

**MEASUREMENT AND CORRELATION OF AXIAL DISPERSION
COEFFICIENT IN A BUBBLE COLUMN WITH A NON-NEWTONIAN LIQUID
PHASE**

by

MARÍA GABRIELA GÓMEZ CARVAJAL

A dissertation submitted in partial fulfillment of the requirements for the
degree of

**DOCTOR OF PHILOSOPHY
in
CHEMICAL ENGINEERING**

**UNIVERSITY OF PUERTO RICO - MAYAGÜEZ CAMPUS
2006**

Approved by:

Jaime Benítez, Ph.D.
Member, Graduate Committee

Date

Moses N. Bogere, Ph.D.
Member, Graduate Committee

Date

Carlos Velázquez, Ph.D.
Member, Graduate Committee

Date

L. Antonio Estévez, Ph.D.
President, Graduate Committee

Date

Nelson Cardona, Ph.D.
Chairperson of the Department

Date

Gustavo Gutiérrez, Ph.D.
Representative of Graduate Studies

Date

José A. Mari Mutt, PhD
Director of Graduate Studies

Date

ABSTRACT

Hydrodynamic characteristics (gas holdup, friction factor, and mixing in the liquid phase) in a bubble column with a non-Newtonian liquid phase (aqueous solutions of carboxymethylcellulose, or CMC, at different concentrations) were measured and correlated. A three-step strategy for this novel approach was devised: first, the rigorous characterization of the rheology of CMC aqueous solutions was conducted to obtain the rheological parameters; second, the hydrodynamic characteristics were measured experimentally; and third, the variables measured were correlated in terms of the rheological parameters of the liquid phase.

The rheological characterization of the aqueous CMC solutions was conducted in a StressTech Rheometer; the power-law model offered an excellent fit of the data and more complex models did not provide substantial improvement to justify their use. Changes in CMC concentrations, sample temperature, and the time of dissolution of the CMC powder in water affected the rheology of these solutions. Additionally, dynamic tests showed a viscoelastic behavior of CMC solutions.

Experiments in a 0.2-m diameter, 2.4-m-high bubble column were carried out to determine pressure drop, gas holdup, and degree of mixing in the liquid phase at various gas and liquid flow rates. The pressure drop, measured with a differential pressure transducer, allowed the calculation of the two-phase friction factor and gas holdup. The gas holdup was also obtained by the disengagement technique. Residence-time distribution experiments were carried out by methylene-blue impulses to characterize the mixing of the liquid phase in two operating modes: batch and continuous.

At the superficial velocities selected, two flow regimes were observed: heterogeneous bubbling flow and heterogeneous churn turbulent flow, and they were identified through the slope changes in the plots of pressure drop and gas holdup. The pressure drop did not seem to be affected by the superficial liquid velocity and it increased as the superficial gas velocity decreased or the CMC concentrations increased. Both techniques used for gas holdup gave similar values (within $\pm 10\%$). Gas holdup

was not affected by the superficial liquid velocity and increased as superficial gas velocity increased. With respect to mixing, two models were used to interpret the experimental data: the axial dispersion model was used in the two operating modes, batch and continuous, and the tanks-in-series model was used just in the case of continuous mode. The axial dispersion model with closed-closed boundary conditions fit experimental data quite well and thus was used to estimate the axial dispersion coefficient. This parameter was higher in batch mode than in continuous mode, and its trend was to increase as superficial gas velocity increased.

The flow behavior and consistency indices of the power-law model, among other standard variables, were used in correlations for the pressure drop, two-phase friction factor, gas holdup, and axial dispersion coefficient in the liquid phase. Inasmuch as possible, dimensionless numbers were used in these correlations. Excellent agreement between predicted and experimental values was obtained. The proposed correlations compared favorably to expressions proposed by other authors.

In summary, a creative and novel approach, holistic in nature, has been pursued. All aspects including rheology, careful experimentation, and rigorous mathematical analysis were taken into account. The results of this work provided an important tool to design bubble column reactors in applications such as fermentation and three-phase catalytic reactions where a powdered catalyst is suspended in a liquid showing a non-Newtonian behavior. Therefore, this work constitutes a significant contribution to the field of heterogeneous reactor modeling.

RESUMEN

Las características hidrodinámicas (retención de gas, factor de fricción y mezclado en la fase líquida) en una columna de burbujeo con un fluido no-Newtoniano (soluciones acuosas de carboximetilcelulosa o CMC a diferentes concentraciones) se midieron y correlacionaron. Se siguió una estrategia de tres etapas en este novedoso desarrollo: primero, se realizó una rigurosa caracterización reológica de soluciones acuosas de CMC para obtener los parámetros reológicos; segundo, se midieron experimentalmente, las características hidrodinámicas; y tercero, se correlacionaron las variables medidas en función de los parámetros reológicos de la fase líquida.

La caracterización reológica de las soluciones acuosas de CMC se realizó en un reómetro StressTech; el modelo de la potencia ofreció un excelente ajuste de los datos reológicos mientras que otros modelos más complejos no proporcionaron mejoras substanciales que justificaran su uso. Cambios en las concentraciones de CMC, temperatura de la muestra y el tiempo de disolución del polvo de CMC en agua afectaron la reología de estas soluciones. Se hicieron además pruebas dinámicas que mostraron un comportamiento viscoelástico de las soluciones.

Se realizaron experimentos en una columna de burbujeo de 0.2 m de diámetro y 2.4 m de altura para determinar caída de presión, retención de gas y el grado de mezclado de la fase líquida a varios flujos de gas y líquido. La caída de presión, medida con un transductor diferencial de presión, permitió el cálculo del factor de fricción bifásico y de la retención de gas. La retención de gas también se obtuvo a través de la técnica de desalojo de gas del sistema. Además, se realizaron experimentos de distribución de tiempos de residencia usando pulsos de azul de metileno para caracterizar el mezclado en la fase líquida bajo dos modos de operación de la columna: semi-continuo y continuo.

Se observaron dos regímenes de flujo a las velocidades superficiales usadas: heterogéneo burbujeante y heterogéneo turbulento. Estos se identificaron a través del cambio de pendiente en las gráficas de caída de presión y retención de gas. La caída de presión no se afectó por la velocidad superficial de líquido y disminuyó al aumentar la velocidad de gas o disminuir la concentración de las soluciones de CMC. Ambas

técnicas usadas para la retención de gas proporcionaron valores similares (dentro de un $\pm 10\%$). La retención de gas no se afectó por la velocidad superficial de líquido y aumentó con la velocidad superficial de gas. Con respecto al mezclado, se usaron dos modelos para interpretar los datos experimentales: el modelo de dispersión axial se usó en los dos modos de operación, semi-continuo y continuo, y el modelo de tanques en serie se usó sólo para el caso continuo. El modelo de dispersión axial con condiciones de borde cerrado-cerrado ajustó bastante bien los datos experimentales y por lo tanto se usó para estimar el coeficiente de dispersión axial. Este parámetro tuvo valores superiores en el caso de modo de operación semi-continuo que en el modo continuo, y su tendencia fue aumentar con el aumento de la velocidad superficial de gas.

Los índices de comportamiento y consistencia del modelo reológico de la ley de potencia, entre otras variables estándares, se usaron en las correlaciones propuestas para el cálculo de la caída de presión, el factor de fricción bifásico, la retención de gas y el coeficiente de dispersión de la fase líquida. Mientras fue posible, se usaron números adimensionales en estas correlaciones. Se obtuvo una concordancia excelente entre los valores predichos por estas correlaciones y los valores experimentales. Las correlaciones propuestas se comparan favorablemente con las expresiones propuestas por otros autores.

En resumen, en este estudio se ha seguido un enfoque creativo y novedoso, de naturaleza holística. Se consideraron todos los aspectos, incluyendo reología, la experimentación cuidadosa y el análisis matemático riguroso. Los resultados de este trabajo constituyen una herramienta importante para el diseño de columnas de burbujeo a usarse como reactores químicos, en aplicaciones como fermentación y reacciones catalíticas trifásicas, donde un catalizador pulverizado está suspendido en un líquido que exhibe un comportamiento no-Newtoniano. Por todo esto, este trabajo constituye una contribución significativa en el campo del modelado de reactores heterogéneos.

To God, Mary and my family ...

ACKNOWLEDGEMENTS

I want to dedicate this section to all people that made possible that today I have reached the yearned goal.

I want to state a sincere acknowledgement to my advisor, Dr. L. Antonio Estévez, for trusting me; he gave me the opportunity to expand my knowledge in process engineering but particularly significant to me in the non-Newtonian fluid area. I received his comprehension, orientation, and support in my studies and in personal life. I also want to thank Dr. Jaime Benítez for his unconditional support, advices, and orientation; he made me feel that the world has hope with very special people like him. I want to thank Dr. Moses Bogere and Dr. Carlos Velázquez for their advices and hallway conversations. Also, I am grateful to Dr. Carlos Rinaldi and Dr. José Colucci and their graduate students for allowing me to use the instruments in their research laboratories. Thank you very much; without your kind support, I would not have been able to finish my research. Thanks to Dr. David Suleiman and graduate committee for giving me the possibility to do the PhD in the Department of Chemical Engineering at UPRM, and for his friendship.

I would not be fair if I did not thank Wilma Irizarry, Angel Zapata, Efren Gregory and Raymond Negrón for their collaboration and help in the laboratory work.

Finally, I want to thank God and Mary for guiding me in my way, thank to my family that has always given me support and encouraged fighting for my dreams and wishes. Thanks to my Puerto Ricans parents who always took care of me.

To all these people, thanks!

TABLE OF CONTENTS

ABSTRACT	ii
RESUMEN	iv
ACKNOWLEDGEMENTS	vii
TABLE OF CONTENTS	viii
LIST OF TABLES	x
LIST OF FIGURES	xvi
LIST OF SYMBOLS	xxiii
1. INTRODUCTION	1
1.1. JUSTIFICATION	1
1.2. OBJECTIVES	1
2. RHEOLOGY. AQUEOUS SOLUTIONS OF CARBOXYMETHYL CELLULOSE	3
2.1. RHEOLOGY	3
General viscous fluid	4
Plastic	6
Viscoelastic materials	7
2.2. RHEOMETRY	9
2.3. A PSEUDOPLASTIC SOLUTION: CARBOXYMETHYL CELLULOSE (CMC) IN WATER	9
2.4. RHEOLOGY PARAMETERS IN BUBBLE COLUMNS	11
3. HYDRODYNAMICS OF BUBBLE COLUMNS	14
3.1. BACKGROUND	14
3.2. FLOW REGIMES	15
3.3. GAS HOLDUP AND PRESSURE DROP	18
3.4. RESIDENCE TIME DISTRIBUTION (RTD)	37
3.4.1. The impulse injection tests	37
3.4.2. The step injection test	39
3.4.3. Moments theory	40
3.5. MATHEMATICAL MODELS. MIXING IN THE LIQUID PHASE	41
3.5.1. Continuous, stirred-tank reactor (CSTR)	42
3.5.2. Plug-flow reactor (PFR)	43
3.5.3. Tank-in-series model	44
3.5.4. The dispersion model (ADM)	46
3.5.5. Modified mixing cell model	69
4. EXPERIMENTAL PROCEDURE	71

4.1. EXPERIMENTAL EQUIPMENT	71
4.2. MATERIALS	76
4.3. EXPERIMENTAL METHOD	76
4.3.1. Rheological characterization of the liquid phase	76
4.3.2. Bubble column experiments	78
4.4. DATA ANALYSIS	82
4.4.1. Rheological characterization of the liquid phase	82
4.4.2. Bubble column experiments	82
5. EXPERIMENTAL RESULTS AND DISCUSSION	84
5.1. RHEOLOGY RESULTS	84
5.1.1. Rheology of CMC solutions at 25 °C	84
5.1.2. Thixotropic behavior of CMC solutions	86
5.1.3. Effect of dissolution time on rheology	90
5.1.4. Effect of temperature on the rheology of CMC solutions	92
5.1.5. Effect of presence of tracers on the rheology of CMC solutions	96
5.1.6. Dynamic tests	100
5.2. BUBBLE COLUMN RESULTS	103
5.2.1. Pressure drop	103
5.2.2. Gas holdup	122
5.2.3. Mixing in the liquid phase	131
6. CONCLUSIONS AND RECOMMENDATIONS	150
7. REFERENCES	153
APPENDIX A. TWO-PHASE FLOW IN PIPES	161
APPENDIX B. CALIBRATION CURVES	169
APPENDIX C. EXPERIMENTAL DATA	176
APPENDIX D. SAMPLE CALCULATIONS	265

LIST OF TABLES

Table 4.1. Experimental runs and conditions	79
Table 4.2. Additional experimental conditions studied	81
Table 5.1. Consistency index for CMC solutions at increasing and decreasing shear rates	89
Table 5.2. Flow index for CMC solutions at increasing and decreasing shear rates	90
Table 5.3. Parameters of the power-law model obtained as a function of temperature (°C).	95
Table 5.4. Values of the power-law parameters with 0.5% and without NaCl	97
Table 5.5. Shear frequency from curves in Figure 5.22	103
Table 5.6. Correlations for pressure drop	109
Table 5.7. Correlations for pressure drop as a function of dimensionless numbers	109
Table 5.8. Correlations for two-phase friction factor	117
Table 5.9. Correlations for two-phase friction factor as a function of dimensionless numbers	118
Table 5.10. Correlations for gas holdup	125
Table 5.11. Correlations for gas holdup as a function of dimensionless numbers	125
Table 5.12. Correlations for axial dispersion coefficient	137
Table 5.13. Correlations for axial dispersion coefficient as a function of dimensionless numbers	138
Table B.1. Calibration of micrometric valve. $u_G < 0.0206$ m/s	169
Table B.2. Calibration of rotameter. $u_G \geq 0.0206$ m/s	170
Table B.3. Calibration of the pump	170
Table B.4. Calibration of spectrophotometer for tap water at $\lambda=300$ nm	171

Table B.5. Calibration of spectrophotometer for 0.10% CMC solution at $\lambda=300$ nm and 24 h of dissolution	172
Table B.6. Calibration of spectrophotometer for 0.20% CMC solution at $\lambda=300$ nm and 24 h of dissolution	173
Table B.7. Calibration of spectrophotometer for 0.30% CMC solution at $\lambda=300$ nm and 24 h of dissolution	174
Table B.8. Calibration of spectrophotometer for 0.40% CMC solution at $\lambda=300$ nm and 24 h of dissolution	175
Table C.1. Experimental data of pressure drop for tap water	176
Table C.2. Experimental data of pressure drop for CMC solutions	177
Table C.3. Correlation data of pressure drop for CMC solutions	178
Table C.4. Gas holdup for tap water through disengagement technique	179
Table C.5. Gas holdup for tap water through pressure drop technique	180
Table C.6. Gas holdup for CMC solutions through disengagement technique	181
Table C.7. Gas holdup of the proposed correlations for CMC solutions calculated through disengagement technique	182
Table C.8. Gas holdup for CMC solutions through pressure drop technique	183
Table C.9. Gas holdup of the proposed correlations for CMC solutions through pressure drop technique	184
Table C.10. Two-phase friction factor for tap water	185
Table C.11. Two-phase friction factor for CMC solutions	186
Table C.12. Tracer concentration for Run 86 ($u_L=0$ m/s, $u_G=0.0112$ m/s, tap water)	187
Table C.13. Tracer concentration for Run 87 ($u_L=0$ m/s, $u_G=0.0206$ m/s, tap water)	188
Table C.14. Tracer concentration for Run 88 ($u_L=0$ m/s, $u_G=0.0010$ m/s, tap water)	189
Table C.15. Tracer concentration for Run 89 ($u_L=0$ m/s, $u_G=0.0055$ m/s, tap water)	190

Table C.16. Tracer concentration for Run 91 ($u_L=0$ m/s, $u_G=0.0055$ m/s, tap water)	191
Table C.17. Tracer concentration for Run 93 ($u_L=0$ m/s, $u_G=0.0034$ m/s, tap water)	192
Table C.18. Tracer concentration for Run 94 ($u_L=0$ m/s, $u_G=0.0112$ m/s, tap water)	193
Table C.19. Tracer concentration for Run 95 ($u_L=0$ m/s, $u_G=0.0462$ m/s, tap water)	194
Table C.20. Tracer concentration for Run 111 ($u_L=0$ m/s, $u_G=0.0027$ m/s, tap water)	195
Table C.21. Tracer concentration for Run 112 ($u_L=0$ m/s, $u_G=0.0308$ m/s, tap water)	196
Table C.22. Tracer concentration for Run 235 ($u_L=0$ m/s, $u_G=0.0083$ m/s, tap water)	197
Table C.23. Tracer concentration for Run 236 ($u_L=0$ m/s, $u_G=0.0385$ m/s, tap water)	198
Table C.24. Tracer concentration for Run 92 ($u_L=0.0025$ m/s, $u_G=0.0010$ m/s, tap water)	199
Table C.25. Tracer concentration for Run 96 ($u_L=0.0025$ m/s, $u_G=0.0034$ m/s, tap water)	201
Table C.26. Tracer concentration for Run 97 ($u_L=0.0025$ m/s, $u_G=0.0112$ m/s, tap water)	203
Table C.27. Tracer concentration for Run 98 ($u_L=0.0025$ m/s, $u_G=0.0462$ m/s, tap water)	205
Table C.28. Tracer concentration for Run 99 ($u_L=0.0017$ m/s, $u_G=0.0010$ m/s, tap water)	207
Table C.29. Tracer concentration for Run 100 ($u_L=0.0017$ m/s, $u_G=0.0034$ m/s, tap water)	209
Table C.30. Tracer concentration for Run 101 ($u_L=0.0017$ m/s, $u_G=0.0112$ m/s, tap water)	210
Table C.31. Tracer concentration for Run 102 ($u_L=0.0017$ m/s, $u_G=0.0462$ m/s, tap water)	212

Table C.32. Tracer concentration for Run 103 ($u_L=0.0017$ m/s, $u_G=0.0027$ m/s, tap water)	213
Table C.33. Tracer concentration for Run 104 ($u_L=0.0025$ m/s, $u_G=0.0027$ m/s, tap water)	214
Table C.34. Tracer concentration for Run 105 ($u_L=0.0025$ m/s, $u_G=0.0308$ m/s, tap water)	216
Table C.35. Tracer concentration for Run 106 ($u_L=0.0007$ m/s, $u_G=0.0034$ m/s, tap water)	217
Table C.36. Tracer concentration for Run 109 ($u_L=0.0017$ m/s, $u_G=0.0112$ m/s, tap water)	219
Table C.37. Tracer concentration for Run 110 ($u_L=0.0017$ m/s, $u_G=0.0112$ m/s, tap water)	220
Table C.38. Tracer concentration for Run 113 ($u_L=0.0017$ m/s, $u_G=0.0112$ m/s, tap water)	221
Table C.39. Tracer concentration for Run 126 ($u_L=0.0045$ m/s, $u_G=0.0308$ m/s, tap water)	222
Table C.40. Tracer concentration for Run 128 ($u_L=0.0045$ m/s, $u_G=0.0112$ m/s, tap water)	224
Table C.41. Tracer concentration for Run 130 ($u_L=0.0045$ m/s, $u_G=0.0206$ m/s, tap water)	226
Table C.42. Tracer concentration for Run 131 ($u_L=0.0045$ m/s, $u_G=0.0206$ m/s, tap water)	228
Table C.43. Tracer concentration for Run 230 ($u_L=0.0045$ m/s, $u_G=0.0083$ m/s, tap water)	230
Table C.44. Tracer concentration for Run 231 ($u_L=0.0045$ m/s, $u_G=0.0145$ m/s, tap water)	231
Table C.45. Tracer concentration for Run 238 ($u_L=0.0045$ m/s, $u_G=0.0385$ m/s, tap water)	232
Table C.46. Tracer concentration for Run 239 ($u_L=0.0045$ m/s, $u_G=0.0010$ m/s, tap water)	233
Table C.47. Tracer concentration for Run 206 ($u_L=0.0$ m/s, $u_G=0.0083$ m/s, 0.20% CMC)	234

Table C.48. Tracer concentration for Run 207 ($u_L=0.0$ m/s, $u_G=0.0145$ m/s, 0.20% CMC)	236
Table C.49. Tracer concentration for Run 208 ($u_L=0.0$ m/s, $u_G=0.0308$ m/s, 0.20% CMC)	238
Table C.50. Tracer concentration for Run 209 ($u_L=0.0$ m/s, $u_G=0.0385$ m/s, 0.20% CMC)	240
Table C.51. Tracer concentration for Run 210 ($u_L=0.0$ m/s, $u_G=0.0462$ m/s, 0.20% CMC)	242
Table C.52. Tracer concentration for Run 216 ($u_L=0.0045$ m/s, $u_G=0.0083$ m/s, 0.20% CMC)	244
Table C.53. Tracer concentration for Run 217 ($u_L=0.0045$ m/s, $u_G=0.0145$ m/s, 0.20% CMC)	245
Table C.54. Tracer concentration for Run 218 ($u_L=0.0045$ m/s, $u_G=0.0308$ m/s, 0.20% CMC)	246
Table C.55. Tracer concentration for Run 219 ($u_L=0.0045$ m/s, $u_G=0.0385$ m/s, 0.20% CMC)	247
Table C.56. Tracer concentration for Run 220 ($u_L=0.0045$ m/s, $u_G=0.0462$ m/s, 0.20% CMC)	248
Table C.57. Tracer concentration for Run 223 ($u_L=0.0045$ m/s, $u_G=0.0010$ m/s, 0.20% CMC)	249
Table C.58. Tracer concentration for Run 213 ($u_L=0.0$ m/s, $u_G=0.0308$ m/s, 0.40% CMC)	251
Table C.59. Tracer concentration for Run 215 ($u_L=0.0$ m/s, $u_G=0.0083$ m/s, 0.40% CMC)	252
Table C.60. Tracer concentration for Run 224 ($u_L=0.0$ m/s, $u_G=0.0145$ m/s, 0.40% CMC)	253
Table C.61. Tracer concentration for Run 226 ($u_L=0.0$ m/s, $u_G=0.0385$ m/s, 0.40% CMC)	254
Table C.62. Tracer concentration for Run 228 ($u_L=0.0$ m/s, $u_G=0.0462$ m/s, 0.40% CMC)	255
Table C.63. Tracer concentration for Run 232 ($u_L=0.0$ m/s, $u_G=0.0010$ m/s, 0.40% CMC)	256

Table C.64. Tracer concentration for Run 239 ($u_L=0.0$ m/s, $u_G=0.0308$ m/s, tap water)	257
Table C.65. Tracer concentration for Run 222 ($u_L=0.0045$ m/s, $u_G=0.0083$ m/s, 0.40% CMC)	258
Table C.66. Tracer concentration for Run 227 ($u_L=0.0045$ m/s, $u_G=0.0308$ m/s, 0.40% CMC)	259
Table C.67. Tracer concentration for Run 229 ($u_L=0.0045$ m/s, $u_G=0.0385$ m/s, 0.40% CMC)	260
Table C.68. Tracer concentration for Run 233 ($u_L=0.0045$ m/s, $u_G=0.0145$ m/s, 0.40% CMC)	261
Table C.69. Tracer concentration for Run 234 ($u_L=0.0045$ m/s, $u_G=0.0462$ m/s, 0.40% CMC)	262
Table C.70. Tracer concentration for Run 237 ($u_L=0.0045$ m/s, $u_G=0.0010$ m/s, 0.40% CMC)	263
Table C.71. Tracer concentration for Run 240 ($u_L=0.0045$ m/s, $u_G=0.0308$ m/s, 0.40% CMC)	264

LIST OF FIGURES

Figure 2.1. Rheological behavior of fluids	4
Figure 2.2. (a) Molecule of glucose. (b) Structural unit of cellulose	10
Figure 2.3. Carboxymethyl cellulose based on β -(1-4)-D-glucofuranose polymer of cellulose (LSBU, 2003)	10
Figure 2.4. Comparison of average shear rate for CMC (taken from Al-Masry, 2001)	13
Figure 3.1. Flow regimes in bubble columns	16
Figure 3.2. Flow-regime map (Ityokumbul <i>et al.</i> , 1994)	18
Figure 3.3. Gas holdup as a function of gas velocity (Deckwer <i>et al.</i> , 1974)	19
Figure 3.4. Cell model (Joshi and Sharma, 1979)	20
Figure 3.5. Gas holdup as a function of viscosity for CMC solutions (Godbole <i>et al.</i> , 1982)	24
Figure 3.6. Holdup model proposed by Walter and Blanch (1983)	25
Figure 3.7. Parity plot of gas holdup observed and calculated through Eq.(3.23) (Walter and Blanch, 1983)	26
Figure 3.8. Gas holdup as a function of superficial gas velocity for different superficial liquid velocity (Ityokumbul <i>et al.</i> , 1993)	30
Figure 3.9. Schematic of the gas holdup behavior (Zahradnik <i>et al.</i> , 1997)	31
Figure 3.10. Radial gas holdup obtained by Moustiri (2001)	34
Figure 3.11. Measurement of residence time distribution with an impulse injection	39
Figure 3.12. Response for a step injection of tracer in the tanks-in-series model (Levenspiel, 1989)	45
Figure 3.13. Response for an impulse injection of tracer in the tanks-in-series model (Levenspiel, 1989)	46
Figure 3.14. Response curves for an impulse injection of tracer in the ADM model with open-open boundary conditions (Levenspiel, 1989)	49

Figure 3.15. Response curves for an impulse injection of tracer in the ADM model with closed-closed boundary conditions (Levenspiel, 1989)	51
Figure 3.16. Axial dispersion coefficient obtained by Ityokumbul <i>et al.</i> (1994) for air-water system	62
Figure 3.17. Axial dispersion coefficient (Degaleesan and Dudukovic, 1998)	63
Figure 4.1. Experimental setup	72
Figure 4.2. Experimental setup	73
Figure 4.3. Differential pressure transducer	73
Figure 4.4. Cecil 3000 spectrophotometer	74
Figure 4.5. StressTech rheometer	74
Figure 4.6. Modules of the rheometer	75
Figure 4.7. Motor/detector module of the rheometer	76
Figure 5.1. Viscosity curves for dissolution time of 2 h	85
Figure 5.2. Flow curves for dissolution time of 2 h	85
Figure 5.3. Consistency index and flow index of the power-law model for CMC solutions for dissolution time of 2 h	86
Figure 5.4. Thixotropy test for 0.15% CMC solution	87
Figure 5.5. Thixotropy test for 0.25% CMC solution	88
Figure 5.6. Thixotropy tet for 0.50% CMC solution	88
Figure 5.7. Effect of the dissolution time on the flow curves at 0.05% of CMC at 25 °C	91
Figure 5.8. Effect of the dissolution time on the flow curves at 0.15% of CMC at 25 °C	91
Figure 5.9. Effect of the dissolution time on the flow curves at 0.25% of CMC at 25 °C	92
Figure 5.10. Viscosity and flow curve for 0.05% aqueous solution of CMC for 2 h of dissolution time	93

Figure 5.11. Viscosity and flow curve for 0.15% aqueous solution of CMC for 2 h of dissolution time	93
Figure 5.12. Viscosity and flow curve for 0.25% aqueous solution of CMC for 2 h of dissolution time	94
Figure 5.13. Viscosity and flow curve for 0.20% aqueous solution of CMC for a dissolution time of 24 h	94
Figure 5.14. Viscosity and flow curve for 0.40% aqueous solution of CMC for a dissolution time of 24 h	95
Figure 5.15. Effect of the addition of sodium chloride to a solution of 0.75% wt of CMC at 25°C and 2 h of dissolution time	96
Figure 5.16. Effect of the addition of phthalic acid monopotassium salt to a solution of 0.05% wt of CMC	98
Figure 5.17. Effect of the addition of 101100 FLT Industrial Red Dye tracer of Tramfloc to a solution of 0.25% wt of CMC	98
Figure 5.18. Effect of the addition of methylene blue to a solution of 0.20% wt of aqueous solution of CMC for 24 h of dissolution	99
Figure 5.19. Effect of the addition of methylene blue to a solution of 0.40% wt of aqueous solution of CMC for 24 h of dissolution	100
Figure 5.20. Storage Modulus at different CMC concentrations	101
Figure 5.21. Loss Modulus at different CMC concentrations	102
Figure 5.22. Storage and Loss Moduli at different CMC weight-percentage concentrations	102
Figure 5.23. Pressure drop for tap water at different liquid superficial velocities	104
Figure 5.24. Pressure drop for 0.20% of CMC in water at different liquid superficial velocities	105
Figure 5.25. Pressure drop for 0.40% of CMC in water at different liquid superficial velocities	105
Figure 5.26. Pressure drop in batch mode at different CMC concentrations	106
Figure 5.27. Pressure drop in continuous mode ($u_L=0.0045$ m/s) at different CMC concentrations	107

Figure 5.28. Flow regimes found in the range of the operation of the bubble column	108
Figure 5.29. Pressure drop for tap water and $u_L = 0$ m/s	110
Figure 5.30. Pressure drop for tap water and $u_L = 0.0045$ m/s	110
Figure 5.31. Comparison between experimental data and equations (5.5) and (5.6) for the pressure drop using tap water	111
Figure 5.32. Pressure drop for 0.20% CMC solutions	112
Figure 5.33. Pressure drop for 0.40% CMC solutions	112
Figure 5.34. Comparison between experimental data and equations (5.7) and (5.8) for the pressure drop with CMC solutions	113
Figure 5.35. Two-phase friction factor for tap water	114
Figure 5.36. Two-phase friction factor for 0.20% CMC solutions	114
Figure 5.37. Two-phase friction factor for 0.40% CMC solutions	115
Figure 5.38. Two-phase friction factor for batch mode ($u_L=0$ m/s)	116
Figure 5.39. Two-phase friction factor for continuous mode ($u_L=0.0045$ m/s)	116
Figure 5.40. Two-phase friction factor for tap water from experimental data fit by equations (5.13) through (5.16)	119
Figure 5.41. Two-phase friction factor for 0.20% CMC solutions from experimental data fit by equations (5.13) through (5.16)	119
Figure 5.42. Two-phase friction factor for 0.40% CMC solutions from experimental data fit by equations (5.13) through (5.16)	120
Figure 5.43. Parity plot of two-phase friction factor at different CMC concentrations and batch mode ($u_L= 0$ m/s)	121
Figure 5.44. Parity plot of two-phase friction factor at different CMC concentrations and continuous mode ($u_L= 0.0045$ m/s)	121
Figure 5.45. Effect of liquid superficial velocity over gas holdup for tap water	122
Figure 5.46. Effect of liquid superficial velocity over gas holdup for 0.20% aqueous solution of CMC	123

Figure 5.47. Effect of liquid superficial velocity over gas holdup for 0.40% aqueous solution of CMC	123
Figure 5.48. Comparison between results of gas holdup obtained by disengagement and pressure drop techniques	124
Figure 5.49. Gas holdup for tap water and batch tests ($u_L=0$ m/s)	126
Figure 5.50. Gas holdup for tap water and continuous tests ($u_L=0.0045$ m/s)	127
Figure 5.51. Gas holdup for 0.20% CMC solution and batch mode ($u_L=0$ m/s)	127
Figure 5.52. Gas holdup for 0.20% CMC solution and continuous mode ($u_L=0.0045$ m/s)	128
Figure 5.53. Gas holdup for 0.40% CMC solution and batch mode ($u_L=0$ m/s)	128
Figure 5.54. Gas holdup for 0.40% CMC solution and continuous mode ($u_L=0.0045$ m/s)	129
Figure 5.55. Comparison between experimental data and equations (5.21) and (5.22) for gas holdup with tap water	130
Figure 5.56. Comparison between experimental data and equations (5.23) and (5.24) for gas holdup with CMC solutions	130
Figure 5.57. Repeatability tests in the exit-tracer concentration for tap water in continuous mode ($u_G=0.0206$ m/s and $u_L=0.0045$ m/s)	131
Figure 5.58. Exit-tracer concentration for tap water in continuous mode ($u_G=0.0112$ m/s and $u_L=0.0017$ m/s) at two radial positions	132
Figure 5.59. Exit-tracer concentration for tap water in batch mode ($u_G=0.0083$ m/s and $u_L=0$ m/s)	133
Figure 5.60. Exit-tracer concentration for 0.20% CMC solution in batch mode ($u_G=0.0308$ m/s and $u_L=0$ m/s)	133
Figure 5.61. Exit-tracer concentration for 0.40% CMC solution in batch mode ($u_G=0.0462$ m/s and $u_L=0$ m/s)	134
Figure 5.62. Exit concentration of an impulse of tracer for tap water at continuous mode ($u_G=0.0010$ m/s and $u_L=0.0025$ m/s)	135
Figure 5.63. Exit concentration of an impulse of tracer for 0.20% of CMC solution in continuous mode ($u_G=0.0462$ m/s and $u_L=0.0045$ m/s)	136

Figure 5.64. Exit concentration of an impulse of tracer for 0.40% of CMC solution in continuous mode ($u_G=0.0462$ m/s and $u_L=0.0045$ m/s)	136
Figure 5.65. Axial dispersion coefficient for tap water at different superficial liquid velocity and $1.04 \times 10^{-3} \leq u_G(m/s) \leq 1.44 \times 10^{-2}$	139
Figure 5.66. Axial dispersion coefficient for tap water at different superficial liquid velocity and $(3.07 \times 10^{-2} \leq u_G(m/s) \leq 4.62 \times 10^{-2})$	139
Figure 5.67. Axial dispersion coefficient for tap water in batch mode ($u_L=0$ m/s) and $1.04 \times 10^{-3} \leq u_G(m/s) \leq 1.44 \times 10^{-2}$	140
Figure 5.68. Axial dispersion coefficient for tap water in continuous mode ($u_L=0.0025$ m/s) and $1.04 \times 10^{-3} \leq u_G(m/s) \leq 1.44 \times 10^{-2}$	141
Figure 5.69. Axial dispersion coefficient for tap water in continuous mode ($u_L=0.0045$ m/s) and $1.04 \times 10^{-3} \leq u_G(m/s) \leq 1.44 \times 10^{-2}$	141
Figure 5.70. Comparison between experimental data and Eq. (5.17) for gas holdup for tap water in the heterogeneous bubbling flow regime	142
Figure 5.71. Axial dispersion coefficient for tap water in batch mode ($u_L=0$ m/s) and $3.07 \times 10^{-2} \leq u_G(m/s) \leq 4.62 \times 10^{-2}$	143
Figure 5.72. Axial dispersion coefficient for tap water in continuous mode ($u_L=0.0045$ m/s) and $3.07 \times 10^{-2} \leq u_G(m/s) \leq 4.62 \times 10^{-2}$	143
Figure 5.73. Comparison between experimental data and Eq. (5.18) for gas holdup for tap water in the heterogeneous churn turbulent flow regime	144
Figure 5.74. Axial dispersion coefficient for 0.20% CMC solution in batch mode ($u_L=0$ m/s)	145
Figure 5.75. Axial dispersion coefficient for 0.20% CMC solution in continuous mode ($u_L=0.0045$ m/s)	145
Figure 5.76. Axial dispersion coefficient for 0.40% CMC solution in batch mode ($u_L=0$ m/s)	146
Figure 5.77. Axial dispersion coefficient for 0.40% CMC solution in continuous mode ($u_L=0.0045$ m/s)	147

Figure 5.78. Comparison between experimental data and equations (5.19) and (5.21) for axial dispersion coefficient and CMC solutions and batch mode ($u_L=0$ m/s) in both heterogeneous flow regimes	148
Figure 5.79. Comparison between experimental data and Eq. (5.20) and (5.22) for axial dispersion coefficient and CMC solutions and continuous mode ($u_L=0.0045$ m/s) in heterogeneous bubbling flow regime	149
Figure A.1. Flow regimes for two-phase flow in vertical pipes (Shoham, 1998)	162
Figure A.2. Flow pattern maps obtained by Taitel <i>et al.</i> (1980) for water-air at 25 °C and 100 kPa	164
Figure A.3. In situ gas holdup and no-slip gas holdup	165
Figure B.1. Calibration of micrometric valve $u_G < 0.0206$ m/s	169
Figure B.2. Calibration of rotameter $u_G \geq 0.0206$ m/s	170
Figure B.3. Curve of calibration of spectrophotometer for tap water at $\lambda=300$ nm	171
Figure B.4. Calibration curve of spectrophotometer for 0.10% CMC solution at $\lambda=300$ nm and 24 h of dissolution	172
Figure B.5. Calibration curve of spectrophotometer for 0.20% CMC solution at $\lambda=300$ nm and 24 h of dissolution	173
Figure B.6. Calibration curve of spectrophotometer for 0.30% CMC solution at $\lambda=300$ nm and 24 h of dissolution	174
Figure B.7. Calibration curve of spectrophotometer for 0.40% CMC solution at $\lambda=300$ nm and 24 h of dissolution	175

LIST OF SYMBOLS

A	flow area, (L^2)
A'	distance between the column axis and the point of maximum vorticity, (L)
A_D	downcomer cross-sectional area, (L^2)
A_r	area ratio of nozzle to column, (-)
A_R	riser cross sectional area, (L^2)
b	constant in equation (2.10), (t)
Bo	Bodenstein number ($Bo = u_g d_c / D_z$), (-)
Bo'	Bond number ($Bo' = g d_c^2 \rho_L / \sigma$), (-)
$c, c(t)$	concentration of the tracer, (M/L^3)
\bar{c}	cross-sectional average concentration, (M/L^3)
c^*	dimensionless concentration of tracer. In Eq. (3.150) defined as $\left(c^* = (c - c_i) / (c_\infty - c_i) \right), (-)$
C'	parameter of the power-law liquid velocity in Eq. (3.42)
c_d	tracer concentration in the downflow liquid flow region, (mol/L^3)
c_E	equilibrium concentration of tracer, (M/L^3)
c_i	initial concentration of the tracer, (M/L^3)
c_{in}	inlet concentration of tracer, (M/L^3)
c_u	tracer concentration in the upflow liquid flow region, (mol/L^3)
c_0	pulse or inlet concentration in the reactor, (M/L^3)
C_0	distribution parameter $\left(C_0 = \frac{\langle \varepsilon_g j \rangle}{\langle \varepsilon_g \rangle \langle j \rangle} \right), (-)$
c_∞	final equilibrium concentration, (M/L^3)
D	constant in Eqs. (3.38) and (3.39)
d, d_c	column diameter, (L)
d_B	bubble diameter, (L)

d_{crit} critical size of the bubble $\left(d_{crit} = \left[0.4\sigma / (\rho_L - \rho_g) g \right]^{1/2} \right)$, (L)

d_0 orifice diameter, (L)

D_{eff} effective axial dispersion $\left[\bar{D}_{zz} = \frac{\int_0^R \varepsilon_L(r) r D_{zz}(r) dr}{\int_0^R r \varepsilon_L(r) dr} \right]$, (L²/t)

D_{Taylor} Taylor-type diffusivity

$$D_{Taylor} = \frac{\int_0^R r \varepsilon_L(r) u_z(r) \left[\int_0^{r'} \frac{\tilde{r} \varepsilon_L(\tilde{r}) \left(u_z(\tilde{r}) - D_{zz}(\tilde{r}) \frac{u_L / \varepsilon_L}{D_{eff}} \right) d\tilde{r}}{r' \varepsilon_L(r') D_{rr}(r')} dr' \right] dr}{\int_0^R r \varepsilon_L(r) dr}, \text{ (L}^2\text{/t)}$$

D_z axial dispersion coefficient, (L²/t)

\bar{D}_{zz} mean axial eddy diffusivity, (L²/t)

e exchange coefficient between flowing and stagnant liquid, (t⁻¹)

E eddy diffusivity, (L²/t)

$E(t)$ external age distribution, (t⁻¹)

F force required to produce the fluid motion, (M·m/s²)

f fraction of stagnant liquid in the modified mixing cell model, (-)

f_{TPL} two-phase friction factor, (-)

f_F Fanning friction factor, (-)

$F(t)$ accumulative distribution, (-)

Fr_i Froude number of the i -phase ($Fr_i = u_i^2 / g d_c$); in the case of Eq. (3.101) the characteristic length is the hydraulic radius of the bed, and in the case of equations (3.110) and (3.111) is defined as ($Fr_i = u_i / \sqrt{g d_c}$) (-)

Fr_M	Froude number of gas-liquid mixture $\left(Fr_M = (u_g + u_L)^2 / g d_c\right)$, (-)
g	gravitational acceleration, (L/t ²)
G	elastic modulus in Hookes' law, (M/L·t ²)
G'	storage modulus, (M/L·t ²)
G''	loss modulus, (M/L·t ²)
G^*	complex shear modulus $(G^* = G' + iG'')$, (M/L·t ²)
Ga	Galilei number $Ga = (g d_c^3 \rho_L^2 / \eta^2)$, (-)
h	reading of a manometer, (L)
H	length of bubbling liquid in the column or operating height, (L)
H_D	length of the downcomer section of the airlift, (L)
H_r	ratio of effective column height to column diameter, (-)
H_0	unexpanded bed height or length of disengaged gas in the columns, (L)
H_I	length of region I, (L)
H_{II}	length of region II, (L)
$\langle j \rangle$	average flux density of the mixture $\left(\langle j \rangle = \frac{Q_l + Q_g}{A}\right)$, (L ³ /t·L ²)
k	consistency index in the power-law model, (M·t ⁿ⁻² /L)
K	liquid velocity profile parameter (-) or constant in Eq. (2.4), (t ^{0.5})
K'	dimensionless constant of Eq. (3.102), (-)
l	linear scale, (L)
L	distance between the two pressure taps, (L)
L_0	height of one cell (0.8 d_c), (L)
m	constant in equation (2.5), (t ^{0.5(n-1)})
M	constant in Eq. (3.39) or total injected mass of tracer, (M)
M_i	centered moment of i -order (independent variable ^{i})
M_i'	non-centered moment of i -order (independent variable ^{i})
Mo_L	liquid Morton number $\left(Mo_L = g \mu_L^4 / (\rho_L - \rho_g) \sigma_L^3\right)$, (-)
n	flow index in the power-law model, (-)

n_u	number of orifices in the gas distributor, (-)
N	total number of tanks, (-)
N'	shape factor for gas holdup, (-)
N_0	mass of tracer, (M)
$P(t)$	statistical distribution (t^{-1})
P_m	energy dissipation rate per unit mass, (L^2/t^2)
Q	volumetric flow rate, (L^3/t)
Q_i	volumetric flow rate of the phase- i , (L^3/t)
r	radial position, (L)
r'	dimensionless radial coordinate ($r' = 2r/d_c$) (in Eq. 3.149, is defined as: $r' = r/H \sqrt{D_z/D_r}$), (-)
r_∞	radial position at which $u_z = -u_{b\infty}$, (L)
R''	radial component of the dimensionless stream function, (-)
Re	Reynolds number $\left[Re = \frac{8u_L^{2-n} d_c^n \rho_L}{k \left(\frac{6n+2}{n} \right)} \right]$ in the case of Eqs. (3.38) and (3.39), (-)
Re_i	Reynolds number of the i -phase $\left(Re_i = \frac{\rho_i u_i d_c}{\mu_i} \right)$, (-). In the case of non-Newtonian fluids, $Re_i = \frac{\rho_i u_i^{2-n} d_c^n}{k}$, (-)
Re_M	mixture Reynolds number $\left(Re_M = \frac{\rho_M v_M d_c}{\mu_M} \right)$, (-)
S	pipe or column perimeter, (L)
Su_L	Suratmann number of liquid, (-)
t	time, (t)
t'	previous time that consider the history of the rate of strain (shear rate) in all particles in the same position, (t)
t_i	time at which tracer first appears in the effluent, (t)

$t_{max,i}$	maximum time required for bubble of class i to disengage, (t)
u	axial velocity, (L/t)
u_b	rise velocity of single bubble, (L/t)
u_B	intercell liquid-circulation velocity, (L/t)
$u_{b\infty}$	slip velocity of a bubble, (L/t)
u_c	average liquid circulation velocity, (L/t)
u_g	superficial velocity of the gas phase, (L/t)
\bar{u}_g	mean gas velocity (u_g at $H/2$), (L/t)
$u_i(r')$	instantaneous liquid velocity, (L/t)
u_L	superficial velocity of the liquid phase, (L/t)
$u_L(r)$	local axial liquid velocity $\left[u_L(r) = \frac{\sum_{j=1}^T u_j(r)}{T} \right]$, (L/t)
\bar{u}_L	average liquid velocity, (L/t)
$u_{Lc}(0)$	centre-line liquid velocity $\left[u_{Lc}(0) = 0.21(gd_c)^{1/2} \left(\frac{u_g^3 \rho_L}{g\mu_L} \right)^{1/8} \right]$, (L/t)
u_r	relative velocities of gas and liquid phases, (L/t)
$u_{r,II}$	rise velocity of the Sauter mean bubble size in the upper section of the column in a stagnant liquid, (L/t)
u_t	terminal bubble rise velocity, (L/t)
u_z	vertical component of the liquid velocity, (L/t)
U_z	absolute vertical component of the bubble velocity, (L/t)
u_0	average vertical component of the liquid velocity, (L/t)
U_0	average of the vertical component of the absolute velocity of bubbles, (L/t)
u_{0b}	average vertical component of liquid velocity, (L/t)
v_M	mixture velocity ($v_M = u_g + u_L$), (L/t)
V	volume of the reactor, (L ³)

V_0	volume of the liquid phase in the bubble column (in the disengagement of the gas phase), (L^3)
w	frequency of the oscillations, (t^{-1})
W	total mass flow rate, (M/t)
x	quality (ratio of the gas mass flow rate to the total mass flow rate across a given sectional area), (-)
z	axial position, (L)
z^*	dimensionless axial position ($z^* = z/H$), (-)

Greek symbols

α	inclination angle of the pipe or column from the horizontal, (rad)
β	height filled with tracer, (L)
β'	dimensionless radial position defined in the boundary condition of Eq. (3.149) ($\beta' = R/H \sqrt{D_z/D_r}$), (-)
$\delta(t)$	Dirac delta function, (t^{-1})
δ_n	roots of equation (3.89)
$\Delta\rho$	density difference ($\Delta\rho = \rho_l - \rho_g$), (M/L^3)
ε_g	overall gas hold-up, (-)
ε'_g	gas holdup with slippage, (-)
ε''_g	gas holdup with no slippage ($\varepsilon''_g = u_g / (u_L + u_g)$), (-)
$\varepsilon_g(t)$	dynamic gas holdup at a time during disengagement, (-)
$\varepsilon_{g,i}$	gas holdup due to i^{th} sized bubbles, (-)
ε_{gd}	gas holdup of the downflow liquid flow, (-)
ε_{gu}	gas holdup of the upflow liquid flow, (-)
$\bar{\varepsilon}_I$	average gas-holdup of section I of the holdup model, (-)
$\bar{\varepsilon}_{II}$	average gas-holdup at section II of the holdup model, (-)

ϕ_i	dimensionless two-phase frictional multiplier of the phase- <i>i</i> , (-)
ϕ'_L	modified dimensionless two-phase frictional multiplier of the liquid phase for shear thinning fluids, (-)
γ^3	skewness, (t ³)
γ	strain, (-)
γ_0	strain amplitude which is small enough for the linearity constraint to be satisfied, (-)
$\dot{\gamma}$	shear rate, (t ⁻¹)
ψ	constant in Eq.(3.21) defined by Eq. (3.22), (-)
η	effective viscosity, (M/L·t)
η'	dynamic viscosity ($G'' = \eta'w$), (M/L·t)
η''	parameter related to dynamic rigidity ($G' = \eta''w$), (M/L·t)
η^*	complex viscosity ($\eta^* = \eta' - i\eta''$), (M/L·t)
η_0	apparent viscosity at zero shear rate, (M/L·t)
η_∞	apparent viscosity at infinite shear rate, (M/L·t)
λ	constant in Eq. (2.3), (t)
μ	Newtonian viscosity in rheology, (M/L·t) or mean residence time in RTD studies, (t)
μ_r	gas-to-liquid viscosity ratio, (M/L·t)
ρ_A	gas density at atmospheric conditions, (M/L ³)
ρ_G	gas density, (M/L ³)
ρ_L	liquid density, (M/L ³)
ρ_M	mixture density $\left(\rho_M = \rho_L(1 - \varepsilon_g) + \rho_g \varepsilon_g = x \left(\frac{1}{\rho_g} - \frac{1}{\rho_L} \right) + \frac{1}{\rho_L} \right)$, (M/L ³)
ρ_w	water density, (M/L ³)
σ^2	variance, (t ²)

σ_{θ}^2	dimensionless second moment of response curve, (-)
σ_L	surface tension of the liquid phase, (M/t ²)
σ_{WA}	surface tension of water at atmospheric conditions, (M/t ²)
τ	mean residence time, (t)
τ	shear stress, (M/L·t ²)
τ_{GL}	gas-liquid frictional stress at the wall, (M/L·t ²)
τ_{rel}	relaxation time of a material, (t)
τ_{yx}	y-x component of the stress tensor, (M/ L·t ²)
τ_y	fluency shear stress or yield stress, (M/ L·t ²)
θ	dimensionless time. In Eq. (3.150) is defined as $D_z t / L^2$), (-)
ν_L	kinematic viscosity of the liquid, (L ² /t)
χ	Lockhart-Marinelli parameter, (-)
χ'	modified Lockhart-Marinelli parameter, (-)

Subscripts

av	average
av,c	average in the cooling coil side
av,j	average in the jacket side
g	gas-phase
L	liquid-phase

1. INTRODUCTION

1.1. Justification

Bubble columns have been used in many applications such as heterogeneous reactors and separation processes because of their simple construction and low installation, operating, and maintenance costs; however, the complexity of their fluid-dynamics increases with scale-up. Some uses of these equipments are wastewater treatment, organic synthesis, desulphurization of gases, and in the biotechnological and pharmaceutical industry. Fermentation is a particular application of a bubble column, where the liquid phase often exhibits non-Newtonian behavior. In the literature, works on bubble column using a non-Newtonian liquid are scarce, particularly with respect to characterization of liquid mixing in a bubble column. Few researchers have studied the flow regimes and the holdup of the phases involved in the bubble column. For this reason, the study of the liquid mixing in bubble columns with a non-Newtonian liquid phase constitutes a significant contribution to the field.

1.2. Objectives

The characterization of bubble columns with a non-Newtonian liquid-phase has received little attention in recent years in spite of their relevant importance in processes such as wastewater, organic synthesis, and fermenters in biotechnological and pharmaceutical industries. In some cases, the liquid phase contains live microorganisms and/or solid particles that give the non-Newtonian characteristics. For these reasons, it is proposed to study a bubble column with a non-Newtonian liquid phase in which the literature is scarce and rigorous less in experimentation and data analysis procedures. The study will target the following main objectives:

- Measurement and correlation of the gas holdup in different flow regimes in the bubble column. The correlation of gas holdup will be a function of superficial velocities and liquid properties.

- Measurement and correlation of the liquid-phase mixing parameter, through a model that gives a good representation of experimental data, as a function of hydrodynamic parameters (superficial velocities and gas holdup), and liquid properties.

Once both parameters are measured, the effect of the non-Newtonian characteristic of the liquid phase used in the system should be established. A rheological model, e.g. the power-law model, will be used to this end.

The three steps that summarize the research strategy of this work are: setup the experimental equipment, conduct experiments, and then analyze the data. As a result of the analysis of the data, models or correlations for the parameters mentioned in the main objectives will be found.

2. RHEOLOGY. AQUEOUS SOLUTIONS OF CARBOXYMETHYLCELLULOSE

2.1. Rheology

The word rheology was coined in 1920 by professor Eugene Bingham at Lehigh University, who studied the flow behavior of concentrated suspensions such as paints. Rheology is the study of flow and deformation of materials, including materials in aeronautic, hydraulic and solid mechanics, but in reality, this science has been restricted to the study of constitutive relations between force and deformation of materials, especially in the case of liquids. A broad definition of rheology would allow studying the behavior of all matter, including the classical extremes of Hookean elastic solids and Newtonian viscous liquids; however, these extremes are viewed by many as being outside rheology (Barnes *et al.*, 1989).

The resistance to flow of a fluid is measured by the viscosity. The force per unit area required to produce the motion is denoted F/A and is known as shear stress and the velocity gradient due to the movement is the shear rate. In the case of a Hookean solid, the shear stress applied over the surface results in an instantaneous deformation that is maintained while stress is applied. The angle formed between the original place of the solid elements and the displaced element is called the strain.

The constitutive equations refer to mathematical expressions that describe the deformations of materials when a force is applied to them. In the case of liquids, the simplest constitutive equation is Newton's law of viscosity that can be expressed in vectorial form as (Macosko, 1994):

$$\boldsymbol{\tau} = -\mu\dot{\boldsymbol{\gamma}} \quad (2.1)$$

where $\boldsymbol{\tau}$ is the stress tensor, μ the Newtonian viscosity, and $\dot{\boldsymbol{\gamma}}$ the rate-of-strain tensor or rate-of-deformation tensor. Examples of these materials are liquids with small molecules such as water and oils.

Not all fluids have a simple behavior as described by Newton's law of viscosity. Figure 2.1 shows different behavior of the fluids sketched in flow and viscosity curves. Therefore, other constitutive relations are used to describe Bingham or plastic fluids, pseudoplastic (materials which become thinner or less viscous at higher shear rates), and dilatant fluids (materials which become thicker or more viscous at higher shear rates).

General viscous fluid

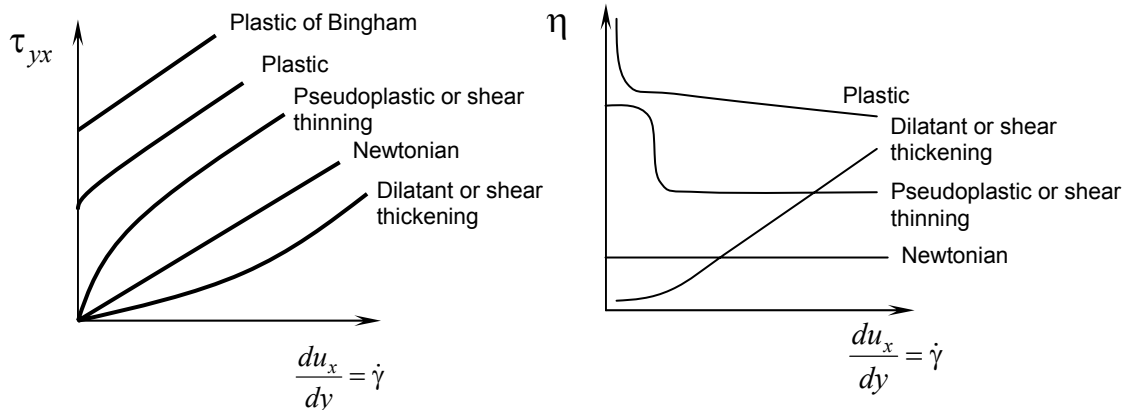
There are several models proposed in literature to describe viscous fluids. These expressions are functions of the shear rate. Some of them are presented in this section.

(a) Power-law model or Ostwald-De Waele relation:

It is the most widely used viscous constitutive relation (Bird *et al.*, 2002):

$$\tau = -\eta\dot{\gamma} = -k\dot{\gamma}^{n-1}\dot{\gamma} \quad (2.2)$$

Here, η is the effective or apparent viscosity, k is the consistency index, n is the flow index, and $\dot{\gamma}$ is the magnitude of the rate-of-strain tensor ($\dot{\gamma} = \sqrt{0.5(\dot{\gamma} : \dot{\gamma})}$).



(a) Flow curves

(b) Viscosity curves

Figure 2.1. Rheological behaviors of fluids

All non-Newtonian materials show regions of shear thinning, $n < 1$; however some materials, e.g., concentrated suspensions, show regions of shear thickening that can be modeled using $n > 1$.

One disadvantage of this model is that it fails to describe the low shear rate region; for $n < 1$, η goes to infinite rather than to a constant η_0 .

(b) Four-parameter Carreau equation:

Carreau (1968) proposed an expression that correlates most rheological data:

$$\frac{\eta - \eta_\infty}{\eta_0 - \eta_\infty} = \left[1 + (\lambda \dot{\gamma})^2 \right]^{(n-1)/2} \quad (2.3)$$

Here, η_0 is the apparent viscosity at zero shear rate, η_∞ is the apparent viscosity at infinite shear rate, and λ and n are constants.

(c) Cross model:

This model was proposed by Cross (1965):

$$\frac{\eta - \eta_\infty}{\eta_0 - \eta_\infty} = \frac{1}{1 + K \dot{\gamma}^n} \quad (2.4)$$

where K is a constant. The last equation is used when $\eta_0 \gg \eta_\infty$

In the intermediate region, the Cross model has power-law behavior:

$$\eta - \eta_\infty \approx (\eta_0 - \eta_\infty) m \dot{\gamma}^{n-1} \quad (2.5)$$

where $m = K^{n-1}$. When $\eta \gg \eta_\infty$:

$$\eta \cong \eta_0 m \dot{\gamma}^{n-1} \quad (2.6)$$

(d) Yasuda model:

This model proposed by Yasuda *et al.* (1981) is equivalent to the Cross model but has an additional adjustable parameter a :

$$\frac{\eta - \eta_{\infty}}{\eta_0 - \eta_{\infty}} = \frac{1}{(1 + \lambda^a \dot{\gamma})^{(1-n)/a}} \quad (2.7)$$

Plastic

A plastic material shows no deformation below a certain level of shear stress at which it begins to flow. Materials such as suspensions of solid particles in Newtonian liquids, paints, margarine, and ketchup show this behavior. These materials are called viscoplastics or Bingham plastics, since Bingham was the first to describe the behavior of these materials through observations of paints. The simplest way to describe these materials as a function of deformation is (Macosko, 1994):

$$\begin{aligned} \tau &= -G\gamma \quad \text{or} \quad \dot{\gamma} = 0, \quad \tau < \tau_y \\ \tau &= -\eta\dot{\gamma} - \tau_y, \quad \tau \geq \tau_y \end{aligned} \quad (2.8)$$

where G is the elastic modulus used in the Hooke's expression of incompressible elastic solid and τ_y is the stress tensor at which a Bingham fluid begins to flow.

Casson (1959) proposed an alternate model to describe viscoplastic fluids which describes the flow of blood and food products better than the Bingham model:

$$\begin{aligned} \dot{\gamma} &= 0, \quad \tau < \tau_y \\ \tau^{1/2} &= -(\eta \dot{\gamma})^{1/2} - \tau_y^{1/2}, \quad \tau \geq \tau_y \end{aligned} \quad (2.9)$$

On the other hand, Papanastasiou (1987) proposed an expression to avoid using a yield criterion, the discontinuity of equations for viscoplastic materials:

$$\tau = \dot{\gamma} \left\{ \eta \frac{\tau_y [1 - \exp(-b \dot{\gamma})]}{\dot{\gamma}} \right\} \quad (2.10)$$

where b is a constant.

Viscoelastic materials

It is not unusual to find in the literature variations of the last expression to describe viscoelastic materials. The word viscoelastic means the simultaneous existence of viscous and elastic properties in a material. Viscous and elastic properties coexist in all materials and the particular response of a material depends on the time-scale of the experiment in relation to the natural time of the material. This means that if the experiment is slow enough, the material will appear to be viscous rather than elastic and, conversely, it would look like elastic rather than viscous if the experiment is relatively fast. For intermediate time-scales, the material would appear to be viscoelastic.

For a linear viscoelastic material, the constitutive equation can be written as (Barnes *et al.*, 1989):

$$\tau = -G\gamma - \eta\dot{\gamma} \quad (2.11)$$

which is well known as Kelvin model.

To study linear viscoelastic materials, small-amplitude oscillatory shear is used, where the strain and the shear rate are expressed as (Barnes *et al.*, 1989):

$$\gamma(t) = \gamma_0 \exp(i\omega t) \quad (2.12)$$

$$\dot{\gamma}(t) = i\omega\gamma_0 \exp(i\omega t) \quad (2.13)$$

where $i = \sqrt{-1}$, ω is the frequency and γ_0 the strain amplitude, which should be small enough for the linearity constraint to be satisfied. Additionally, a complex shear modulus G^* is defined in oscillatory shear (Barnes *et al.*, 1989):

$$\tau = G^*(\omega)\gamma(t) \quad (2.14)$$

where the complex shear modulus can be written as (Barnes *et al.*, 1989):

$$G^* = G' + iG'' \quad (2.15)$$

where G' is the storage or elastic modulus and G'' the loss modulus. Using the Maxwell model (this model considers a differential equation for linear viscoelasticity of the form: $\tau_{yx} = \tau_{rel} \dot{\tau}_{yx} = \eta \dot{\gamma}_{yx}$, where τ_{rel} is the relaxation time), each term is defined as:

$$G' = \frac{\eta \tau_{rel} \omega^2}{1 + \omega^2 \tau_{rel}^2} \quad (2.16)$$

$$G'' = \frac{\eta \omega}{1 + \omega^2 \tau_{rel}^2} \quad (2.17)$$

where τ_{rel} is the relaxation time or the time taken for the shear stress of a fluid that obeys the Maxwell model to reduce to 1/e of its original equilibrium value on the cessation of steady shear flow (Barnes *et al.*, 1989). Other representation of the oscillatory motion is through the complex viscosity η^* :

$$\eta^* = \eta' + i\eta'' \quad (2.18)$$

where η' is the dynamic viscosity and η'' is a parameter related to dynamic rigidity. The mathematical definitions are (Barnes *et al.*, 1998):

$$G' = \eta'' \omega \quad (2.19)$$

$$G'' = \eta' \omega \quad (2.20)$$

All dynamic properties increase in value when molecular weight increases at a given frequency. Low-molecular-weight polymers, which have few entanglements, present a little or no-plateau region in a plot $\log G'$ or $\log G''$ versus $\log \omega$. However, high-molecular-weight polymers have plateau regions which cover several decades (log cycles) in frequency and, in these regions, both moduli are independent of molecular weight because the effective molecular weight between entanglements becomes constant (Nielsen, 1977). A log-log plot of these moduli versus the frequency permits to establish the predominant trend of the material as a function of the shear frequency (the frequency at which both moduli become equal).

2.2. Rheometry

Many instruments exist to measure viscosity and other rheological properties of liquid and molten polymers. Most of these instruments are capable of measuring rheological properties as a function of temperature and shear rate. They can be steady-state instruments such as: simple shear viscometer, coaxial-cylinder viscometers, capillary rheometers, capillary and plate viscometers, and parallel-plate viscometers; or non-steady-state instruments used to measure complex viscosity such as: dynamic rheometers, rheogoniometers (rheometer designed for the measurement of normal as well as shear components of the stress tensor) and orthogonal rheometers (the axes of the two parallel disks are not quite colinear, producing an eccentric oscillatory motion). Additionally, another class of instruments is capable to measure tensile viscosity and normal stresses. Some instruments measure both viscosity and normal stresses.

2.3. A pseudoplastic solution: Carboxymethyl cellulose (CMC) in water

Cellulose is one of many polymers found in nature. Wood, paper, and cotton all contain cellulose, and in smaller quantities it is also found in certain bacteria (Acetobacter) and in sea animals (Tunicin). As shown in Figure 2.2, cellulose is made of repeated units of the monomer glucose: reason why it is considered a polysaccharide (LSBU, 2003).

Cellulose is a long chain of β -D-glucose units linked together by 1,4-glycosidic bonds. The primary hydroxyl on the sixth carbon atom is sterically the most readily available.

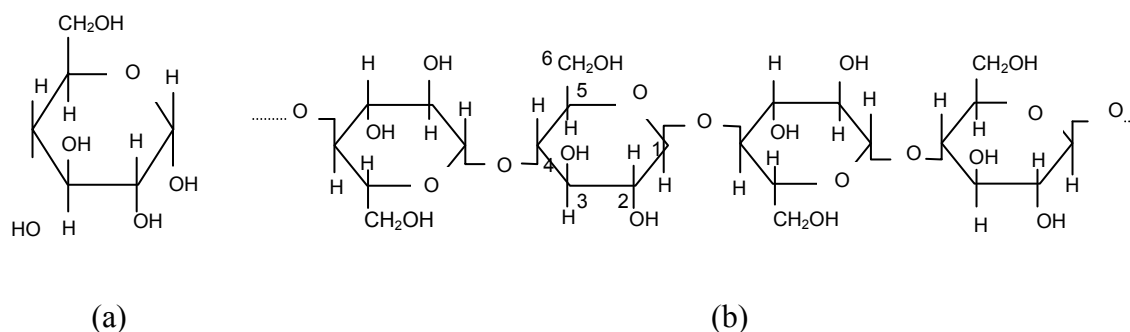
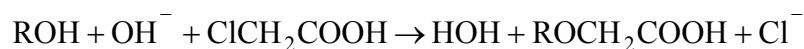


Figure 2.2. (a) Molecule of glucose. (b) Structural unit of cellulose

The polymer to be used in this research is carboxymethyl cellulose that is formed by an etherification reaction (cellulose hydroxyl in its alcoholate form reacts with chloroacetic acid):



The structure of the resulting polymer is shown in Figure 2.3.

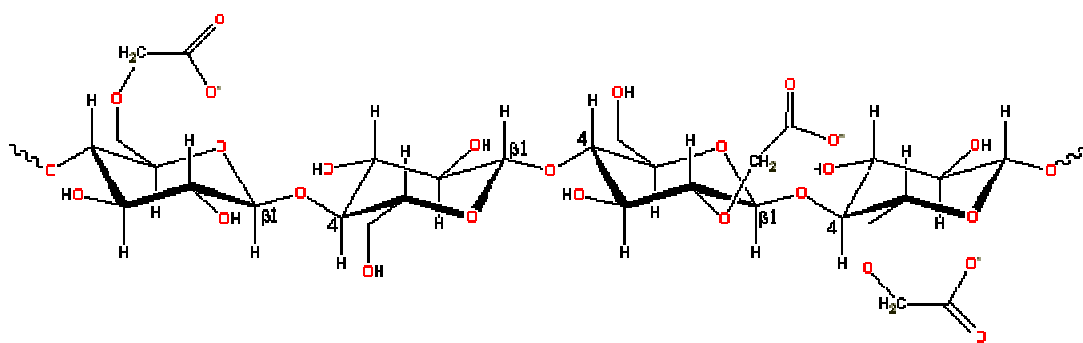


Figure 2.3. Carboxymethyl cellulose based on β -(1-4)-D-glucopyranose polymer of cellulose (LSBU, 2003)

The hydrogen of the carboxyl group sometimes is substituted by a sodium atom and, in this case, the carboxymethyl cellulose is called either sodium cellulose glycolate or sodium carboxymethyl cellulose. It has been used as:

- Adhesive, sizing, and thickening agent in textile and paper industries.

- Protective colloid: keeps suspended stable particles in suspension.
- For retarding staling and reducing fat uptake into fried food.

Carboxymethylcellulose is a polymer that dissolves in water and the resulting solutions have a pseudoplastic rheological behavior.

2.4. Rheology parameters in bubble columns

In bubble columns, the superficial gas velocity is the principal parameter that permits to relate hydrodynamic parameters to rheology parameters through the shear rate. Some researchers have been studying an empirical relation between last two parameters.

Nishikawa *et al.* (1977) worked with a 0.15 and 0.05 m of internal diameter provided with a double jacket and a cooling coil. They proposed relations of shear rate with superficial gas velocity for CMC solutions in 0.15 m column diameter:

$$\dot{\gamma}_{av} = 50.0 u_g \quad (u_g \geq 0.04 \text{ m/s}) \quad (2.21)$$

$$\dot{\gamma}_{av,c} = 100 u_g^{0.5} \quad (u_g \leq 0.04 \text{ m/s}) \quad (2.22)$$

$$\dot{\gamma}_{av,j} = 0.195 u_g^{5.0} \quad (u_g \leq 0.04 \text{ m/s}) \quad (2.23)$$

where u_g is the superficial gas velocity expressed in cm/s and the subscripts av , av,c and av,j refer to average, average in the cooling coil side, and average jacket side respectively. As shown, the researchers measured the shear stress punctually and obtained an average depending on the superficial gas velocity. It is important to mention that Eq. (2.21) corresponds to heterogeneous flow regime.

Schumpe and Decker (1982) used aqueous solutions of CMC in two bubble columns with diameters of 0.14 and 0.102 m and heights of 2.70 and 2.36 m, respectively. They used the expression proposed by Nishikawa *et al.* (1977) emphasizing that the expression was obtained in a 0.15-m diameter bubble column. They mentioned that for low gas velocities, the shear rates in the wall region are lower

and those in the center of the column are higher than predicted by Nishikawa *et al.* (1977) equation. However, they claim that the correlation holds for the whole cross-sectional area and it can be used for CMC concentrations at $u_g \geq 0.04$ m/s.

Godbole *et al.* (1982) worked with CMC solutions at concentrations between 0.01 and 0.5 wt % in 0.305-m diameter and 2.44-m height bubble column. They used the expression of apparent viscosity originally proposed by Nishikawa *et al.* (1977), but with superficial gas velocity expressed in m/s:

$$\eta = k(5000 u_g)^{n-1} \quad (2.24)$$

Godbole *et al.* (1984), using a larger bubble column (3.4-m high), Haque *et al.* (1986), Popovic and Robinson (1987), Popovic and Robinson (1988), Bukur and Patel (1989), and Popovic and Robinson (1993) used the equation proposed by Nishikawa *et al.* (1977) in their work to relate shear rate to superficial gas velocity.

Eickenbusch *et al.* (1995) used the expression proposed by Schumpe and Deckwer (1987) to relate the shear rate to superficial gas velocity:

$$\dot{\gamma} = 2800u_g \quad (2.25)$$

Al-Masry and Dukkan (1998) proposed the following expressions obtained for xanthan gum and CMC solutions:

$$\dot{\gamma} = 14795u_g^2 + 128.76u_g + 0.4996 \quad (\text{for xanthan gum}) \quad (2.26)$$

$$\dot{\gamma} = 27625u_g^2 + 358.32u_g + 22.54 \quad (\text{for CMC}) \quad (2.27)$$

Al-Masry (2001) worked with an airlift of 0.15 m diameter and 2.5 m height. They compared the results obtained of shear rate as a function of superficial gas velocity by different researchers as shown in Figure 2.4.

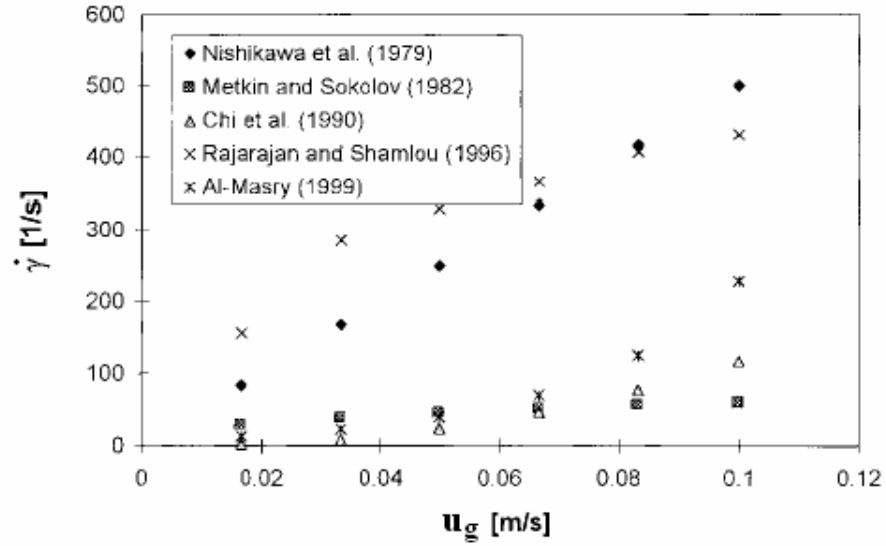


Figure 2.4. Comparison of average shear rate for CMC (taken from Al-Masry, 2001)

The correlations shown in Figure 2.4 are the following:

- Shi *et al.* (1990):

$$\dot{\gamma} = 14800u_g^2 - 351u_g + 3.26 \quad (2.28)$$

- Rajarajan and Shamlou (1996):

$$\dot{\gamma} = \frac{8u_L}{d_c(1-\varepsilon_g)} \left(\frac{1+3n}{4n} \right) \quad (2.29)$$

where ε_g is the holdup of the gas phase and d_c the diameter of the bubble column.

- Al-Masry (1999):

$$\dot{\gamma} = 3.36(1-u_g)^{-32.56} \left(1 + \frac{A_D}{A_R} \right)^{0.89} H_D^{0.44} \quad (2.30)$$

where A_D is the downcomer cross sectional area, A_R the riser cross sectional area, and H_D is the length of the downcomer section of the airlift.

3. HYDRODYNAMICS OF BUBBLE COLUMNS

3.1. Background

Bubble columns have been widely used as chemical reactors, and can be used to carry out various types of reactions. Among these, the following can be cited:

- Two-phase gas-liquid reactions: Most gas-liquid reactions use a homogeneous dissolved catalyst. Examples of these reactions are: partial oxidation of ethylene to acetaldehyde, isobutene separation from C₄ cracking, production of dichloroethane.
- Three-phase, gas-liquid-solid reactions: Within these, there is a variety of operation modes (capacities, flow directions, moving or fixed). Some processes are: production of hydrogen peroxide, Fischer Tropsch synthesis, and biotechnological processes.

Another possible use of bubble columns is in separation processes such as treatment of various types of water (drinking, underground or wastewaters). Velázquez and Estévez (1992) demonstrated the potential that bubble columns have in the removal of trihalomethanes from drinking water and, by extension, of any volatile organic chemical (VOC).

Also, bubble columns can be operated in different flow directions. The gas normally enters at the bottom, e.g., through a gas distributor. The liquid may be contained in the column (not flowing); this is often called semibatch or simply batch operation. The liquid may alternatively flow continuously at the bottom of the column, giving rise to a cocurrent or parallel flow operation. Less frequently, the liquid may flow downward and the operation is then called countercurrent. Even less frequently, the gas and the liquid are fed at the top of the column in a cocurrent downward flow operation. Liquid phase properties have been found to have an effect on the flow regime as it will be mentioned in next section. Additionally, the superficial velocities of the

phases have also an effect on flow regimes. In bubble columns, aspect ratio (L/d) between 3 and 6 are recommended, although greater values have been used (Deckwer, 1992).

In bubble-column design several parameters have been found to be relevant. Among these, the following may be cited: holdups, mass-transfer parameters, pressure drop, superficial velocities, and parameters related to the mixing of the phases. This dissertation focuses on gas holdup, pressure drop, and mixing of the liquid phase. There are numerous works of mixing and gas holdup in bubble columns with a Newtonian liquid phase. Unfortunately that is not the case for columns with a non-Newtonian liquid phase where the few studies found in literature do not show rigorously the behavior of gas holdup and mixing of the liquid phase for each flow regime and show no attempt to relate these parameters to the parameters in a rheological model, something done in this work.

3.2. Flow regimes

Flow regimes in one-phase flow are laminar and turbulent. When more phases are present (two- and three-phase flow), the situation is more complex and flow regimes refer to the various distinct patterns in which the various phases distribute in space and flow. The phase distribution determines the gas and the liquid holdup, which are the volumetric fractions of the gas and liquid phases in the vessel. The relative motion of the two phases causes the occurrence of interfacial shear stresses that under some flow conditions contributes significantly to the pressure drop (Shoham, 1998).

The ways that two phases distribute in the space within the conduit are referred to as flow patterns (Fernandes, *et al.*, 1983). Any attempt to get a unique and general solution for two-phase problems for all configurations is impossible. However, all configurations are grouped in flow patterns (Shoham, 1998). The existing flow pattern in a given two-phase flow system depends on: gas and liquid flow rates, geometrical

variables (diameter and small deviations of vertical alignment of the cylindrical sections), and the physical properties of the two phases (gas and liquid densities, viscosities and the surface tensions).

Ramachandran and Chaudhari (1983) identified the following flow regimes for Newtonian liquid phase in bubble columns, which are depicted in Figure 3.1:

Homogeneous bubbling flow: Observed at low superficial gas velocities (less than 0.05 m/s) and characterized by bubbles of similar size, uniformly distributed throughout the column.

Heterogeneous bubbling flow: It occurs at superficial gas velocities higher than 0.07 m/s. Bubbles coalesce giving rise to a wide distribution of bubble sizes.

Slug flow: Observed at high superficial gas velocities and small column diameters (less than 0.15 m). The diameter of the bubbles formed through bubble coalescence is similar to the column diameter. Big bubbles, often called Taylor bubbles, are stabilized by the column walls and small bubbles flow together along the column.

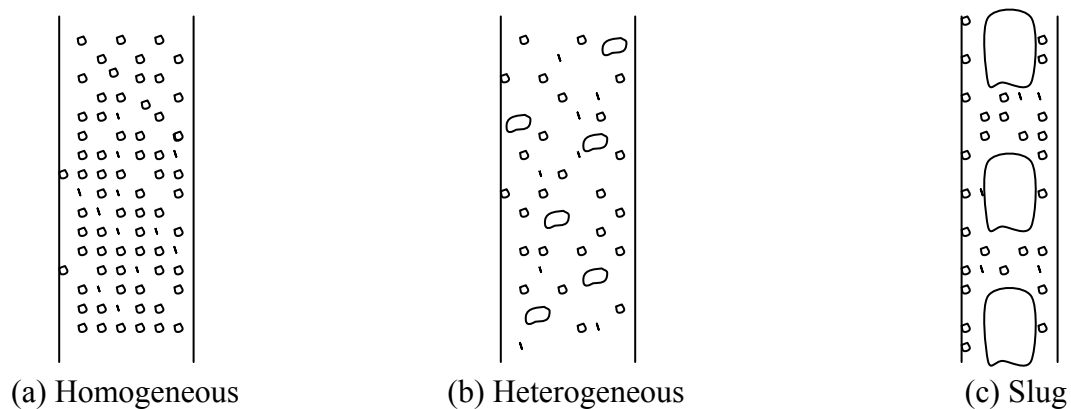


Figure 3.1. Flow regimes in bubble columns

Bubble columns with an aspect ratio greater than 4 may have similarities to flow in vertical pipes (see Appendix A).

Zuber and Findlay (1965) provided a general method to predict the gas holdup, which is useful in the analysis of experimental data and to establish the prevailing flow regime at given experimental conditions. They plotted the ratio between superficial gas velocity and gas holdup (u_G/ε_G) versus the sum of the superficial gas and liquid velocities ($\langle j \rangle$) obtaining straight lines with different slopes and intercept depending on the flow regime. They proposed the following expressions to help determining the prevailing flow regimes:

Homogeneous flow:

$$\frac{u_G}{\varepsilon_G} = \langle j \rangle \quad (3.1)$$

A plot of the previous equation gives a straight line through the origin with a slope of 1.

Turbulent flow:

$$\frac{u_G}{\varepsilon_G} = C_0 \langle j \rangle + 1.53 \left(\frac{\sigma g (\rho_L - \rho_G) \rho}{\rho_L^2} \right)^{1/4} \quad (3.2)$$

Slug flow:

$$\frac{u_G}{\varepsilon_G} = C_0 \langle j \rangle + 0.35 \left(\frac{\sigma g (\rho_L - \rho_G)}{\rho_L^2} \right)^{1/2} \quad (3.3)$$

where C_0 is a distribution parameter.

A plot of u_G/ε_G as a function of $\langle j \rangle$ of Equation (3.2) or (3.3) gives a straight line with an intercept different from 0 and a slope different from 1.

Ityokumbul *et al.* (1994) used a 0.06-m diameter and 1.06-m height bubble column with a porous stainless steel plate (average pore size of 134 μm) as gas distributor. The fluids were tap water and air and the setup was operated in countercurrent. They measured pressure drop to estimate the gas holdup and obtained the flow regime map shown in Figure 3.2 by plotting the bubble rise velocity vs. the superficial gas velocity.

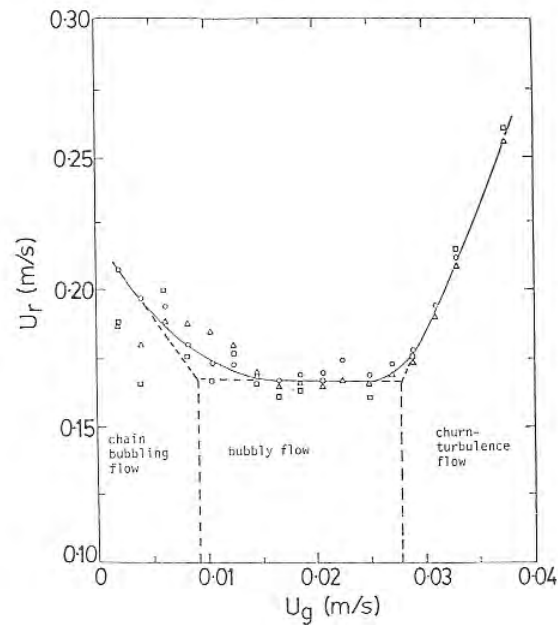


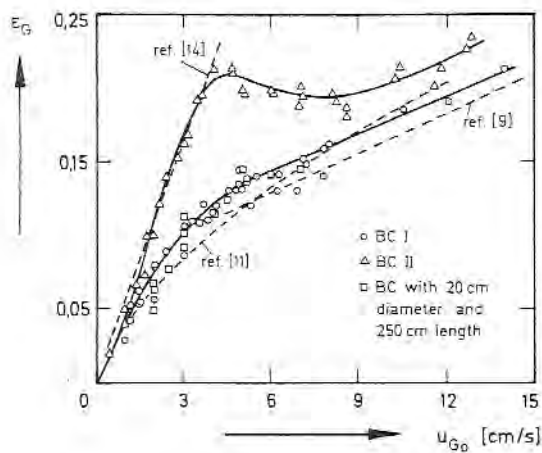
Figure 3.2. Flow-regime map (Ityokumbul *et al.*, 1994). The symbol u_r in the figure refers to bubble rise velocity (u_b)

3.3. Gas holdup and pressure drop

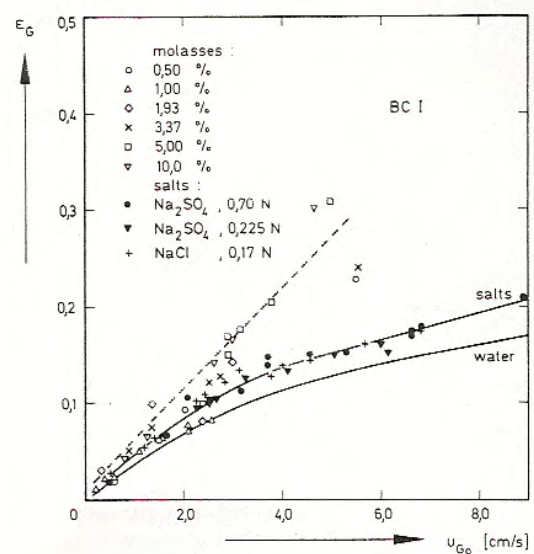
The holdup of any given phase is defined as the ratio between the volume occupied by that phase and the total volume occupied by all phases in the system. In the case of two-phase, gas-liquid systems, the gas holdup is determined experimentally by measuring the volume of the aerated liquid in operation, V , and the volume of non-aerated liquid, V_0 , after phase flows have been halted and phases have disengaged. The gas holdup is then expressed as:

$$\varepsilon_G = \frac{V - V_0}{V} \quad (3.4)$$

Deckwer *et al.* (1974) worked with two different bubble columns: BC I (0.20 m in diameter and 0.72 m in length) and BCII (0.15 m diameter and 0.44 m length). The liquid was tap water, aqueous solutions of sodium sulphate or sodium chloride, or aqueous solutions of molasses at various concentrations. After a time of bubbling of 1 h they found good reproducibility when tap water and electrolytes solutions were used. On the contrary, scattering of gas holdup was found in solutions of molasses. Both trends were shown in Figure 3.3.



(a) Tap water



(b) Bubble column of 0.2-m diameter

Figure 3.3. Gas holdup as a function of gas velocity (Deckwer *et al.*, 1974)

Eissa and Schügerl (1975) studied the effect of the liquid properties on gas holdup and backmixing. In cases of foam formation, they considered the height of a continuous surface as seen through the column wall to determine the gas holdup. Additionally, the gas holdup was obtained from pressure drop measurements. In a batch operation, they obtained that gas holdup increases with superficial gas velocity. On the other hand, at

constant gas velocity the gas holdup increased at increasing viscosities reaching a maximum at about 3 cP followed by a rather sharp decrease up to viscosities of about 11 cP, and a slow decrease afterwards. They explained this behavior in terms of the hindered gas bubble motion in viscous fluids in which, at relatively low viscosities, drag forces are not large enough to cause bubble coalescence. They asseverate that these moderate forces could contribute to more uniform distribution of bubbles giving rise to higher gas holdups; but higher drag forces promote coalescence causing lower gas holdups. Moreover, they found an increase of gas holdup with surface tension.

Joshi and Sharma (1979) proposed a circulation cell model in which the fluid goes up at the center and goes down at the wall of the column in a toroidal form as shown in Figure 3.4. The model was applied to a column of 1.0-m diameter and an aspect ratio of 1.

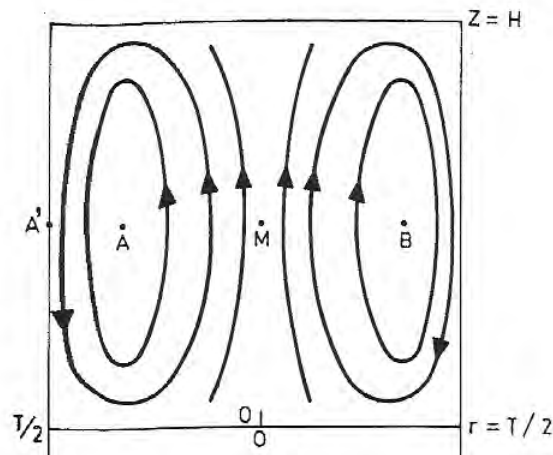


Figure 3.4. Cell model (Joshi and Sharma, 1979)

Joshi (1980) analyzed different concepts in multiphase contactors. He proposed two expressions to evaluate gas holdups in Newtonian fluids when bubbles rise at their terminal velocity, u_t :

Batch liquid and continuous gas:

$$\varepsilon_G = \frac{u_G}{u_t} \quad (3.5)$$

Continuous co-current gas and liquid phases:

$$\varepsilon_G = \frac{u_G}{u_t + \left[u_L / (1 - \varepsilon_G) \right]} \quad (3.6)$$

Hikita *et al.* (1980) constructed a 0.10-m diameter and 1.50-m high bubble column that was operated in batch mode with air, hydrogen, carbon dioxide, methane and nitrogen as gas phase and non-electrolyte (water, different concentrations of sucrose, aniline, n-butanol, and methanol) and electrolyte (aqueous NaCl, Na₂SO₄, CaCl₂, AlCl₃, KCl, K₃PO₄, and KNO₃) solutions. They proposed for non-electrolyte solutions the following equation:

$$\varepsilon_G = 0.672 \left(\frac{u_G \mu_L}{\sigma} \right)^{0.573} \left(\frac{\mu_L^4 g}{\rho_L \sigma^3} \right)^{-0.131} \left(\frac{\rho_G}{\rho_L} \right)^{0.062} \left(\frac{\mu_G}{\mu_L} \right)^{0.107} \quad (3.7)$$

where the applicability ranges of the equation are:

$$1.1 \times 10^{-3} < (u_G \mu_L / \sigma) < 8.9 \times 10^{-2}$$

$$2.5 \times 10^{-11} < (\mu_L^4 g / \rho_L \sigma^3) < 1.9 \times 10^{-3}$$

$$8.4 \times 10^{-5} < (\rho_G / \rho_L) < 1.9 \times 10^{-3}$$

$$1.0 \times 10^{-2} < (\mu_G / \mu_L) < 1.8 \times 10^{-2}$$

Godbole *et al.* (1982) studied the gas holdup in highly viscous Newtonian and non-Newtonian media using glycerine and carboxymethylcellulose (CMC) solutions. They worked in a 0.306-m diameter and 2.44-m high bubble column. The conical section was packed with Berl saddles for a more uniform gas-phase distribution. They measured the dynamic gas holdup as a function of time. For n bubble sizes, the dynamic gas holdup was presented by authors through the following expression:

$$\varepsilon_G(t) = \sum_{i=1}^n \varepsilon_{G,i} \left(1 - \frac{t}{t_{\max,i}} \right) \quad (3.8)$$

where $t_{\max,i}$ is the maximum time required for bubble of class i to disengage and $\varepsilon_{G,i}$ is the gas holdup due to the i -th bubble size. They presented the previous expression for two sizes of bubbles:

$$\varepsilon_G(t) = \varepsilon_{G,l} \left(1 - \frac{t}{t_{\max,l}} \right) + \varepsilon_{G,s} \left(1 - \frac{t}{t_{\max,s}} \right) \quad (3.9)$$

where subscripts l and s refers to large and small bubbles respectively. When the large bubbles are disengaged:

$$\varepsilon_G(t) = \varepsilon_{G,s} \left(1 - \frac{t}{t_{\max,s}} \right) \quad (3.10)$$

They worked with CMC solutions at concentrations by weight between 0.01 and 0.5% which had flow indexes between 1 and 0.5 respectively.

Godbole *et al.* (1982) found that the gas holdup increases as gas velocity does, but it is lower in small diameter columns ($d_c \leq 0.15$ m) when they compared it with the works of Eissa and Schügerl (1975), Bach and Pilhofer (1978), and Buchholz *et al.* (1978). Researchers observed a weak maximum in the gas holdup with respect to the viscous Newtonian liquid viscosity (at 0.002 Pa·s). This observation agrees with others' found in literature (Eissa and Schügerl, 1975; Buchholz *et al.*, 1978; Bach and Pilhofer, 1978) and it is explained through the hindered gas bubble motion in viscous fluids, in which the drag forces are not large enough to cause the coalescence in bubbles at low viscosities. They correlated their experimental data through the following expression:

$$\varepsilon_G = 0.319 u_G^{0.476} \mu_L^{-0.058} \quad (3.11)$$

The last equation is valid only in the range of 0.004 to 0.25 Pa·s of viscosity. For non-Newtonian liquids, Godbole *et al.* (1982) agree with results obtained with the use

of correlations of Akita and Yoshida (1973), Mersmann (1978) and Hikita *et al.* (1980) for viscosities less than 0.08 Pa·s; but in highly viscous solutions these correlations failed. Godbole *et al.* (1982) found a maximum with respect to liquid viscosity as shown in Figure 3.5. Additionally, they found two bubble sizes at CMC concentrations below 0.15% wt. They did not observe the bubbly flow regime (homogeneous regime) within their range of superficial gas velocity ($u_G > 0.02$ m/s). Moreover, they plotted u_G/ε_G as a function of u_G and obtained a straight line with an intercept that increased with the CMC concentration, but a unique intercept was observed for all CMC concentrations above 0.25%. They proposed an empirical correlation in the range of apparent viscosities between 0.018 and 0.230 Pa·s (for pseudoplastic solutions) and in columns with diameters larger than 0.3 m:

$$\varepsilon_G = 0.225 u_G^{0.532} \eta^{-0.146} \quad (3.12)$$

Also, Godbole *et al.* (1982) proposed a correlation for highly viscous CMC solutions ($\mu_L \geq 0.02$ Pa·s):

$$\varepsilon_G = 0.42 u_G^{0.624} \quad (3.13)$$

and, to take into account the effect of bubble column diameter on gas holdup, proposed:

$$\varepsilon_G = 0.239 u_G^{0.634} d_c^{-0.50} \quad (3.14)$$

Schumpe and Deckwer (1982) obtained several gas holdup correlations depending on bubble column diameter and the gas distributor. These expressions are:

For homogeneous flow, both studied diameters and CMC ≥ 0.8 wt%:

$$\varepsilon_G = 0.0908 \bar{u}_G^{0.85} \quad (3.15)$$

where \bar{u}_G is the mean superficial gas velocity (u_G at $H/2$) (cm/s)

For homogeneous flow, 2-mm perforated plate, 0.14-m diameter bubble column and CMC ≥ 0.8 wt%:

$$\varepsilon_G = 0.0258 \bar{u}_G^{-0.876} \quad (3.16)$$

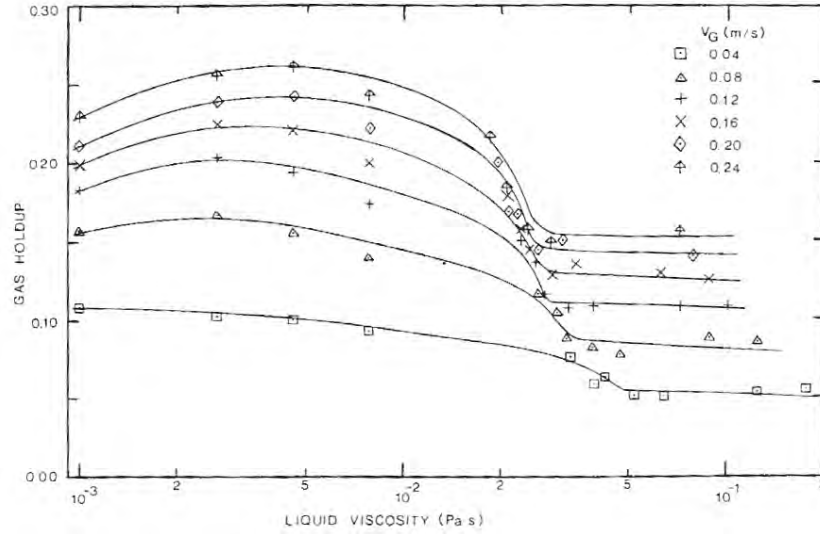


Figure 3.5. Gas holdup as a function of viscosity for CMC solutions (Godbole *et al.*, 1982)

For slug flow, any sparger type, 0.14-m diameter bubble column and CMC ≥ 0.8 wt%:

$$\varepsilon_G = 0.0322 \bar{u}_G^{-0.674} \quad (3.17)$$

For slug flow, any sparger type, 0.102-m diameter bubble column and CMC ≥ 0.8 wt%:

$$\varepsilon_G = 0.0404 \bar{u}_G^{-0.627} \quad (3.18)$$

Walter and Blanch (1983) measured the velocity profile, the gas holdup and the bubble size distribution. They divided the column into two regions to express the holdup (Figure 3.6):

$$\bar{\varepsilon}_G = \frac{H_I}{H} \bar{\varepsilon}_I + \frac{H - H_I}{H} \bar{\varepsilon}_{II} \quad (3.19)$$

where $\bar{\varepsilon}_I$ is the average gas-holdup of section I, $\bar{\varepsilon}_{II}$ the average gas-holdup at section II, H_I the length of region I, and H the total height of liquid in the column.

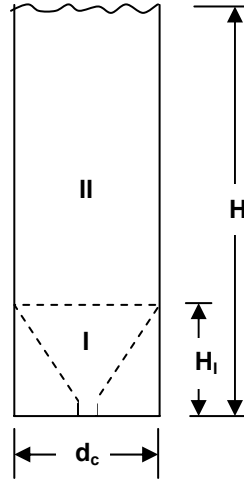


Figure 3.6. Holdup model proposed by Walter and Blanch (1983)

In the case of sparger holes distributed uniformly, the length of region I is presented as:

$$H_I = 1.125 \frac{d_c}{\sqrt{n_u}} \quad (3.20)$$

where n_u is the number of orifices in the gas distributor. In the upper region (section II) the bubble-size distribution is uniform and the bubbles rise with terminal velocity with respect to the surrounding fluid (Walter and Blanch, 1983). The gas holdup for this region is presented by these authors as follows:

$$\bar{\varepsilon}_{II} = \frac{u_G}{u_{r,II} + \Psi \bar{u}_L} \quad (3.21)$$

where $u_{r,H}$ is the rise velocity of the Sauter mean bubble size (diameter of a bubble obtained from the ratio between volume and superficial area representative of a spray sample) in the upper section of the column in a stagnant liquid, \bar{u}_L the average liquid velocity and ψ is a constant expressed as:

$$\psi = \frac{2(N'+1)}{N'} \left[\frac{1}{N'+2} + \frac{1}{2(N'+4)} + \bar{\alpha} \left(\frac{-\gamma^{N'}}{N'+4} + \frac{1}{2N'+4} \right) \right] \quad (3.22)$$

where N' is the shape factor of the gas holdup profile of the equation:

$$\varepsilon_G = \bar{\varepsilon}_G \frac{N'+2}{N'} \left[1 - \left(\frac{r}{R} \right)^{N'} \right] \quad (3.23)$$

With these expressions, the authors obtained good results as it is seen in Figure 3.7.

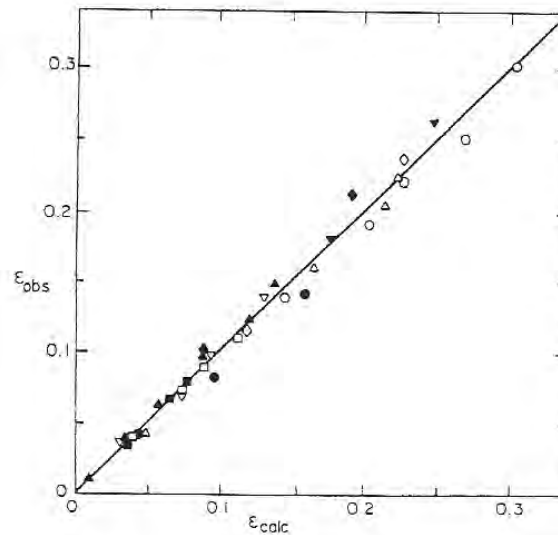


Figure 3.7. Parity plot of gas holdup observed and calculated through Eq.(3.23) (Walter and Blanch, 1983)

Godbole *et al.* (1984) used CMC solutions to characterize experimentally the gas holdup and mass transfer in a 0.306-m diameter bubble column, in the heterogeneous bubbling flow regime. They found a transition from churn turbulent to slug flow at 0.1

Pa's. The correlation obtained from experimental data for churn-turbulent flow regime was:

$$\varepsilon_G = 0.207 u_G^{0.6} \eta^{-0.19} \quad (3.24)$$

Haque *et al.* (1986) used CMC solutions (0 – 2 wt %), and various spargers. They found two flow regimes: churn turbulent and slug flow, in 0.10, 0.20, 0.38 and 1.0 m column diameters. They proposed the following equation for the gas holdup in the churn turbulent regime:

$$\varepsilon_G = 0.171 u_G^{0.6} \eta^{-0.22} d_c^{-0.15} \quad (3.25)$$

Rice and Littlefield (1987) worked in a 0.14-m diameter and 2.44-m height bubble column and water and air as fluids. They proposed the following expression for batch operation:

$$u_G = \left(\frac{2g}{15\nu_L^{0.5}} \right)^{2/3} d_B \varepsilon_G (1 - \varepsilon_G)^2 \quad (3.26)$$

where d_B is the bubble diameter. The variables are in c.g.s. units system.

Bukur and Patel (1989) worked with CMC solutions and *n*-butanol in batch mode. They proposed a modification of the Akita and Yoshida (1974) correlation to calculate the gas holdup. The equation is:

$$\frac{\varepsilon_G}{(1 - \varepsilon_G)} = 0.032 \left(\frac{gd_c^2 \rho_L}{\sigma} \right)^{-0.056} \left(\frac{gd_c^3}{\nu_L^2} \right)^{0.31} \left(\frac{u_G}{\sqrt{gd_c}} \right)^{1.2} \left(\frac{\rho_G u_G^2 d_c^4}{n_u^2 d_0^3 \sigma} \right)^{0.25} \quad (3.27)$$

where d_0 is the orifice diameter. This equation predicts the gas holdup within a 20% error.

Vatai and Tekic (1989) worked with bubble columns of 0.05, 0.10, 0.15 and 0.20 m in diameter and 2.50-m high with water and CMC solutions in batch mode. They found

no effect of the column diameter on gas holdup for water, but when they used CMC solutions, the gas holdup increased as diameter decreased because the walls stabilized large bubbles permitting the transition to a slug flow regime so that the holdup increased. Otherwise, for large diameters, the flow regime is churn turbulent and the transition to slug regime occurs at high viscosity liquids at high superficial gas velocity. Vatai and Tekic (1989) got correlations for churn turbulent and slug flow regimes:

$$\varepsilon_G = 0.19n^{-0.6} \left[\frac{u_G}{(gd_c)^{0.5}} \right]^{0.84-0.14n} \left(\frac{gd_c^3 \rho_L^2}{\eta^2} \right)^{0.07} \quad (\text{churn-turbulent regime}) \quad (3.28)$$

$$\eta = k\dot{\gamma}^{n-1} = k \left(\frac{u_G}{d_c/2} \right)^{n-1}$$

$$\varepsilon_G = 0.13 u_G^{0.534} d_c^{-0.5} \quad (\text{slug flow regime}) \quad (3.29)$$

The authors commented that they obtained a mean deviation of 16.4% from experimental data.

Kawase *et al.* (1992) used the concept of energy dissipation rate. This rate is high in bubble columns because of the liquid circulation generated by gas flow. Manipulating the proposed expressions to represent the energy dissipation rate they obtained the following equation to evaluate gas holdup:

$$\frac{\varepsilon_G}{1-\varepsilon_G} = 2^{-(3n+5)/(n+1)} n^{-(n+2)/2(n+1)} \left(\frac{k}{\rho_L} \right)^{-1/2(n+1)} g^{-n/2(n+1)} u_G^{(n+2)/2(n+1)} \quad (3.30)$$

In the case of Newtonian fluids ($n = 1$), Eq. (3.30) reduces to:

$$\frac{\varepsilon_G}{1-\varepsilon_G} = 0.0625 \left(\frac{u_G^3 \rho_L}{\mu_L g} \right)^{1/4} \quad (3.31)$$

Kawase *et al.* (1992) obtained good results with Eq. (3.31) in viscous Newtonian media in the range of $0.002 \leq \mu_L \text{ (Pa} \cdot \text{s)} \leq 0.02$, while in case of non-Newtonian fluids,

Eq. (3.30) fits experimental data in fluids represented rheologically by the power-law model in the following ranges of its parameters: $0.87 \geq n \geq 0.54$ and $0.0035 \leq k(\text{Pa} \cdot \text{s}^n) \leq 0.53$. In both cases, a parity plot showed that the points are within the $\pm 30\%$ error bars.

Ityokumbul *et al.* (1994) observed that gas holdup was independent of liquid velocity for gas velocities in the range of 0 to 0.008 m/s. For this range, the gas holdup was between 0 and 0.025 and they proposed the following expression for this parameter:

$$\varepsilon_G = 5.9 u_G \quad (3.32)$$

The experimental data showed in Figure 3.8 exhibit almost no dependence of gas holdup from liquid velocity.

Eickenbusch *et al.* (1995) worked in batch mode with three bubble columns of different diameters: 0.19, 0.29 and 0.6 m and 2.80, 4.50 and 5.7-m high, respectively. The liquid phase was aqueous solutions of xantham gum and hydropropyl guar (HPG), which exhibits pseudoplastic behavior. They proposed the following correlation for gas holdup obtained from experimental data mainly in the heterogeneous flow regime:

$$\varepsilon_G = 0.20 \text{Bo}'^{-0.13} \text{Ga}^{0.11} \text{Fr}_G^{0.54} \quad (3.33)$$

where Bo' is the Bond number and Ga the Galilei number. The effective viscosity used in the Galilei number was obtained from the power-law model in which the shear rate is related to superficial gas velocity through the linear expression proposed by Schumpe and Deckwer (1987).

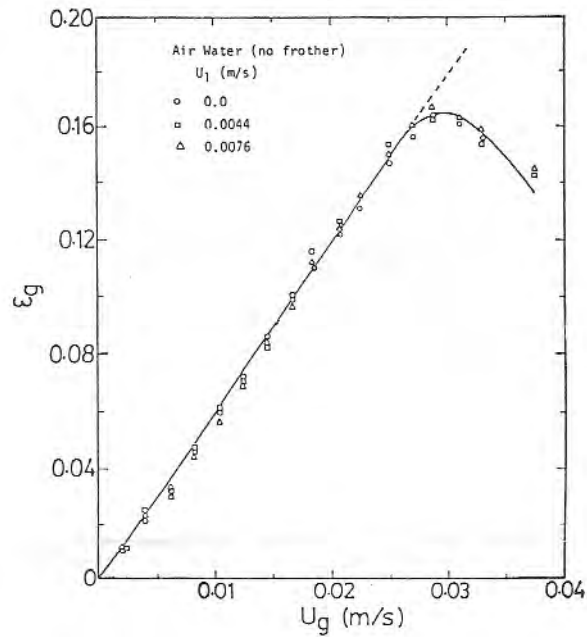


Figure 3.8. Gas holdup as a function of superficial gas velocity for different superficial liquid velocity (Ityokumbul *et al.*, 1993)

Zahradnik *et al.* (1997) used three bubble columns with diameters: 0.14, 0.15, and 0.29 m and with aspect ratios between 1 and 29. They evaluated the gas holdup through the expansion method and pressure drop. They obtained the following expression to evaluate gas holdup from pressure drop measurements:

$$\varepsilon_G = \frac{\Delta H - \Delta h}{\Delta H} \quad (3.34)$$

where ΔH is the distance between the two pressure taps and Δh the difference between readings of the two respective manometers. Figure 3.9 shows, schematically, their results and the flow regimes they found. They proposed expressions for the gas holdup in each flow regime therein:

$$\varepsilon_G = \frac{u_G}{u_t} \frac{A_c}{1 - \varepsilon_G} \quad (\text{homogeneous bubbling regime}) \quad (3.35)$$

$$\varepsilon_G = \frac{u_G}{2.02 u_G + 0.257} \quad (\text{heterogeneous bubbling regime}) \quad (3.36)$$

where A_c is an empirical coefficient with a value of 0.79 determined by the data regression, and u_t is the terminal bubble rise velocity.

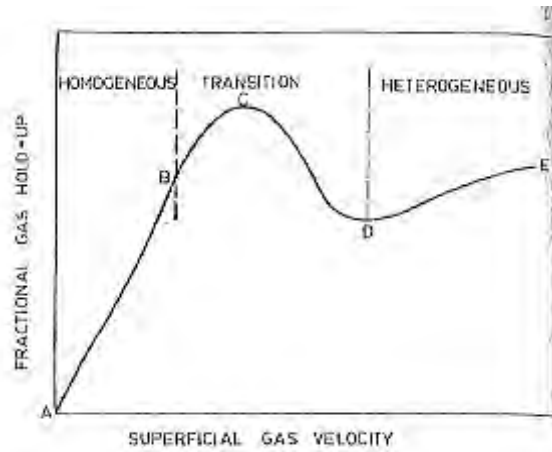


Figure 3.9. Schematic of the gas holdup behavior (Zahradnik *et al.*, 1997)

Al-Masry (2001) explained the three contributions to total pressure drop: hydrostatic head, frictional losses and momentum flux (due to changes in the available flow areas at the top and bottom of the riser in the airlift or bubble column). They neglected the contribution by momentum in small columns and expressed the gas holdup as:

$$\varepsilon_G = \frac{\Delta h}{\Delta z} + \frac{4\tau_{GL}}{d_c \rho_L g} \quad (3.37)$$

where h is the height in the manometer, z the distance between the manometer ports, and τ_{GL} the gas-liquid frictional stress at the wall.

Al-Masry (2001) mentioned the frictional stress of two phases at the wall expressions derived by Metkin and Sokolov (1982):

For laminar flow:

$$\frac{\tau_{GL}}{\tau_L} = \left(\frac{1}{1 - \varepsilon_G} \right)^n \left[1 + \frac{D(1 - \varepsilon_G)^{1+n}}{\left(\frac{\tau_L}{\rho_L} \right)^{\frac{1+n}{n}} \left(1 + \frac{D(1 + \varepsilon_G)^{1+n}}{\left(\frac{\tau_L}{\rho_L} \right)^{\frac{1+n}{n}}} \right)^{n/2}} \right]^{\frac{n^2}{2(1+n)}}, \tau_L = \frac{8\rho_L u_L^2}{\text{Re}} \quad (3.38)$$

For turbulent flow:

$$\frac{\tau_{GL}}{\tau_L} = \left(\frac{1}{1 - \varepsilon_G} \right)^{\frac{2Mn}{n(M-1)+2}} \left[1 + \frac{D(1 - \varepsilon_G)^{\frac{2M(n+1)}{n(M-1)+2}}}{\left(\frac{\tau_L}{\rho_L} \right)^{\frac{1+n}{n}} \left(1 + \frac{D(1 + \varepsilon_G)^{\frac{2M(n+1)}{n(M-1)+2}}}{\left(\frac{\tau_L}{\rho_L} \right)^{\frac{1+n}{n}}} \right)^{\frac{2Mn}{n(M-1)+2}}} \right]^{\frac{Mn^2}{(n+1)[n(M-1)+2]}}$$

$$\tau_L = \frac{0.316n^{0.121} \rho_L u_L^2}{8 \text{Re}^{\frac{2}{n(M-1)+2}}} \quad (3.39)$$

where:

$$\text{Re} = \frac{8u_L^{2-n} d_c^n \rho_L}{k \left(\frac{6n+2}{n} \right)}$$

$$D = 2 \frac{2(1+n)}{n} \left(\frac{k}{\rho_L} \right)^{1/n} g \varepsilon_G (1 - \varepsilon_G)^2 \left(\frac{u_G}{\varepsilon_G} - \frac{u_L}{1 - \varepsilon_G} \right)$$

$$M = 0.7n^{-0.59}$$

Al-Masry compared gas holdup calculated from experimental data with calculated from a correlation obtained in a previous work Al-Masry and Dukkan (1998):

$$\varepsilon_G = 0.3245 u_G^{0.9032} \eta^{-0.0925} \quad (3.40)$$

The result of this comparison was the underestimation of gas holdup with the previous equation. Al-Masry and Dukkan (1998) obtained an empirical correlation using aqueous solutions of CMC in an airlift of 0.225-m diameter of riser and downcomer and 6.2-m height. For xanthan gum solutions, the expression of gas holdup obtained by them was:

$$\varepsilon_G = 0.9856 u_G^{0.8747} \eta^{-0.0577} \quad (3.41)$$

Moustiri *et al.* (2001) used two bubble columns of 0.15 and 0.20 m in diameter, and 4.25 and 4.50 m high respectively, tap water and compressed air as work fluids. The bubble columns had a flexible membrane sparger (4 holes/cm²) that covered all cross-sectional area of each bubble column. The superficial gas and liquid velocities were in the range of 0.0052 to 0.055 m/s and 0.0062 to 0.0216 m/s respectively. They measured pressure drop to determine average gas holdup and an optical probe to determine local gas holdup to establish the radial gas holdup profiles. These authors found that the gas holdup depends on column diameter and gas and liquid velocities, being the last the less influent; an increase in liquid velocity resulted in a slight decrease in gas holdup. Additionally, they found that, at low gas velocities, the homogeneous bubbly flow regime prevailed and that the gas holdup varied linearly with superficial gas velocity up to 0.045 m/s. At higher gas velocities, bubbles were large and rose fast; this caused that gas holdup to decrease with an increase in superficial gas velocity. Moreover, in larger

diameter columns, Moustiri *et al.* (2001) found a decreasing gas holdup with superficial gas velocity due to wall effect (wall effect reduces the bubble rise velocity causing an increase in average gas holdup).

The local (radial) gas holdup obtained by Moustiri *et al.* (2001) shown in Figure 3.10 is importantly affected by superficial gas velocity. At low superficial gas velocities (homogeneous regime), the local gas holdup profiles are relatively flat while at high gas velocities (heterogeneous regime), the profiles have an arched shape with a maximum at the center of the column.

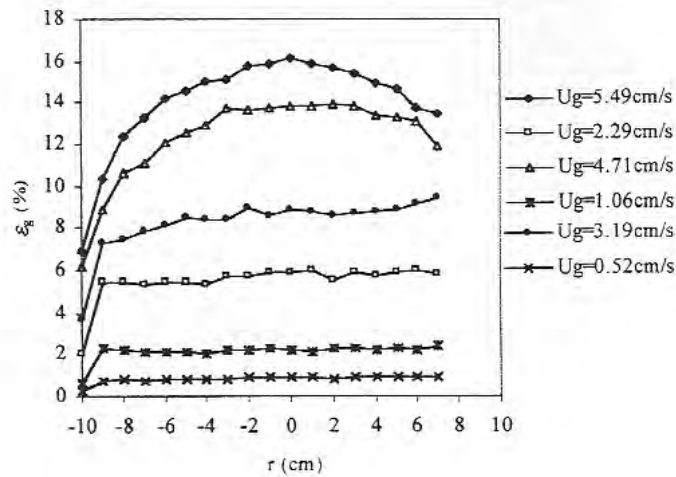


Figure 3.10. Radial gas holdup obtained by Moustiri (2001)

Wu *et al.* (2001) derived an expression for the axial liquid velocity in the column with a non-Newtonian liquid that follows the power-law model in terms of parameters proposed by Montserrat and García-Calvo (1996) and García-Calvo and Leton (1994). Wu *et al.* (2001) evaluated the gas holdup through the Luo and Svendsen (1991) that used the same power-law parameters of the proposed axial liquid velocity equation; this expression is as follows:

$$\varepsilon_G = \bar{\varepsilon}_G \left(\frac{N+2}{N+2-2C'} \right) \left[1 - C' \left(\frac{r}{R} \right)^N \right] \quad (3.42)$$

where $\bar{\varepsilon}_G$ is the cross-sectional average gas holdup, N and C' are parameters of the power-law liquid velocity given by the following expressions:

$$\begin{aligned} N &= 2.188 \times 10^3 \text{Re}_G^{-0.598} \text{Fr}_G^{0.146} \text{Mo}_L^{-0.004} \\ C' &= 4.32 \times 10^{-2} \text{Re}_G^{0.249} \\ \text{Re}_G &= \frac{d_c u_G (\rho_L - \rho_G)}{\mu_L} \end{aligned}$$

The expression proposed by Wu *et al.* (2001) for the liquid velocity was obtained by fitting data obtained experimentally through the computer automated radioactive particles tracking (CARPT) obtaining:

$$\frac{u_L(r)}{u_{Lc}(0)} = 1 - 2.65 N^{0.44} C' \left(\frac{r}{R} \right)^{2.65 N^{0.44} C'} \quad (3.43)$$

Forret *et al.* (2003) in a 1-m diameter bubble column with air-water in batch mode used the gas holdup correlation developed by Schweitzer *et al.* (2001) verified and validated in the same column using an optical probe. This correlation is:

$$\varepsilon_G(r') = \varepsilon_G \left[-1.638(r'^6 - 1) + 1.228(r'^4 - 1) - 0.939(r'^2 - 1) \right] \quad (3.44)$$

where r' is the dimensionless radial coordinate ($r' = 2r/d_c$)

Shirsat *et al.* (2003) worked in a 0.05-m diameter and 1.5-m length downflow bubble column with CMC solutions as liquid phase and air as gas phase. The liquid and gas flow rates were in the ranges of 1.03×10^{-4} to 2.44×10^{-4} m³/s and 0.15×10^{-4} to 2.06×10^{-4} m³/s respectively, obtaining a bubbly two phase flow pattern. They proposed from the multiple regression method of their experimental data the following expression:

$$\varepsilon_G = 1.5063 \text{Re}_L^{-0.168} \text{Mo}_L^{-0.034} \text{Su}_L^{-0.048} \mu_r^{0.076} A_r^{-0.031} H_r^{0.215} \quad (3.45)$$

where Mo_L is the Morton number of the liquid, Su_L the Suratmann number of liquid, μ_r the viscosity ratio between gas to liquid, A_r the area ratio of nozzle to column, and H_r ratio of effective column height to column diameter. Their correlation agrees within a 10% with their experimental data. Additionally, they measured the total pressure drop and calculated the friction pressure drop taking into account the contribution due to gravity (Eq. A.15 of Appendix A). They proposed a correlation to estimate the friction factor evaluated from a pressure drop balance defined by Eq. (A.10) of Appendix A, in which they neglected the acceleration contribution because of the uniform cross-sectional area .:

$$\Delta P_f = \Delta P_t - g\Delta z \left[(1 - \varepsilon_G) \rho_L + \varepsilon_G \rho_G \right] \quad (3.46)$$

The difference this time is that they defined a two-phase friction factor based on superficial liquid velocity as follows:

$$f_{TPL} = 0.5 \left(\frac{\Delta P_f}{\rho_L g \Delta z} \right)_L \left(\frac{gd_c}{u_L^2} \right) \quad (3.47)$$

Finally, the correlation proposed by Shirsat *et al.* (2003) is:

$$f_{TPL} = 4.1258 \times 10^{-6} \text{Re}_L^{-2.069} \text{Mo}_L^{-1.152} \text{Su}_L^{0.016} \quad (3.48)$$

This correlation represented the experimental data with a 9% error.

Mandal *et al.* (2004) presented a similar analysis in downflow bubble column with air and non-Newtonian liquid (CMC solutions). They neglected the contribution of the gas density in Eq. (3.46) obtaining the following expression to evaluate de two-phase friction factor:

$$f_{TPL} = 0.5 \left[\frac{\Delta P_t}{\rho_L g \Delta z} - (1 - \varepsilon_G) \right] \left(\frac{gd_c}{u_L^2} \right) \quad (3.49)$$

The final expression of the two-phase friction factor, obtained through the regression of experimental data by Mandal *et al.* (2004) is:

$$f_{TPL} = 0.356 \times 10^4 \text{Re}_L^{-1.702} \text{Mo}_L^{-0.384} A_r^{0.201} H_r^{-1.069} \quad (3.50)$$

This correlation has an average error of 10.6%.

3.4. Residence Time Distribution (RTD)

The idea of the residence time distribution was shown by MacMullin and Weber (1935); however the concept was exposed extensively in the 1950s by Danckwerts (1953). The residence time is the time that a particle or fluid element stays inside of the vessel. The residence time distribution (RTD) allows characterizing the mixing in a chemical reactor or vessel by a fit of the data obtained using RTD experiments to a proposed mathematical model, which includes parameters related to the mixing phenomenon. Two extreme cases are normally used as reference: a plug flow reactor (PFR) where there is no axial mixing and a continuous stirred-tank reactor (CSTR) that presents the opposite behavior with perfect mixing inside the vessel.

To determine the experimental RTD, an inert tracer is injected at the feed of the vessel and its concentration is measured at the exit. The tracer should be non reactive, easy to detect in the system, completely soluble in the mixture, and should not alter the physical properties to the fluid to which it is injected. The tracer can be injected as an impulse or as a step.

3.4.1. The impulse injection tests

In an impulse injection, a small amount of tracer is injected swiftly at the feed of the vessel and mathematically, this kind of injection is represented through the Dirac function, $\delta(t)$. The exit concentration is measured as a function of time and the resulting

response is shown schematically in Figure 3.11. The mass of tracer exiting in a period of time between t and $t + \Delta t$ is described by the expression:

$$\Delta N = c(t) Q \Delta t \quad (3.51)$$

where Q is the volumetric flow rate, $c(t)$ is the exit tracer concentration at time t , and ΔN is the mass of tracer that exits in the time interval between t and $t + \Delta t$.

If Eq. (3.51) is divided through by the total mass injected in the system, N_0 , the following expression is obtained:

$$\frac{\Delta N}{N_0} = \frac{Q c(t)}{N_0} \Delta t \quad (3.52)$$

It is possible to define a statistical function called external age distribution $E(t)$. This is a normalized (although not dimensionless) function that describes the residence time of the tracer particles in the system. It can be expressed as follows in the case of an impulse injection:

$$E(t) = \frac{Q c(t)}{N_0} \quad (3.53)$$

From equation (3.51) it is possible to write:

$$N_0 = \int_0^{\infty} Q c(t) dt \quad (3.54)$$

and if Q is constant, thus:

$$E(t) = \frac{c(t)}{\int_0^{\infty} c(t) dt} \quad (3.55)$$

If experimental data are consistent, the Eq. (3.54) must be satisfied.

$$c(t) = c_0 \int_0^t E(t') dt' \quad (3.58)$$

The function $F(t)$, which represents the fraction of fluid that has been in the reactor for a time less than t , is defined mathematically as:

$$F(t) \equiv \int_0^t E(t) dt \quad (3.59)$$

Experimental data can be related to $F(t)$ through the expression:

$$F(t) = \frac{c(t)}{c_0} \quad (3.60)$$

3.4.3. Moments theory

The k -th moment around $x=a$ of any distribution $P(x)$ is defined by:

$$M_k = \int_0^{\infty} (x - a)^k P(x) dx \quad (3.61)$$

If $a = 0$ (origin), the moment is considered a non-central moment:

$$M'_k = \int_0^{\infty} x^k P(x) dx \quad (3.62)$$

when $k = 0$, the zero-th moment is obtained:

$$M'_0 = \int_0^{\infty} P(x) dx \quad (3.63)$$

Three important moments of the distribution function $E(t)$ are:

- The mean residence time (μ): represents the center of gravity of the distribution function with respect to the origin. It is a non-centered first moment of $E(t)$:

$$M_1' = \mu = \int_0^{\infty} t E(t) dt \quad (3.64)$$

- Variance: it is a measure of the spread of the distribution around the mean value; it is the square of the standard deviation. It is a centered second moment of $E(t)$:

$$M_2 = \sigma^2 = \int_0^{\infty} (t - \mu)^2 E(t) dt \quad (3.65)$$

- Skewness: it is a measure of asymmetry of the distribution with respect to the mean. If the skewness is zero, the distribution is symmetrical. It is a centered third moment of $E(t)$:

$$M_3 = \gamma^3 = \int_0^{\infty} (t - \mu)^3 E(t) dt \quad (3.66)$$

3.5. Mathematical models. Mixing in the liquid phase

Many models can be used to describe bubble column reactors. Some aspects to take into account when it is proposed a model are the mathematical nature of the equations and the degree of complexity of their solution (Deckwer, 1992).

The liquid phase mixing has an important effect on mass transfer capabilities of a bubble column. Mixing in bubble columns is due to liquid circulation caused by the rise of the bubbles through liquid phase, reducing or eliminating the concentration gradient in the system. Because of the ratio between length and diameter is high, the radial gradients are often neglected compared to axial gradients (Walter and Blanch, 1983).

Several mathematical models have been proposed in the literature to describe mixing based on conservation laws or simply based on empirical relations. It is common to use an injection of a tracer at the feed and then measure tracer concentrations at the exit. These collected data are analyzed using, for example, the moment's theory or the transfer function of a mathematical model that could represent the behavior of these experimental data. The disadvantage of the moments method is that moments can be quite sensitive to measurement errors at the tail of the function $E(t)$, (Ostergaard and Michelsen, 1969). In the case of bubble columns, mixing or backmixing of each phase (degree of turbulence) is due to flow or movement of the fluids through the column. The rising bubbles cause turbulent stochastic diffusion processes and large-scale steady circulation flows (Riquarts, 1981).

Some of the mathematical models found in literature are presented in this section. Models as perfect mixing (CSTR), partial mixing (ADM) and tubular flow (PFR) may be found in gas and liquid phases operations (Deckwer, 1992).

3.5.1. Continuous, stirred-tank reactor (CSTR)

The continuous-stirred-tank reactor is a perfectly mixed tank with steady-state inlet and exit flow streams. Therefore, the concentration in the reactor, $c(t)$, is only function of time. The expression obtained from a mass balance for an impulse of tracer is (Froment and Bischoff, 1979):

$$c(t) = \frac{N_0}{V} \exp(-t/\tau) \quad (3.67)$$

where N_0 is the mass of tracer added initially as an impulse, V is the fluid volume in the tank (considered constant), t is the time and, $c(t)$ is the exit concentration of the tracer, which is the same as the concentration inside the reactor at the any particular time, and τ is the residence time defined as the relation between reactor volume, V and volumetric flow rate of the feed, Q .

The Eq. (3.67) can be expressed in terms of the age distribution function as:

$$E(t) = \frac{1}{\tau} \exp(-t/\tau) \quad (3.68)$$

For a step injection, the solution of the tracer mass balance, for a zero initial concentration in the system is:

$$c(t) = c_0 [1 - \exp(-t/\tau)] \quad (3.69)$$

where c_0 is the input concentration for $t \geq 0$. When a step injection is used, the cumulative function $F(t)$ is used instead of the distribution function $E(t)$, and the resulting expression for a continuous stirred tank is:

$$F(t) = 1 - \exp(-t/\tau) \quad (3.70)$$

3.5.2. Plug-flow reactor (PFR)

In an ideal, plug-flow reactor (considered tubular), the fluid is assumed to travel through the system at uniform velocity and in straight streamlines; therefore there are no radial concentration gradients. Under these conditions, the concentration in the reactor, $c(t,z)$, is a function of time and axial position in the reactor. A tracer mass balance on a differential element of fluid inside the reactor, taking into account as initial condition, $c(0,z) = 0$ in the case of an impulse injection, gives the final expression:

$$c(t,L) = N_0 \delta(t - \tau) \quad (3.71)$$

where L is the exit point (i.e., the length of the reactor).

In case of a step injection, the exit concentration will be given by:

$$c(t,L) = c_0 H(t) \quad (3.72)$$

where c_0 is the maximum concentration that corresponds to feed concentration of tracer and $H(t)$ is the Heaviside function that gives the step form of the obtained answer.

3.5.3. Tank-in-series model

This model is a modified CSTR model, where a mass balance of the tracer is made in a generic tank “ n ” of a series of identical tanks that constitute the system. When the resulting equation from the mass balance is manipulated and the initial and the boundary conditions are applied, the final expression is obtained for each form of tracer injection:

For step injection tests (Levenspiel, 1999):

$$F(t) = 1 - \exp\left(-N \frac{t}{\tau}\right) \sum_{n=1}^N \frac{(nt/\tau)^{n-1}}{\Gamma(n)} \quad (3.73)$$

where N is the number of tanks in the system.

For impulse injection tests (Froment and Bischoff, 1979):

$$E(t) = \frac{N^N}{\tau^N} \frac{t^{N-1} \exp(-N t / \tau)}{\Gamma(N)} \quad (3.74)$$

If any of the two previous equations is substituted into the defining equation of each moment, equations (3.64) to (3.66), the following expressions are obtained:

$$\frac{\mu}{\langle t \rangle} = 1 \quad (3.75)$$

$$\frac{\sigma^2}{\langle t \rangle^2} = \frac{1}{N} \quad (3.76)$$

$$\frac{\gamma^3}{\langle t \rangle^3} = \frac{2}{N^2} \quad (3.77)$$

The plots of equations (3.73) and (3.74) are presented by Levenspiel (1989) and they are shown in figures (3.12) and (3.13) respectively.

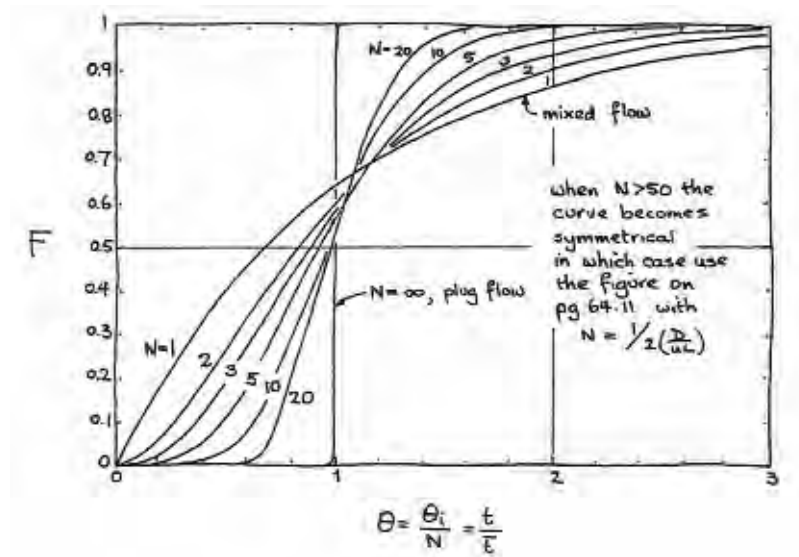


Figure 3.12. Response for a step injection of tracer in the tanks-in-series model (Levenspiel, 1989)

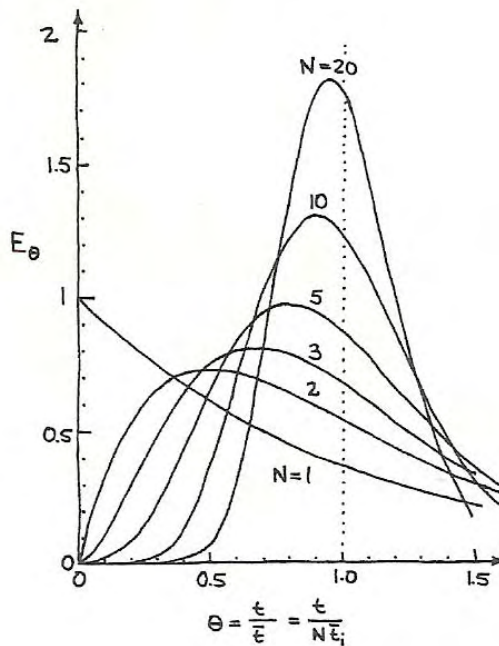


Figure 3.13. Response for an impulse injection of tracer in the tanks-in-series model (Levenspiel, 1989)

3.5.4. The dispersion model

The dispersion model is used to describe tubular non-ideal reactors. It considers that there is a Fickian dispersion of matter, i.e., described by a constitutive equation similar to the Fick's law of diffusion. The expression of the model results from a tracer mass balance considered that is injected at the feed of the system. The model takes into account two effects: convection, which represents the bulk flow, and dispersion, which results from the molecular and turbulent diffusion. There are two types of contributions to dispersion: radial and axial (Riquarts, 1981). The radial effect is negligible in comparison to axial effect when the aspect ratio L/D is greater than 4. The model is then called axial-dispersion model. In this case, the concentration $c(t,z)$ is a function of time and axial position in the reactor, and it is described by the following expression:

$$\frac{\partial c}{\partial t} = D_z \frac{\partial^2 c}{\partial z^2} - u \frac{\partial c}{\partial z} \quad (3.78)$$

where c is the concentration of the tracer, u the fluid velocity, D_z the axial dispersion coefficient, z the axial coordinate, and t the time. This equation can be written in dimensionless form:

$$\frac{\partial c^*}{\partial \theta} = \frac{1}{\text{Bo}_z} \frac{\partial^2 c^*}{\partial z^{*2}} - \frac{\partial c^*}{\partial z^*} \quad (3.79)$$

where the new variables are defined as:

$$c^* = \frac{c}{c_0} \quad (3.80)$$

$$\theta = \frac{t u}{L} \quad (3.81)$$

$$z^* = \frac{z}{L} \quad (3.82)$$

$$\text{Bo}_z = \frac{u L}{D_z} \quad (3.83)$$

where L is the characteristic length (in this case, the length of the reactor) and Bo_z is the Bodenstein number in the axial direction. For simplicity, the Bodenstein number will be expressed as Bo instead Bo_z .

The Bodenstein number is the ratio of the transport rate by convection to the transport rate by dispersion. The inverse of the Bodenstein number is called dispersion number.

The solution to the differential equation depends on the boundary conditions. Two boundary conditions are needed; one at $z = 0$, the injection point, and one at $z = L$, the point at which the response is measured. Each condition depends on whether there is

dispersion before the injection point ($z = 0$) and after the response point ($z = L$). If there is dispersion on both sides of any of these points, it is called an open boundary; otherwise it is called a closed boundary. All four combinations are possible for a reactor: open-open, open-closed, closed-open and closed-closed. Closed boundaries result in a mathematical discontinuity in concentration, produced by a discontinuity in dispersion.

When open-open boundary conditions are used, they can be written as:

$$\begin{aligned}c^*(-\infty, 0) &= \text{finite} \\c^*(\infty, 0) &= \text{finite}\end{aligned}$$

The corresponding analytical solution of equation (3.79) at $z^* = 1$ is (Froment and Bischoff, 1979):

$$c^* = \frac{c}{c_0} = \frac{1}{2} \sqrt{\frac{\text{Bo}}{\pi \theta}} \exp\left(\frac{-\text{Bo}(1-\theta)^2}{4\theta}\right) \quad (3.84)$$

This solution leads to the following expressions for the moments using the definitions of equations (3.64) to (3.66):

$$\frac{\mu}{\tau} = 1 + \frac{2}{\text{Bo}} \quad (3.85)$$

$$\frac{\sigma^2}{\tau^2} = \frac{2}{\text{Bo}} + \frac{8}{\text{Bo}^2} \quad (3.86)$$

$$\frac{\gamma^3}{\tau^3} = \frac{12}{\text{Bo}^2} + \frac{64}{\text{Bo}^3} \quad (3.87)$$

and the response curves for an impulse injection is shown in Figure 3.14.

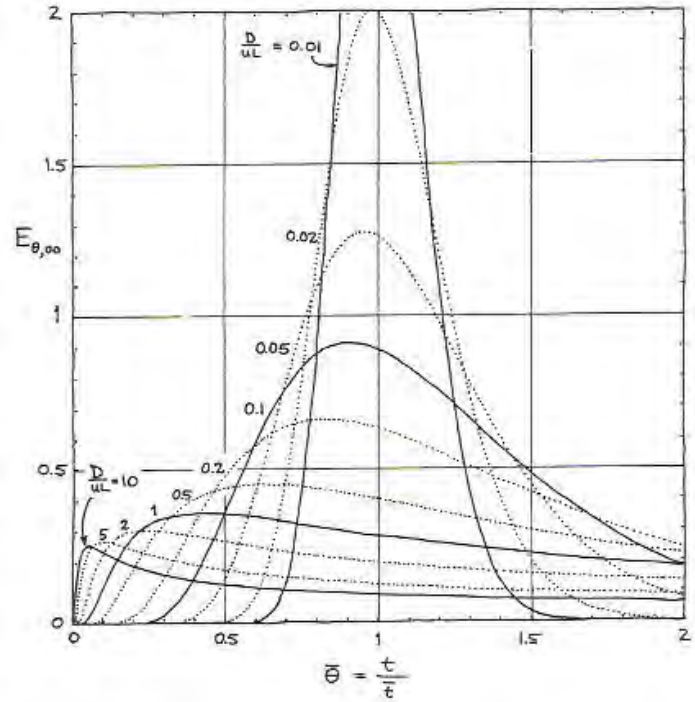


Figure 3.14. Response curves for an impulse injection of tracer in the ADM model with open-open boundary conditions (Levenspiel, 1989)

On the other hand, the following closed-closed boundary conditions, normally called Danckwerts boundary conditions, may be used:

$$z^* = 0, \quad -\frac{1}{Bo} \left. \frac{\partial c^*}{\partial z^*} \right|_{0+} + c^* \Big|_{0+} = 1$$

$$z^* = 1, \quad \left. \frac{\partial c^*}{\partial z^*} \right|_{1+} = 0$$

and the corresponding analytical solution at $z^* = 1$ is (Froment and Bischoff, 1979):

$$c^* = \frac{c}{c_0} = 4 \sum_{n=0}^{\infty} \frac{\delta_n (Bo \sin \delta_n + 2 \delta_n \cos \delta_n)}{Bo^2 + 4 Bo + 4 \delta_n} \exp \left[\frac{Bo}{2} - \frac{(Bo^2 + 4 \delta_n^2)}{4 Bo} \theta \right]$$

(3.88)

where the eigenvalues δ_n of this series solution are the roots of the following equation:

$$\cot \delta_n = \frac{1}{2} \left(\frac{2\delta_n}{\text{Bo}} - \frac{\text{Bo}}{2\delta_n} \right) \quad (3.89)$$

The moments for closed-closed boundary conditions, using the definitions of equations (3.64) to (3.66), are as follows:

$$\frac{\mu}{\tau} = 1 \quad (3.90)$$

$$\frac{\sigma^2}{\tau^2} = \frac{2}{\text{Bo}} - \frac{2}{\text{Bo}^2} [1 - \exp(-\text{Bo})] \quad (3.91)$$

$$\frac{\gamma^3}{\tau^3} = \frac{24}{\text{Bo}^3} \left[\left(\frac{\text{Bo}}{2} - 1 \right) + \left(\frac{\text{Bo}}{2} + 1 \right) \exp(-\text{Bo}) \right] \quad (3.92)$$

Figure 3.15 shows the response curves for impulse injection of tracer in these boundary conditions.

On the other hand, when there are at least two phases in the system, the equation (3.78) needs to be modified as follows:

$$\frac{\partial c}{\partial t} = -\frac{u_L}{1 - \varepsilon_G} \frac{\partial c}{\partial z} + D_z \frac{\partial^2 c}{\partial z^2} \quad (3.93)$$

where c is the tracer concentration in the liquid phase.

When figures 3.13 through 3.15 are compared, the trends of figures 3.13 and 3.15 are similar because both models consider that the mixing is inside the system and in enter and exit zones there are not mixing.

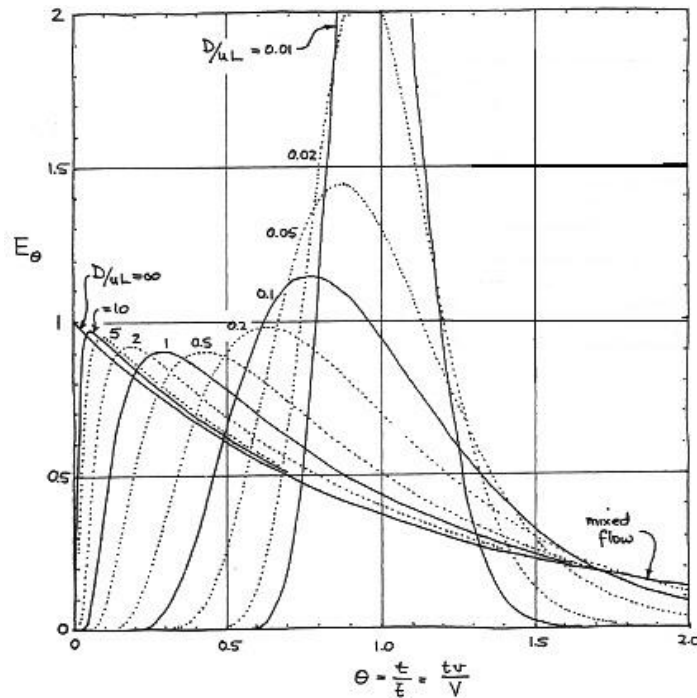


Figure 3.15. Response curves for an impulse injection of tracer in the ADM model with closed-closed boundary conditions (Levenspiel, 1989)

Many researchers have studied the backmixing in bubble columns showing the dependence on the column diameter, gas distributor, and gas velocity, but the influence of the velocity and properties of the liquid phase on the mixing of the same phase, especially when the liquid phase is non-Newtonian is not known. Some experimental and mathematical works are described below.

Ohki and Inoue (1970) determined longitudinal dispersion coefficient in batch bubble column with 0.04, 0.08 and 0.16 m diameters. They stated that the one-dimensional diffusion model is valid when the distance between injection tracer and measuring points are sufficiently long. They use the one-dimensional diffusion model resulting from Eq. (3.78) when the convective term is neglected:

$$\frac{\partial c}{\partial t} = D_z \frac{\partial^2 c}{\partial z^2} \quad (3.94)$$

The boundary conditions used by authors are:

$$\frac{\partial c}{\partial z} = 0 \text{ at } z = 0 \text{ and } z = L$$

while the initial conditions is:

$$c(z, 0) = \begin{cases} c_0 & \text{for } 0 \leq z \leq \beta \\ 0 & \text{for } z \geq \beta \end{cases}$$

where β is a height filled with tracer. The solution to the differential equation is:

$$\frac{c(t, z)}{c_E} = 1 + \frac{2L}{\pi\beta} \sum_{n=1}^{\infty} \left\{ \frac{1}{n} \sin\left(\frac{n\pi}{L}\beta\right) \cos\left(\frac{n\pi}{L}z\right) \exp\left[-\left(\frac{n\pi}{L}\right)^2 D_z t\right] \right\} \quad (3.95)$$

where c_E is related through the expression:

$$c_E L = c_0 \beta \quad (3.96)$$

The researchers determined the dispersion coefficient from the expression:

$$D_z = \left(\frac{L}{\pi}\right)^2 \frac{\Delta\theta}{\Delta t} \quad (3.97)$$

D_z is obtained from the fitting of Eq. (3.95) to experimental data, where the authors plotted c/c_E as a function of $\pi D_z t/L$ and took $\Delta\theta$ as the distance in the abscise marked when the value of $c/c_E = 0.7$ and $c/c_E = 0.3$ intercept the curve obtained from the model for a z/L . The authors correlated the data and proposed two expressions that depend on prevailing flow regime:

Homogeneous regime:

$$D_z = 0.30 d_c^2 u_G^{1.2} + 170d_0 \quad (3.98)$$

Slug flow regime:

$$D_z = \frac{14d_c}{(1 - \varepsilon_G)^2} \quad (3.99)$$

They got agreement of the proposed expressions with experimental data.

Kim *et al.* (1972) worked with a rectangular bubble column in the range of superficial velocities of 0.014 to 0.10 m/s for the gas phase and 0 to 0.27 m/s for the liquid phase. They defined a height of liquid phase axial mixing unit HMU:

$$HMU = \frac{2H}{Bo} \quad (3.100)$$

where H is the expanded bed height (ft). They used an impulse and step perturbation with tracer to get the complete mixing behavior. Experimental data were correlated in terms of liquid- and gas-phase dimensionless numbers. The expression they obtained is:

$$\frac{HMU}{H_0} = 3.89 \left(\frac{Fr_L \rho_G}{\rho_L} \right)^{-0.134} \left(\frac{Fr_G \rho_L}{\rho_G} \right)^{0.229} (Re_G Re_L)^{-0.274} \quad (3.101)$$

where Fr_i and Re_i are the Froude and Reynolds numbers of the i -phase respectively, and H_0 is the unexpanded bed height.

Deckwer *et al.* (1974) did the mixing experiments with tap water as liquid phase. They used the stationary and transient methods, where tracer concentrations were measured upwards the bulk flow of liquid. They defined the mixing time as that time which is needed to distribute an amount of tracer (introduced as Dirac pulse) uniformly or to distinct degree homogeneity c/c_0 (introduced as step injection of the tracer). They found scattered points at 5 cm/s of gas velocity in the plot of dispersion coefficient

versus superficial gas velocity, and they explained this phenomenon through the transition between homogeneous and heterogeneous regimes.

Baird and Rice (1975) worked in the turbulent region and developed the isotropic turbulence model. A variety of eddy sizes were present, but the largest are generated continuously by an energy source such a moving grid or impeller, breaking in smaller eddies due to viscosity. If the scale of the process is greater than the minimum eddy size, the rate depends mainly on the energy dissipation. This basis is applied mainly in stirred tank processes. The authors presented the eddy diffusivity using dimensional analysis:

$$E = K' l^{4/3} P_m^{1/3} \quad (3.102)$$

where E is the Eddy diffusivity, K' dimensionless constant, l the linear scale, and P_m the energy dissipation rate per unit mass. They deduced expressions of the energy dissipation rate per unit mass for different types of columns. For bubble columns the expression of P_m is:

$$P_m = u_G g \quad (3.103)$$

For bubble columns, Baird and Rice (1975) used the column diameter as the linear scale. They finally proposed the following expression to estimate the order-of-magnitude under turbulent conditions giving advertences about its use in small diameter column (because of the possibility of the slug flow presence) or when the ratio of length to column diameter was less than 5:

$$D_z = 0.35 d_c^{4/3} (u_G g)^{1/3} \quad (3.104)$$

Eissa and Schügerl (1975) made the tracer injection at the top or at the bottom in cocurrent or countercurrent, respectively. They measured the liquid conductivity at the column exit in steady-state operation, and they applied the axial-dispersion-model in

steady state. They observed an increase in the dispersion coefficient with superficial velocities and in countercurrent the values were highest.

The mixing of a fluid is usually divided into: micromixing (intimacy of mixing of various molecules or entities in a flow system; it includes all aspects of mixing not defined by residence time distribution, as molecular diffusion, depending only on the time association between various molecules) and macromixing (the fluid is considered as independent entities and provides information on the residence time; it is a result of convective diffusion). The extreme cases of macromixing are complete mixing and plug flow (Shah *et al.*, 1978).

Shah *et al.* (1978) mentioned that models for backmixing are divided into two groups: differential models (i.e. axial dispersion model) and stagewise models (i.e. tanks-in-series model). The former results in differential equations while the latter results in algebraic equations in steady-state conditions. The parameters defined to characterize backmixing are usually equivalent. In the axial dispersion model as it was mentioned previously, the parameter of the model is the dimensionless Bodenstein number (sometimes called Péclet), where the characteristic length is the diameter of the column or the diameter of the bubble in spray or bubble columns, while in fixed bed is the diameter of the packing. Additionally, they analyzed the expression obtained by Ohki and Inoue (1970) for batch systems and for flow systems, mentioning the error obtained in tailed RTD when Bodenstein number is obtained from moment theory. They suggested the time-domain solution proposed by Michell and Furzer (1972) for axial dispersion model with closed-closed boundary condition:

$$c(t) = \frac{M}{A\sqrt{4\pi D_z t}} \exp\left[\frac{-(L_z - ut)^2}{4D_z t}\right] \quad (3.105)$$

where u is the real mean velocity and M the injected mass of tracer. The authors recommended a non-linear regression of the data using the Eq. (3.105).

Shah *et al.* (1978) discussed the determination of Bodenstein number through the method proposed by Ostergaard and Michelsen (1969). Shah *et al.* (1978) commented on the error in this procedure for smallest or longest values of s that permits values of τs between 2 and 5 in packed beds. These values were proposed originally by Hopkins *et al.* (1969).

Shah *et al.* (1978) mentioned some empirical correlations obtained by different researchers:

Towel and Ackerman (1972):

$$D_z = 1.23 d_c^{1.5} u_G^{0.5} \quad (3.106)$$

Deckwer et al. (1974):

$$D_z = 2.7 d_c^{1.4} u_G^{0.3} \quad (3.107)$$

where the column diameter is expressed in cm, the velocity in cm/s and the dispersion coefficient in cm²/s.

Cova (1974):

$$D_z = 73.7 u_G^{0.32} \rho_L^{0.07} \quad (\text{obtained in 1.8-in tube for single orifice gas sparger}) \quad (3.108)$$

$$D_z = 23.6 u_G^{0.45} \rho_L^{0.40} \quad (\text{obtained in 0.75-in tube for single orifice gas sparger}) \quad (3.109)$$

where u_g is expressed in ft/min, ρ_L in g/cm³ and D_z in ft²/h. Cova (1974) found no effect of surface tension or viscosity on axial dispersion coefficient.

Hikita and Kikukawa (1974):

$$D_z = (0.15 + 0.69 u_G^{0.77}) d_c^{1.25} (1/\mu_L)^{0.12} \quad (3.110)$$

where μ_L is in cP.

Alexander and Shah (1976):

$$\frac{u_G d_c}{D_z} = \frac{13 Fr_G}{1 + 6.5 Fr_G^{0.8}} \quad (3.111)$$

Reith et al. (1968):

$$Bo_L = \frac{u_r d_c}{D_z} = 3.0 \pm 0.3 \quad (3.112)$$

where u_r is the relative velocity between gas and liquid phases defined by authors as two times the superficial gas velocity minus the rise velocity of a single bubble. This correlation was obtained in 0.14- and 0.29-m column diameters, at superficial gas velocities ranging from 0.10 to 0.45 m/s. The authors found that radial-dispersion coefficient was 10 times smaller than axial-dispersion coefficient at a same superficial gas velocity.

Joshi (1980) analyzed various concepts in multiphase contactors and proposed an expression to evaluate the liquid dispersion coefficient in bubble columns as follows:

$$D_z = 0.33(u_c + u_L)d_c \quad (3.113)$$

where u_c is the liquid circulation.

Riquarts (1981) describes the flows in the column qualitatively. He explains that, in the center of the column, both effects (convective and diffusive) have the same direction whereas near the column wall, the convective movement is descendant and diffusive is ascendant. He proposed an empirical expression to evaluate the axial dispersion; the form of the equation is:

$$D_z = 0.068 d_c (d_c g)^{1/2} \left(\frac{\rho_L u_G^3}{\mu_L g} \right)^{1/8} \quad (3.114)$$

Walter and Blanch (1983) proposed $Bo = 1.65$ for $Re > 1000$ and explained that axial mixing is due to the liquid circulation profiles.

Kawase and Moo-Young (1986) proposed the following expression for the Bodenstein number:

$$Bo = \frac{u_G d_c}{D_L} = 2.92 n^{8/3} Fr_G^{1/3} \quad (3.115)$$

They used this correlation to compare the different expressions obtained by others for Newtonian and non-Newtonian fluids. In the case of non-Newtonian fluids, they compared their correlation with the one proposed by Deckwer *et al.* (1982). Kawase and Moo-Young (1986) concluded that equation (3.115) fits better their experimental data for both Newtonian and non-Newtonian fluids.

Haque *et al.* (1986) presented a modification of the Levenspiel's model based on an idea developed by Nishiwaki and Shinkawa (1980). They represented the mixing in terms of stirred tanks in series with interstage circulation. For four circulation cells, the expression is:

$$\frac{c_4}{c_0} = 1 + \exp\left(-2 \frac{u_B t}{L_0}\right) - \left\{ \frac{2 - \sqrt{2}}{2} \exp\left[\left(2 + \sqrt{2}\right) \frac{u_B t}{L_0}\right] \right\} - \left\{ \frac{2 + \sqrt{2}}{2} \exp\left[-\left(2 - \sqrt{2}\right) \frac{u_B t}{L_0}\right] \right\} \quad (3.116)$$

where c_0 is the pulse effective concentration (mass of tracer divided by reactor volume), u_B intercell liquid circulation velocity, calculated by an expression proposed by Joshi (1980), and L_0 height of one cell ($0.8 d_c$). This model provided a good fit of the experimental data.

Rice and Littlefield (1987) used the Baird and Rice (1975) model to start their analysis and obtained the following correlation for batch bubble columns:

$$D_z = d_B^{4/3} (g u_G)^{1/3} \quad (3.117)$$

where the parameters are substituted in c.g.s. unit system.

Rustemeyer *et al.* (1989) worked with two bubble columns in batch mode: column A with 0.15 m diameter and 2.57 m height and column B with 0.20 m diameter and 6.18 m height. They used the model developed by Ohki and Inoue (1970) where they defined D_{eff} (the effective dispersion coefficient) instead the simple axial dispersion coefficient D_z . When Rustemeyer *et al.* (1989) plotted the effective dispersion as a function of dimensionless radial position, they found a maximum at the wall and a minimum at the center radial position and this trend is very important when the point in which concentration is measured is most far from the injection point. Additionally, they found that the effective dispersion coefficient increases as superficial gas velocity does. Taking into account these results, the authors decided to propose a two-dimensional mixing model that considers the radial profiles of the mean axial velocities of the liquid. This model has three adjustable parameters: the number of mixing cells, their height, and the axial dispersion coefficient in the flow regions. They found that their model fits the experimental data quite well.

Wilkinson *et al.* (1993) worked in a batch bubble column injecting 30 ml of 4 M NaCl solution at the bottom of the column at 1.5 MPa as tracer and measured it with conductivity probe. They used a simplified mode of the axial dispersion model in which do not consider de convective term in the tracer balance, using the final expression proposed by Siemes and Weis (1957):

$$\frac{c(t) - c(t=0)}{c(t=\infty) - c(t=0)} = 1 + 2 \sum_{m=1}^{\infty} \cos\left(\frac{m\pi}{H} z\right) \exp\left(-\frac{m^2 \pi^2}{H^2} D_z t\right) \quad (3.118)$$

They also commented about the circulation pattern inside the column in which the liquid flows upward in the center of the column and downward near the column wall; this phenomenon is assumed to be the main cause of liquid mixing besides liquid

turbulence. They proposed an expression for the axial mixing coefficient in the liquid phase:

$$D_z = 0.43 d_c^{4/3} [g(u_G - \varepsilon_G u_b)]^{1/3} \quad (3.119)$$

Wilkinson *et al.* (1993) found that the dispersion coefficient increases slightly as pressure increases, while gas holdup increases considerably with pressure.

They proposed the following correction for axial-dispersion coefficient at high pressures:

$$D_z(\text{high pressure}) \cong D_z(\text{atmospheric pressure}) \frac{\varepsilon_L(\text{atmospheric pressure})}{\varepsilon_L(\text{high pressure})} \quad (3.120)$$

The authors emphasized that Eq. (3.120) is based on limited number of experimental results and they recommended developing this proposal.

Additionally, García-Calvo and Letón (1994) developed an expression for the so-called energy dissipation rate, which is due to the liquid motion. This expression comes from an energy balance, previously formulated by Kawase and Moo-Young (1986) for turbulent flow. The expression was then combined with a circulation cell model, developed by Joshi and Sharma (1979) to obtain the following equations:

$$D_z = 0.35 d_c^{4/3} E_m^{*1/3} \quad (3.121)$$

$$E_m^{*1/3} = \frac{W}{H_0 \rho_L} \quad (3.122)$$

$$W = \frac{0.64 (2)^{3K/2} K^3 n^2 \rho_L H_0 u_{L0}^3}{d_c} \left[\frac{1}{2(3K-1)} + \frac{1}{(3K-1)} - \frac{2^{0.5}}{3K} \right] \quad (3.123)$$

where E_m^* is the rate of energy consumed by the liquid motion per unit mass, K is a liquid velocity profile parameter (the best value found by the authors was 2.3), H_0 the

clear-liquid height, u_{L0} the linear velocity of the liquid at $r = 0$, and W the energy dissipation rate. The authors obtained results within a $\sim 30\%$ error.

Ityokumbul *et al.* (1994) measured axial mixing through the injection of an impulse of concentrated hydrochloric acid at the liquid feed. They measured the pH at the bottom of the column to estimate the tracer concentration and based on their measures, and they obtained one expression for each flow regime encountered by them as it is shown:

Region I (chain bubbling flow that occurs at $u_G \leq 0.009$ m/s or $Fr_G \leq 1.25 \times 10^{-4}$):

$$D_z = 0.675 d_c^{1.235} g^{0.235} u_G^{0.53} \quad (3.124)$$

Region II (bubbly flow that occurs at $0.009 \leq u_G$ (m/s) ≤ 0.025 or $1.25 \times 10^{-4} \leq Fr_G \leq 7.24 \times 10^{-4}$):

$$D_z = 0.674 d_c^{1.5} g^{0.5} \quad (3.125)$$

Region III (churn-turbulent flow that occurs at $u_G \geq 0.025$ m/s or $Fr_G \geq 7.24 \times 10^{-4}$):

$$D_z = 28.5 d_c^{0.69} g^{-0.31} u_G^{1.62} \quad (3.126)$$

Figure 3.16 shows these correlations graphically.

Degaleesan and Dudukovic (1998) analyzed the liquid mixing and axial dispersion coefficient based on a Taylor-type expression that considers an effective axial-dispersion coefficient in terms of convective recirculation and (axial and radial) eddy diffusion. The analysis was developed considering low superficial liquid velocities, in which the cross-sectional average liquid velocity relative to local liquid velocities is negligible; a continuous stream of liquid tracer introduced uniformly at the top of the column, and steady state operation. The convection-diffusion equation proposed under the previous considerations is:

$$\frac{1}{r} \frac{\partial}{\partial r} \varepsilon_L(r) D_{rr}(r) r \frac{\partial c}{\partial r} = \varepsilon_L(r) u_z(r) \frac{\partial c}{\partial z} - \varepsilon_L(r) D_{zz}(r) \frac{\partial^2 c}{\partial z^2} \quad (3.127)$$

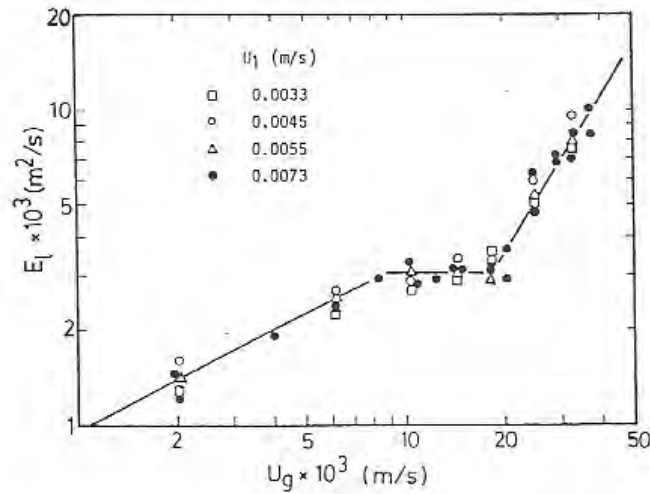


Figure 3.16. Axial dispersion coefficient obtained by Ityokumbul *et al.* (1994) for air-water system

Eq. (3.127) is written for the well-developed flow region (middle portion of the recirculation cell) where ε_L , u_z , D_{rr} and D_{zz} are functions of radial position only. The authors made some mathematical manipulations to demonstrate that Eq. (3.127) can be simplified to:

$$D_{eff} \frac{d^2 \bar{c}}{dz^2} - \bar{u} \frac{d\bar{c}}{dz} = 0 \quad (3.128)$$

where \bar{c} is the cross-sectional average concentration and D_{eff} the effective axial dispersion considered as the contribution of two terms: a Taylor-type diffusivity D_{Taylor} and \bar{D}_{zz} the mean axial eddy diffusivity.

Experimental data obtained by the authors and other researchers are shown in Figure 3.17.

Krishna *et al.* (2000) worked with 4-m high bubble columns of three different diameters: 0.174, 0.38 and 0.63 m. The fluids used were demineralized water or oil as the liquid phase and air as the gas phase, being batch liquid the mode of operation. The correlation proposed by the authors is:

$$D_z = 0.31 u_{Lc} d_c \quad (3.129)$$

where u_{Lc} is the center-line liquid velocity.

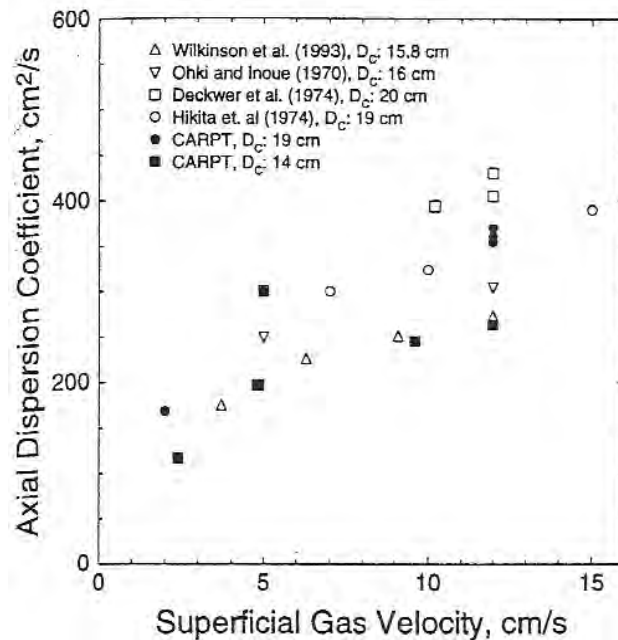


Figure 3.17. Axial dispersion coefficient (Degaleesan and Dudukovic, 1998)

Moustiri *et al.* (2001) made an analysis of the expressions proposed in single-phase flow of the Péclet number and the changes that experiments to be applied in two-phase flow using the proposal of Joshi (1980). They proposed for two-phase flow the following expressions:

$$\text{Pe} = \frac{1.3H \text{Re}_L^{0.1}}{d_c(1-\varepsilon_G) \left[\left(\frac{1}{1-\varepsilon_G} \right) + \left(\frac{1}{235} \right) \left(\frac{\text{Re}_L}{\text{Fr}_G^{1/3}} \right)^{-2/3} \text{Ga}^{0.6} \right]} \quad (3.130)$$

$$\text{Bo} = \frac{1.3 \text{Re}_L^{0.1}}{(1-\varepsilon_G) \left[\left(\frac{1}{1-\varepsilon_G} \right) + \left(\frac{1}{235} \right) \left(\frac{\text{Re}_L}{\text{Fr}_G^{1/3}} \right)^{-2/3} \text{Ga}^{0.6} \right]} \quad (3.131)$$

where authors defined Péclet and Bodenstein number as $\text{Pe} = u_L H / (1 - \varepsilon_G) D_z$ and $\text{Bo} = u_L d_c / (1 - \varepsilon_G) D_z$ respectively.

Bin *et al.* (2001) determined the liquid dispersion coefficient in a 0.15-m diameter and 5.5-m high with water and ozone as liquid and gas phase respectively; in different modes of operation: co-current, counter-current, and batch. The flow rates were in the ranges of 0.3 to 1.2 STP m³/h for the gas and 0.10 to 0.45 m³/h for the liquid phase. They obtained that the liquid dispersion coefficient increases with the liquid velocity in operating modes. Additionally, the liquid dispersion coefficient was between 1×10^{-3} and 7×10^{-3} m²/s. The expression used to evaluate the liquid dispersion coefficient was Eq. (3.78) with the following initial and boundary conditions:

$$\begin{aligned} z > z_0 \wedge t \leq 0 &\Rightarrow c = 0 \\ z = z_0 \wedge t > 0 &\Rightarrow c = f(t) \\ z \rightarrow \infty \wedge t > 0 &\Rightarrow c \rightarrow 0 \end{aligned}$$

where $f(t)$ is the injection pulse. The solution of Eq. (3.93) in the Laplace space is:

$$\bar{c}_2(s) = \bar{c}_1(s) \exp \left[\frac{H}{2D_z} \left(u_L - \sqrt{u_L^2 + 4sD_z} \right) \right] \quad (3.132)$$

where $\bar{c}_1(s)$ and $\bar{c}_2(s)$ are the tracer concentrations measured at points 1 and 2 respectively, in the column in the Laplace space. The authors calculated the moments from the transmittance $F(s)$:

$$F(s) = \frac{\bar{c}_2(s)}{\bar{c}_1(s)} = \exp\left[\frac{H}{2D_z}\left(u_L - \sqrt{u_L^2 + 4sD_z}\right)\right] \quad (3.133)$$

The moments are:

$$\Delta\mu = \frac{F'(s)}{F(s)} = \mu_2 - \mu_1 \quad (3.134)$$

$$\Delta\sigma^2 = \frac{d}{ds}\left[\frac{F'(s)}{F(s)}\right] = \sigma_2^2 - \sigma_1^2 \quad (3.135)$$

From these equations, the residence time of the tracer and the Péclet number can be expressed as:

$$\tau = \frac{\Delta\mu}{\sqrt{1 - 2s\Delta\sigma^2/\Delta\mu}} = \frac{H}{u_L} \quad (3.136)$$

$$\text{Pe}_L = \frac{u_L H}{D_z} = 2 \frac{(\Delta\mu)^2}{\Delta\sigma^2} \sqrt{1 - 2s \frac{\Delta\sigma^2}{\Delta\mu}} \quad (3.137)$$

Wild *et al.* (2003) mentioned that mixing is purely dispersive and the ADM model is used to represent it in bubble columns. Aris (1959) showed that a perfect pulse function is unnecessary if the transient tracer concentration is measured at two points in the system. The additional advantages of this technique are: (i) the method can be used to determine the parameters of any model that can be represented by a transfer function and (ii) the detector dynamics can be neglected in data processing if the detectors are identical (Ostergaard and Michelsen, 1969). The disadvantage is that the determination of the dispersion coefficient or the Bodenstein number is usually based on the calculus of the second moment from experimental concentration-time data in two points located in the system (due the tails of experimental data), which causes error on the second moments.

The expressions proposed by Ostergaard and Michelsen (1969) to study the mixing in an open system are the following:

$$\mu_2 - \mu_1 = \tau \quad (3.138)$$

$$\sigma_2^2 - \sigma_1^2 = \frac{2\tau^2}{Bo} \quad (3.139)$$

where Bodenstein number is defined as Eq. (3.81) but the characteristic length is the distance between measuring points. Equation (3.139) was proposed originally by Aris (1959) who simplify the original expression for open-open boundary condition presented in Eq. (3.82).

The moments were computed by authors as follows (Ostergaard and Michelsen, 1969):

$$\mu_j = \frac{\sum_i^N c_i(t) t_i \Delta t}{\sum_i^N c_i(t) \Delta t} \quad j=1,2 \quad (3.140)$$

$$\sigma_j^2 = \frac{\sum_i^N c_i(t) t_i^2 \Delta t}{\sum_i^N c_i(t) \Delta t} - \mu_j^2 \quad j=1,2 \quad (3.141)$$

The form of transfer function is described through the expression:

$$F(s) = \frac{c_2(s)}{c_1(s)} = \frac{\int_0^\infty c_2(t) \exp(-st) dt / \int_0^\infty c_2(t) dt}{\int_0^\infty c_1(t) \exp(-st) dt / \int_0^\infty c_1(t) dt} \quad (3.142)$$

$F(s)$ is calculated assuming arbitrary values of s having n values of $F(s)$ permitting evaluate numerically the parameters of the model.

When Laplace transform is applied to axial dispersion model, the following expression is obtained:

$$F(s) = \exp \left\{ \frac{\text{Bo}}{2} \left[1 - \left(1 + \frac{4s\tau}{\text{Bo}} \right)^{1/2} \right] \right\} \quad (3.143)$$

Ostergaard and Michelsen (1969) proposed a manipulation of the last equation to plot in the easy way to obtain the Bo number:

$$\left[\ln \left(\frac{1}{F(s)} \right) \right]^{-1} = \tau s \left[\ln \left(\frac{1}{F(s)} \right) \right]^{-2} - \frac{1}{\text{Bo}} \quad (3.144)$$

where the intercept of a plot of $\left[\ln \left(\frac{1}{F(s)} \right) \right]^{-1}$ as a function of $s \left[\ln \left(\frac{1}{F(s)} \right) \right]^{-2}$ gives the inverse of negative Bo number and the slope, τ .

Forret *et al.* (2003) determined the liquid velocity with an improved Pitot tube and the liquid backmixing by conductivity measurements of tracer concentrations. They determined the axial-dispersion coefficient based on the upflow and downflow regions inside bubble column. They took simultaneous series-tracer samples at dimensionless radial positions of 0.35 (upflow region) and 0.85 (downflow region). They weighted these two concentrations by the liquid-phase holdups to obtain an average concentration, \bar{c} :

$$\bar{c} = \frac{(1 - \varepsilon_{Gu})c_u + (1 - \varepsilon_{Gd})c_d}{2(1 - \varepsilon_G)} \quad (3.145)$$

where ε_{Gd} and ε_{Gu} are the gas holdups of the downflow and upflow liquid flow and c_d and c_u are the tracer concentration in the downflow and upflow liquid flow region, respectively. They ran simulations of the one- and two-dimensional dispersion models to compare them to each other. They wrote the one- and two-dimensional dispersion models as follows:

$$\frac{\partial \bar{c}}{\partial t} = D_{ax,1D} \frac{1}{H^2} \frac{\partial^2 \bar{c}}{\partial z^{*2}} \quad (3.146)$$

$$\frac{\partial c}{\partial t} = D_{ax,2D} \frac{1}{H^2} \frac{\partial^2 c}{\partial z^{*2}} - u_L(r') \frac{1}{H} \frac{\partial c}{\partial z^*} + \frac{D_{rad,2D}}{[1 - \varepsilon_G(r')]} \frac{\partial}{\partial r'} \left\{ [1 - \varepsilon_G(r')] \frac{\partial c}{\partial r'} \right\} + \frac{D_{rad,2D}}{r'} \frac{\partial c}{\partial r'} \quad (3.147)$$

where $D_{ax,1D}$ and $D_{ax,2D}$ are the axial-dispersion coefficient determined by the one- and two-dimensional models, $D_{rad,2D}$ is the radial-dispersion coefficient determined by the two-dimensional model, and $u_L(r')$ the local axial liquid velocity represented as:

$$u_L(r') = \frac{u_{Lc}(0)}{1.128} \left[2.976 \exp(-0.943r'^2) - 1.848 \right] \quad (3.148)$$

In the cases that researchers did not use internals in the bubble column formed by 56 tubes of 63 mm diameter arranged in a square pitch of 108 mm, the one- and two-dimensional models gave similar results at superficial gas velocity of 0.15 m/s, $z^*=0.42$. The axial dispersion coefficient of one-dimensional model was 0.5 m²/s. For the two-dimensional model, the axial dispersion coefficient to radial dispersion coefficient ratio was 20. At the same conditions, both models differ greatly obtaining the best fit with two-dimensional model at $D_{ax,2D}/D_{rad,2D} = 400$. The authors explained this behavior through the increase of liquid recirculation velocity and decrease in fluctuating velocity and recommended the use of one-dimensional model in large bubble columns without internals.

Camacho *et al.* (2004) worked in 0.193-m diameter and 2.3-m high bubble column with tap and salt water as liquid phase and superficial gas velocity up to 0.051 m/s. They considered the dispersion coefficient in radial and axial directions in their study obtaining that radial is 1% of the axial dispersion coefficients under any given condition.

The dimensionless tracer mass balance proposed by Camacho *et al.* (2004) is:

$$\frac{\partial c^*}{\partial \theta} = \frac{\partial^2 c^*}{\partial z^{*2}} - \frac{u_L H}{(1 - \varepsilon_G) D_z} \frac{\partial c^*}{\partial z^*} + \frac{1}{r'} \frac{\partial c^*}{\partial r'} + \frac{\partial^2 c^*}{\partial r'^2} \quad (3.149)$$

They considered the case of batch operation mode in the liquid phase and applied the following boundary conditions:

$$\begin{aligned} r' = 0, \quad \partial c^* / \partial r' &= 0 \\ r' = R/H\sqrt{D_z/D_r} = \beta', \quad \partial c^* / \partial r' &= 0 \\ \theta > 0 \text{ and } z^* = 0, \quad \partial c^* / \partial z^* &= 0 \text{ (at the surface of the dispersion)} \\ \theta > 0 \text{ and } z^* = 1, \quad \partial c^* / \partial z^* &= 0 \text{ (at the bottom of the system)} \end{aligned}$$

The authors solved Eq. (3.149) resulting in:

$$c^* = \sum_{j=1}^{\infty} \frac{J_0(v_j r')}{J_0^2(v_j \beta')} \exp(-v_j^2 \theta) \left[1 + 2 \sum_{m=1}^{\infty} \cos(m\pi z^*) \exp(-m^2 \pi^2 \theta) \right] \quad (3.150)$$

Camacho *et al.* (2004) found that the axial-dispersion model gives a slight underestimation of the axial-dispersion coefficient; the latter is consistent with published empirical expressions to evaluate this parameter.

3.5.5. Modified mixing cell model

The model assumes that each cell contains stagnant and flowing regions, occurring mass exchange between both regions. When the number of cells is large, the model is represented through differential equations that Deans (1963) as Shah *et al.* (1978) solved for a pulse injection:

$$E(t) = \exp(-e\tau) \delta(t - t_i) + \left(\frac{e^2\tau}{f}\right) \exp\left\{-e\tau\left[2 + \left(\frac{t-\tau}{f\tau}\right)\right]\right\} \left\{ \frac{I_1\left[2e\tau\left(1 + \frac{t-\tau}{f\tau}\right)^{1/2}\right]}{e\tau\left(1 + \frac{t-\tau}{f\tau}\right)^{1/2}} \right\} \quad (3.151)$$

where e (exchange coefficient between flowing and stagnant liquid) and f (fraction of stagnant liquid) are the parameters of the model. These parameters are calculated from the manipulation of the following expressions:

$$f = 1 - \left(\frac{t_i}{\tau}\right) \quad (3.152)$$

$$\sigma_\theta^2 = \frac{2f^2}{e\tau} \quad (3.153)$$

where t_i is the time at which tracer first appears in the effluent and σ_θ^2 is the dimensionless second moment of response curve.

4. EXPERIMENTAL PROCEDURE

In this section, a description of experimental setup, materials, and data analysis is presented.

4.1. Experimental equipment

The experimental setup is shown in Figure 4.1. The main components are: a column made up by two cylindrical sections of Plexiglas of 0.20 m of inner diameter and an entrance cone, a self-metering pump, two plastic feed tanks, filter devices, a rotameter to measure the gas flow rate, and a pressure transducer connected to a data acquisition system. The cylindrical sections have 7 equally-spaced sampling ports alongside, used to measure local pressure or to draw samples; the pump is Milton-Roy, model HMRB1-0711-140SM designed to be used with liquids and slurries or suspensions; the tanks are Nalgene 400 L each; and rotameter is from Brooks Instrument with a rate range of 6×10^{-4} to 6×10^{-3} m³/s; and the differential pressure transducer, from Omega, part no. PX771A-300WDI, and a range of 0-50 to 0-300 in H₂O is connected to a data acquisition system, a Data Logger of the series OM-CP-PROCESS101 from Omega. The pressure transducer and data acquisition system were used to measure the pressure drop between top and bottom in the bubble column. Figure 4.2 shows a photograph of the experimental setup while Figure 4.3 shows a photograph of the pressure transducer.

To measure the tracer concentrations and to study the rheological behavior of polymeric solutions, a spectrophotometer and a rheometer respectively, are available in laboratories in the Chemical Engineering Department.

A spectrophotometer Cecil 3000 was used to analyze samples taken from the top of the bubble column when an impulse of tracer (methylene blue) was injected at the bottom of the column. This was done to study the mixing of the liquid phase by using residence time distribution (RTD) experiments. Figure 4.4 shows a photograph of this spectrophotometer.

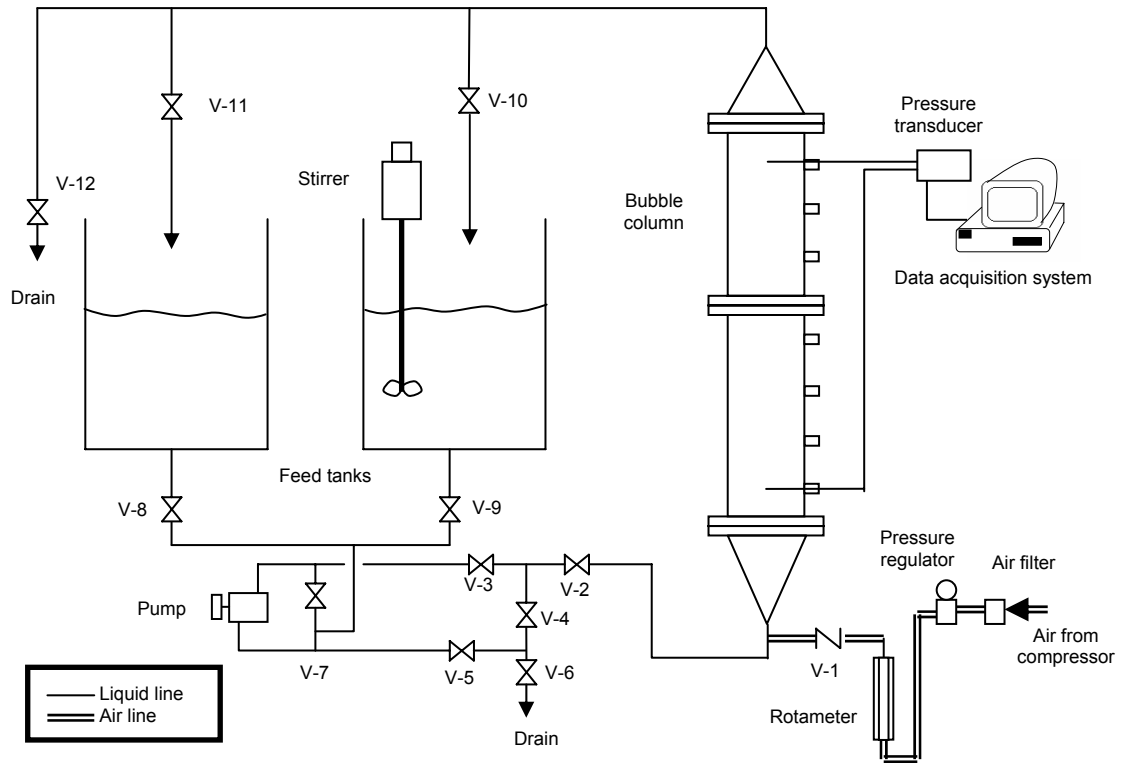


Figure 4.1. Experimental setup



Figure 4.2. Experimental setup



Figure 4.3. Differential pressure transducer



Figure 4.4. Cecil 3000 spectrophotometer

A StressTech rheometer of ATS Rheosystem was used for the rheological characterization of the CMC aqueous solutions at different conditions (concentrations, time of dilution, and temperature). A photograph of this rheometer is shown in Figure 4.5.



Figure 4.5. StressTech rheometer

The rheometer has a normal force sensor, which provides a wide dynamic range and can be used for both user-selectable, constant-force loading and quantitative normal-force measurements. Neither the normal force nor torque signals interfere with the motion or apply any external forces on the air bearing. The instrument has automatic, real time, inertia compensation (not a software correction after the data are collected) and automatic temperature compensation of the gap during temperature sweep experiments. The instrument is built of modules as shown in the Figure 4.6.

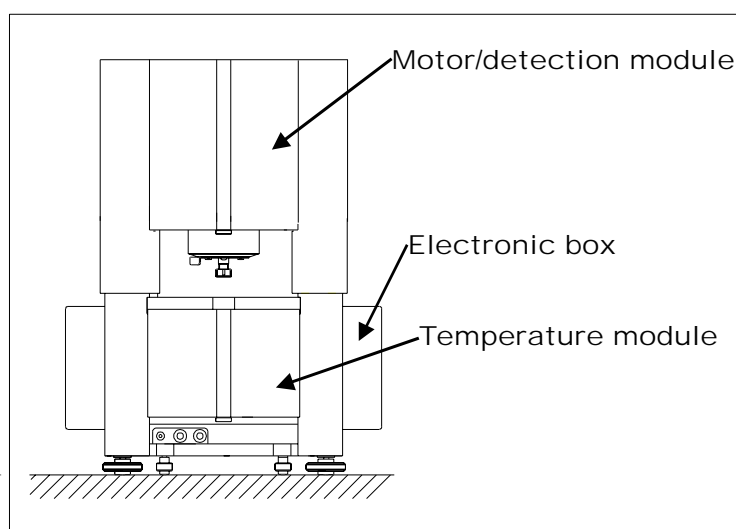


Figure 4.6. Modules of the rheometer

The motor/detector module is shown in Figure 4.7. The drag-cup motor applies a torque to the rotor and the position sensor measures the angular deflection during rotation. The rotational speed depends on the properties of the sample. The whole system runs on an air bearing to avoid friction between rotating and static parts. The spindle attached to the chuck in Figure 4.7 spins close to a static base (not shown). Various geometries for the spindle/base combination can be used depending on the viscosity range of the sample. Available geometries in this laboratory are double gap, plane plates, and cone-plate. The temperature is manipulated and controlled by a temperature module, a water jacket, which is used with an external liquid circulator.

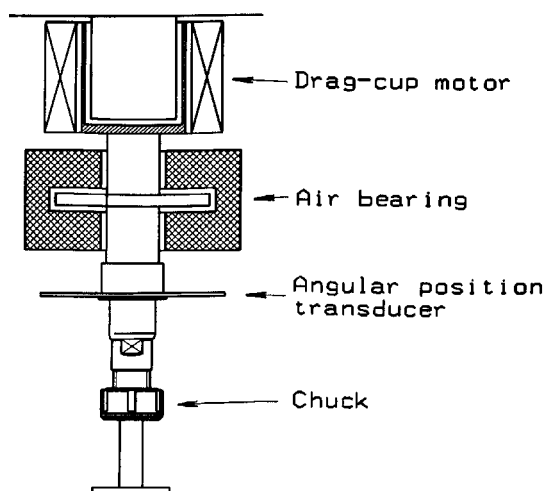


Figure 4.7. Motor/detector module of the rheometer

4.2. Materials

Aqueous solutions of carboxymethylcellulose (provided by Noviant) at different concentrations, which are known to exhibit non-Newtonian behavior, were used in the experiments. Methylene blue was used as the tracer in the residence time distribution (RTD) experiments. The tracer was injected in the form of concentrated aqueous solutions. Filtered air from a compressor was used as the gas phase in this research.

4.3. Experimental method

This section shows the description of the procedure followed. It contains two parts: the rheological characterization of the liquid phase and the experiments in the bubble column to measure gas holdup and the liquid-mixing parameter.

4.3.1. Rheological characterization of the liquid phase

Aqueous CMC solutions were characterized rheologically through the StressTech Rheometer of ATS Reologica. Different concentrations of CMC solutions were

analyzed in the rheometer changing the shear rate to obtain the viscosity and shear stress as function of this variable; then, viscosity and flow curves were plotted. From flow curves, experimental data were fit to the power-law rheological model and its parameters were regressed as a function of CMC concentration. In addition, an analysis of the rheology of CMC solutions at various times of dissolution was done. The CMC provided by Noviant is a powder that dissolves in water. Therefore agitation with a magnetic stirrer is used. Once the powder is dissolved in water, a timer is started. The rheological behavior of the solution is measured at various dissolution times. Additionally, the effect of the temperature on the rheology of the CMC solutions was also studied. Due to the possibility of CMC degradation because of the presence of some chemicals used as tracer in RTD experiments, both the original CMC solution (with no tracer) and corresponding solution with a tracer dissolved in it were subjected to a rheometric characterization, doing a regression of the parameters of the power-law model as a function of temperature. Finally, to complete the rheology studies of aqueous CMC, dynamic tests were carried out to determine the viscoelastic behavior of the polymeric solutions, including their characteristic moduli.

The tests in the rheometer were done placing 11 ml of the sample to be analyzed inside a double-gap geometry, and the viscosity and shear stress curves were measured at different shear rates. These data were plotted and fit to a rheological model, obtaining the best estimates of the parameters of such model. These rheological parameters were used in the correlations of pressure drop, two-phase factor, gas holdup and liquid-phase mixing parameter obtained in this work.

The dynamic tests are done in general to study linear viscoelastic materials at small-amplitude oscillatory shear. Qualitative analyses can be made when storage and loss moduli are plotted versus oscillation frequency in the same graph. If these curves intersect, the material will have a viscoelastic behavior. The frequency at which these curves cross over (intersect) is called shear frequency. This shear frequency divides the graph in two regions: a region where the material's behavior is mostly viscous ($G' > G''$) and a region where it is mostly elastic ($G' < G''$). As a consequence of the

addition of dynamic tests, a complete characterization of CMC solutions was achieved in this work.

4.3.2. Bubble column experiments

Two types of experiments were carried out: continuous (the gas and liquid phases are fed continuously in the column in the bottom of the column, flowing in this case in ascendant and cocurrent mode) and semicontinuous modes (the gas phase flow in ascendant mode while the liquid phase was charged to the column at the beginning of the operation). First the CMC solution was prepared in one of the feed tanks. Runs were carried out at various gas and liquid superficial velocities and at various concentrations of CMC.

By opening the appropriate valves and turning on the pump, the column was filled with the liquid phase. Using the micrometering valve, the air flow was set to a desired value of a gas superficial velocity following the calibration curve done previously and presented in figures B.1 and B.2 of Appendix B, similarly, a calibration curve was done for the pump at different positions of the axis that permits to change the flow rate of liquid in it (Table B.3 of the Appendix B shows the calibration curve of the pump). When the column reached steady state, a pulse of tracer (aqueous methylene blue solution) was injected at the lowest sampling port and the samples were drawn from the highest sampling port. The samples were taken from the top until the blue color of the injected tracer tone down totally (continuous tests) or becomes homogeneous in all bubble column (batch tests). In addition, the pressure drop was recorded continuously by means of the pressure transducer and the data acquisition system. Then, the inlet valves of air and liquid were closed and the pump turned off. The final height of the liquid in the column was measured after phase disengagement.

The procedure for semicontinuous operation was similar except that bubble column was filled with liquid, the pump was turned off and the exit valve of the pump to bubble column closed.

On the other hand, concentration of the tracer injected in the column was measured by means of a spectrophotometer, in which absorbance of each sample was measured and converted to concentration through a calibration curve made previously for each concentration of polymer in the liquid phase (Figures B.4 through B.8 of the Appendix B).

The experimental design considered was a factorial of three factors with mixture levels: three levels of concentration of polymer in the liquid phase, six levels for gas superficial velocity (three levels for each flow regime found) and two levels for liquid superficial velocity. The first runs done to observe the behavior of the bubble column at different superficial velocities of the phases permitted to conclude that liquid superficial velocity have no influence over parameters considered in this work in the range permitted by the pump of the experimental setup. The experimental conditions considered are shown in Table 4.1.

Table 4.1. Experimental runs and conditions

Run	Polymer concentration (% wt)	u_G (m/s)	u_L (m/s)
88, 90	0	0.0010	0
235	0	0.0083	0
225	0	0.0145	0
112	0	0.0308	0
236	0	0.0385	0
95	0	0.0462	0
239	0	0.0010	0.0045
230	0	0.0083	0.0045
231	0	0.0145	0.0045
126	0	0.0308	0.0045
238	0	0.0385	0.0045
127	0	0.0462	0.0045
212	0.20	0.0010	0
206, 214	0.20	0.0083	0
207	0.20	0.0145	0

Table 4.1. Experimental runs and conditions (cont.)

Run	Polymer concentration (% wt)	u_G (m/s)	u_L (m/s)
208	0.20	0.0308	0
209	0.20	0.0385	0
210	0.20	0.0462	0
223	0.20	0.0010	0.0045
216	0.20	0.0083	0.0045
217	0.20	0.0145	0.0045
218	0.20	0.0308	0.0045
219	0.20	0.0385	0.0045
220	0.20	0.0462	0.0045
232	0.40	0.0010	0
215	0.40	0.0083	0
224	0.40	0.0145	0
213	0.40	0.0308	0
226	0.40	0.0385	0
228	0.40	0.0462	0
237	0.40	0.0010	0.0045
222	0.40	0.0083	0.0045
233	0.40	0.0145	0.0045
227	0.40	0.0308	0.0045
229	0.40	0.0385	0.0045
234	0.40	0.0462	0.0045

Additionally, other experimental conditions were studied previously to establish the flow regimes that are present in the system and select the superficial velocities to be considered. These conditions are shown in Table 4.2.

Table 4.2. Additional experimental conditions studied

Run	Polymer concentration (% wt)	u_G (m/s)	u_L (m/s)
111	0	0.0027	0
82	0	0.0034	0
93	0	0.0034	0
89	0	0.0055	0
86	0	0.0112	0
94	0	0.0112	0
87	0	0.0206	0
106	0	0.0034	0.0007
108	0	0.0112	0.0007
107	0	0.0308	0.0007
99	0	0.0010	0.0017
103	0	0.0027	0.0017
100	0	0.0034	0.0017
101, 102, 110, 113	0	0.0112	0.0017
109	0	0.0112	0.0017
92	0	0.0010	0.0025
104	0	0.0027	0.0025
96	0	0.0034	0.0025
97	0	0.0112	0.0025
105	0	0.0308	0.0025
98	0	0.0462	0.0025
129	0	0.0027	0.0045
128	0	0.0112	0.0045
130, 131	0	0.0206	0.0045
164, 165	0.05	0.0010	0.0045
203	0.10	0.0010	0
204, 205	0.10	0.0083	0
201, 202	0.15	0.0010	0
166	0.15	0.0385	0
178	0.15	0.0385	0.0025
211	0.30	0.0308	0

4.4. Data Analysis

The experimental data obtained in this work were analyzed as follows:

4.4.1. Rheological characterization

As a result of the rheological measurements made with a StressTech rheometer of ATS Rheosystem, the apparent viscosities, shear rate, and shear stress are obtained for each polymer concentration. Flow curves were plotted and the parameters of the power-law model were obtained from the fit of these experimental data. The rheological parameters were obtained as a function of the polymer concentration in aqueous solutions of CMC. Additionally, the data obtained of viscosity and shear stress as a function of shear stress were used to study the effect of temperature on the rheology of CMC solutions and from this analysis the data of flow curves were regressed to obtain the power-law parameters as a function of temperature.

Also, the results of dynamic tests were plotted to analyze the viscoelastic behavior of the CMC solutions, and determine which effect prevails (viscosity or elasticity).

4.4.2. Bubble column experiments

The experimental data obtained from the bubble column were used to determine the pressure drop, the two-phase friction factor, the mean gas holdup, and liquid-mixing parameter.

The pressure drop measurements were plotted to study the effect of liquid and gas superficial velocities on this variable. Similar plots were done to obtain the effect of CMC concentrations. Due to the presence of two slopes in these plots, two flow regimes were identified confirming the visual observations.

Taking into account the complete force balance, the two-phase friction factor was calculated from the total pressure drop measured, neglecting only the accelerational contribution due to the constant sectional, no phase changes and incompressible liquid.

The two-phase friction factor was plotted as a function of superficial velocities and CMC concentrations, and as result of these plots, this friction factor was correlated as a function of gas superficial velocity for each liquid superficial velocity.

The operation and clear liquid heights upon phase disengagement were used to calculate the mean gas holdup. Additionally, the pressure drop obtained from the pressure transducer allowed to check the gas holdup obtained from the disengagement method, using a simplified force balance in the bubble column.

The data of gas holdup and pressure drop were correlated considering the two slopes observed in gas holdup and pressure drop versus gas superficial velocity plots for Newtonian (tap water) and non-Newtonian (CMC solutions) fluids. Several expressions were obtained from regression of these experimental data for each flow regime as a function of superficial gas velocity and rheological parameters of the power-law model obtained at the temperature of the solution during the experimental session in the bubble column.

Finally, exit concentrations of tracer in the residence time distribution experiments were analyzed through the axial dispersion model and tank-in-series model using the moment theory and direct fit of the experimental data to the model. As a result of this procedure, the number of tanks in series, Bodenstein number and axial dispersion coefficient in the liquid phase were found, taking into account the multiphase system used in this case (gas and liquid phases involved in the experiments). Axial dispersion coefficient data were correlated for each flow regime as a function of superficial velocities of gas and liquid phases, and rheological parameters of the power-law model.

The expressions of gas holdup and axial dispersion coefficient obtained were compared to another expressions proposed by other authors. A comparison of two-phase friction factor to Shirsat *et al.* (2003) and Mandal *et al.* (2004) correlations was tried but it was not possible and it is discussed in Chapter 5.

5. EXPERIMENTAL RESULTS AND DISCUSSION

The results obtained in this dissertation following the procedures and strategies described in Chapter 4 are presented in this chapter. Results include those corresponding to the rheological study, which are presented first, and those corresponding to the bubble column experiments. All values obtained in this work were tabulated in Appendix C.

5.1. Rheology results

The rheology results are structured in different subsections as follows.

5.1.1. Rheology of CMC solutions at 25 °C

Figure 5.1 and Figure 5.2 show the results obtained at 25°C, for solutions of the weight percents: 0.05, 0.10, 0.15, 0.20, 0.25, 0.30, 0.50, and 0.75%. All solutions showed a shear-thinning behavior as indicated by the viscosity decrease with shear rate shown in Figure 5.1. Consequently, the shear-stress-versus-shear-rate curves shown in Figure 5.2 are concave. It is important to mention that the curves showed in these two figures were obtained at a dissolution time of two hours.

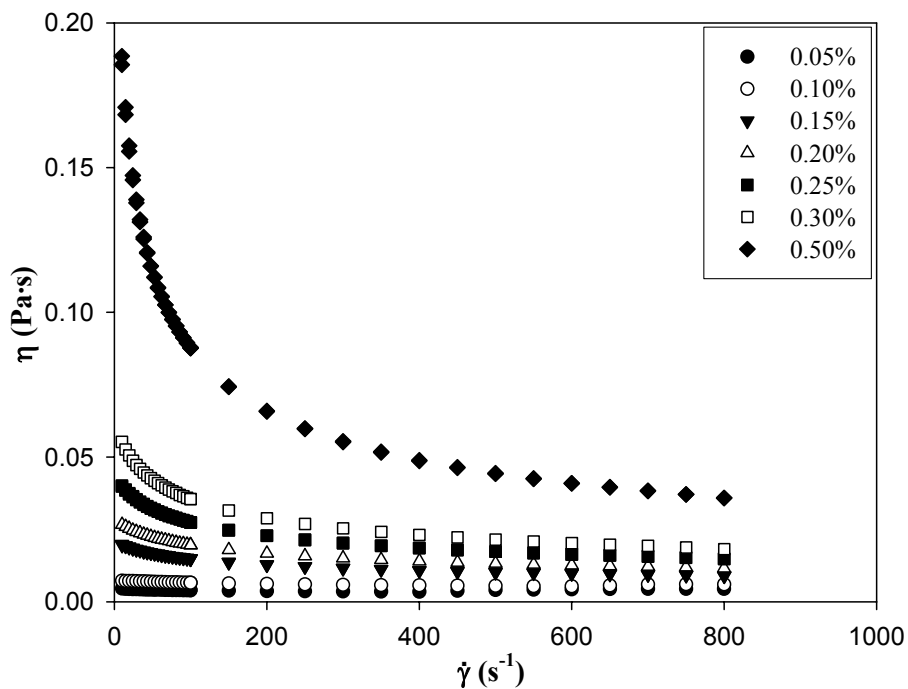


Figure 5.1. Viscosity curves for dissolution time of 2 h

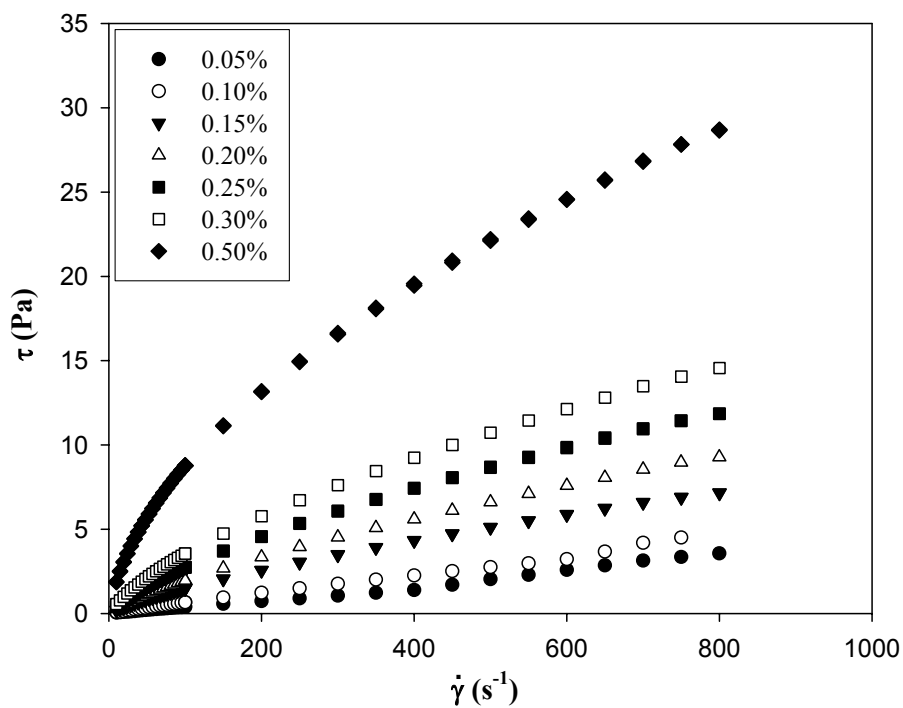


Figure 5.2. Flow curves for dissolution time of 2 h

Figure 5.3 shows the power-law model parameters obtained at varying concentrations of the CMC solutions prepared at 25°C and with two hours of the polymer dissolution. It is observed that k increases with CMC concentration, due to the increase of the flow resistance (viscosity), while n decreases with CMC concentration. The value of n is less than 1 indicating that CMC solutions are shear-thinning; also, higher CMC concentrations produce an increase in their shear-thinning behavior.

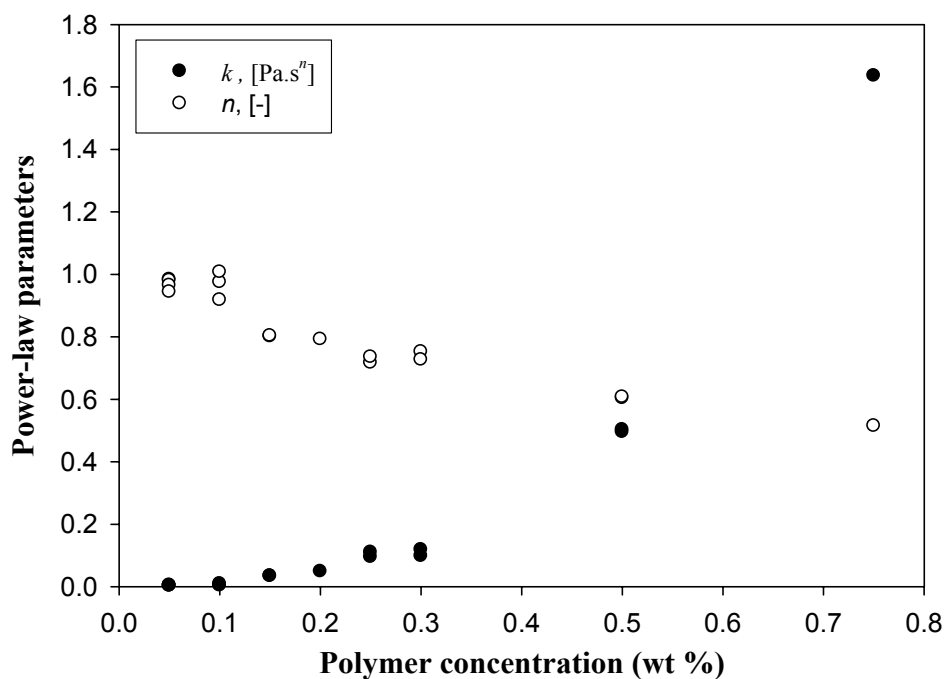


Figure 5.3. Consistency index (k) and flow index (n) of the power-law model for CMC solutions for dissolution time of 2 h

5.1.2. Thixotropic behavior of CMC solutions

Although it is not uncommon to see a thixotropic behavior in polymer solutions, this was not observed for CMC solutions. To illustrate this, Figure 5.4 shows results for 0.15% by weight CMC solution. Open circles represent points for increasing shear rates while crosses represent those for decreasing shear rates. Both resulting curves coincide indicating no thixotropic behavior. Similar analyses were made at other CMC concentrations of 0.25% and 0.50% (Figures 5.5 and 5.6, respectively) by weight and no

thixotropic behavior was observed. The corresponding data were fit quite well through the power-law model, in which the values of the parameters k and n obtained by regression of the data for increasing and decreasing shear rate, as shown in Tables 5.1 and 5.2.

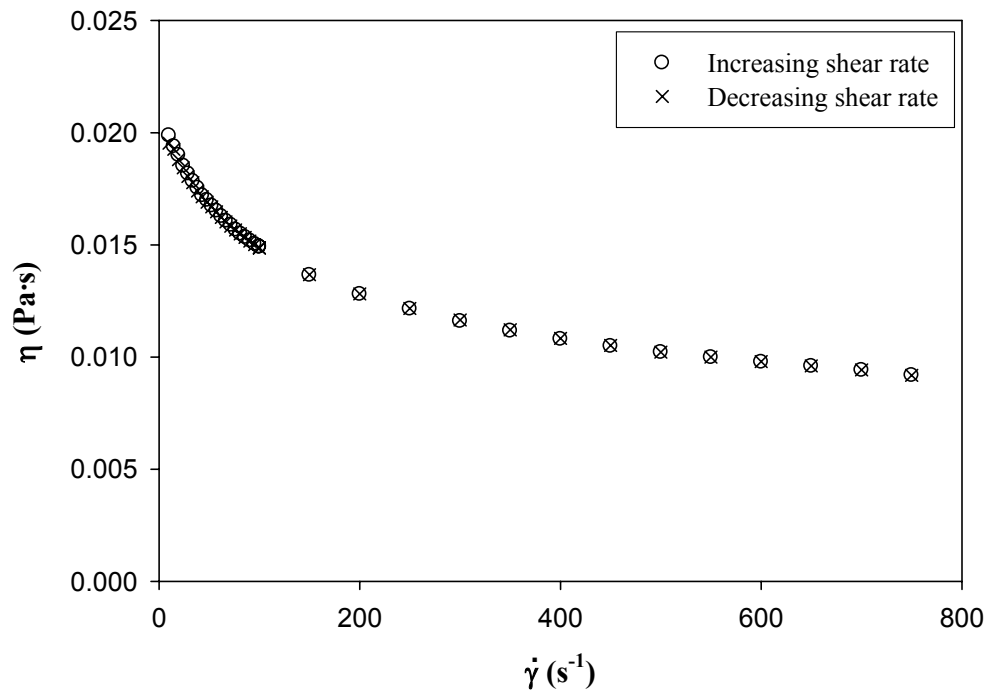


Figure 5.4. Thixotropy test for 0.15% CMC solution

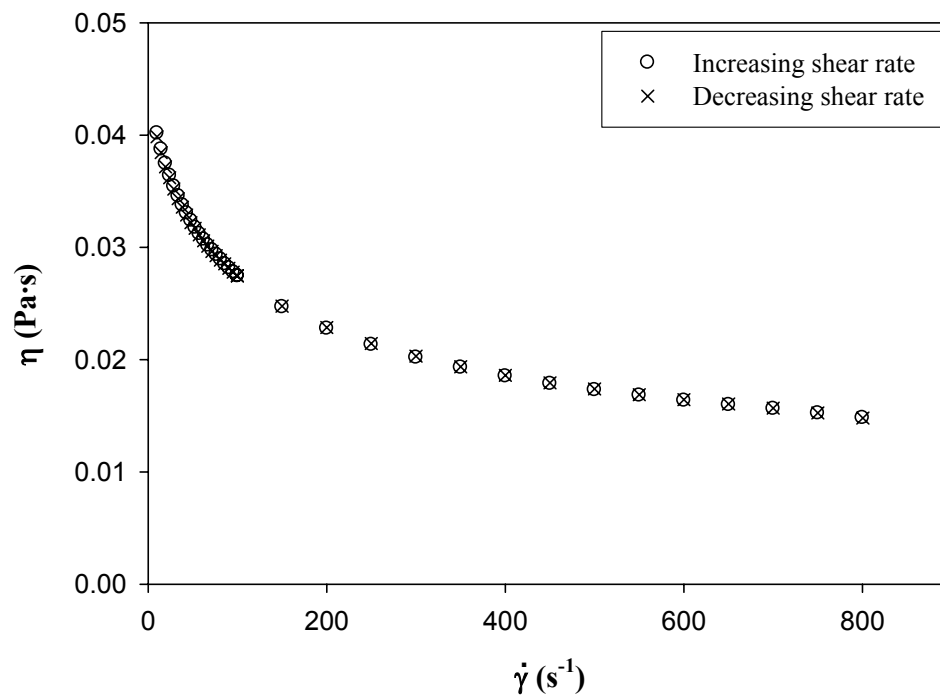


Figure 5.5. Thixotropy test for 0.25% CMC solution

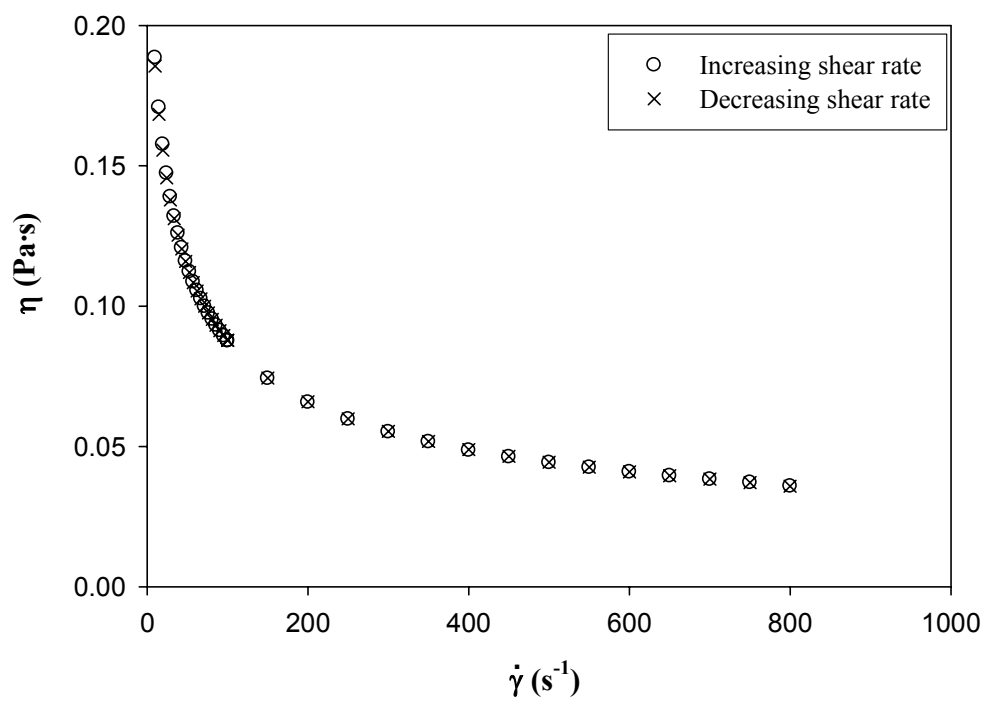


Figure 5.6. Thixotropy test for 0.50% CMC solution

Table 5.1. Consistency index for CMC solutions at increasing and decreasing shear rates

Polymer concentration (%wt)	Condition	Consistency index k , (Pa·s ^{<i>n</i>})
0.15	Increasing shear rate (R ² =0.9997)	$(4.3 \pm 0.3) \times 10^{-2}$ 99% confidence interval: $4.1 \times 10^{-2} \leq k \leq 4.7 \times 10^{-2}$
	Decreasing shear rate (R ² =0.9996)	$(4.3 \pm 0.3) \times 10^{-2}$ 99% confidence interval: $4.1 \times 10^{-2} \leq k \leq 4.6 \times 10^{-2}$
0.25	Increasing shear rate (R ² =0.9996)	$(1.02 \pm 0.06) \times 10^{-1}$ 99% confidence interval: $9.5 \times 10^{-2} \leq k \leq 1.08 \times 10^{-1}$
	Decreasing shear rate (R ² =0.9995)	$(1.01 \pm 0.07) \times 10^{-1}$ 99% confidence interval: $9.4 \times 10^{-2} \leq k \leq 1.08 \times 10^{-1}$
0.50	Increasing shear rate (R ² =0.9997)	$(6.0 \pm 0.2) \times 10^{-1}$ 99% confidence interval: $5.7 \times 10^{-1} \leq k \leq 6.2 \times 10^{-1}$
	Decreasing shear rate (R ² =0.9995)	$(6.0 \pm 0.2) \times 10^{-1}$ 99% confidence interval: $5.7 \times 10^{-1} \leq k \leq 6.2 \times 10^{-1}$

Table 5.2. Flow index for CMC solutions at increasing and decreasing shear rates

Polymer concentration (%wt)	Condition	Flow index n , (-)
0.15	Increasing shear rate ($R^2=0.9997$)	$(7.6 \pm 0.1) \times 10^{-1}$ 99% confidence interval: $7.5 \times 10^{-1} \leq n \leq 7.7 \times 10^{-1}$
	Decreasing shear rate ($R^2=0.9996$)	$(7.7 \pm 0.1) \times 10^{-1}$ 99% confidence interval: $7.6 \times 10^{-1} \leq n \leq 7.8 \times 10^{-1}$
0.25	Increasing shear rate ($R^2=0.9996$)	$(7.1 \pm 0.1) \times 10^{-1}$ 99% confidence interval: $7.0 \times 10^{-1} \leq n \leq 7.2 \times 10^{-1}$
	Decreasing shear rate ($R^2=0.9995$)	$(7.2 \pm 0.1) \times 10^{-1}$ 99% confidence interval: $7.1 \times 10^{-1} \leq n \leq 7.3 \times 10^{-1}$
0.50	Increasing shear rate ($R^2=0.9997$)	$(5.8 \pm 0.2) \times 10^{-1}$ 99% confidence interval: $5.7 \times 10^{-1} \leq n \leq 5.9 \times 10^{-1}$
	Decreasing shear rate ($R^2=0.9995$)	$(5.8 \pm 0.1) \times 10^{-1}$ 99% confidence interval: $5.7 \times 10^{-1} \leq n \leq 5.9 \times 10^{-1}$

5.1.3. Effect of dissolution time on rheology

The dissolution process was described in Chapter 4. The time elapsed from the addition of the CMC powder until they were analyzed analyzed in the rheometer, or used in the bubble column, was found to affect the properties of the CMC solutions, as shown in Figures 5.7 through 5.9. However, this effect becomes negligible beyond dissolution times of 24 h. Therefore, the CMC solutions used in the bubble column experiments were prepared with a dissolution time of 24 h.

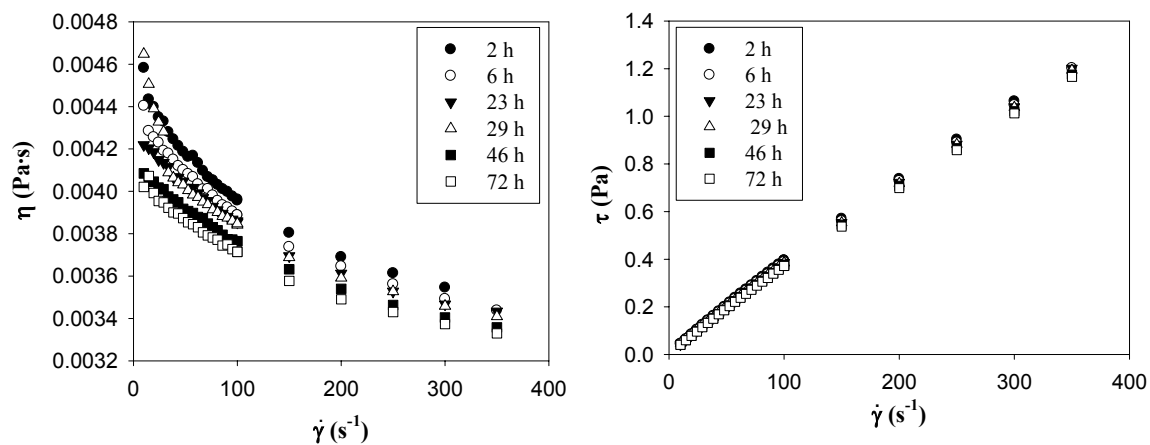


Figure 5.7. Effect of the dissolution time on the flow curves at 0.05% of CMC at 25 °C

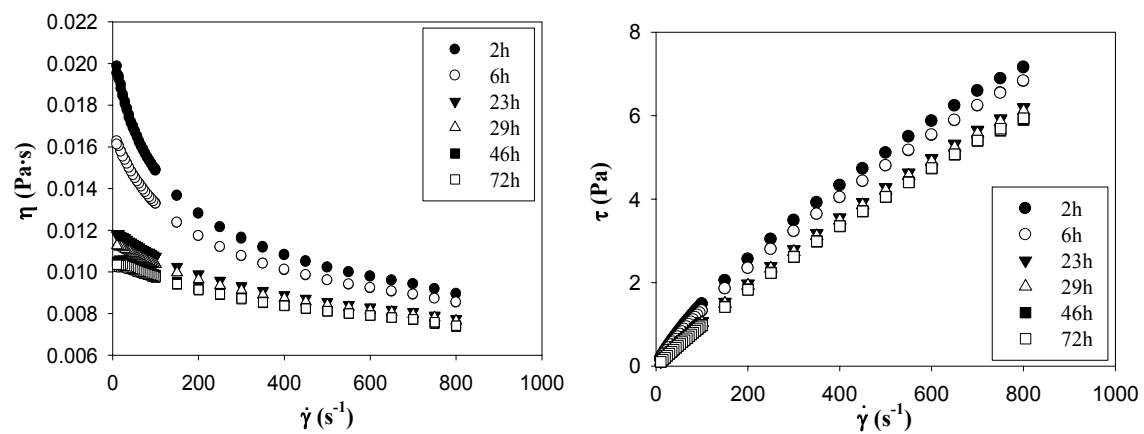


Figure 5.8. Effect of the dissolution time on the flow curves at 0.15% of CMC at 25 °C

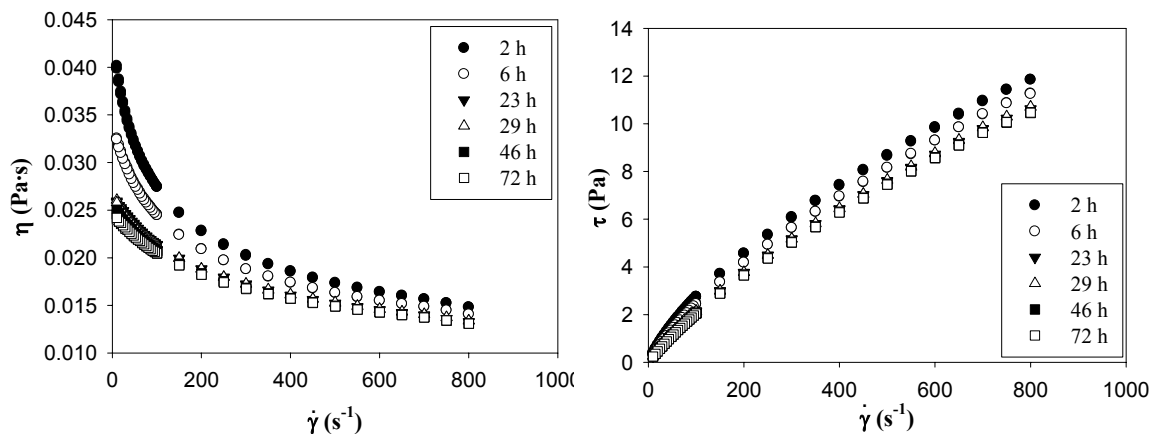


Figure 5.9. Effect of the dissolution time on the flow curves at 0.25% of CMC at 25 °C

5.1.4. Effect of temperature on the rheology of CMC solutions

A study of the temperature effect on the behavior of solutions was carried out. Figure 5.10 shows the effect of this variable on viscosity and flow curves of a 0.05% wt of CMC solution. Similar tendency, but with increasing temperature effect was observed for 0.15 and 0.25% wt concentrations (Figures 5.11 and 5.12, respectively). It is important to mention that these curves correspond to solutions with two hours of polymer dissolution. The curves obtained for 24 h hours of time of polymer dilution are shown in Figures 5.13 and 5.14 that correspond to 0.20 and 0.40 % wt of CMC.

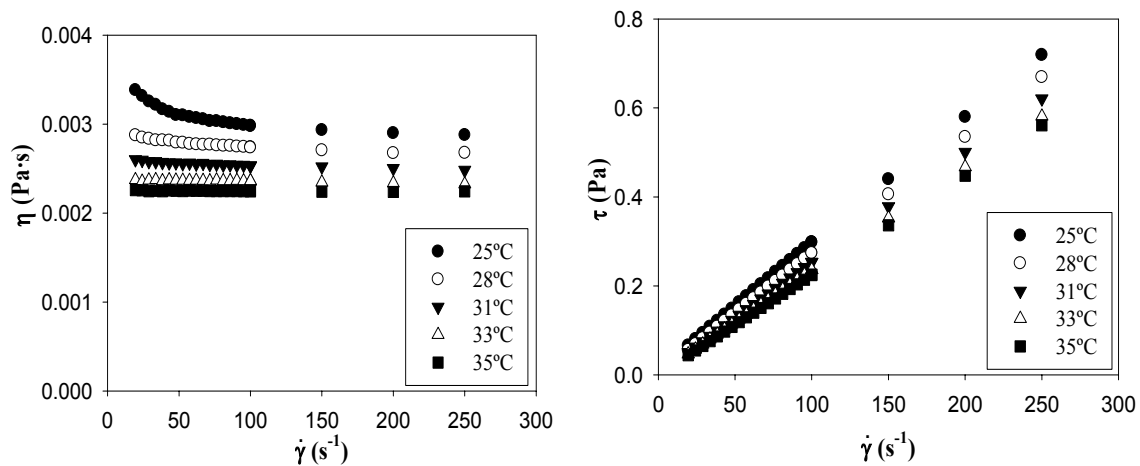


Figure 5.10. Viscosity and flow curve for 0.05% aqueous solution of CMC for 2 h of dissolution time

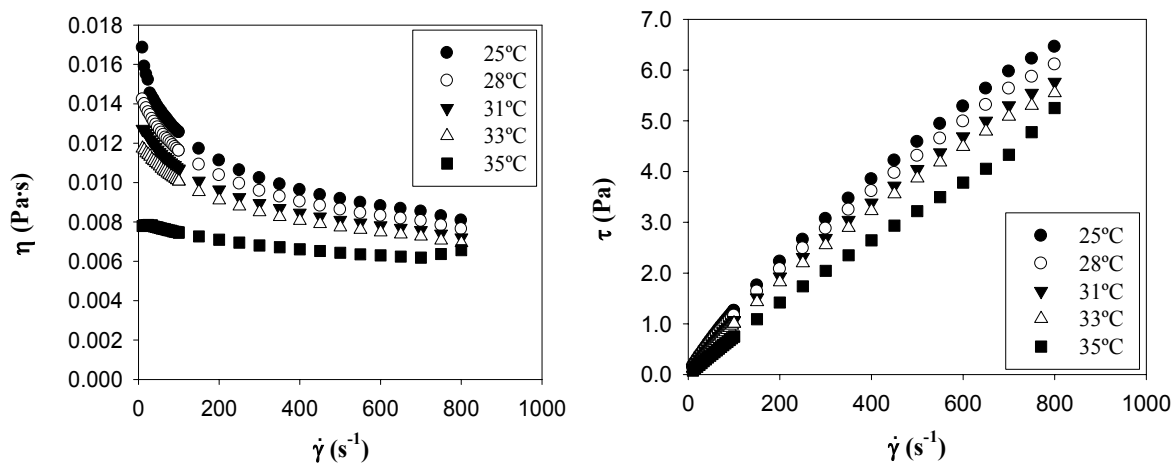


Figure 5.11. Viscosity and flow curve for 0.15% aqueous solution of CMC for 2 h of dissolution time

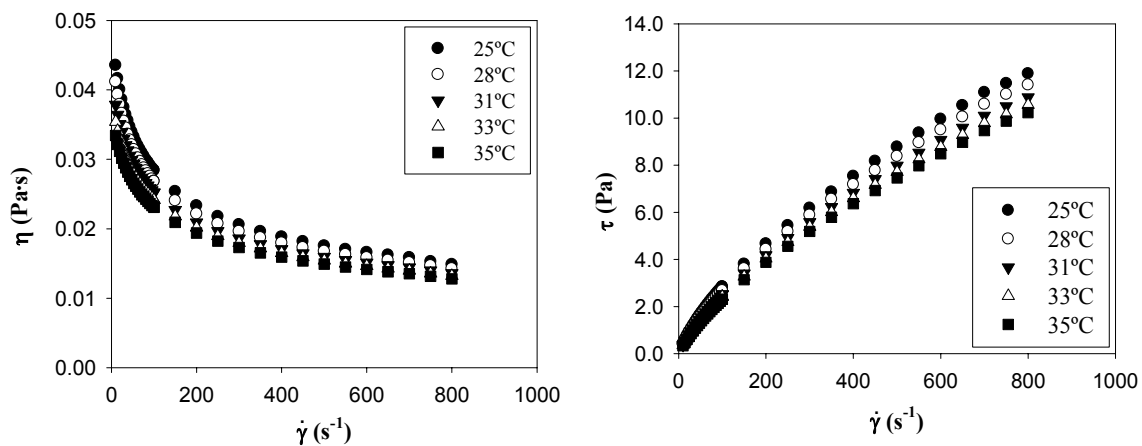


Figure 5.12. Viscosity and flow curve for 0.25% aqueous solution of CMC for 2 h of dissolution time

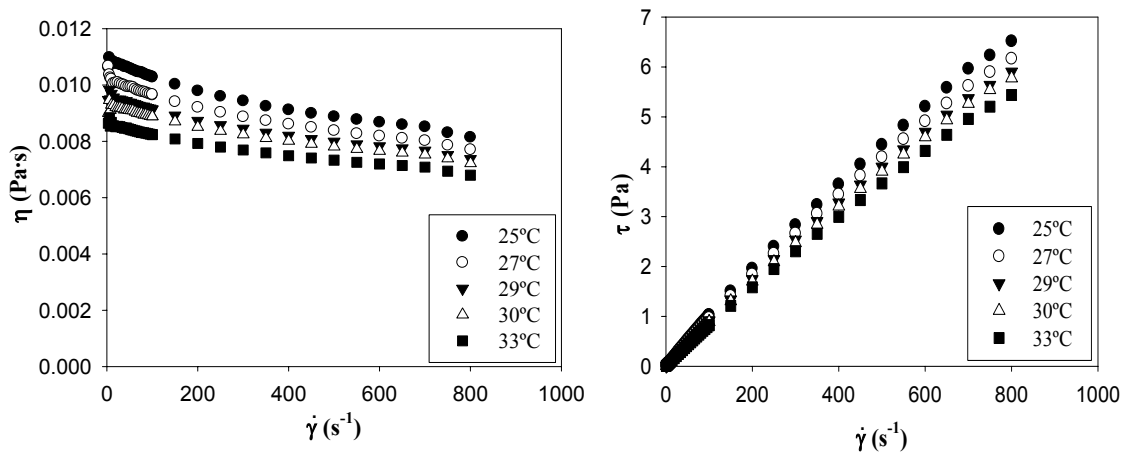


Figure 5.13. Viscosity and flow curve for 0.20% aqueous solution of CMC for a dissolution time of 24 h

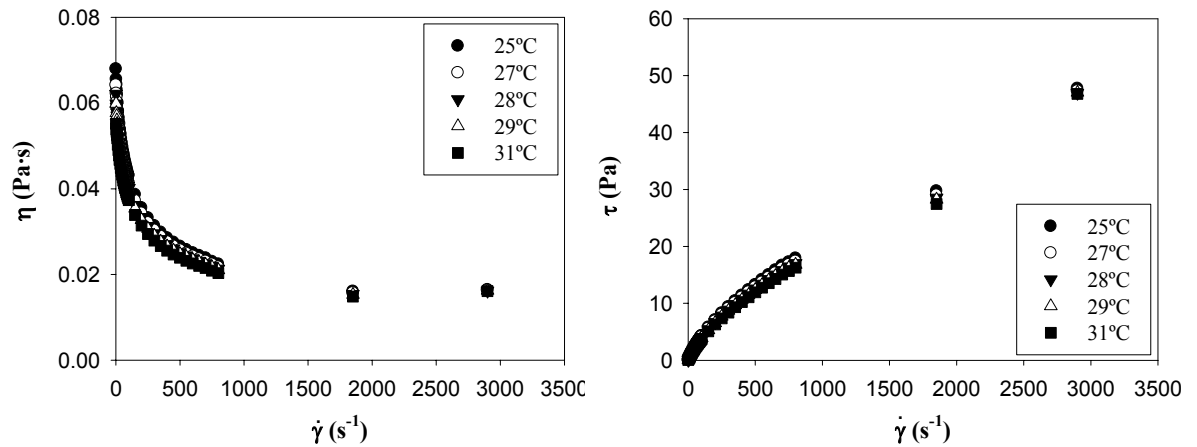


Figure 5.14. Viscosity and flow curve for 0.40% aqueous solution of CMC for a dissolution time of 24 h

From the previous flow curves obtained at different temperatures, the parameters of the power-law model were found and correlated as a function of temperature. The results are shown in Table 5.3. These expressions allow finding rheological parameters of the power-law model at the real temperature of CMC solution in the range of $25 \leq T(^{\circ}C) \leq 33$.

Table 5.3. Parameters of the power-law model obtained as a function of temperature ($^{\circ}C$)

Polymer concentration (% wt)	Dissolution time (h)	k (Pa·s ⁿ)	n (-)
0.05	2	$0.00001T^2 - 0.0008T + 0.0177$	$-0.0005T^2 + 0.0353T + 0.374$
0.15	2	$0.00003T^2 - 0.0029T + 0.08$	$-0.00003T^2 + 0.0061T + 0.6964$
0.20	24	$0.00006T^2 - 0.004T + 0.08$	$-0.0003T^2 + 0.0198T + 0.608$
0.25	2	$-0.0026T + 0.1566$	$0.0002T^2 - 0.0093T + 0.844$
0.40	24	$-0.0037T + 0.1965$	$0.000004T^3 - 0.00009T^2 - 0.0007T + 0.8$

* The expressions are valid only in the interval $25 \leq T(^{\circ}C) \leq 33$

5.1.5. Effect of presence of tracers on the rheology of CMC solutions

One of the bases for the selection of the tracer in the bubble-column experiments was its effect on the rheology of the CMC solutions. To assess this effect rheological tests were done on aqueous CMC solutions with and without the potential tracer. The chemicals considered as possible tracer were sodium chloride (used in all references consulted on RTD studies), phthalic acid monopotasium salt, a dye tracer used in water treatment plants called 101100 FLT Industrial Red Dye tracer of Tramfloc, Inc., and methylene blue.

Figure 5.15 shows the results obtained when sodium chloride was added to a 0.75% CMC solution.

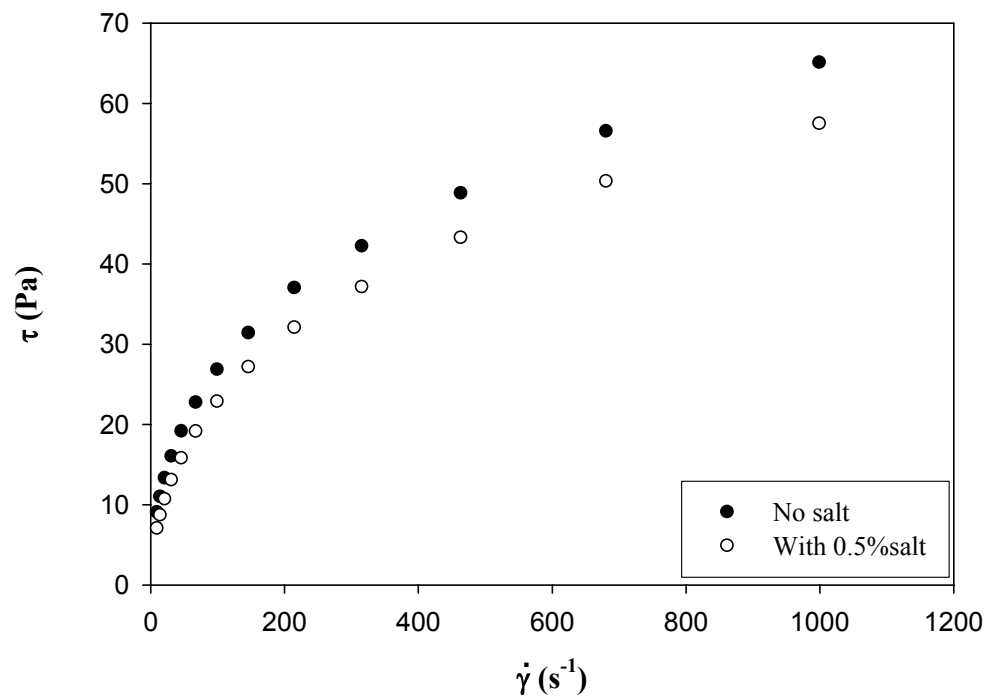


Figure 5.15. Effect of the addition of sodium chloride to a solution of 0.75% wt of CMC at 25°C and 2 h of dissolution time

Figure 5.15 shows a clear difference between curves of shear stress without salt and with 0.5% salt. The effect of the addition of sodium chloride to solutions at other CMC concentrations was determined and the results are shown in Table 5.4. The presence of

salt changed the values of the power-law parameters; the value of the index flow, n increased while the consistency index, k , decreased with the presence of NaCl. The presence of salt in the solution apparently acts over the polyelectrolyte characteristic of the CMC causing some changes in the polymer molecule.

Table 5.4. Values of the power-law parameters with 0.5% and without NaCl

CMC concentration (%wt)	Without NaCl		With NaCl	
	k (Pa·s ^{<i>n</i>})	n (-)	k (Pa·s ^{<i>n</i>})	n (-)
0.00	0.0008	1.000	0.0008	1.000
0.25	0.1428	0.709	0.0402	0.815
0.50	1.2132	0.508	0.5987	0.577
0.60	2.4883	0.470	1.1295	0.527
0.75	3.4596	0.430	2.4883	0.459
1.00	8.3592	0.366	6.7271	0.390

* These tests were done as part of the preliminary tests in an ARES rheometer of the Polymeric Research Group at Simón Bolívar University in Caracas, Venezuela.

Similar results were found when phthalic acid monopotassium salt and 101100 FLT Industrial Red Dye tracer of Tramfloc were used as shown in Figures 5.16 and 5.17.

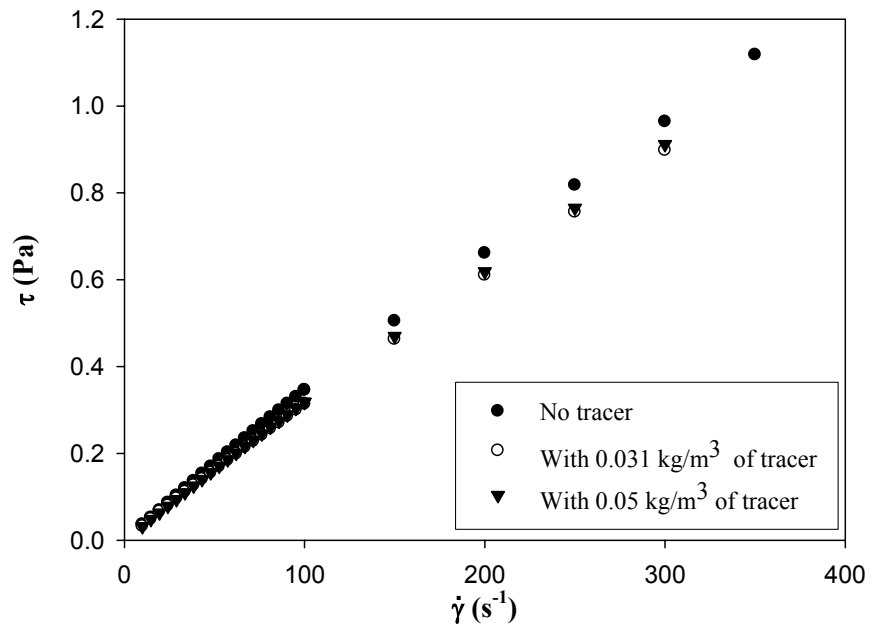


Figure 5.16. Effect of the addition of phthalic acid monopotassium salt to a solution of 0.05% wt of CMC

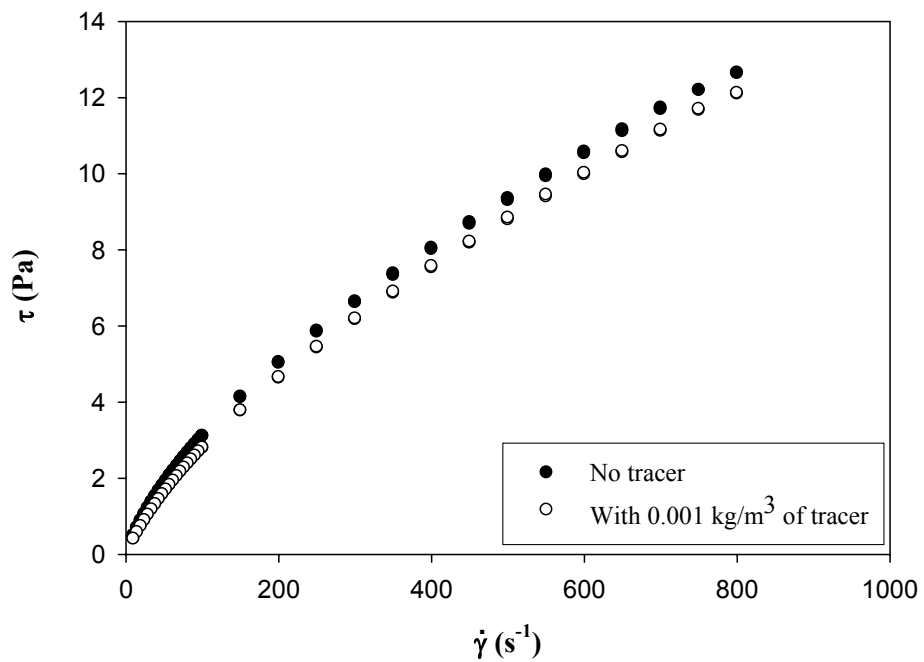


Figure 5.17. Effect of the addition of 101100 FLT Industrial Red Dye tracer of Tramfloc to a solution of 0.25% wt of CMC

On the contrary, the methylene blue has no important effect on the CMC molecule. The results are shown in Figures 5.18 and 5.19 for 0.20 and 0.40 % wt concentration of CMC in the solution, respectively.

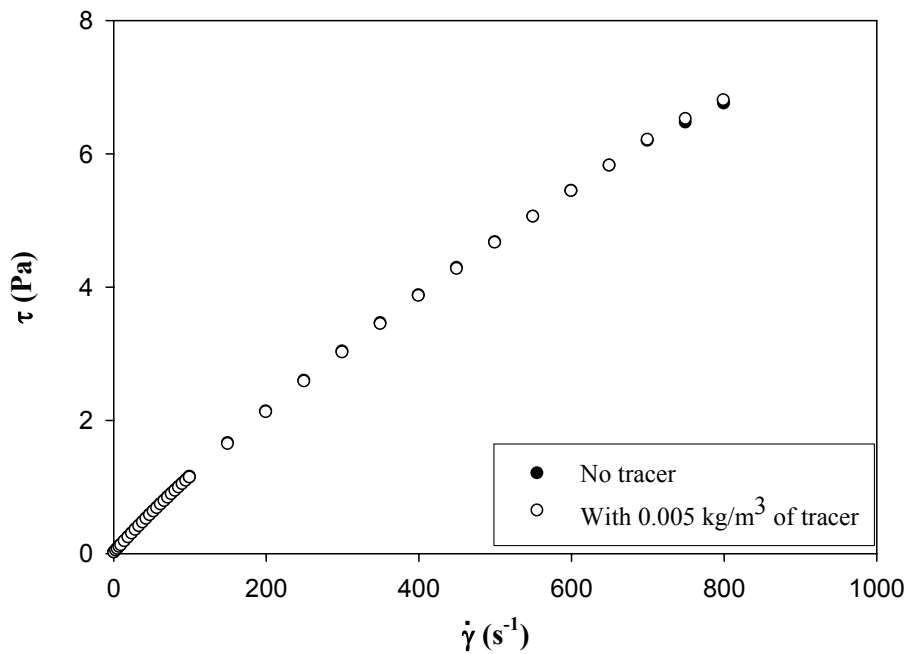


Figure 5.18. Effect of the addition of methylene blue to a solution of 0.20% wt of aqueous solution of CMC for 24 h of dissolution

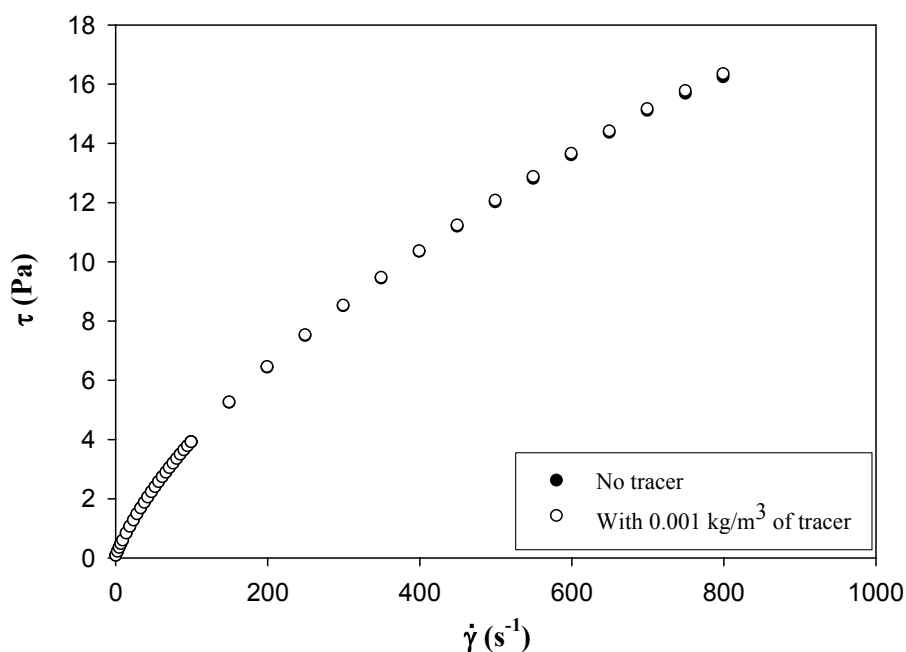


Figure 5.19. Effect of the addition of methylene blue to a solution of 0.40% wt of aqueous solution of CMC for 24 h of dissolution

The tracer selected to be used as tracer in the bubble column was methylene blue because the others change the behavior of the polymer in solution as it is observed in the rheology results obtained in this study.

5.1.6. Dynamic tests

A dynamic test was performed to study the viscoelastic properties. These properties include the storage modulus, related to the elastic behavior of the solution, and the loss modulus, a measure of the viscous behavior of the solution. Figure 5.20 shows the storage modulus (in logarithm scale), as a function of the frequency; negligible effect of CMC concentration on this parameter was observed. Therefore, the elastic behavior of the solutions was not affected by the presence of the CMC.

The loss modulus is presented in Figure 5.21, which shows an increase of this modulus with CMC concentration thus confirming the trends obtained for viscosity in Figure 5.1.

Additionally, a displacement was observed for the cross-over point of these moduli for a given sample. Figure 5.22 shows that, as CMC concentration increased, the shear frequency increased. At frequencies lower than the shear frequency, the loss modulus is higher than the storage modulus indicating that the predominant effect of the material is viscous. At frequencies higher than the shear frequency, the elastic behavior dominates. Table 5.5 shows the shear frequency at each CMC concentration.

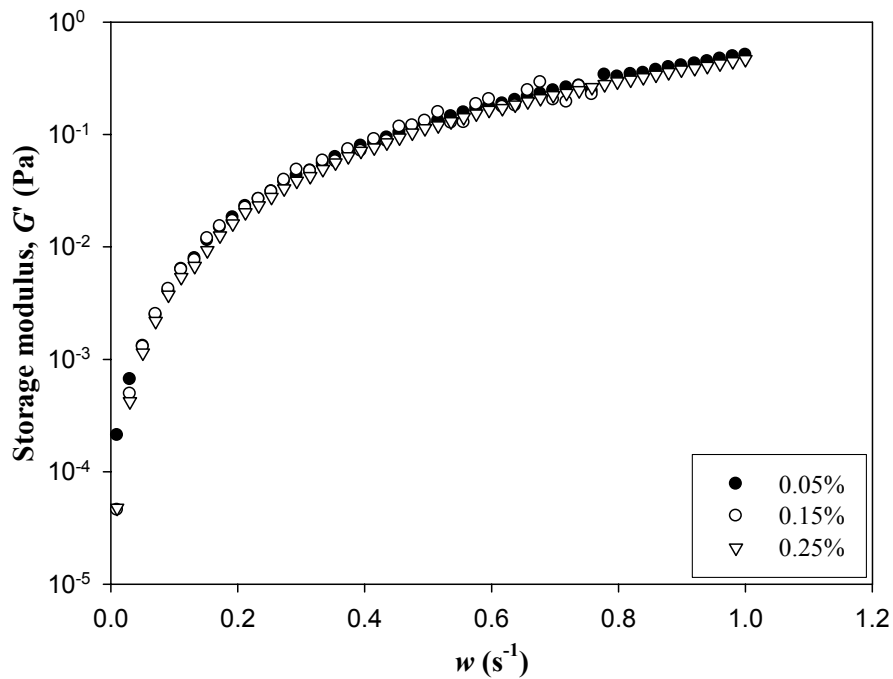


Figure 5.20. Storage Modulus at different CMC concentrations

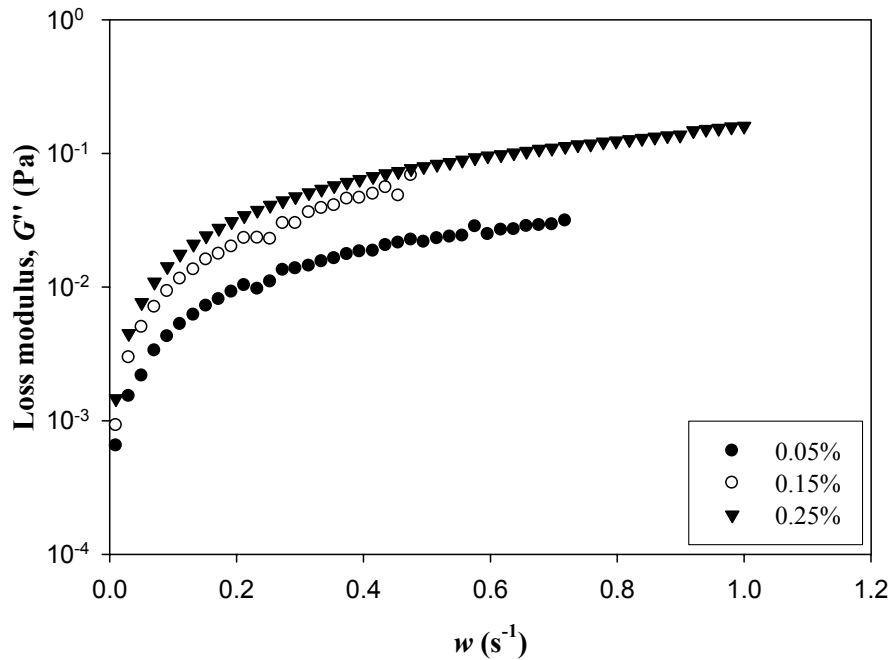


Figure 5.21. Loss Modulus at different CMC concentrations

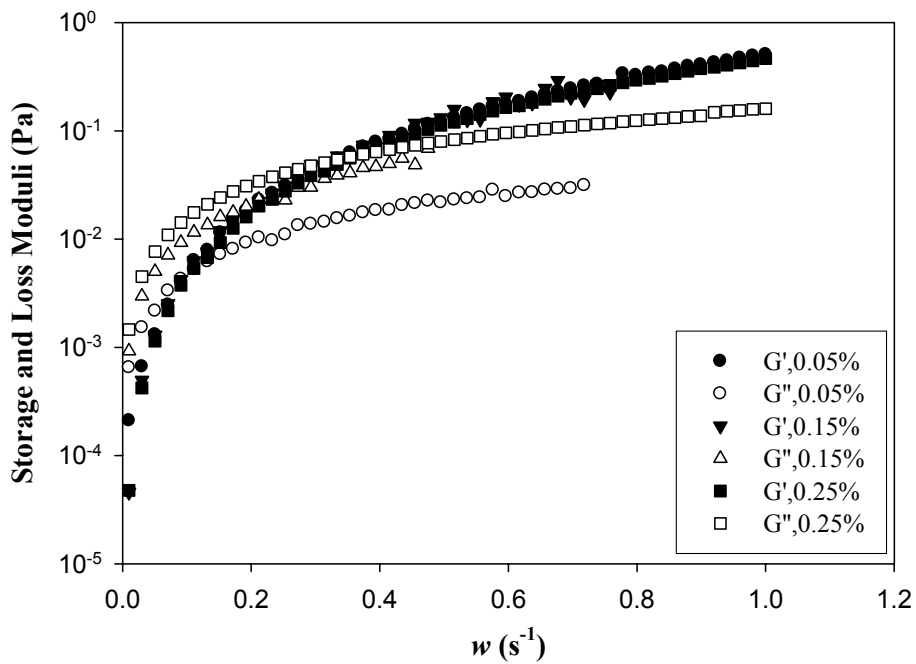


Figure 5.22. Storage and Loss Moduli at different CMC weight-percentage concentrations

Table 5.5. Shear frequency from curves in Figure 5.22

CMC concentration (wt %)	Shear frequency (s ⁻¹)
0.05	0.091
0.15	0.212
0.25	0.374

5.2. Bubble column results

A number of experiments were carried out in the bubble column at varying gas and liquid flow rates and varying CMC concentrations. For each run, the pressure drop, the gas holdup, the flow regimes, and the mixing in the liquid phase were determined. These results are presented in this section.

5.2.1. Pressure drop

The pressure drop obtained for tap water at different liquid superficial velocities through the differential pressure transducer is shown in Figure 5.23. This plot shows no effect on the pressure drop of the superficial liquid velocity in the range studied. Additionally, it is seen that pressure drop decreased as superficial gas velocity increased, and this observation could be explained through the reduction of the mixture viscosity (because of the increase of gas holdup in the bubble column) that caused the reduction of the shear stress in its component τ_z and so that the pressure drop decreased.

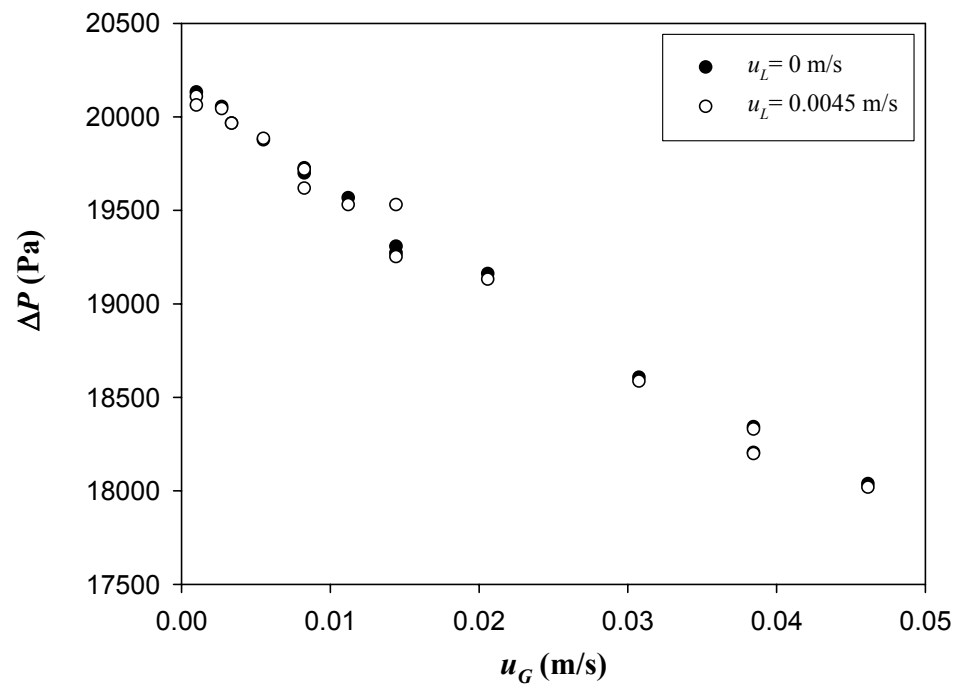


Figure 5.23. Pressure drop for tap water at different liquid superficial velocities

Figures 5.24 and 5.25 show similar plots, but for 0.20 and 0.40% aqueous solutions of CMC.

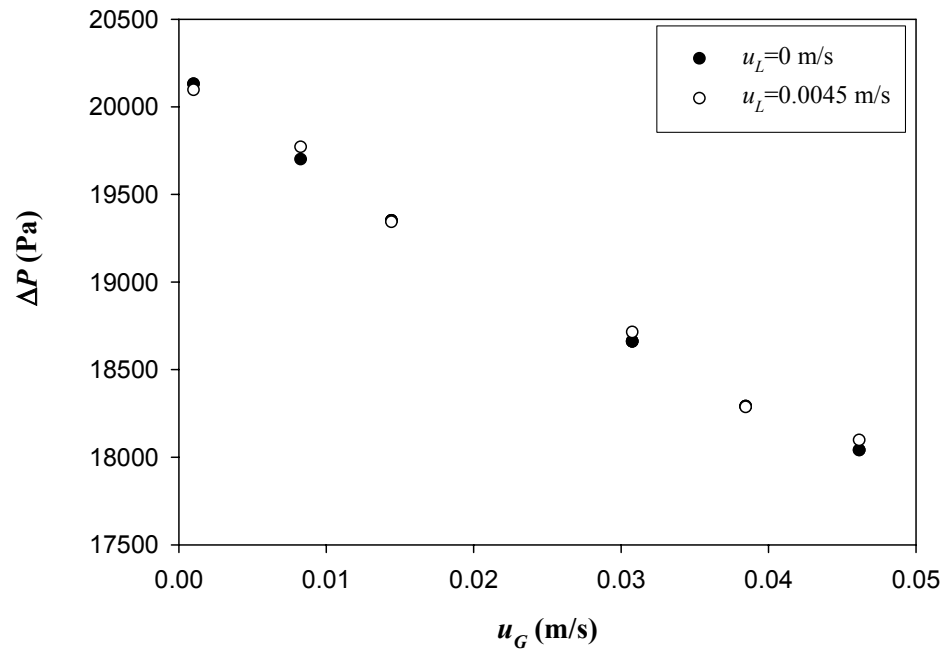


Figure 5.24. Pressure drop for 0.20% of CMC in water at different liquid superficial velocities

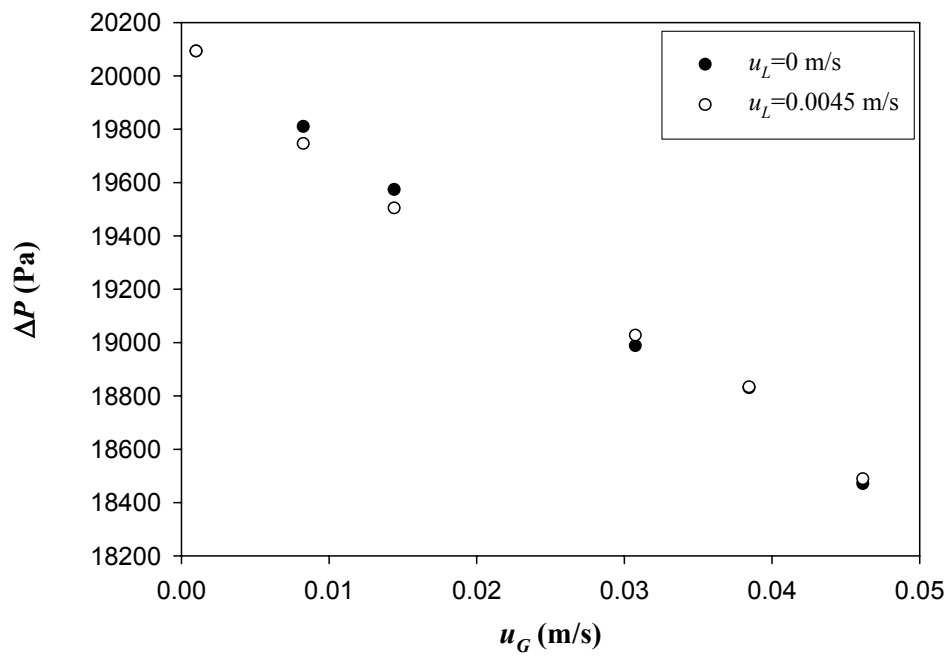


Figure 5.25. Pressure drop for 0.40% of CMC in water at different liquid superficial velocities

In Figure 5.26 the comparison between CMC concentrations is presented in batch mode of liquid ($u_L=0$ m/s). In this figure it is observed that pressure drop increases as CMC concentration in the liquid phase does due to the increase in the viscosity of the solution such as it is seen in Figure 5.1. The effect it is undistinguished at low superficial gas velocity. The same trend was found in Figure 5.27 that corresponds to continuous mode ($u_L=0.0045$ m/s).

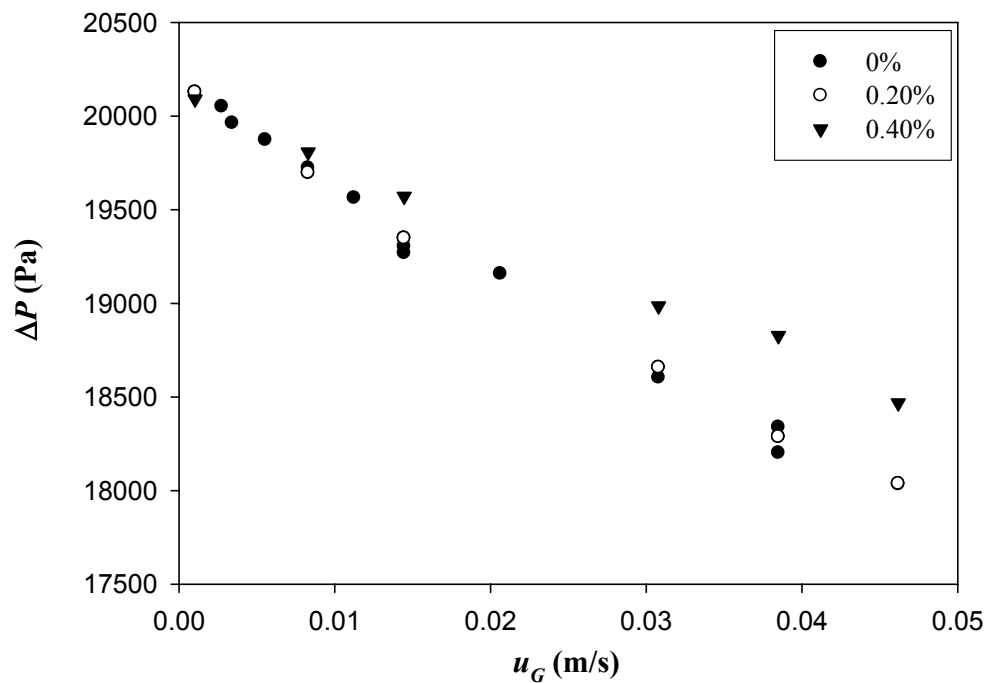


Figure 5.26. Pressure drop in batch mode at different CMC concentrations

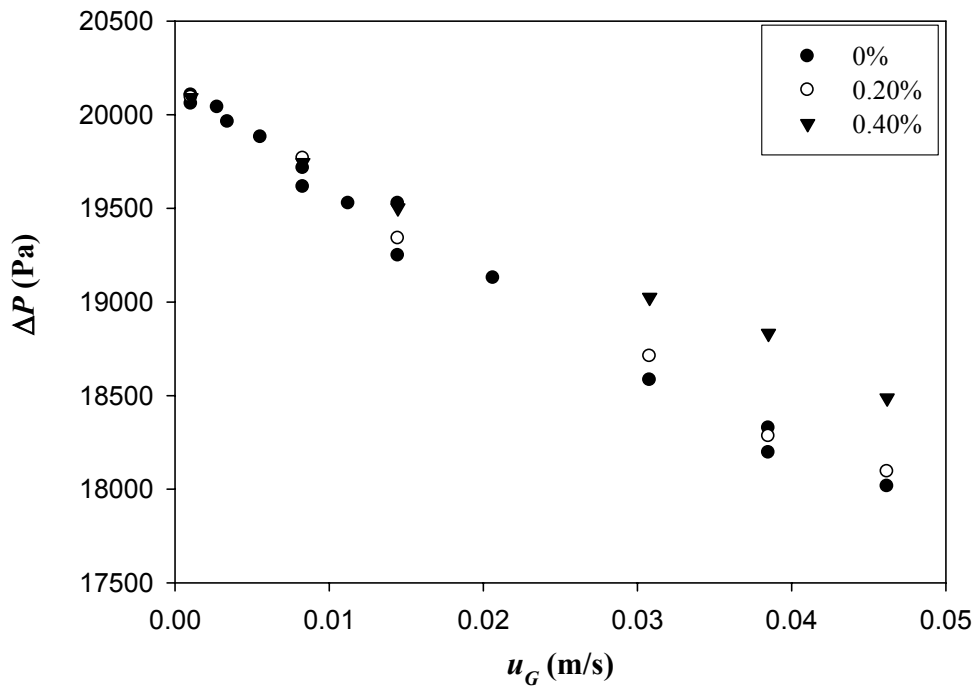
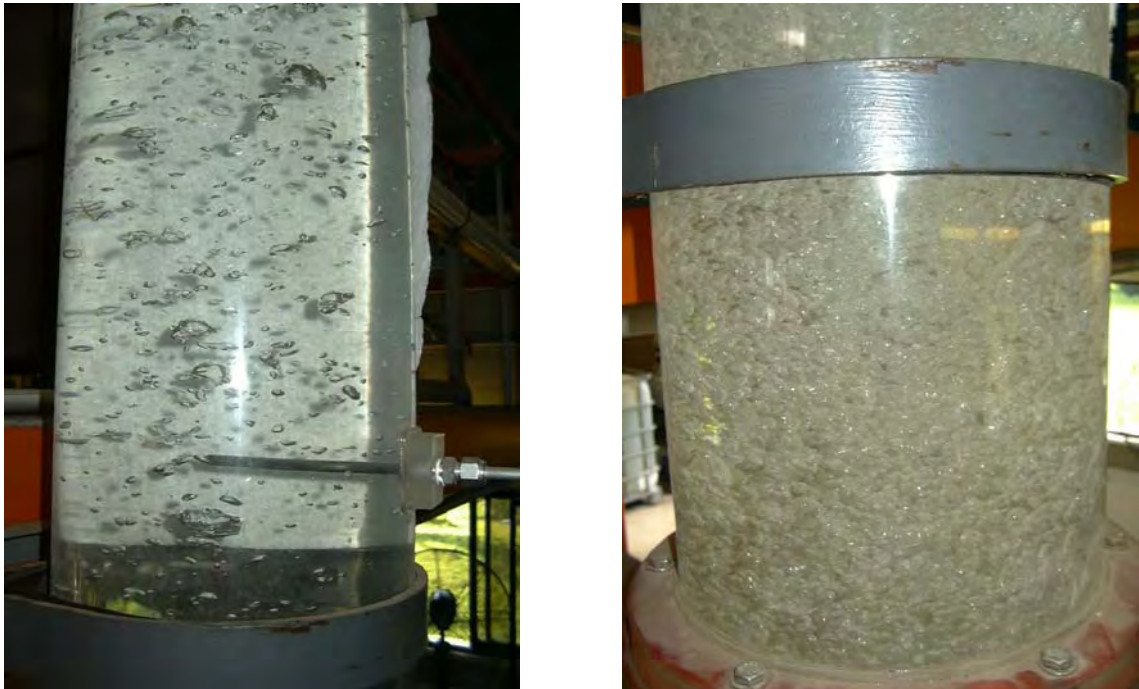


Figure 5.27. Pressure drop in continuous mode ($u_L=0.0045$ m/s) at different CMC concentrations

Two flow regimes were observed in the bubble column in all concentrations of CMC. Both were heterogeneous because the presence of different bubble sizes in the bubble column; but the movement inside of them were different establishing two heterogeneous regimes: heterogeneous bubbling flow (described by Ramanchadran and Chaudri, 1983) and heterogeneous churn turbulent flow (found by Vatai and Tekic, 1989, Soham, 1982). Two pictures were taken to illustrate both regimes and they are shown in Figure 5.28.



(a) Heterogeneous bubbling flow

(b) Heterogeneous churn turbulent

Figure 5.28. Flow regimes found in the range of the operation of the bubble column

Taking into account the effect of CMC concentration (in terms of the power-law parameters) and the superficial gas velocity on pressure drop, it is possible to propose expressions to predict the last parameter as a function of the formers in both flow regime and for Newtonian (tap water) and non-Newtonian solutions. These expressions are shown in Table 5.6, and Table 5.7 shows analogous expressions but as a function of dimensionless numbers. It is important to mention that regression coefficients of equivalent expressions from Tables 5.6 and 5.7 were similar; for this reason, the next figures corresponds to the correlations calculated from the Table 5.7.

Table 5.6. Correlations for pressure drop

Fluid	Regime	Correlation
Newtonian	Heterogeneous bubbling flow regime ($1.04 \times 10^{-3} \leq u_G (m/s) \leq 1.44 \times 10^{-2}$)	$\Delta P (Pa) = 18323 u_G^{-0.014}$ (5.1)
	Heterogeneous churn turbulent flow regime ($3.07 \times 10^{-2} \leq u_G (m/s) \leq 4.62 \times 10^{-2}$)	$\Delta P (Pa) = 14230 u_G^{-0.077}$ (5.2)
Non-Newtonian	Heterogeneous bubbling flow regime ($1.04 \times 10^{-3} \leq u_G (m/s) \leq 1.44 \times 10^{-2}$)	$\Delta P (Pa) = 18943 u_G^{-0.014n} k^{0.0064n}$ (5.3)
	Heterogeneous churn turbulent flow regime ($3.07 \times 10^{-2} \leq u_G (m/s) \leq 4.62 \times 10^{-2}$)	$\Delta P (Pa) = 15791 u_G^{-0.086n} k^{0.027n}$ (5.4)

Table 5.7. Correlations for pressure drop as a function of dimensionless numbers

Fluid	Regime	Correlation
Newtonian	Heterogeneous bubbling flow regime ($1.04 \times 10^{-3} \leq u_G (m/s) \leq 1.44 \times 10^{-2}$)	$\Delta P (Pa) = 20995 Re_G^{-0.014}$ (5.5)
	Heterogeneous churn turbulent flow regime ($3.07 \times 10^{-2} \leq u_G (m/s) \leq 4.62 \times 10^{-2}$)	$\Delta P (Pa) = 29529 Re_G^{-0.077}$ (5.6)
Non-Newtonian	Heterogeneous bubbling flow regime ($1.04 \times 10^{-3} \leq u_G (m/s) \leq 1.44 \times 10^{-2}$)	$\Delta P (Pa) = 18514 n^{-0.042} Re_G^{-0.0028n} Fr_G^{-0.010n}$ (5.7)
	Heterogeneous churn turbulent flow regime ($3.07 \times 10^{-2} \leq u_G (m/s) \leq 4.62 \times 10^{-2}$)	$\Delta P (Pa) = 16108 n^{0.16} Re_G^{-0.039n} Fr_G^{-0.037n}$ (5.8)

* The Reynolds number in the case of non-Newtonian fluids was calculated follows the definition of this number for this kind of fluids.

* k and n are the rheological parameters of the power-law model.

Figure 5.29 shows the behavior of correlations (Equations 5.5 and 5.6) obtained for water in both flow regimes for batch runs compared to experimental data, while Figure

5.30 shows analogous plot but at $u_L = 0.0045$ m/s. It is observed that proposed correlations fits experimental data.

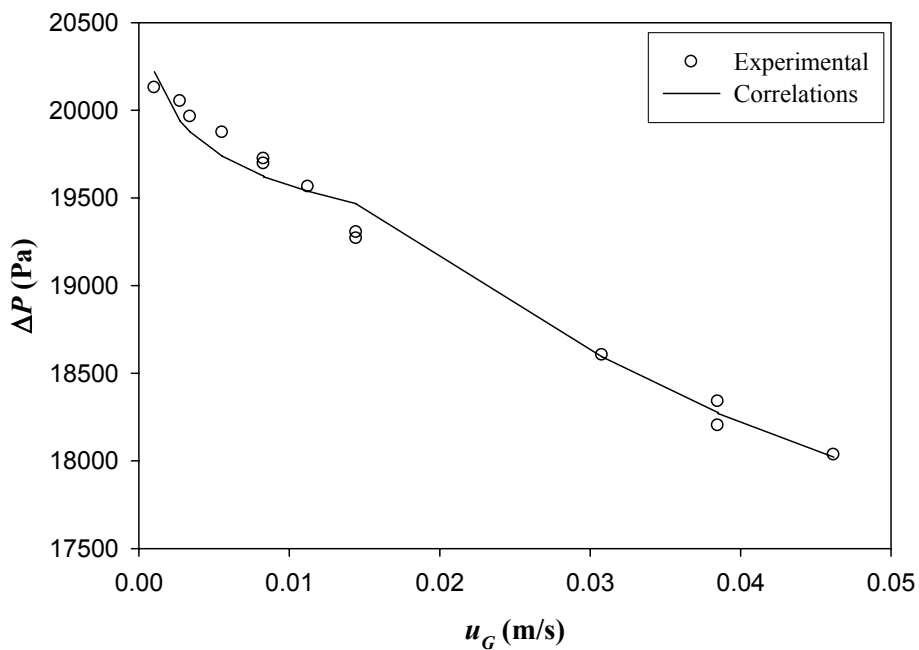


Figure 5.29. Pressure drop for tap water and $u_L = 0$ m/s

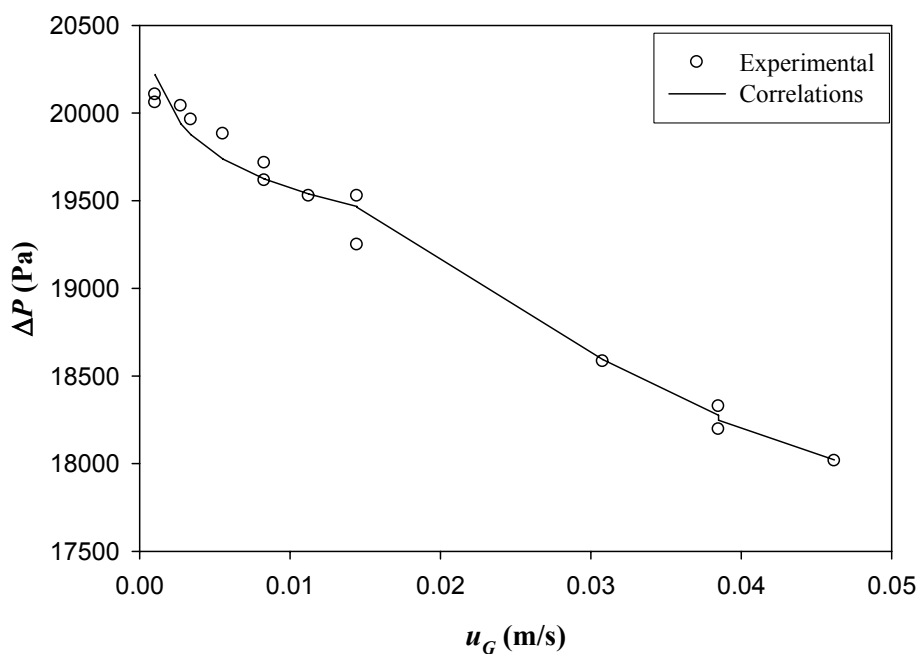


Figure 5.30. Pressure drop for tap water and $u_L = 0.0045$ m/s

The parity plot shown in Figure 5.31 compares the pressure drop obtained from experimental data and by equations (5.5) and (5.6) in the case of tap water as used fluid. The values calculated with the proposed correlations are inside the 2% of deviation bars respect to straight line of 45°, indicating that data were fit quite well through the proposed correlations.

Figures 5.32 and 5.33 show the experimental data obtained with 0.20 and 0.40% CMC solutions respectively and the fit of the correlations proposed through equations (5.7) and (5.8). Again, the plots showed the good fit of the correlations.

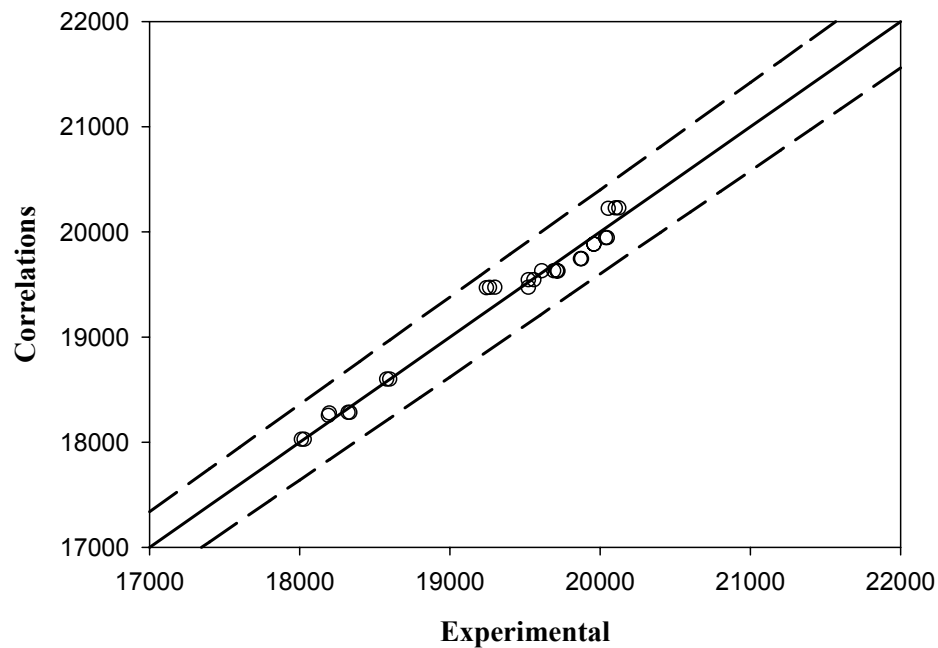


Figure 5.31. Comparison between experimental data and equations (5.5) and (5.6) for the pressure drop using tap water

The symbols used in figures 5.32 and 5.33 are shown as follows:

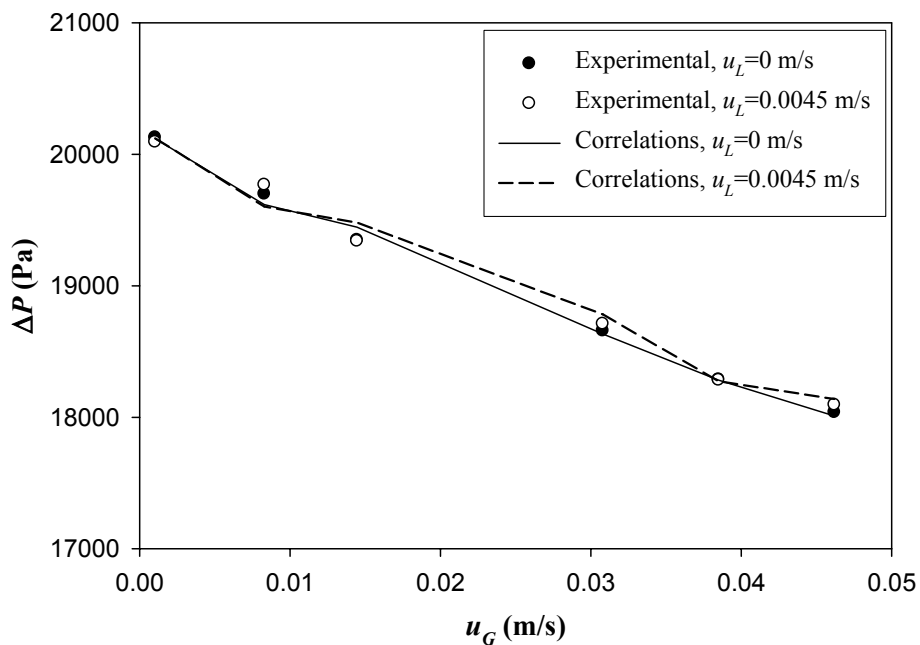


Figure 5.32. Pressure drop for 0.20% CMC solutions

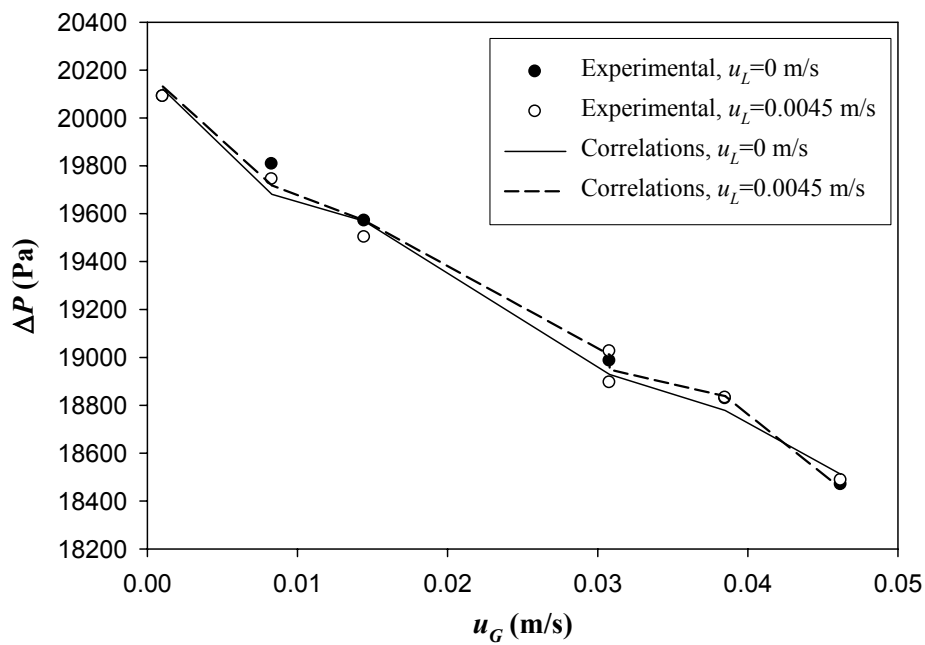


Figure 5.33. Pressure drop for 0.40% CMC solutions

Figure 5.34 shows a parity plot that compares the pressure drop obtained from experimental data and by equations (5.7) and (5.8) for CMC solutions. The values calculated with the proposed correlations are within $\pm 2\%$ of the straight line at 45° , indicating that the proposed correlations fit quite well the experimental data.

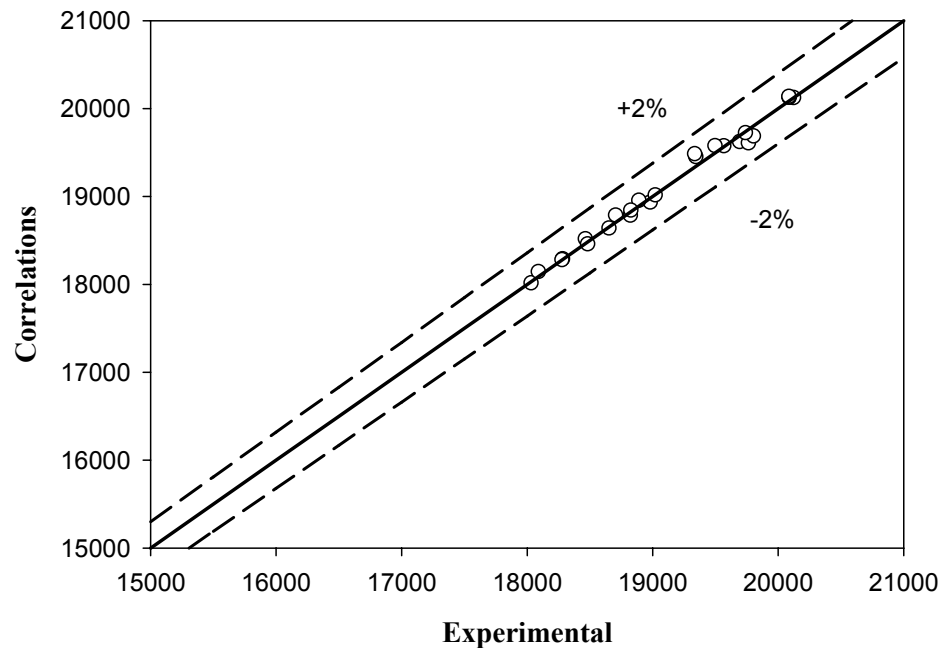


Figure 5.34. Comparison between experimental data and equations (5.7) and (5.8) for the pressure drop with CMC solutions

From the analysis developed in vertical pipes and presented in Appendix A, the friction factor for two phases was calculated from pressure drop measurements. The results are shown in Figures 5.35 through 5.37 in which the effect of liquid and gas superficial velocities are shown. The increase of gas velocity decreased the friction factor due to the decrease in liquid holdup. Additionally, the friction factor is higher for $u_L=0$ m/s than $u_L=0.0045$ m/s. It could be explained because of the increase of the superficial velocity of the mixture that causes the increase in the friction force and as a result the decrease of the friction factor considering that this is the proportionality constant between kinetic energy (for this reason, the superficial mixture velocity) and friction force.

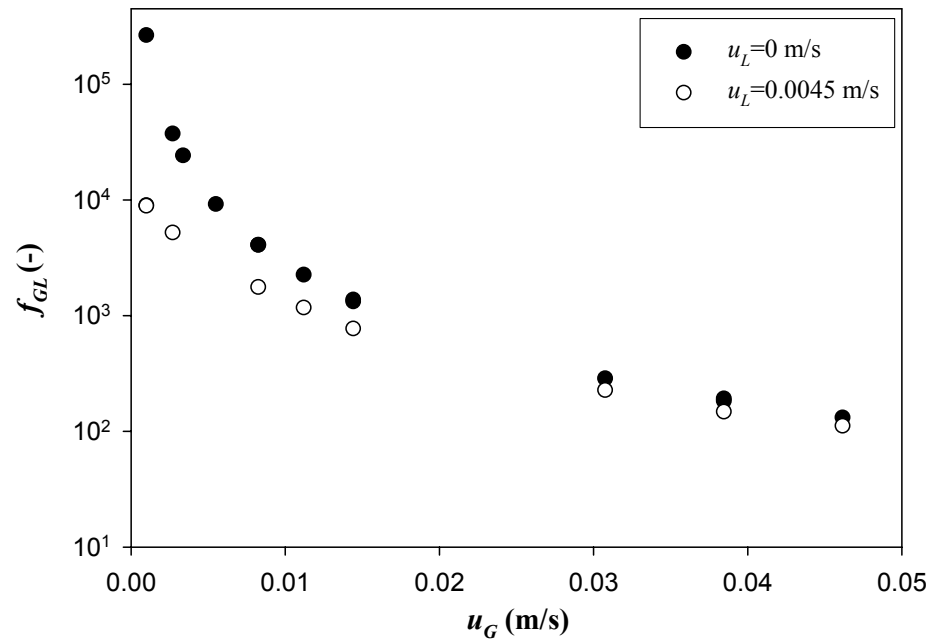


Figure 5.35. Two-phase friction factor for tap water

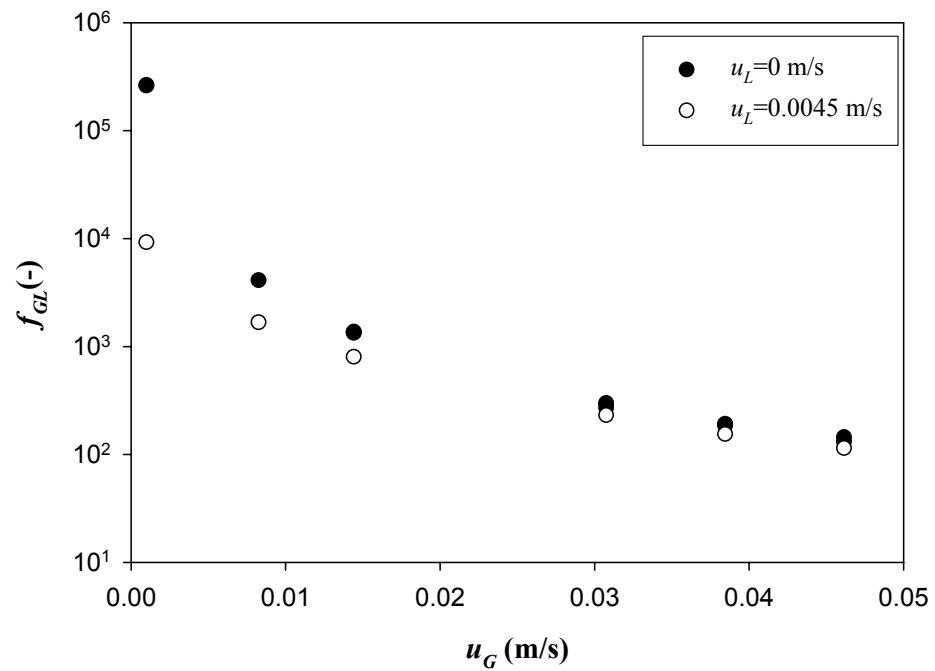


Figure 5.36. Two-phase friction factor for 0.20% CMC solutions

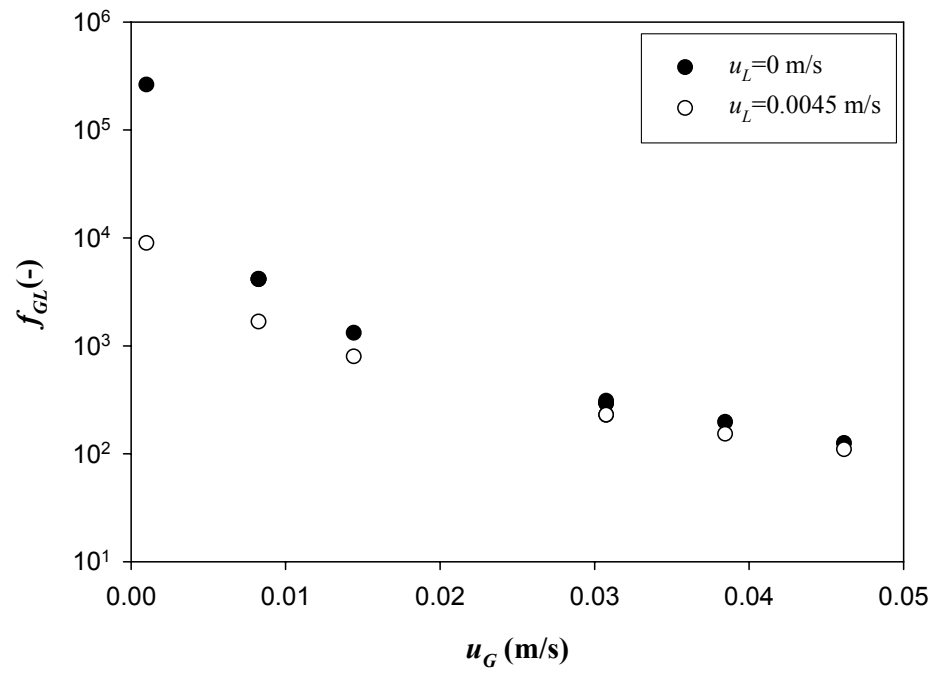


Figure 5.37. Two-phase friction factor for 0.40% CMC solutions

Figures 5.38 and 5.39 show the negligible effect of CMC two-phase friction factor in the range of concentrations considered.

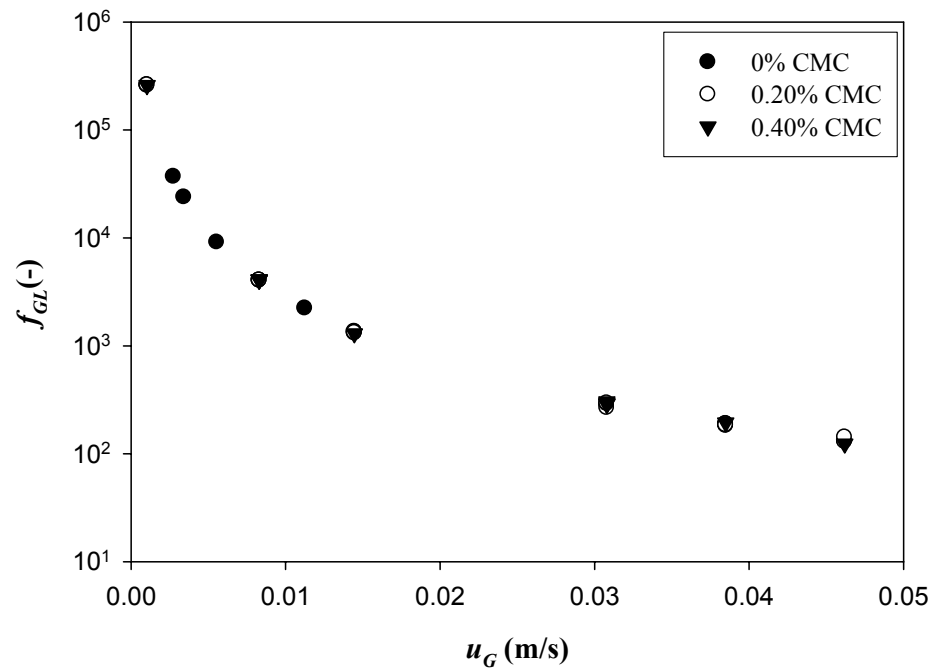


Figure 5.38. Two-phase friction factor for batch mode ($u_L=0$ m/s)

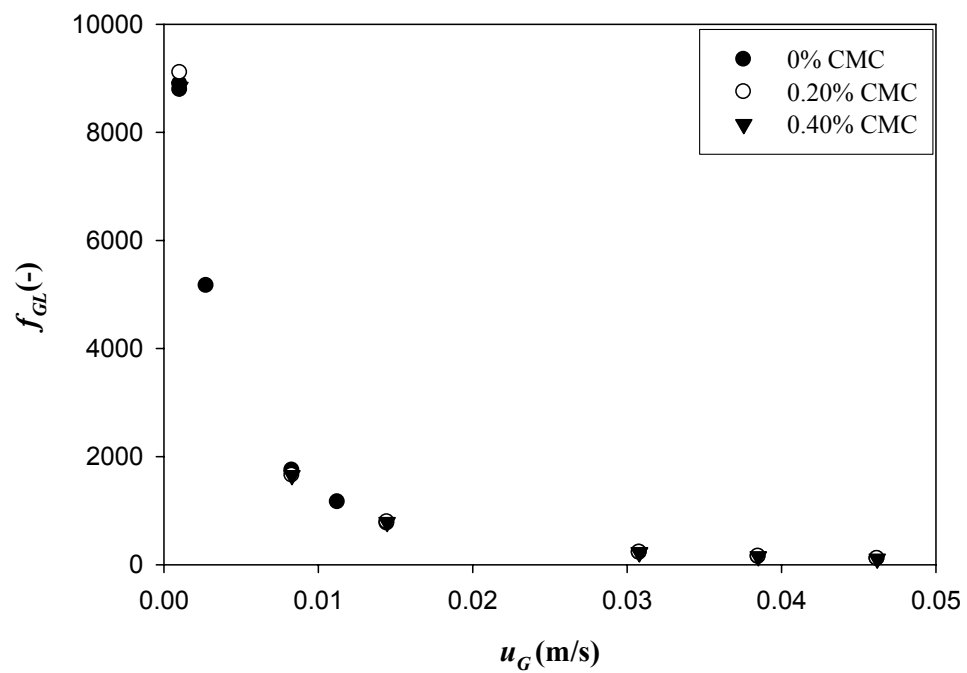


Figure 5.39. Two-phase friction factor for continuous mode ($u_L=0.0045$ m/s)

The trends observed in Figures 5.35 to 5.39 are similar to those obtained by Shirsat *et al.* (2003), but the correlation of these researchers was obtained for the downflow bubble column. For this reason, these results were not plotted to be compared to the results obtained in this work.

The regression of experimental data gives the following expression for all concentrations of CMC solutions and tap water, only depending on the liquid flow regime found. These expressions are shown in Tables 5.8 and in Table 5.9 the correlations proposed are functions of dimensionless numbers.

Table 5.8. Correlations for two-phase friction factor

u_L (m/s)	Regime	Correlation
0.0000	Heterogeneous bubbling flow regime $(1.04 \times 10^{-3} \leq u_G (m/s) \leq 1.44 \times 10^{-2})$	$f_{GL} = 0.279u_G^{-2.00}$ (5.9)
	Heterogeneous churn turbulent flow regime $(3.07 \times 10^{-2} \leq u_G (m/s) \leq 4.62 \times 10^{-2})$	$f_{GL} = 0.292u_G^{-1.98}$ (5.10)
0.0045	Heterogeneous bubbling flow regime $(1.04 \times 10^{-3} \leq u_G (m/s) \leq 1.44 \times 10^{-2})$	$f_{GL} = 761u_G^{-0.375} \exp(-115u_G)$ (5.11)
	Heterogeneous churn turbulent flow regime $(3.07 \times 10^{-2} \leq u_G (m/s) \leq 4.62 \times 10^{-2})$	$f_{GL} = 0.447u_G^{-1.79}$ (5.12)

Table 5.9. Correlations for two-phase friction factor as a function of dimensionless numbers

u_L (m/s)	Regime	Correlation
0.0000	Heterogeneous bubbling flow regime ($1.04 \times 10^{-3} \leq u_G (m/s) \leq 1.44 \times 10^{-2}$)	$f_{GL} = 0.136 \text{Re}_G^{0.00117} \text{Fr}_G^{-2.01}$ (5.13)
	Heterogeneous churn turbulent flow regime ($3.07 \times 10^{-2} \leq u_G (m/s) \leq 4.62 \times 10^{-2}$)	$f_{GL} = 0.187 \text{Re}_G^{-0.00336} \text{Fr}_G^{-1.92}$ (5.14)
0.0045	Heterogeneous bubbling flow regime ($1.04 \times 10^{-3} \leq u_G (m/s) \leq 1.44 \times 10^{-2}$)	$f_{GL} = 670 \text{Fr}_G^{-0.375} \exp(-161 \text{Fr}_G)$ (5.15)
	Heterogeneous churn turbulent flow regime ($3.07 \times 10^{-2} \leq u_G (m/s) \leq 4.62 \times 10^{-2}$)	$f_{GL} = 0.248 \text{Re}_G^{-0.00139} \text{Fr}_G^{-1.79}$ (5.16)

* The Reynolds number in the case of non-Newtonian fluids was calculated follows the definition of this number for this kind of fluids.

* k and n are the rheological parameters of the power-law model.

Figures 5.40 through 5.42 show the behavior of the correlations obtained for each range of superficial gas velocity for tap water, and 0.20 and 0.40% of CMC concentration. In each plot, the two ranges of gas velocities studied in this work were considered. These figures show that the correlations fit well the experimental data.

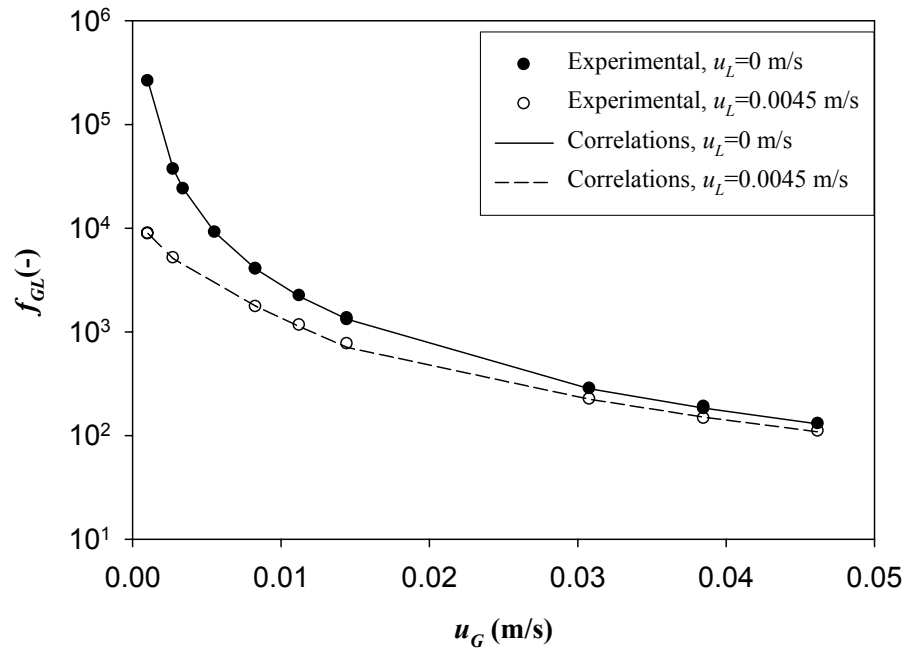


Figure 5.40. Two-phase friction factor for tap water from experimental data fit by equations (5.13) through (5.16)

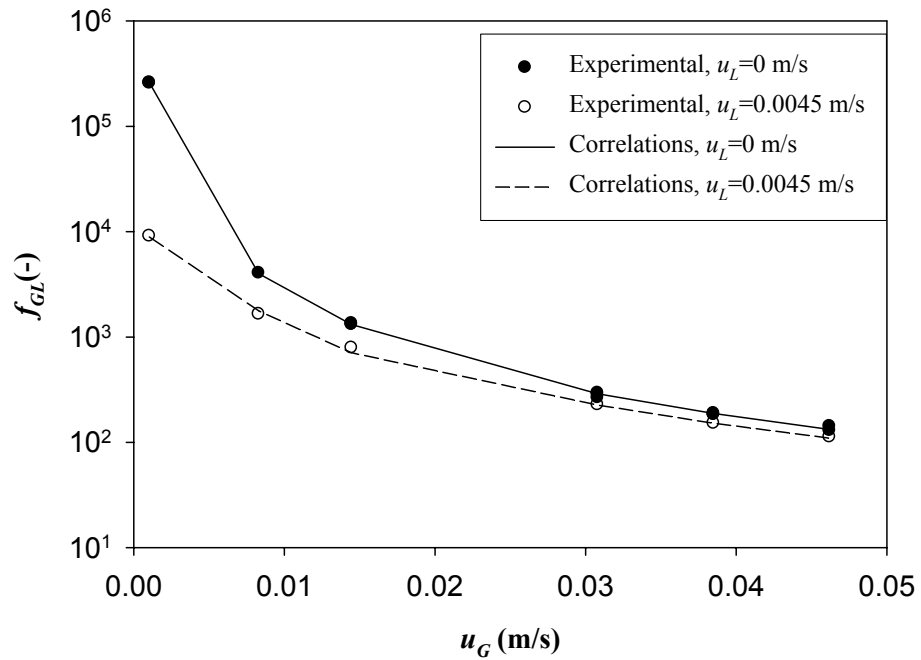


Figure 5.41. Two-phase friction factor for 0.20% CMC solutions from experimental data fit by equations (5.13) through (5.16)

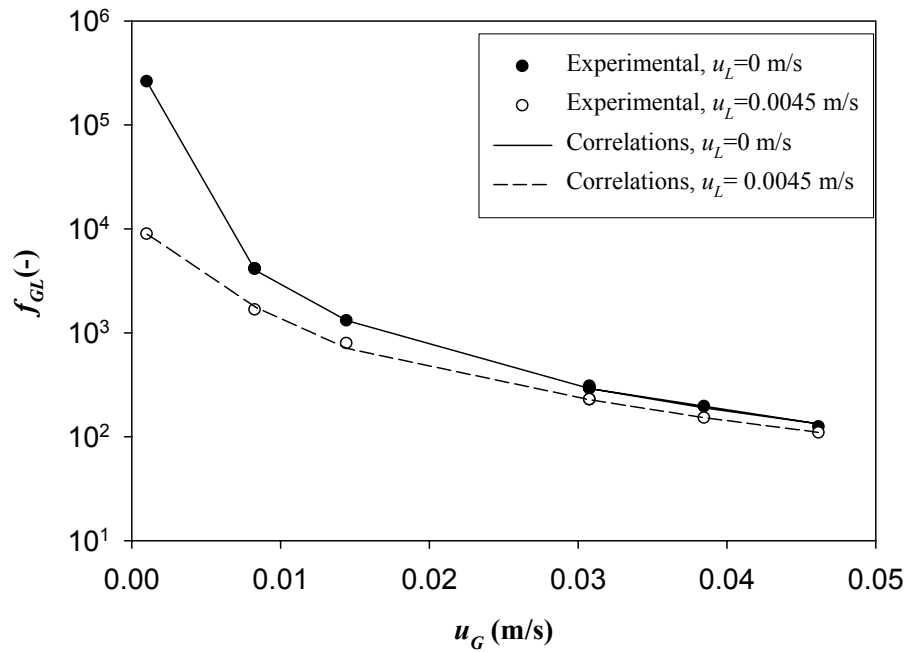


Figure 5.42. Two-phase friction factor for 0.40% CMC solutions from experimental data fit by equations (5.13) through (5.16)

The comparison between experimental data to the correlations proposed in equations (5.13) through (5.16) is shown in the parity plot in Figures 5.43 and 5.44 for $u_L = 0$ m/s and $u_L = 0.0045$ m/s respectively. The figures show that the proposed correlations fit quite well the experimental data, within $\pm 10\%$.

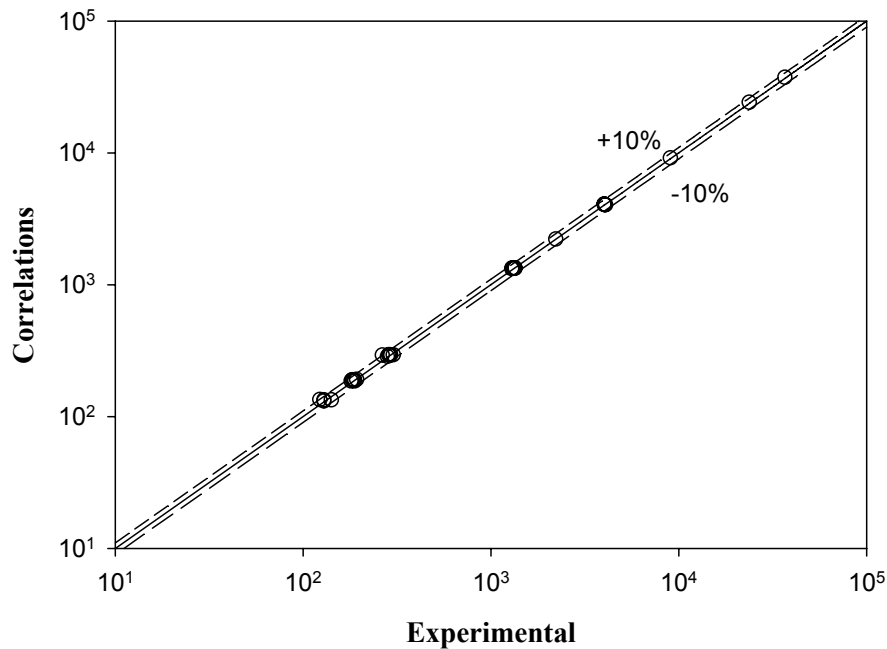


Figure 5.43. Parity plot of two-phase friction factor at different CMC concentrations and batch mode ($u_L = 0$ m/s)

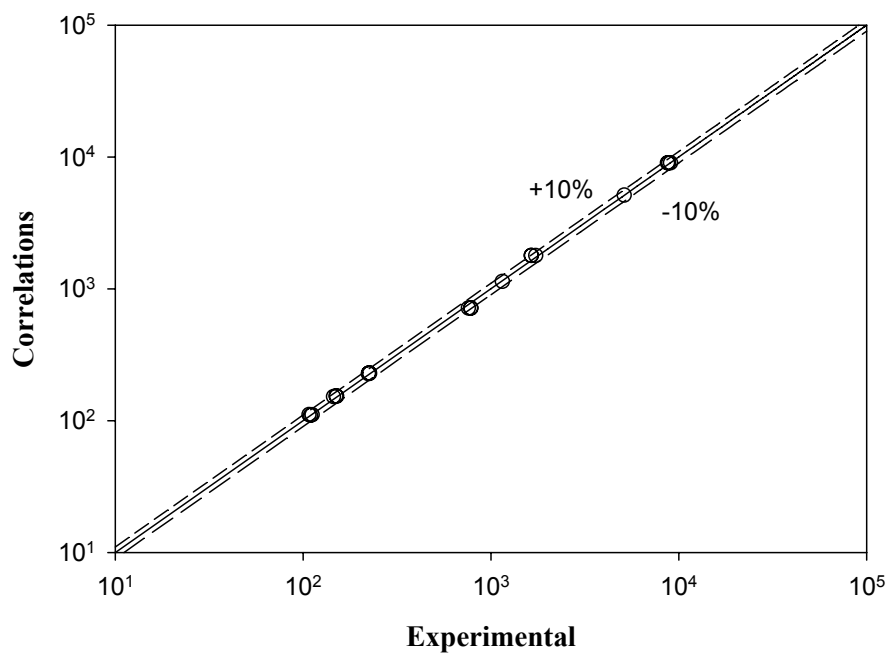


Figure 5.44. Parity plot of two-phase friction factor at different CMC concentrations and continuous mode ($u_L = 0.0045$ m/s)

5.2.2. Gas holdup

The gas holdup was determined by two techniques: the disengagement and pressure drop techniques, described in Chapter 4.

Figure 5.45 shows the effect of superficial velocities the gas and liquid phases on gas holdup obtained with the disengagement technique. While the increase of superficial gas velocity strongly increased the gas holdup, the effect of superficial liquid velocity was rather negligible. Similar trends were found in the case of 0.20 and 0.40% of CMC solutions. The corresponding results are shown in Figures 5.46 and 5.47.

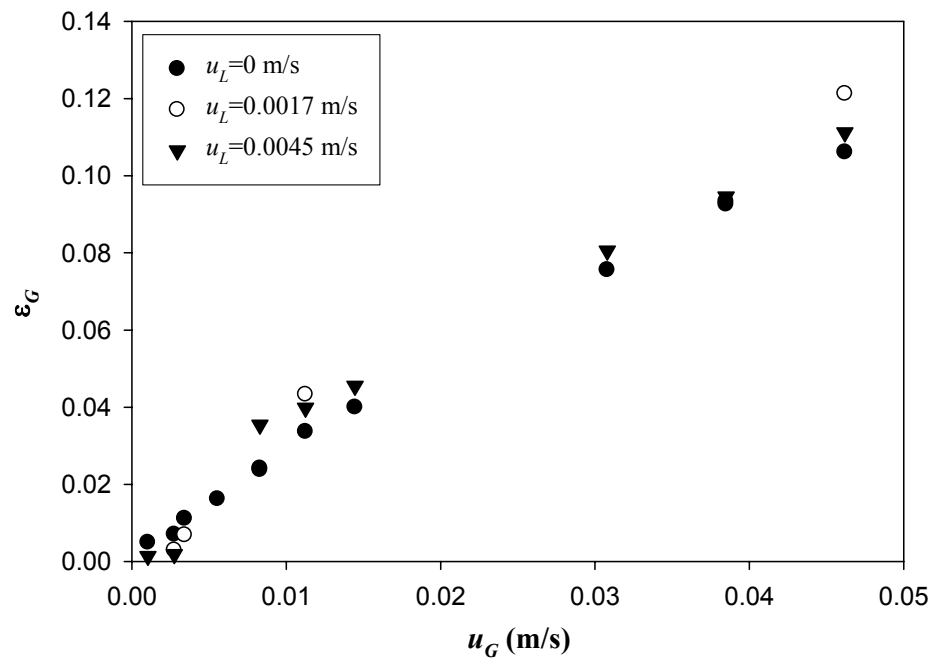


Figure 5.45. Effect of superficial liquid velocity over gas holdup for tap water

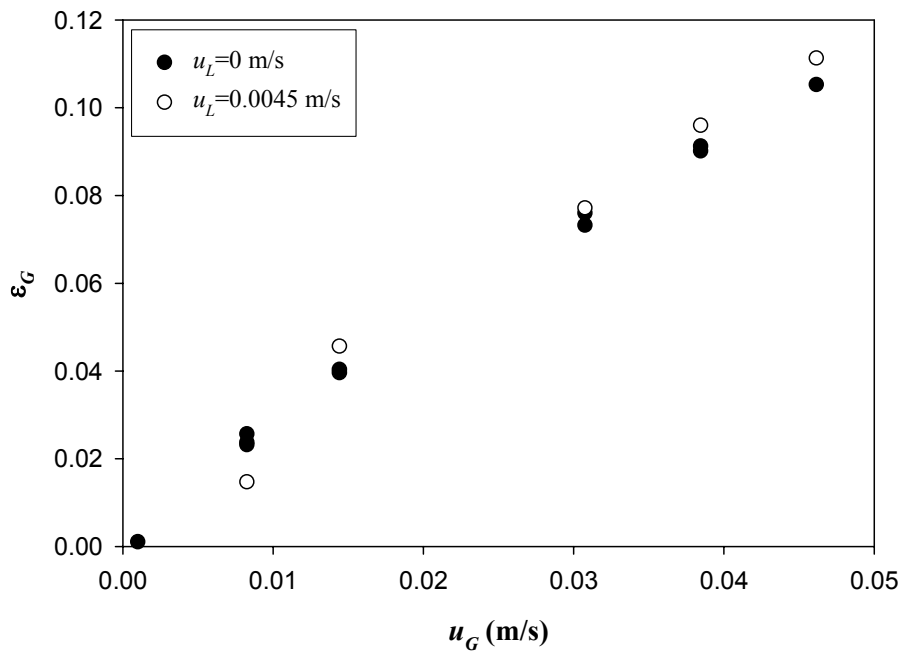


Figure 5.46. Effect of superficial liquid velocity over gas holdup for 0.20% aqueous solution of CMC

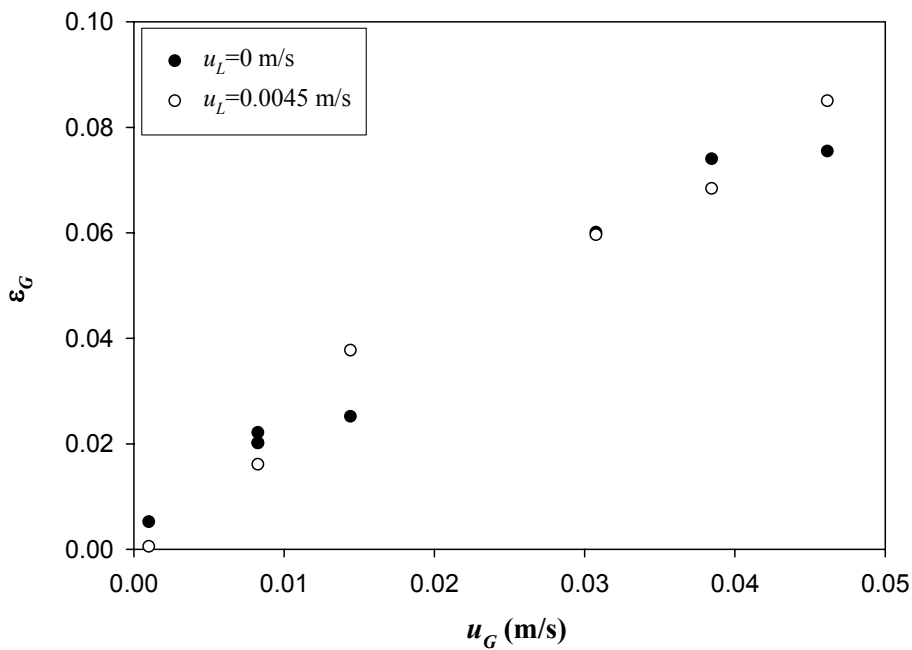


Figure 5.47. Effect of superficial liquid velocity over gas holdup for 0.40% aqueous solution of CMC

Analogous trends were obtained with the pressure drop technique. The comparison between results obtained by both techniques is shown in Figure 5.48. In this figure it is observed that the values have a deviation of $\pm 10\%$ bar lines respect to the straight line of 45° indicating that both techniques provide similar values of gas holdup.

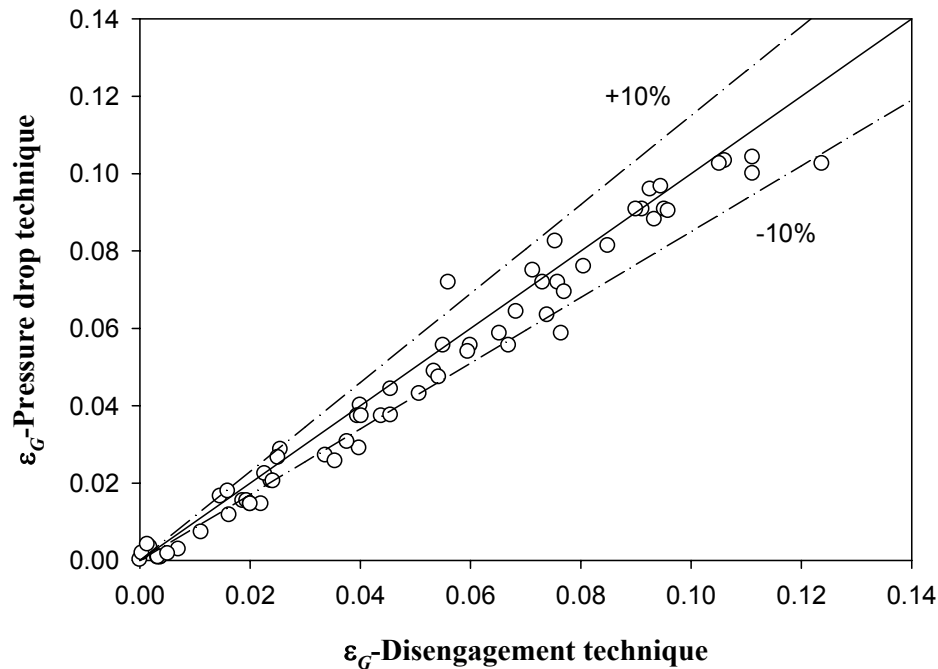


Figure 5.48. Comparison between results of gas holdup obtained by disengagement and pressure drop techniques

In Figures 5.45 through 5.47, two zones are present identifying the two flow regimes mentioned previously (visual observations in the bubble column during each run confirm the trend of the data). For these two regimes, and taking into account whether the fluid is Newtonian or non-Newtonian, four expressions were obtained by each of the two techniques described. They are shown in Table 5.10. In this table, the values obtained from both techniques are used to obtain the correlations in each flow regime and both kinds of fluids considered. Table 5.11 shows the correlations to calculate gas holdup as a function of dimensionless numbers. Both tables, comparing the equivalent expressions for each kind of fluids and regime flow, give similar regression coefficients.

For this reason, the following figures correspond to the correlations proposed in Table 5.11.

Table 5.10. Correlations for gas holdup

Fluid	Regime	Correlation
Newtonian	Heterogeneous bubbling flow regime ($1.04 \times 10^{-3} \leq u_G (m/s) \leq 1.44 \times 10^{-2}$)	$\varepsilon_G = 5.58 u_G^{1.14}$ (5.17)
	Heterogeneous churn turbulent flow regime ($3.07 \times 10^{-2} \leq u_G (m/s) \leq 4.62 \times 10^{-2}$)	$\varepsilon_G = 1.57 u_G^{0.87}$ (5.18)
Non-Newtonian	Heterogeneous bubbling flow regime ($1.04 \times 10^{-3} \leq u_G (m/s) \leq 1.44 \times 10^{-2}$)	$\varepsilon_G = 4.52 n^{5.07} u_G^{1.16n} k^{-0.04n}$ (5.19)
	Heterogeneous churn turbulent flow regime ($3.07 \times 10^{-2} \leq u_G (m/s) \leq 4.62 \times 10^{-2}$)	$\varepsilon_G = 0.184 n^{-2.26} u_G^{0.909n} k^{-0.466n}$ (5.20)

Table 5.11. Correlations for gas holdup as a function of dimensionless numbers

Fluid	Regime	Correlation
Newtonian	Heterogeneous bubbling flow regime ($1.04 \times 10^{-3} \leq u_G (m/s) \leq 1.44 \times 10^{-2}$)	$\varepsilon_G = 1.92 \times 10^{-5} \text{Re}_G^{1.32} \text{Fr}_G^{-0.18}$ (5.21)
	Heterogeneous churn turbulent flow regime ($3.07 \times 10^{-2} \leq u_G (m/s) \leq 4.62 \times 10^{-2}$)	$\varepsilon_G = 1.01 \times 10^{-2} \text{Re}_G^{0.52} \text{Fr}_G^{0.28}$ (5.22)
Non-Newtonian	Heterogeneous bubbling flow regime ($1.04 \times 10^{-3} \leq u_G (m/s) \leq 1.44 \times 10^{-2}$)	$\varepsilon_G = 8.70 n^{5.60} \text{Re}_G^{0.031n} \text{Fr}_G^{1.17n}$ (5.23)
	Heterogeneous churn turbulent flow regime ($3.07 \times 10^{-2} \leq u_G (m/s) \leq 4.62 \times 10^{-2}$)	$\varepsilon_G = 0.374 n^{-1.97} \text{Re}_G^{0.450n} \text{Fr}_G^{0.409n}$ (5.24)

Experimental data were compared to the proposed correlations and to other correlations proposed by other authors. These results are shown in the following figures.

Figures 5.49 through 5.54 show that experimental data are fit by proposed correlations in this work (the curves described by the proposed correlations are near to

experimental data) while the correlations proposed by other authors under predict the gas holdup in the majority of the cases except in the case of the correlation proposed by Ityokumbul *et al.* (1994) that over predicts the gas holdup at low superficial gas velocity.

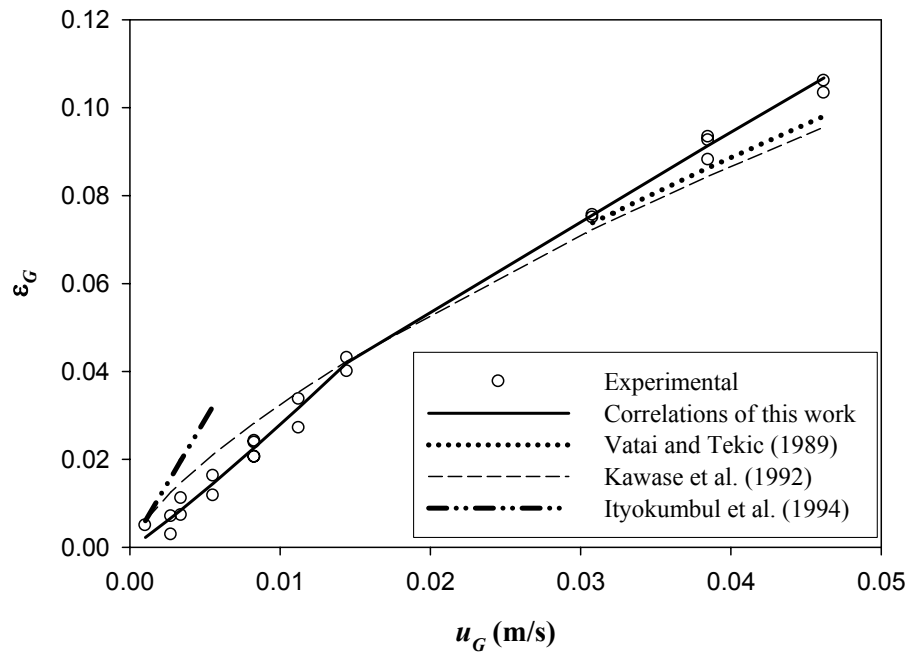


Figure 5.49. Gas holdup for tap water and batch tests ($u_L=0$ m/s)

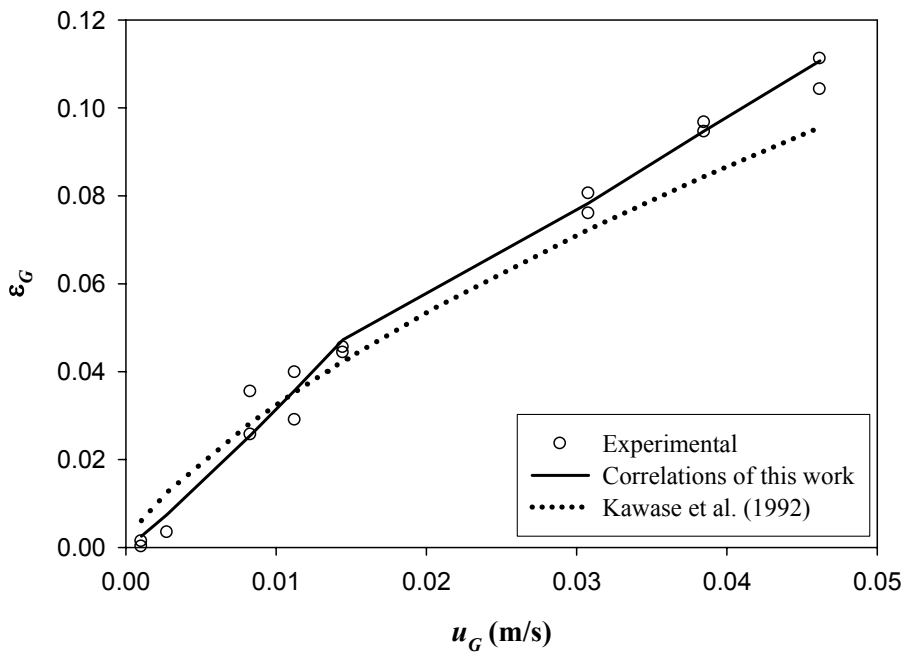


Figure 5.50. Gas holdup for tap water and continuous tests ($u_L=0.0045$ m/s)

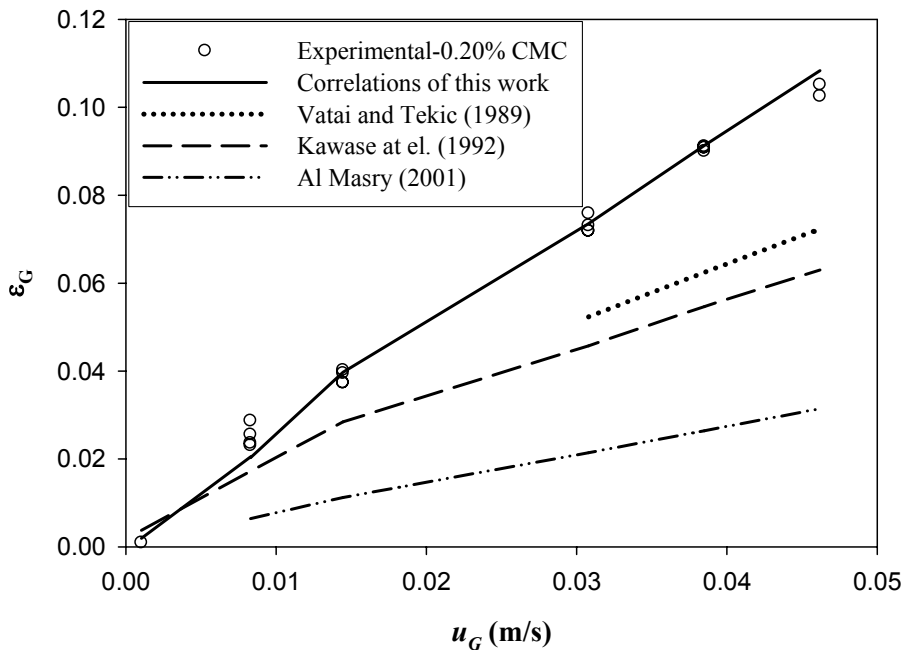


Figure 5.51. Gas holdup for 0.20% CMC solution and batch mode ($u_L=0$ m/s)

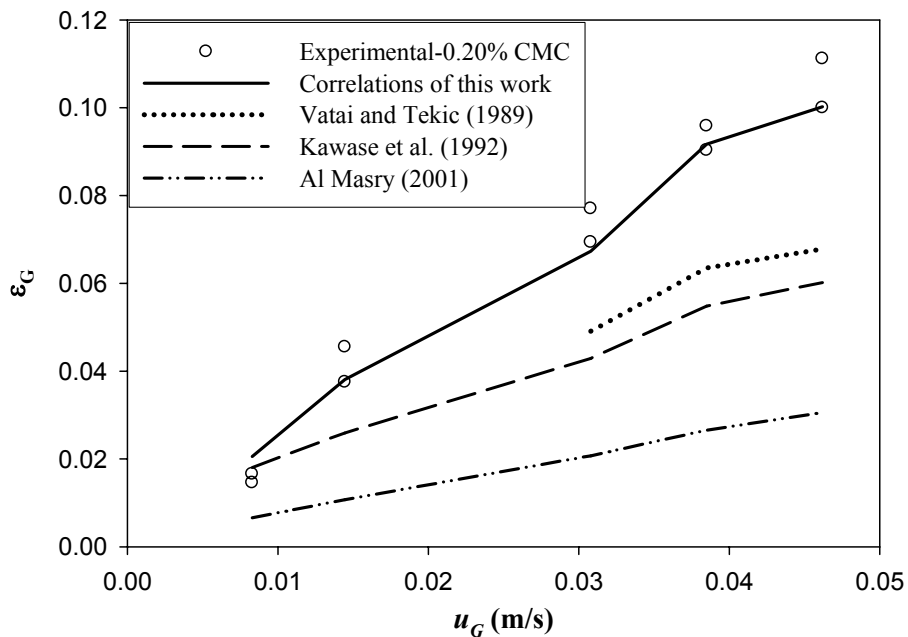


Figure 5.52. Gas holdup for 0.20% CMC solution and continuous mode ($u_L=0.0045$ m/s)

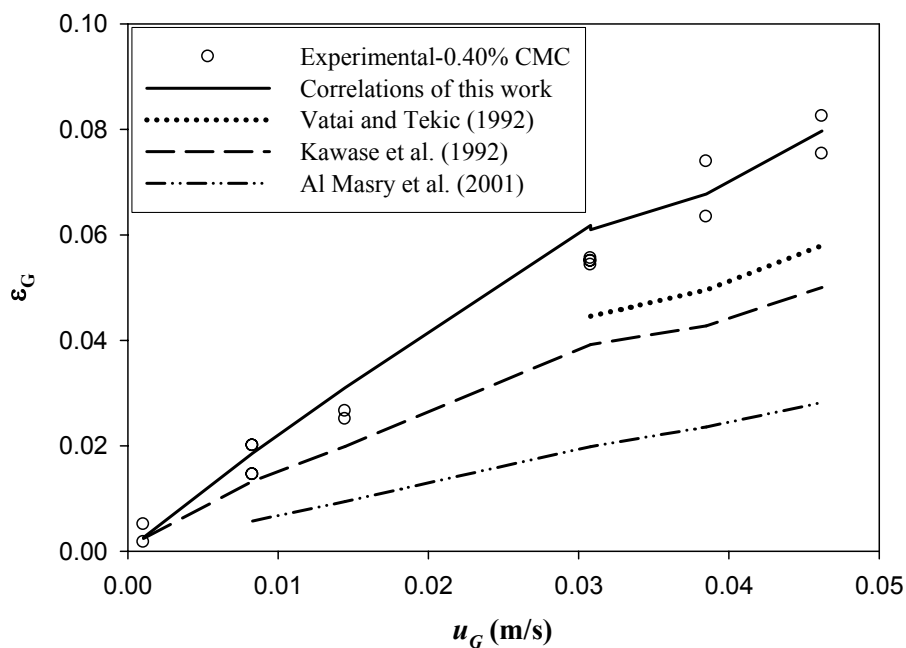


Figure 5.53. Gas holdup for 0.40% CMC solution and batch mode ($u_L=0$ m/s)

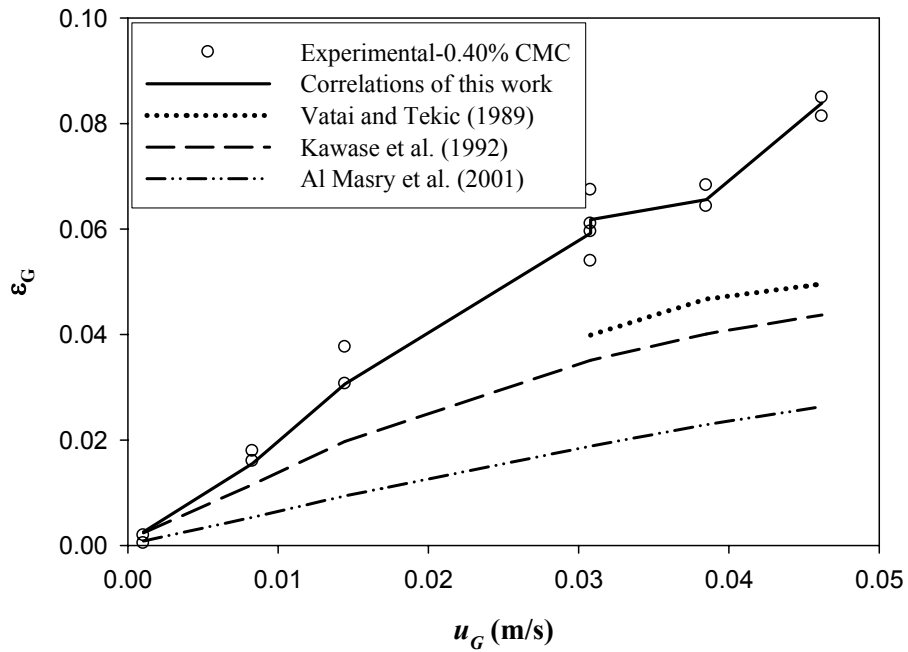


Figure 5.54. Gas holdup for 0.40% CMC solution and continuous mode ($u_L=0.0045$ m/s)

The comparison between experimental data and the proposed correlations are presented in the two following parity plots. Figures 5.55 and 5.56 show that proposed correlations provide deviation of $\pm 10\%$ bar lines respect to the straight line of 45° , indicating that data were fit quite well proposed correlations.

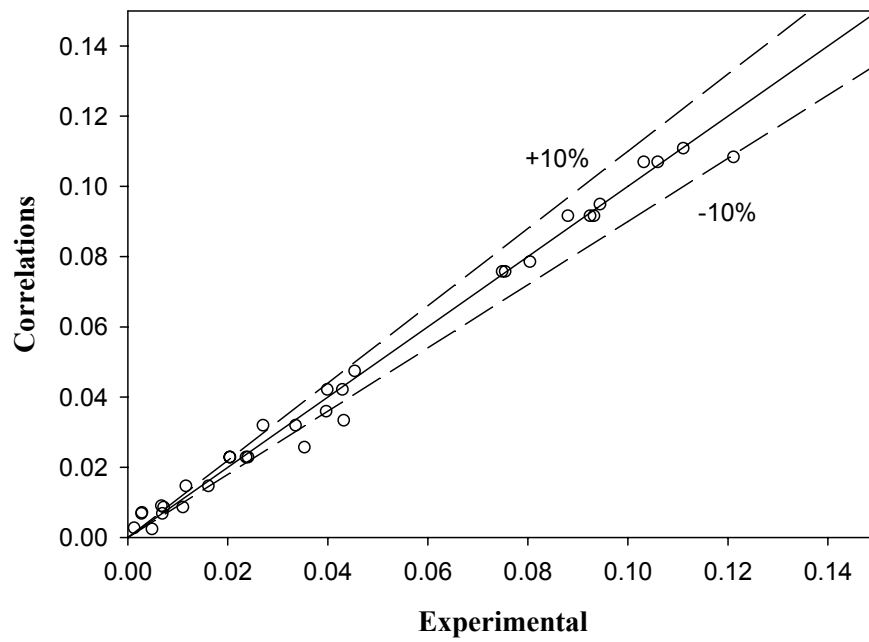


Figure 5.55. Comparison between experimental data and equations (5.21) and (5.22) for gas holdup with tap water

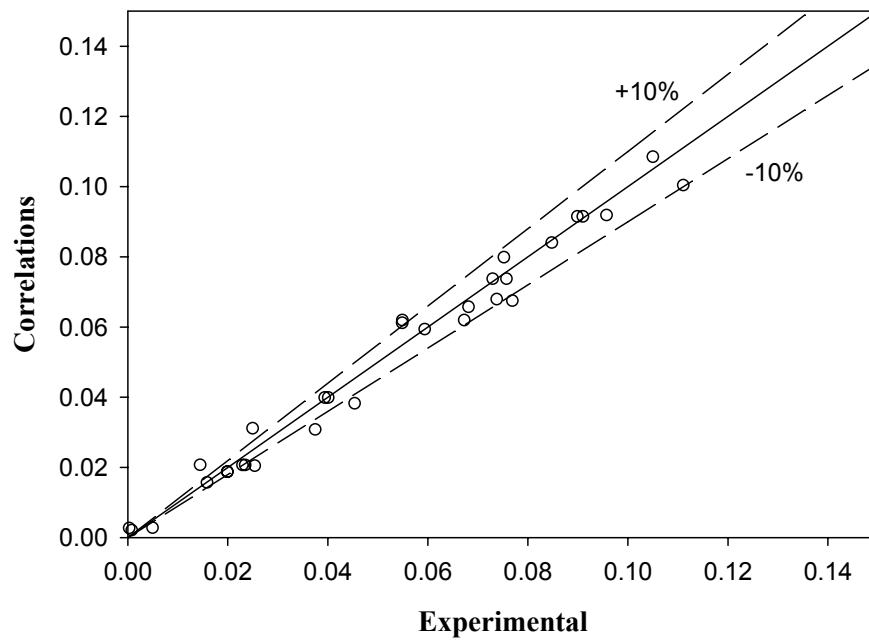


Figure 5.56. Comparison between experimental data and equations (5.23) and (5.24) for gas holdup with CMC solutions

5.2.3. Mixing in the liquid phase

The results of the injection of a tracer impulse in the liquid feed are shown in this section. Additionally, the fit of experimental data by a proposed correlation through the minimization of the sum of squares of errors using a Mathcad® subroutine is presented, together with the best estimate of the parameter and the moments calculated from the parameter.

To show the consistency in the measurements of tracer concentrations, some runs were repeated (repeatability in exit-tracer measures). Figure 5.57 shows the repeatability in the two runs with tap water at $u_G=0.0206$ m/s and $u_L=0.0045$ m/s.

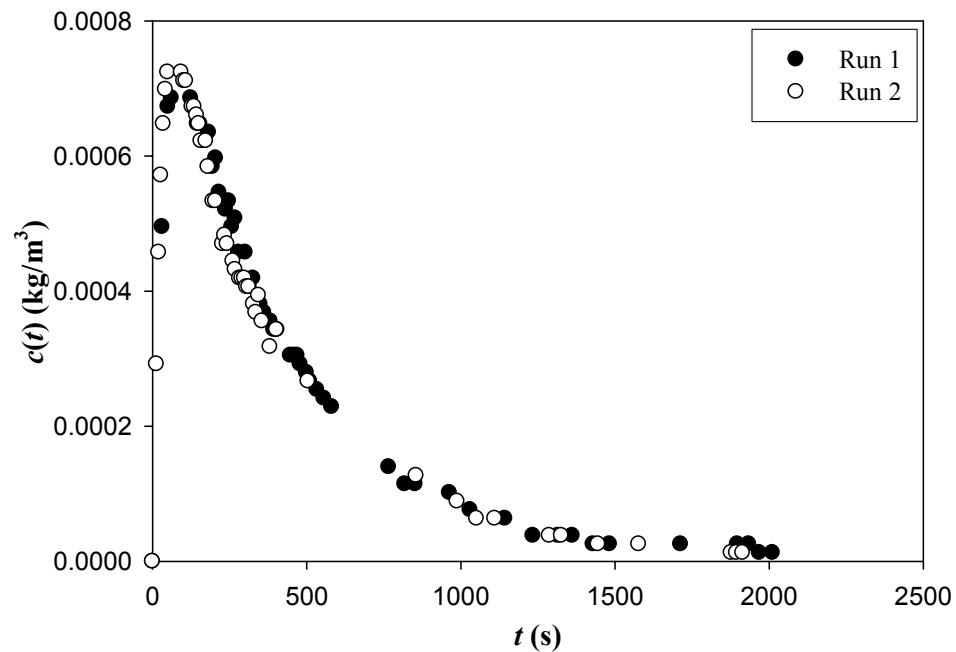


Figure 5.57. Repeatability tests in the exit-tracer concentration for tap water in continuous mode ($u_G=0.0206$ m/s and $u_L=0.0045$ m/s)

To rule out the existence of difference in dispersion in the radial direction, two runs were done at two different radial positions: at $r=0$ and $r=R/2$. Figure 5.58 shows there is not a significant difference in the exit-tracer concentration between the two radial positions; therefore, it is reasonable to consider only the effect of axial position in the dispersion model.

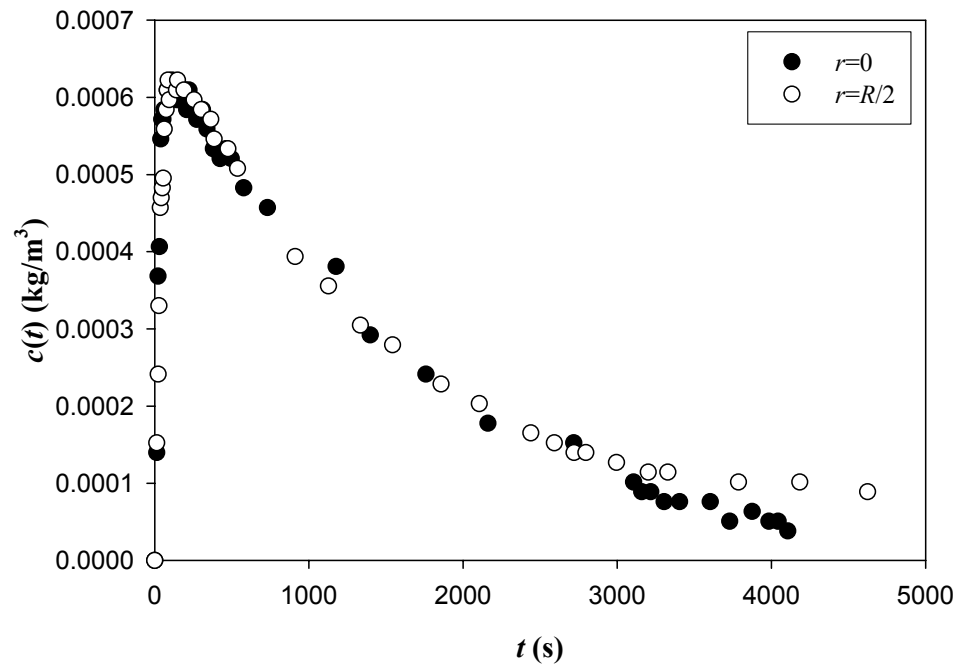


Figure 5.58. Exit-tracer concentration for tap water in continuous mode ($u_G=0.0112$ m/s and $u_L=0.0017$ m/s) at two radial positions

The mixing in the liquid phase was studied considering the operation mode. In each case (batch and continuous mode), experimental data and the equation of the model considered could fit these data were plotted. The parameter of the proposed model was adjusted to find its best value that permitted the best fit. This procedure was developed through Mathcad® software and its minimization technique.

In the case of batch mode, the programmed expression was Eq. (3.95) and the results of this model shows that it fitted quite well experimental data as it is observed in Figure 5.59 for tap water. Similar plots are shown in Figures 5.60 and 5.61 for 0.20 and 0.40% CMC solutions.

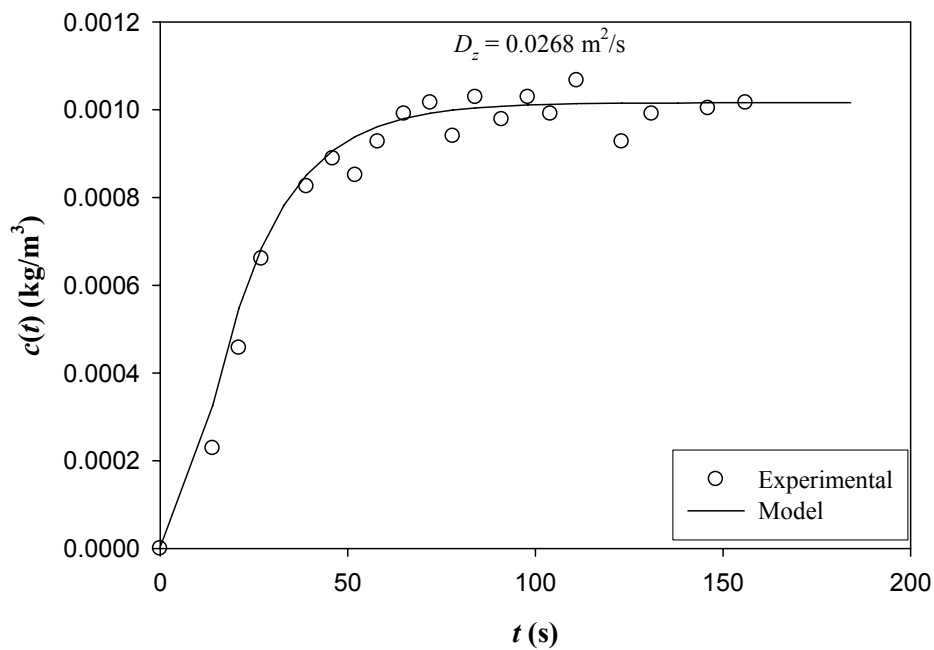


Figure 5.59. Exit-tracer concentration for tap water in batch mode ($u_G=0.0083 \text{ m/s}$ and $u_L=0 \text{ m/s}$)

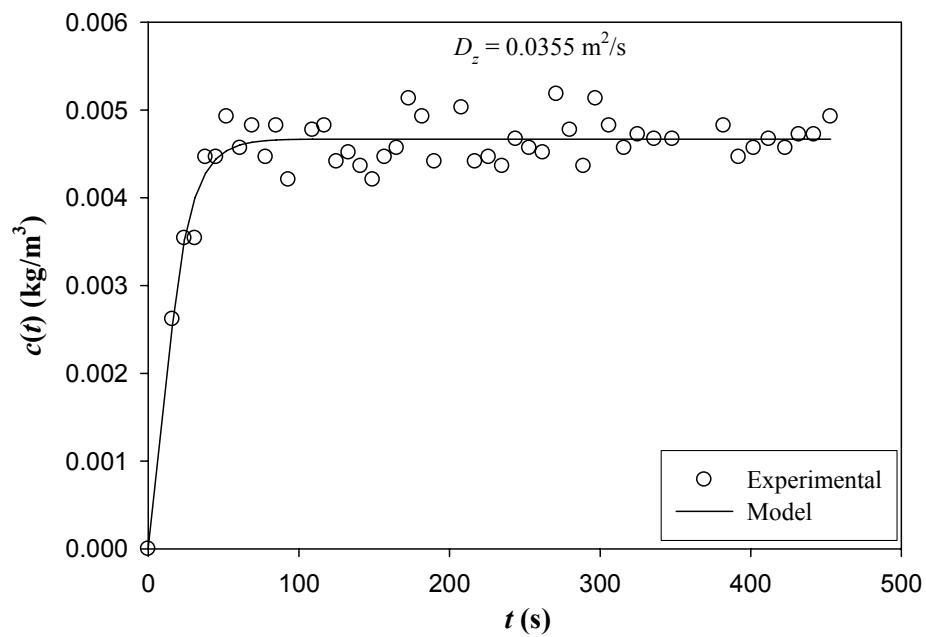


Figure 5.60. Exit-tracer concentration for 0.20% CMC solution in batch mode ($u_G=0.0308 \text{ m/s}$ and $u_L=0 \text{ m/s}$)

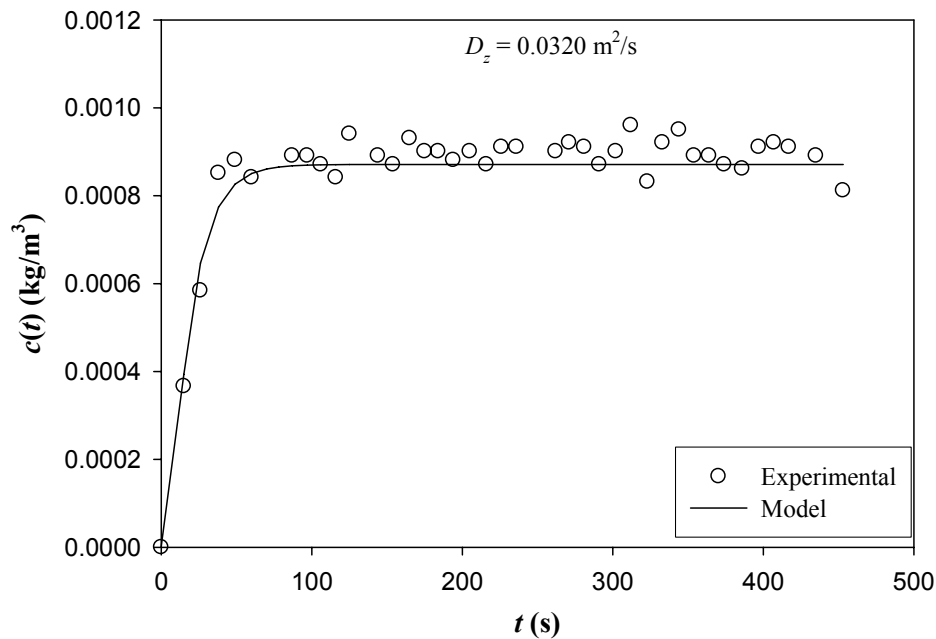


Figure 5.61. Exit-tracer concentration for 0.40% CMC solution in batch mode ($u_G=0.0462$ m/s and $u_L=0$ m/s)

In continuous mode, Eq. (3.74) for the tanks-in-series model and Eq. (3.84) for the axial dispersion model with boundary conditions open-open were programmed in Mathcad®. In Chapter III, the similarity between tanks-in-series model and axial dispersion model with closed-closed boundary conditions was mentioned. The easiest procedure was to fit the tanks-in-series model to experimental data through the minimization of the sum of squares of errors using the parameter N and, when this value was found, it was substituted in equations (3.75) through (3.77) to calculate the moments of this model. Each result was equaled to moments expressions of axial dispersion model with closed-closed boundary conditions (equations 3.90 through 3.92) and the Bodenstein number was calculated from second and third moments, following verification of the first moment condition of this model. A similar procedure was followed with the axial dispersion model with open-open boundary conditions.

In all cases of this work, the first dimensionless moment was near to one, that is consistent with the expression of this dimensionless moment for tanks-in-series and axial

dispersion model with closed-closed boundary condition models. Additionally, when Eq. (3.84) of axial dispersion model with open-open boundary conditions was plotted, no fit of this model was found.

Figure 5.62 shows the experimental data and the models tested for tap water. It is observed that the axial dispersion model (ADM) with open-open boundary conditions does not fit the experimental data. Figures 5.63 and 5.64 show results for 0.20 and 0.40% CMC solutions that were similar to those obtained with tap water. These results were similar at the other gas and liquid superficial velocities considered.

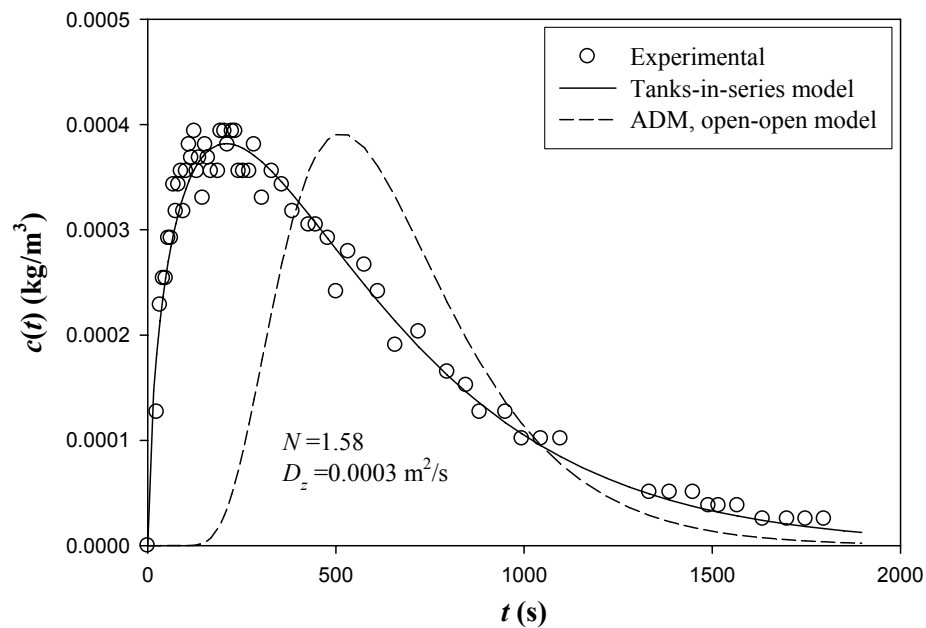


Figure 5.62. Exit concentration of an impulse of tracer for tap water at continuous mode ($u_G=0.0010 \text{ m/s}$ and $u_L=0.0025 \text{ m/s}$)

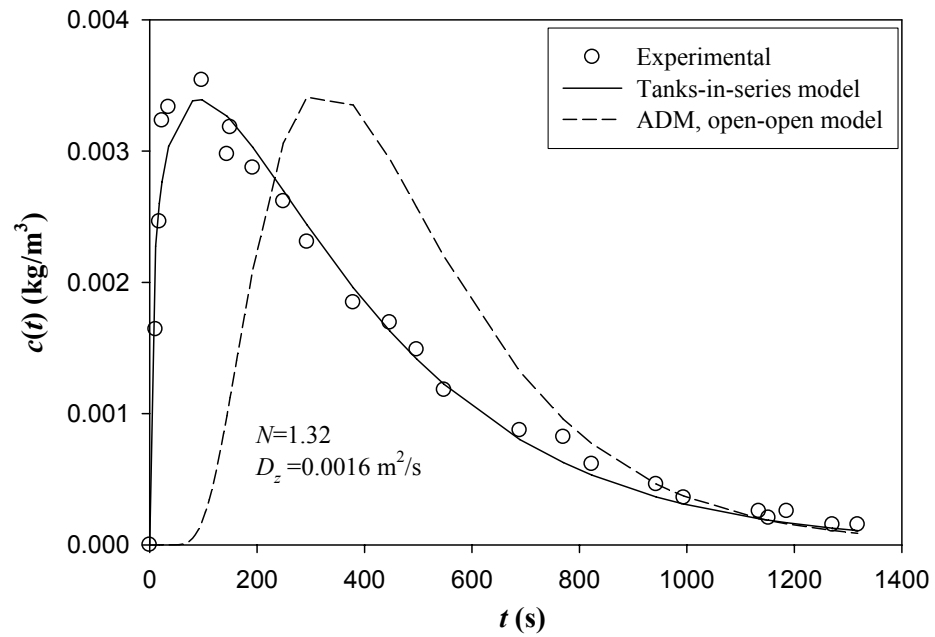


Figure 5.63. Exit concentration of an impulse of tracer for 0.20% of CMC solution in continuous mode ($u_G=0.0462 \text{ m/s}$ and $u_L=0.0045 \text{ m/s}$)

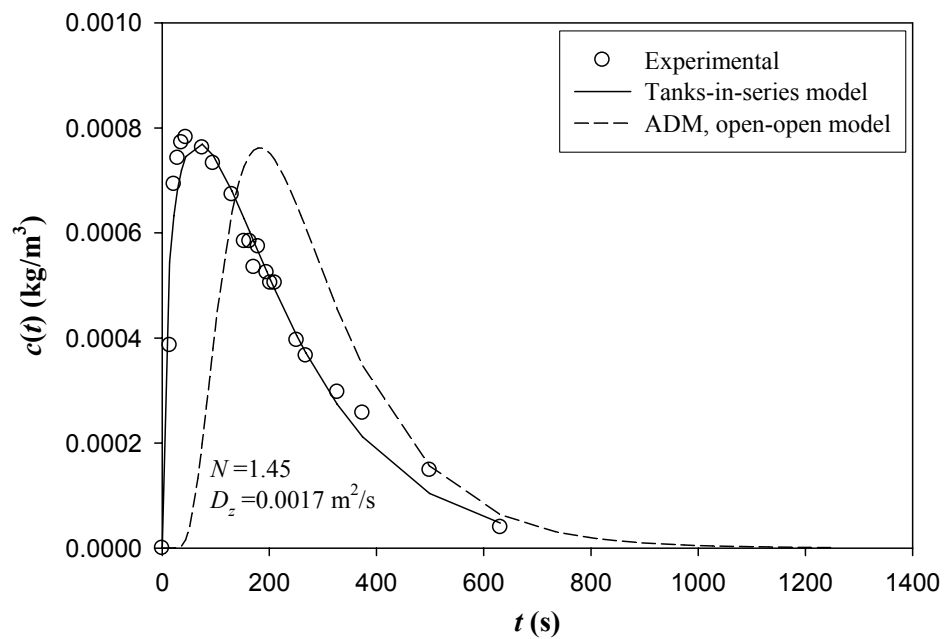


Figure 5.64. Exit concentration of an impulse of tracer for 0.40% of CMC solution in continuous mode ($u_G=0.0462 \text{ m/s}$ and $u_L=0.0045 \text{ m/s}$)

From the fit of the models to the experimental data (as it is illustrated in Appendix D), some empirical expressions were proposed to evaluate the axial dispersion coefficient for Newtonian and non-Newtonian fluids. These expressions are presented in Table 5.12. Table 5.13 shows the correlations for Newtonian fluids that were found as a function of dimensionless numbers with the similar regression coefficient, but it is not the case for non-Newtonian fluids because of the high dependency of the correlations of the consistency index (k) of the power-law model of rheology. For this reason, correlations to calculate the axial dispersion coefficient as a function of dimensionless number were not proposed.

Table 5.12. Correlations for axial dispersion coefficient

Fluid	Regime	Correlation
Newtonian	Heterogeneous bubbling flow regime $(1.04 \times 10^{-3} \leq u_G (m/s) \leq 1.44 \times 10^{-2})$	$D_z = 0.027u_G^{0.039} + 3.11u_L - 0.066u_L^{0.16}$ (5.17)
	Heterogeneous churn turbulent flow regime $(3.07 \times 10^{-2} \leq u_G (m/s) \leq 4.62 \times 10^{-2})$	$D_z = 0.095u_G^{0.41} + 11u_L - u_L^{0.52}$ (5.18)
Non-Newtonian	Heterogeneous bubbling flow regime $(1.04 \times 10^{-3} \leq u_G (m/s) \leq 1.44 \times 10^{-2})$	$D_z = 6.8u_G^{4.3(1-n)} k^{\left(\frac{-1.1n}{1.8-0.77n}\right)}$ for $u_L = 0$ m/s (5.19) $D_z = 0.68u_G^{2.5(1-n)} k^{\left(\frac{0.42n}{2.5-2.2n}\right)}$ for $u_L = 0.0045$ m/s (5.20)
	Heterogeneous churn turbulent flow regime $(3.07 \times 10^{-2} \leq u_G (m/s) \leq 4.62 \times 10^{-2})$	$D_z = 0.02u_G^{-0.09} k^{\left(\frac{1.6n}{8.5-9.9n}\right)}$ for $u_L = 0$ m/s (5.21) $D_z = 2.6u_G^{6.0(1-n)} k^{\left(\frac{0.38n}{1.2-0.92n}\right)}$ for $u_L = 0.0045$ m/s (5.22)

* k and n are the rheological parameters of the power-law model

Table 5.13. Correlations for axial dispersion coefficient as a function of dimensionless numbers

Fluid	Regime	Correlation
Newtonian	Heterogeneous bubbling flow regime $(1.04 \times 10^{-3} \leq u_G (m/s) \leq 1.44 \times 10^{-2})$	$D_z = 0.0245 Fr_G^{0.0227} + 0.00441 Re_L - 0.00476 Re_L^{0.989}$ (5.23)
	Heterogeneous churn turbulent flow regime $(3.07 \times 10^{-2} \leq u_G (m/s) \leq 4.62 \times 10^{-2})$	$D_z = 0.0232 (Re_G Fr_G)^{0.0328} \times (1 + Re_L)^{-0.258}$ (5.24)

Experimental data were compared to the proposed correlations and to others proposed by other researchers. These results are shown in the next figures.

Figure 5.65 shows the behavior of the axial dispersion coefficient for tap water at different liquid superficial velocities in the heterogeneous bubbling flow regime. In this figure it is observed that the values of the axial dispersion coefficient are higher in the case of batch mode than in the continuous mode. Additionally, it is seen that in continuous mode, this parameter increases as superficial liquid velocity increases. In batch mode this phenomenon could be explained because of the internal movement of liquid (recirculation of the liquid phase) induced only by gas movement in the bubble column in which prevails the stochastic mixing caused by the motion of the rising bubbles (an eddy dispersion term), while in continuous mode, a convective contribution is present due the circulation of the liquid phase in the system (a Taylor dispersion term) so that, it is possible that the liquid causes a drag of the phases to be out of the system, diminishing the eddies contribution and therefore, the axial dispersion coefficient. In this figure, the proposed Eq. (5.17) fits quite well the experimental data. Similar results were obtained in the heterogeneous churn turbulent regime, in which Eq. (5.18) fits the experimental data at different liquid superficial velocities (Figure 5.66).

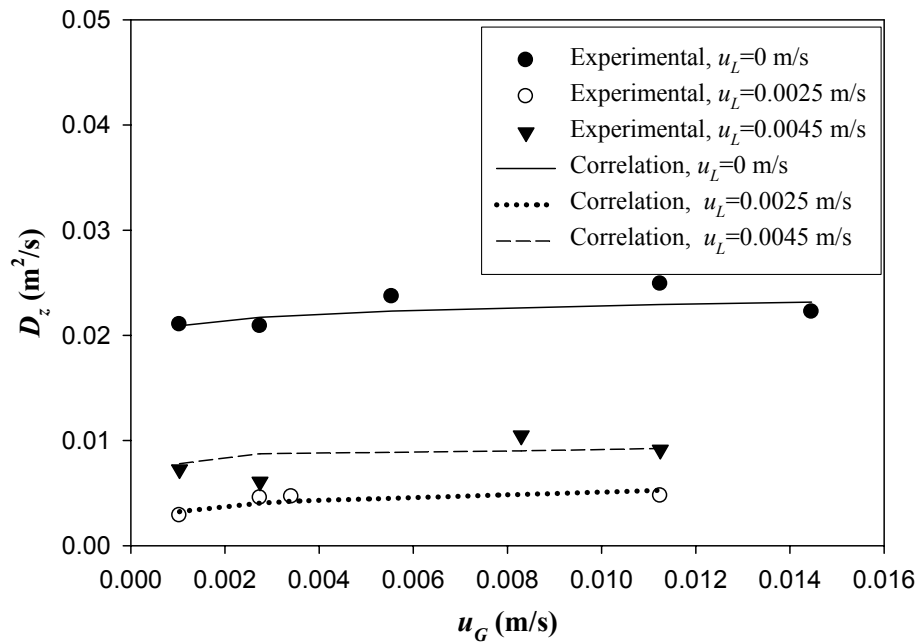


Figure 5.65. Axial dispersion coefficient for tap water at different superficial liquid velocity and $1.04 \times 10^{-3} \leq u_G$ (m/s) $\leq 1.44 \times 10^{-2}$

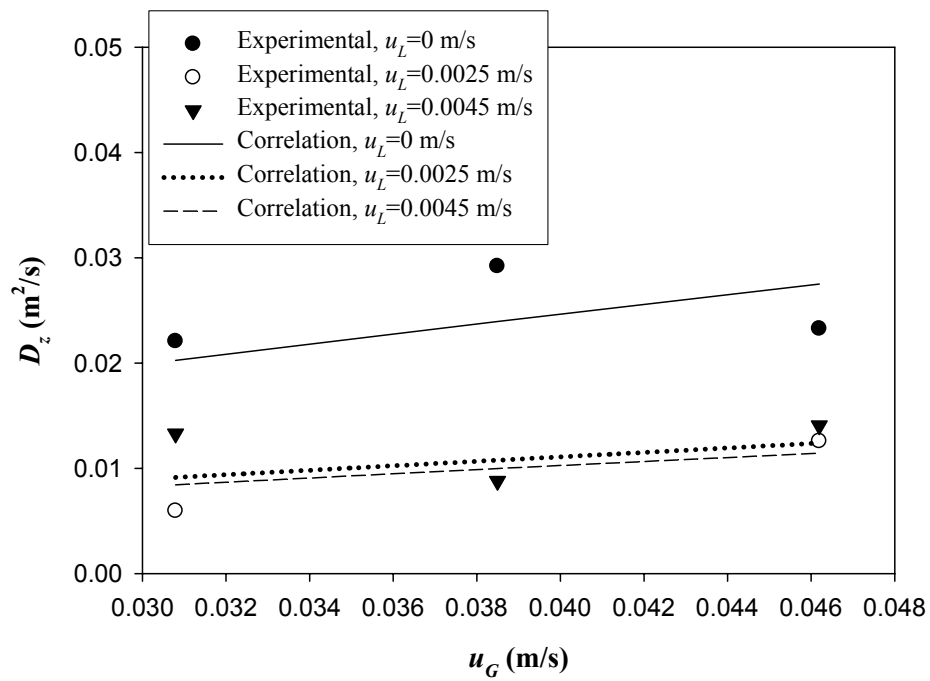


Figure 5.66. Axial dispersion coefficient for tap water at different superficial liquid velocity and $(3.07 \times 10^{-2} \leq u_G$ (m/s) $\leq 4.62 \times 10^{-2})$

For each flow regime, experimental data and proposed correlations were compared to expressions proposed by other authors. The results obtained are presented in figures 5.67 through 5.69 for heterogeneous bubbling flow regime. In Figure 5.67, that corresponds to batch mode, it is observed that correlation proposed by Kawase and Moo Young (1986) under predicts the values of axial dispersion coefficient while correlation of Hikita and Kikukawa (1974) and expression proposed by Alexander and Shah (1976) predicts quite near the experimental data; however, Eq. (5.17) gives a better fit of them.

Figure 5.68 shows an over prediction of Kawase and Moo Young (1986), Riquarts (1981) and Towel and Ackerman (1972) correlation of the axial dispersion coefficient while Eq. (5.17) fits quite well experimental data.

Figure 5.69 shows the over prediction of Kawase and Moo Young (1986) correlation instead while Towel and Ackerman (1972) expression under predicts the experimental values of the axial dispersion coefficient.

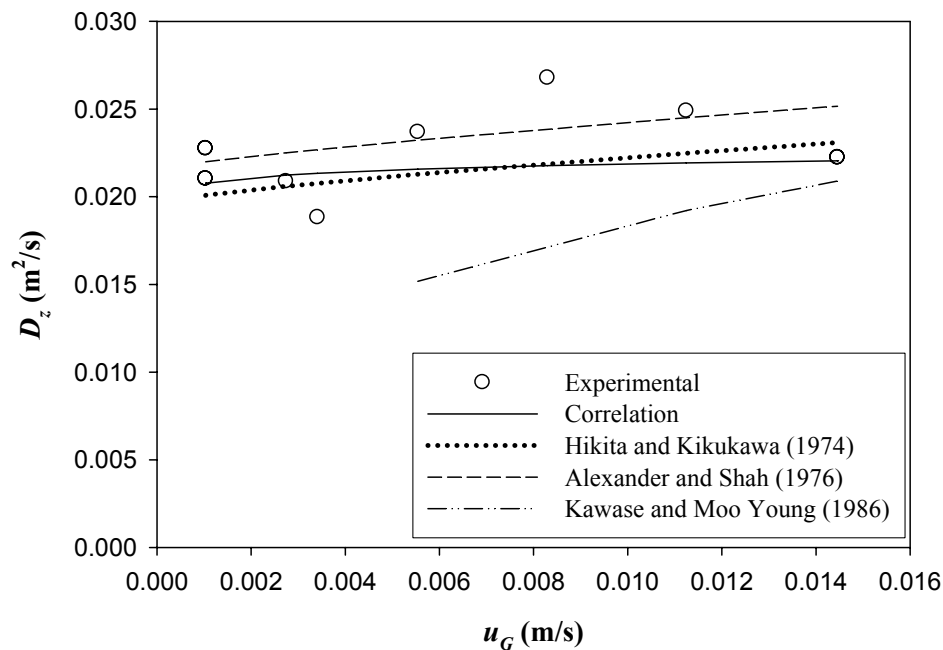


Figure 5.67. Axial dispersion coefficient for tap water in batch mode ($u_L=0$ m/s) and $1.04 \times 10^{-3} \leq u_G$ (m/s) $\leq 1.44 \times 10^{-2}$

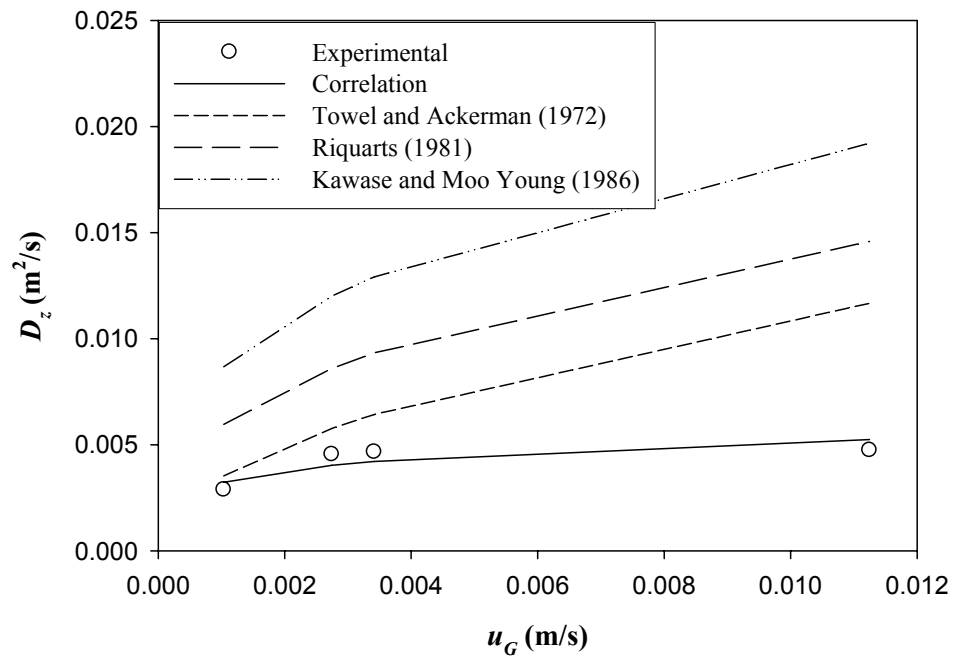


Figure 5.68. Axial dispersion coefficient for tap water in continuous mode ($u_L=0.0025$ m/s) and $1.04 \times 10^{-3} \leq u_G (m/s) \leq 1.44 \times 10^{-2}$

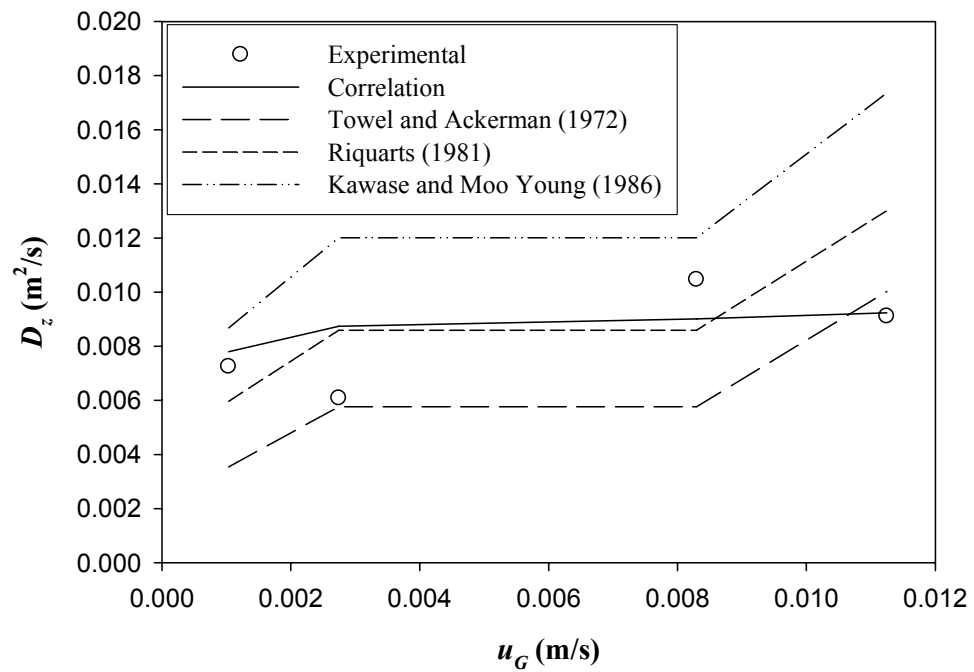


Figure 5.69. Axial dispersion coefficient for tap water in continuous mode ($u_L=0.0045$ m/s) and $1.04 \times 10^{-3} \leq u_G (m/s) \leq 1.44 \times 10^{-2}$

Figure 5.70 shows the parity plot values calculated through Eq. (5.17) and experimental data. It is observed that the values are inside the $\pm 10\%$ deviation lines of the straight line of 45° indicating the correlation fit quite well experimental data in the heterogeneous bubbling flow regime for tap water.

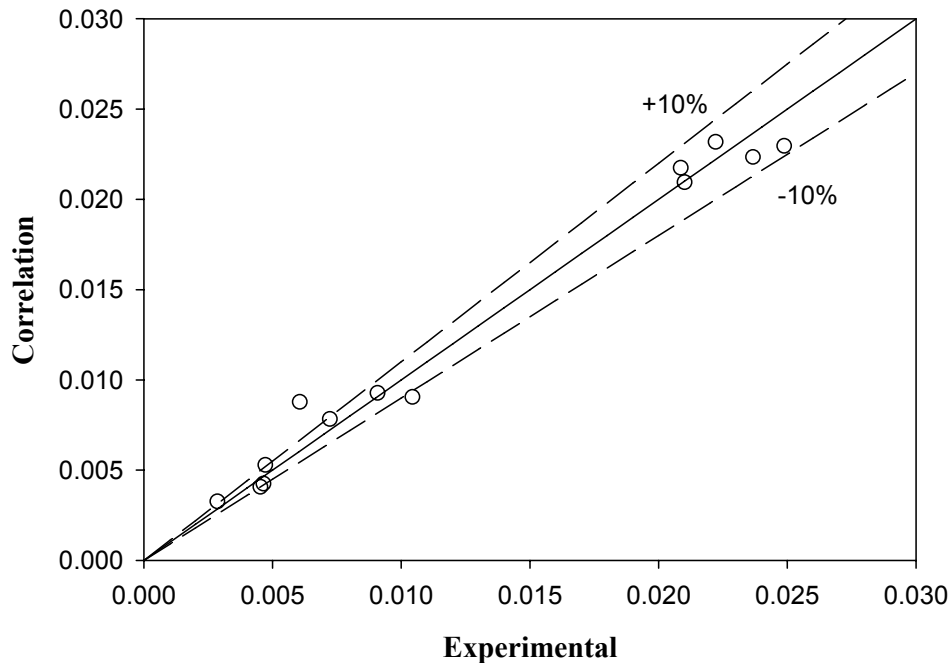


Figure 5.70. Comparison between experimental data and Eq. (5.17) for gas holdup for tap water in the heterogeneous bubbling flow regime

Results for tap water in the heterogeneous churn turbulent flow regime are presented in figures 5.71 and 5.72. In Figure 5.71, that corresponds to the batch mode, it is observed that the correlations proposed by Kawase and Moo Young (1986), Alexander and Shah (1976) and, Hikita and Kikukawa (1974) over predict the values of axial dispersion coefficient. In the case of continuous mode (Figure 5.72), the correlations proposed by Kawase and Moo Young (1986), Riquarts (1981) and Towel and Ackerman (1972) over predict the axial dispersion coefficient too.

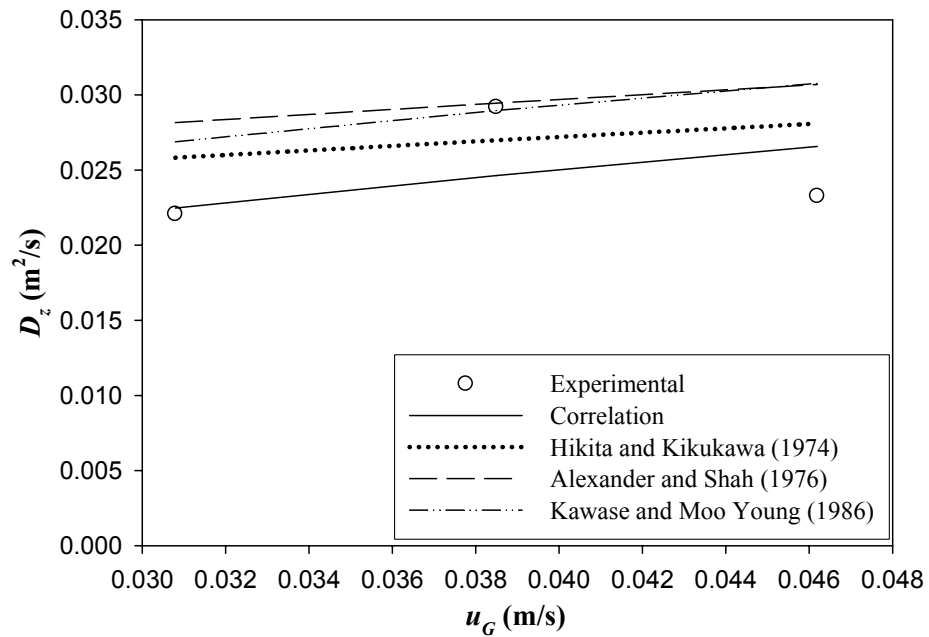


Figure 5.71. Axial dispersion coefficient for tap water in batch mode ($u_L=0$ m/s) and $3.07 \times 10^{-2} \leq u_G$ (m/s) $\leq 4.62 \times 10^{-2}$

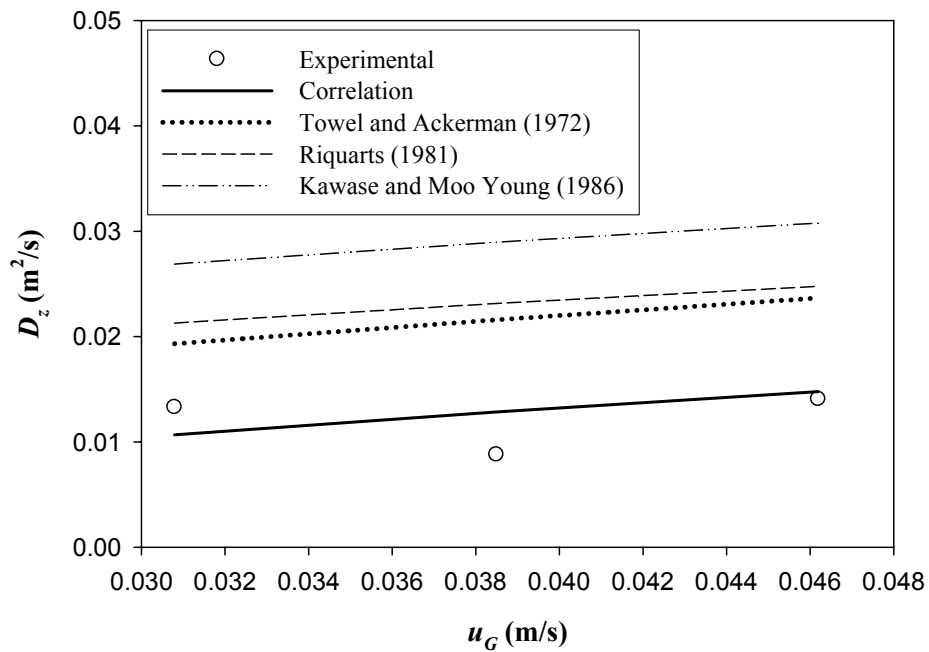


Figure 5.72. Axial dispersion coefficient for tap water in continuous mode ($u_L=0.0045$ m/s) and $3.07 \times 10^{-2} \leq u_G$ (m/s) $\leq 4.62 \times 10^{-2}$

Figure 5.73 shows the comparison between experimental data and Eq. (5.18). It is observed that the values are inside the $\pm 15\%$ deviation lines of the straight line of 45° indicating the correlation fit quite well the experimental data in the heterogeneous churn turbulent flow regime for tap water.

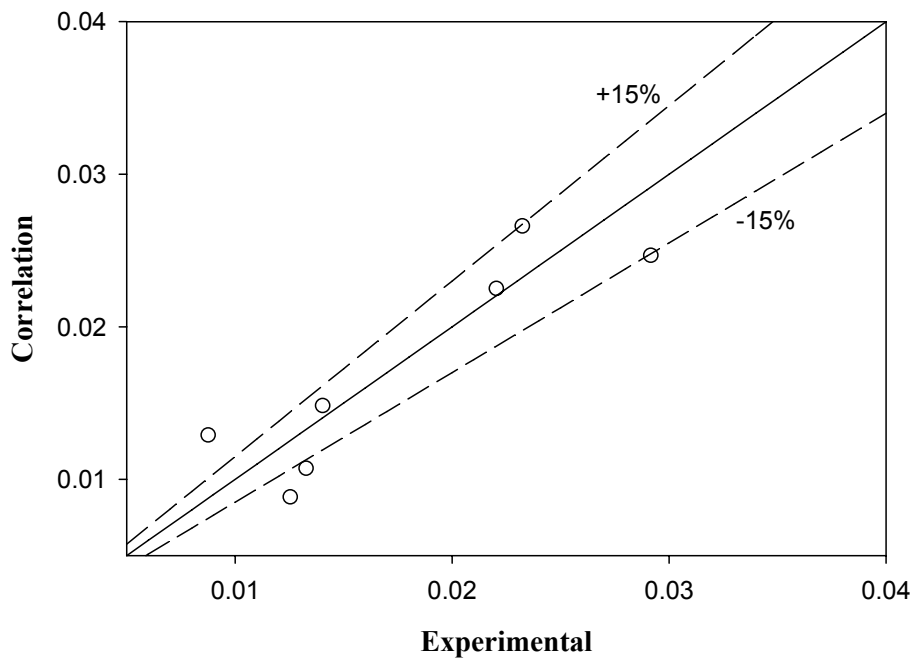


Figure 5.73. Comparison between experimental data and Eq. (5.18) for gas holdup for tap water in the heterogeneous churn turbulent flow regime

Figures 5.74 and 5.75 show a trend of axial dispersion coefficient to increase as superficial gas velocity does, but as the consequence of the impossibility to maintain constant the temperature in the laboratory, the CMC solutions of many runs were different as it is observed in these figures, having in some cases both effects: temperature and superficial velocities. The temperature in the laboratory is a factor that changes the rheological behavior of the CMC solution as it showed previously in this work. In the case of batch mode (Figure 5.74), the correlation of Kawase and Moo Young (1986) are in the region of experimental data but not fit them, however in continuous mode (Figure 5.75), this correlation over predict the axial dispersion coefficient.

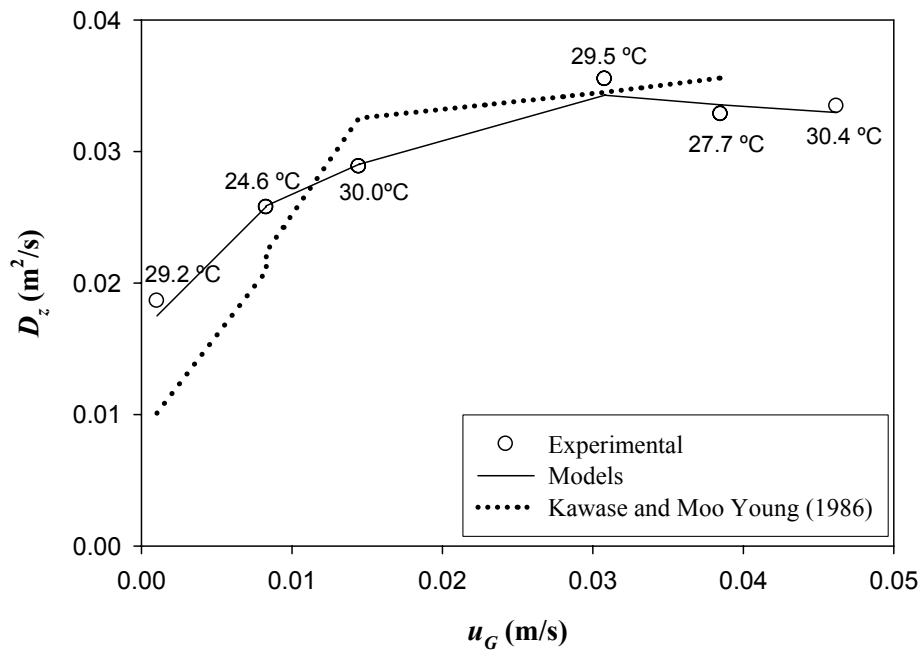


Figure 5.74. Axial dispersion coefficient for 0.20% CMC solution in batch mode ($u_L=0$ m/s)

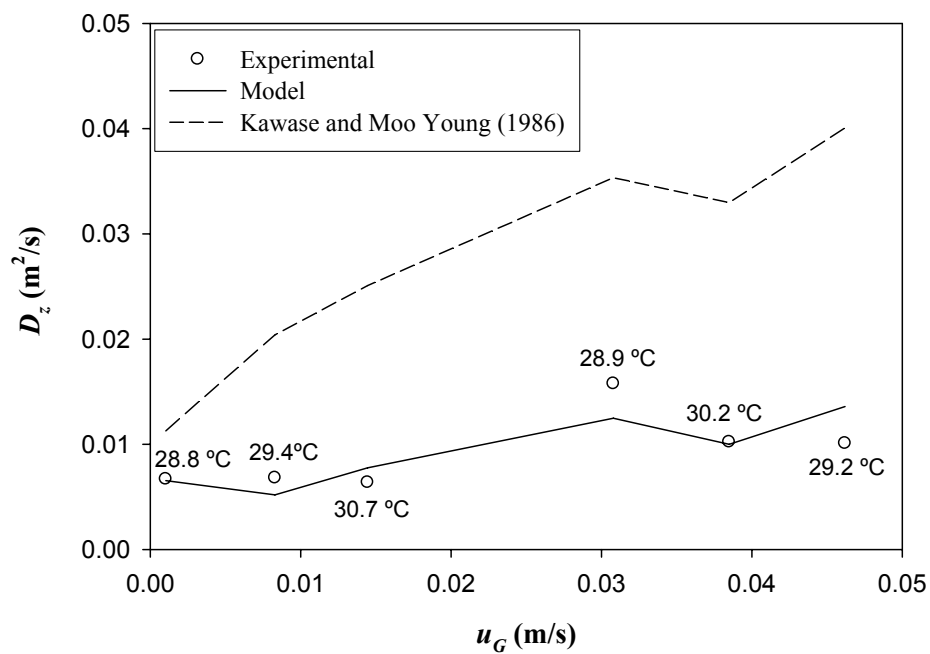


Figure 5.75. Axial dispersion coefficient for 0.20% CMC solution in continuous mode ($u_L=0.0045$ m/s)

Figures 5.76 and 5.77 show the axial dispersion coefficient for 0.40% CMC solutions at $u_L=0$ m/s and $u_L=0.0045$ m/s, respectively. In both figures similar trends were obtained compared to 0.20% CMC solutions. The difference in temperature in the laboratory caused the changes in the rheological parameters of the solution; this is the reason of the two points at $u_G=0.0308$ m/s in both figures.

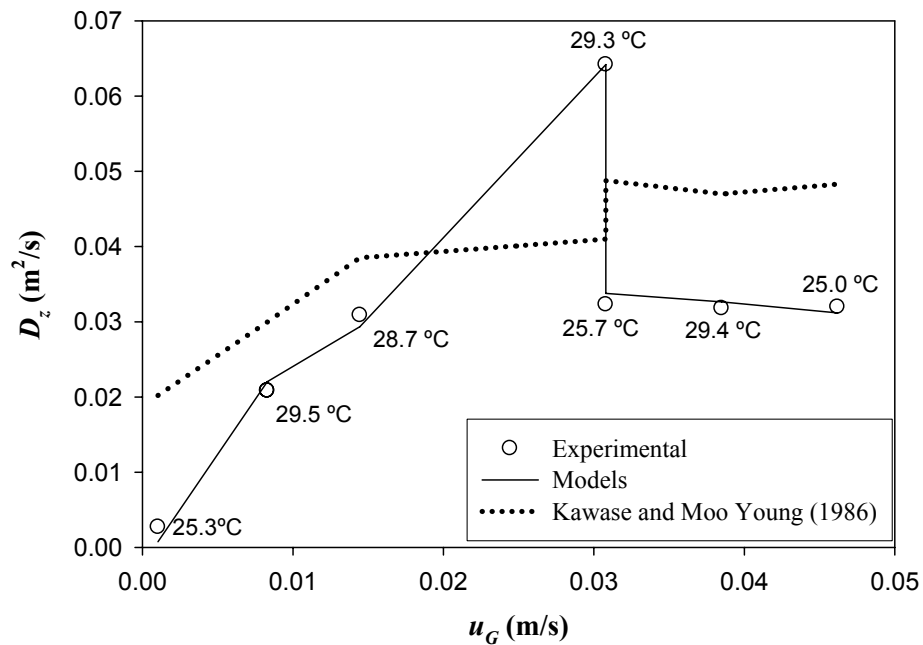


Figure 5.76. Axial dispersion coefficient for 0.40% CMC solution in batch mode ($u_L=0$ m/s)

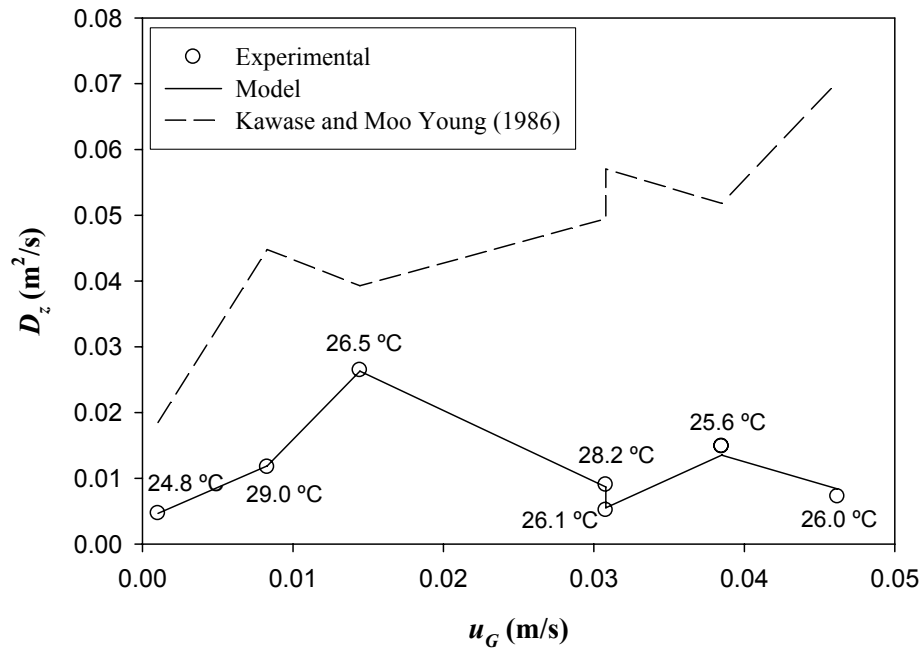


Figure 5.77. Axial dispersion coefficient for 0.40% CMC solution in continuous mode ($u_L=0.0045$ m/s)

To establish the comparison between experimental axial dispersion coefficient and the calculated through equations (5.19) and (5.21), a parity plot is shown in Figure 5.78. In this figure is observed that proposed correlations fit quite well experimental values of this parameter because the values are inside the $\pm 10\%$ deviation lines from straight line of 45° .

Figure 5.79 shows the comparison between experimental data and equations (5.20) and (5.22). In this case, the values are within the $\pm 15\%$ deviation lines from straight line of 45° .

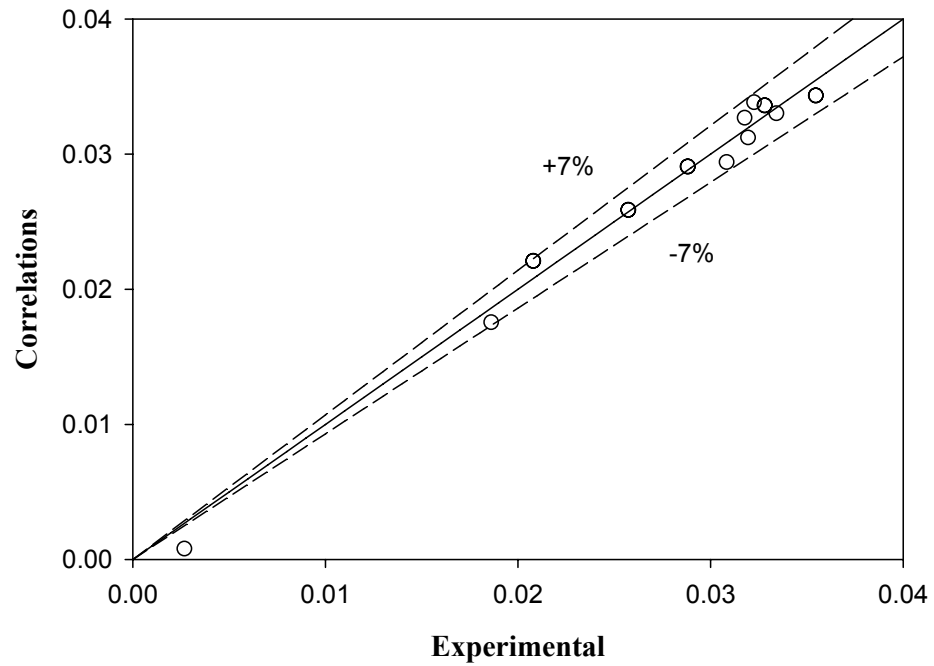


Figure 5.78. Comparison between experimental data and equations (5.19) and (5.21) for axial dispersion coefficient and CMC solutions and batch mode ($u_L=0$ m/s) in both heterogeneous flow regimes

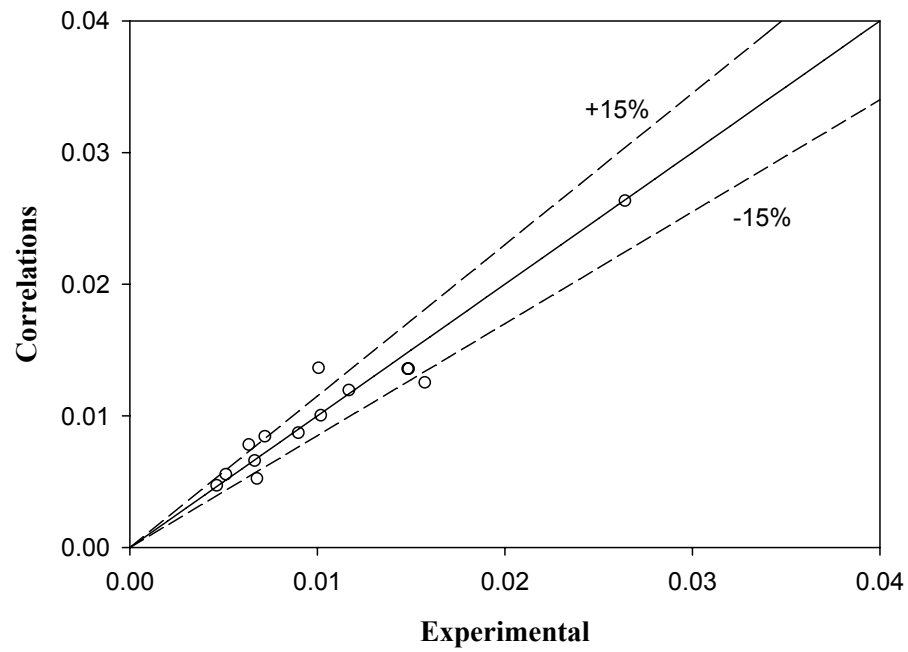


Figure 5.79. Comparison between experimental data and Eq. (5.20) and (5.22) for axial dispersion coefficient and CMC solutions and continuous mode ($u_L=0.0045$ m/s) in heterogeneous bubbling flow regime

6. CONCLUSIONS AND RECOMMENDATIONS

A study of the gas holdup, pressure drop, two-phase friction factor and the mixing in the liquid phase were developed with the available resources in a bubble column of 0.2-m diameter with Newtonian (tap water) and non-Newtonian (CMC solutions) fluids. In it, rheological properties of the liquid phase were considered, characterizing the liquid phase used in the study. This work gives a rigorous study in which two flow regimes were found and important parameters in bubble columns, such as pressure drop, gas holdup and the mixing of the liquid phase were measured and correlated as a function of operational variables as superficial velocities of the phases involved in the column, and the rheological parameters of the power-law model. The rheological parameters were carefully calculated taking into account the effect of the time required to the complete dissolution of the CMC when aqueous polymeric solutions were prepared, the temperature of each experiment in the column, the chemical used as a tracer in RTD experiments. All these parameters were checked at the beginning and at the ending of each experiment to be sure to obtain the best representation of the reality of this process.

The main and specific conclusions to be mentioned are the following:

Relative to rheological characterization:

CMC solutions exhibited a shear thinning behavior in the range of concentrations considered (0.05 to 0.75% by weight).

The power-law model represented the behavior of CMC solutions

CMC solutions did not exhibit thixotropy behavior in the concentrations considered.

The time of dissolution of CMC powder to prepare aqueous solutions of the polymer affected the rheology of the solution; the solution reached no changes in viscosity and flow curves in 23 h approximately.

Temperature is another variable that affected the rheology of CMC solutions. When the temperature increased, the curvature of the viscosity curves tended to decrease and the slopes of the flow curves decreased. For this reason, expressions of the parameters of

the power-law model were proposed as a function of temperature for each CMC solution concentrations.

The effect of the presence of some chemicals used as tracer in bubble column studies was considered. The most common chemical, sodium chloride in the range to be detected by a conductivity meter affected the rheology of CMC solutions. Similar results were obtained with phthalic acid monopotassium salt and 101100 FLT Industrial Red Dye tracer of Tramfloc, Inc. Methylene blue did not change the rheology of CMC solutions in the range of tracer concentration to be detected by the spectrophotometer.

Dynamic tests were developed to characterize the linear viscoelastic behavior of CMC solutions. The principal effect of the CMC is viscosity over elasticity when the polymer concentration was considered.

Relative to bubble column:

The superficial liquid velocity did not affect the pressure drop in the range of liquid velocities considered.

Two flow regimes were found in the bubble column studied: heterogeneous bubbling flow and heterogeneous churn turbulent flow.

Empirical correlations were proposed to calculate the pressure drop for Newtonian and non-Newtonian fluids for the two flow regimes.

The two-friction factor was calculated and plotted finding higher values in the batch mode compared to the continuous mode.

The CMC concentration has no effect over the two-phase friction factor in the range of concentrations considered.

Expressions to calculate the two-phase friction factor were proposed for the superficial liquid velocity and flow regimes studied.

The gas holdup was calculated through disengagement and pressure drop techniques. The comparison between both techniques gave a deviation of $\pm 10\%$, which confirmed the consistency between them.

Superficial liquid velocity did not have effect on gas holdup, while superficial gas velocity increases cause the increase of gas holdup.

Empirical correlations were proposed for Newtonian and non-Newtonian fluids for each flow regime to calculate the gas holdup.

The tracer concentration curves showed repeatability verifying the consistency of the data and of the technique used to take samples and their measurements of concentration through calibration curves of absorbance.

In the bubble column, no changes in the concentration curves at the same operating conditions were found at different radial positions.

The dispersion model for semicontinuous mode fit quite well experimental data and tanks-in-series model fit well experimental data for continuous mode. The calculations of the axial dispersion coefficient from the model with closed-closed boundary conditions showed consistency in the expressions of the three moments derived for this model. The axial dispersion model with open-open boundary conditions did not fit experimental data.

Axial dispersion coefficient exhibited higher values in the batch mode than in continuous mode.

Empirical models were proposed to calculate the dispersion axial coefficient. In heterogeneous bubbling flow regime, the trend was an increase as superficial gas velocity did.

Some recommendations are:

It is proposed to complete the study using at least other polymer, but it is necessary select one that not produce foam when it be aerated, for example, polyacrylamide. In this way, a complete validation of proposed correlations will be done to other non-Newtonian fluids.

The design and built of a cone with another angle of entrance (less angle that the actual cone) in the region of the phases feed could allow the find another regime flow in the bubble column.

7. REFERENCES

- Akita, K. and Yoshida, F., "Bubble size, interfacial area, and liquid-phase mass transfer coefficient in bubble columns," *Ind. Eng. Chem. Process Des. Develop.* 13, 84-91 (1974).
- Alexander, B. F. and Shah Y. T., "Axial dispersion coefficient in bubble columns," *Chem. Eng. J.*, 11, 153 (1976). Cited by Shah et al. (1978).
- Al-Masry, W. A. and Dukkan, A. R., "Hydrodynamics and mass-transfer studies in a pilot-plant airlift reactor: non-Newtonian systems," *Ind. Eng. Chem. Res.*, 37, 41-48 (1998). Cited by Al-Masry (2001).
- Al-Masry, W. A., "Gas holdup in circulating bubble columns with pseudoplastic liquids," *Chem. Eng. Technol.*, 24, 71-76 (2001).
- Aris, R., "Notes on the diffusion-type model for longitudinal mixing in flow," *Chem. Eng. Sci.*, 9, p. 266-267 (1959). Cited by Ostergaard and Michelsen (1969).
- Bach, H. F., and Pilhofer, T., "Variation of gas hold-up in bubble columns with physical properties of liquids and operating parameters of columns," *Ger. Chem. Eng.*, 1, 270-275 (1978). Cited by Godbole et al. (1982).
- Baird, M. H. I., and Rice, R. G., "Axial dispersion in large unbaffled columns," *The Chem. Eng. J.*, 9, 171-174 (1975).
- Barnes, H. A., Hutton, J. F., and Walters, K. *An Introduction to Rheology*; 1st edition, Elsevier Science Publishers B.V., p.199 (1989).
- Bin, A. K., Duczmal, B., and Machniewski, P., "Hydrodynamics and ozone mass transfer in a tall bubble column," *Chem. Eng. Sci.*, 56, 6233-6240 (2001).
- Bird, R.B., Stewart, W.E. and, Lightfoot, E.N., *Transport Phenomena*; 2nd edition, John Wiley & Sons, Inc, USA, p. 895 (2002).
- Buchholz, H., Buchholz, R., Niebeschütz, H., and Schügerl, K., "Absorption of oxygen in highly viscous Newtonian and non-Newtonian fermentation model media in

- bubble column bioreactors,” *Eur. J. of Appl. Microbiology and Biotechnology*, 6, 115-126 (1978).
- Bukur, D. B. and Patel, S. A., “Hydrodynamic studies with foaming and non-Newtonian solutions in bubble columns,” *Canadian J. of Chem. Eng.* 67, 741-751 (1989).
- Camacho, F., Sánchez, A., Cerón, M. C., García, F., Molina, E., and Chisti, Y., “Mixing in bubble columns: a new approach for characterizing dispersion coefficients,” *Chem. Eng. Sci.*, 59, 4369-4376 (2004).
- Carreau, P.J., *PhD thesis*; University of Wisconsin, Madison (1968). Cited by Bird et al. (2002).
- Casson, N., *Rheology of Disperse Systems*; Mill, C. C., Ed.; Pergamon: London, p. 84. (1959).
- Cova, D. R., “Axial mixing in the liquid phase in gas-sparged columns,” *Ind. Eng. Chem. Process Design Dev.*, 13(3), 292-296 (1974). Cited by Shah et al. (1978)
- Cross, M. M., “Rheology of Non-Newtonian fluids: a new flow equation for pseudoplastic systems,” *J. Colloid Sci.*, 20, 417-437 (1965).
- Danckwerts, P. V., “Continuous flow systems. Distribution of residence times,” *Chem. Eng. Sci.*, 2, 1-13 (1953).
- Davis, W. J., “The effect of Froude number in estimating vertical two phase gas-liquid friction losses,” *British Chem. Eng.*, 8, 462-468 (1963). Cited by Mandal et al. (2004).
- Deans, H. A., “A mathematical model for dispersion in the direction of flow in porous media,” *Soc. Petrol. Eng. J.*, 3, 49 (1963). Cited by Shah et al. (1978).
- Deckwer, W. D., Burckhart, R. and Zoll, G., “Mixing and mass transfer in tall bubble columns,” *Chem. Eng. Sci.*, 29, 2177 (1974).
- Deckwer, W.D., Nguyen-Tien, K., Schumpe, A. and Serpemen, Y., “Oxygen mass transfer into aerated CMC solutions in a bubble column”. *Biotechnol. Bioengng.* 24, 461-481 (1982). Cited by Kawase and Moo-Young (1986).

- Deckwer, W.D. Bubble Column Reactors, John Wiley & Sons. New York. pp.533. (1992).
- Dukler, A. E., Wicks, M. and Cleveland, R.G., "Frictional pressure drop in two phase flow. B. An approach through similarity analysis," *AIChE J.*, 10, 1, 44-51 (1964). Cited by Shoham (1998).
- Eickenbusch, H., Brunn, P. O., and Schumpe, A, "Mass transfer into viscous pseudoplastic liquid in large-diameter bubble columns," *Chem. Eng. and Processing*, 34, 479-485 (1995).
- Eissa, S. H. and Shügerl, K., "Holdup and backmixing investigations in cocurrent and countercurrent bubble columns," *Chem. Eng. Sci.*, 30, 1251-1256 (1975).
- Fernandes, R. C., Semiat, R., and Dukler, A. E., "Hydrodynamic model for gas-liquid slug flow in vertical tubes," *AIChE J.*, 29, 6, 981-989 (1983).
- Forret, A., Schweitzer, J.-M., Gauthier, T., Krishna, R. and Schweich, D., "Liquid dispersión in large diameter bubble columns, with and without internal," *Can. J. Chem. Eng.*, 81, 360-366 (2003).
- Froment, G. and Bischoff, K., *Chemical Reactor Analysis and Design*, John Wiley & Sons. New York. pp.764. (1979).
- García-Calvo, E. and Letón, P., "Prediction of fluid dynamics and liquid mixing in bubble columns", *Chem. Eng. Sci.*, 49, 21, 3642-3649 (1994).
- Godbole, S. P., Schumpe, Honath, M. F., and Shah, Y. T., "Holdup structure in highly viscous Newtonian and non-Newtonian liquids in bubble columns," *Chem. Eng. Commun.*, 16, 119-134 (1982).
- Godbole, S. P., Schumpe, A., Shah, Y. T., and Carr, N. L., "Hydrodynamics and mass transfer in non-Newtonian solutions in a bubble column," *AIChE J.*, 30(2), 213-220 (1984).

- Haque, M. W., Nigam, D. P., and Joshi, J. B., "Hydrodynamics and mixing in highly viscous pseudo-plastic non-Newtonian solutions in bubble columns," *Chem. Eng. Sci.*, 41(9), 2321-2331 (1986).
- Hikita, H., and Kikukawa, H. "Liquid-phase mixing in bubble columns: effect of liquid properties," *Chem. Eng. J.*, 8 191-197 (1974). Cited by Shah et al. (1978).
- Hikita, H., Asai, S., Tanigawa, K., Segawa, K., and Kitao, M., *The Chem. Eng. J.*, 20, 59-67 (1980). Cited by Yoshida et al. (1982).
- Hopkins, M. J., Sheppard, A. J., and Eisenklam, P., "The use of transfer functions in evaluating residence time distribution curves," *Chem. Eng. Sci.*, 24, 1131-1137 (1969). Cited by Shah et al. (1978).
- Ityokumbul, M. T., Kosaric, N., and Bulani, W., "Gas hold-up and liquid mixing at low and intermediate gas velocities. I. Air-water system," *The Chem. Eng. J.*, 53, 167-172 (1994).
- Joshi, J. B., and Sharma, M. M., "Mass transfer characteristics of horizontal sparged contactors," *Trans. Inst. Chem. Engrs.*, 54, 42-53 (1976). Cited by Shah et al. (1978).
- Joshi, J. B. and Sharma, M. M., "A circulation cell model for bubble columns," *Trans. Inst. Chem. Eng.*, 57, 244-249 (1979). Cited by García-Calvo and Letón (1994).
- Joshi, J. B., "Axial mixing in multiphase contactors-a unified correlation," *Trans. Inst. Chem. Eng.*, 58, 155-165 (1980). Cited by Haque et al. (1986).
- Kawase, Y. and Moo-Young, M., "Liquid phase mixing in bubble columns with Newtonian and non-Newtonian fluids," *Chem. Eng. Sci.*, 41(8), 1969-1977 (1986).
- Kawase, Y., Umeno, S., and Kumagai, T., "The prediction of gas hold-up in bubble column reactors: Newtonian and non-Newtonian fluids," *The Chem. Eng. J.*, 50, 1-7 (1992).

- Kim S.D., Baker, G.J. and Bergougnou, M. A., "Hold-up and axial mixing characteristics of two and three phase fluidized beds", *The Canadian J. of Chem., Eng.*, 50, 695-701 (1972).
- Levenspiel, O., *Chemical Reaction Engineering*, 3rd edition, John Wiley & Sons, pp.668 (1999).
- London South Bank University (LSBU). Rheology primer of hydrocolloid science. <http://www.lsbu.ac.uk/water/hyrhe.html#pseud> (2003).
- Luo, H. and Svendsen, H., "Turbulent circulation in bubble columns from eddy viscosity distributions of single-phase pipe flow," *Can. J. Chem. Eng.*, 69, 1389-1394 (1991). Cited by Wu and Al-Dahhan (2001).
- MacMullin, R. B. and Weber, M., Jr., "The theory of short-circuiting in continuous-flow mixing vessels in series and kinetics of chemical reactions in such systems," *Trans. Am. Inst. Chem. Eng.*, 31(2), 409-458 (1935).
- Macosko, C. W., *Rheology: Principles, Measurements and Applications*. VCH Publishers, N.Y., pp. 550 (1994).
- Mandal, A., Kundu, G., and Mukherjee, D., "Studies on frictional pressure drop of gas-non-Newtonian two-phase flow in a cocurrent downflow bubble column," *Chem. Eng. Sci.*, 59, 3807-3815 (2004).
- Mersmann, A., Design and Scale-up of Bubble and Spray Columns," *Ger. Chem. Eng.*, 1, 1-11 (1978). Cited by Yoshida et al. (1982).
- Metkin, V. P. and Sokolov, V. N., "Hydraulic resistance to flow of gas-liquid mixtures having Non-Newtonian properties," *J. Appl. Chem. USSR*, 55, 558-563 (1982). Cited by Al-Masry (2001).
- Michell, R. W., and Furzer, I. A., "Mixing in trickle flow through packed beds," *Chem. Eng. J.*, 4, 53 (1972). Cited by Shah et al. (1978).
- Montserrat, T. and García-Calvo, E., "Prediction of hydrodynamic behavior in bubble columns," *J. of Chem. Tech. and Biotech.*, 66, 199-205 (1996). Cited by Wu and Al-Dahhan (2001).

- Moustiri, S., Hebrard, G., Thakre, S. S. and Roustan, M., "A unified correlation for predicting liquid axial dispersion coefficient in bubble columns," *Chem. Eng. Sci.*, 56, 1041-1047 (2001).
- Nielsen, L. E., *Polymer Rheology*; Marcel Dekker, INC, p.203 (1977).
- Nishikawa, M., Kato, H., and Hashimoto, K., "Heat transfer in aerated tower filled with non-Newtonian liquid," *Ind. Eng. Chem. Process Des. Dev.*, 16(1), 133-137 (1977).
- Ohki, Y. and Inoue, H., "Longitudinal mixing of the liquid phase in bubble columns", *Chem. Eng. Sci.*, 25, 1-16 (1970).
- Ostergaard, K. and Michelsen, M.L., "On the use of the imperfect tracer pulse method for determination of hold-up and axial mixing," *The Canadian J. of Chem. Eng.*, 47, 107 (1969).
- Papanastasiou, T. C., "Flows of materials with yield," *J. of Rheol.*, 31(5), 385-404 (1987).
- Popovic, M. and Robinson, C. W., "The specific interfacial area in external-circulation-loop airlifts and a bubble column—II. Carboxymethyl cellulose/sulphite solution," *Chem. Eng. Sci.*, 42, 12, 2825-2832 (1987).
- Popovic M. and Robinson, C. W., "External-circulation-loop airlift bioreactors: study of the liquid circulating velocity in highly viscous non-Newtonian liquids," *Biotechnology and Bioengineering*, 32, 301-312 (1988).
- Popovic M. and Robinson, C. W., "Mixing characteristic of external-loop airlifts: non-Newtonian systems," *Chem. Eng. Sci.*, 48, 8, 1405-1413 (1993).
- Ramachandran, P.A. and Chaudhari, R.V., *Three-phase catalytic reactors*, Gordon and Breach Science Publishers, Inc (1983).
- Reith, T., Renken, S., and Israel, B. A., "Gas hold-up and axial mixing in the fluid phase of bubble columns," *Chem. Eng. Sci.*, 23, 619-629 (1968). Cited by Shah et al. (1978).
- Rice, R. G. and Littlefield, M.A., "Dispersion coefficients for ideal bubbly flow in truly vertical bubble columns," *Chem. Eng. Sci.*, 42, 8, 2045-2053 (1987).

- Riquarts H.-P., "A physical model for axial mixing of the liquid phase for heterogeneous flow regime in bubble columns," *Ger. Chem. Eng.*, 4, 18-23 (1981).
- Rustemeyer, U., Pauli, J., Menzel, Th., Buchholz, R., and Onken, U., "Liquid-phase mixing model for hydrodynamics of bubble columns," *Chem. Eng. Process*, 26, 165-172 (1989).
- Schumpe, A. and Deckwer, W-D, "Gas holdups, specific interfacial areas, and mass transfer coefficients of aerated carboxymethyl cellulose solutions in a bubble column," *Ind. Eng. Chem. Process Des. Dev.*, 21, 706-711 (1982).
- Schweitzer, J.-M., Bayle, J., and Gauthier, T., "Local gas holdup measurements in fluidized bed and slurry bubble column," *Chem. Eng. Sci.*, 56, 1103-1110 (2001). Cited by Forret et al. (2003).
- Shirsat, S., Mandal, A., Kundu, G., and Mukherjee, D., "Hydrodynamic studies on gas-liquid downflow bubble column with Non-Newtonian liquids," *IE (I) Journal*, 84, 38-43 (2003).
- Siemes, W. and Weis, W., "Flüssigkeitsdurchmischung in engen blasensesäulen," *Chemie-Ingr-Techn.*, 29, 727-732 (1957). Cited by Wilkinson et al. (1993).
- Shah, Y.T., Stiegel, G. J., and Sharma, M. M., "Backmixing in gas-liquid reactors," *AIChE J.*, 24(3), 369-400 (1978).
- Shoham, O., *Flow Pattern Transition and Characterization in Gas Liquid Two Phase Flow in Inclined Pipes*, Ph.D. Dissertation, Tel Aviv University (1982).
- Shoham, O., Course Handout: *Two-Phase Flow Modeling*, Department of Petroleum Engineering, The University of Tulsa (1998).
- Taitel, Y., Bornea, D., and Dukler, A. E., "Modelling flow pattern transitions for steady upward gas-liquid flow in vertical tubes," *AIChE J.*, 26, 3, 345-354 (1980).
- Towel, G. D., and Ackerman, G. H., "Axial mixing of liquid and gas in large bubble reactors," *Proceedings of the fifth european/second international symposium on Chemical Reaction Engineering*, p.B 3-1, Amsterdam (1972) . Cited by Shah et al. (1978).

- Vatai, GY. And Tekic, M. N, "Gas hold-up and mass transfer in bubble columns with pseudoplastic liquids," *Chem. Eng. Sci.*, 44, 10, 2402-2407 (1989).
- Velázquez, C. and Estévez, L.A., "Stripping of trihalomethanes from drinking water in a bubble-column aerator," *AIChE J.*, 38 (2), 211-218 (1992).
- Wild, G., Li, H.-Z., Poncin, S., and Olmos, E., "Some aspects of the hydrodynamics of bubble columns," *International J. of Chem. Reactor Eng*, 1, 1-36 (2003).
- Yasuda, K., Armstrong, R. C., and Cohen, R. E., "Shear flow properties of concentrated solutions of linear and star branched polystyrenes," *Rheol. Acta*, 20,163-178 (1981).
- Walter, J. F., and Blanch, H. W. "Liquid circulation patterns and effect on gas hold-up and mixing in bubble columns," *Chem. Eng. Commun.*, 19, 243-262 (1983).
- Wilkinson, P. M, Haringa, H., Stokman, F. P.A., van Dierendonck, L. L., "Liquid mixing in a bubble column under pressure," *Chem. Eng. Sci.*, 48, 10, 1785-1791 (1993).
- Wu, Y., Ong, B., and Al-Dahhan, M. H., "Predictions of radical gas holdup profiles in bubble column reactors," *Chem. Eng. Sci.*, 56, 1207-1210 (2001). Cited by Wu and Al-Dahhan (2001).
- Wu, Y. and Al-Dahhan, M. H., "Prediction of axial liquid velocity profile in bubble columns," *Chem. Eng. Sci.*, 56, 1127-1130 (2001).
- Zahradnik, J., Fialová, M., Ruzicka, M., Drahos, J., Kastánek, F., and Thomas, N.H., "Duality of the gas-liquid flow regimes in bubble column reactors," *Chem. Eng. Sci.*, 52, 21/22, 3811-3826 (1997).
- Zuber, N. and Findlay, J.A., "Average volumetric concentration in two-phase flow systems," *J. Heat Transfer*, 87, 453-458 (1965).

APPENDIX A. TWO-PHASE FLOW IN PIPES

A.1. Introduction

Bubble columns with an aspect ratio (L/d_c) higher than 4 can be considered with a developed flow and when it is heterogeneous (liquid and gas phases are involved), the results obtained from their analysis could be used in two-phase flow in pipes.

A.2. Types of two-phase flow in pipes

Shoham (1982) defined flow patterns based on experimental data obtained from different configurations of the pipe (inclination angle, horizontal flow, upward and downward inclined and vertical flow). For vertical and sharply inclined flow, the flow patterns observed are (Shoham, 1982):

Bubble flow: The gas phase is dispersed into small discrete bubbles in a continuous liquid phase. The distribution is homogeneous throughout the cross section. This regime is divided into bubbly flow and dispersed bubble flow that differ in the flow mechanism. The bubbly flow is observed at low liquid flow rates when slippage between gas and liquid phases occurs (the gas and the liquid velocities differs). The dispersed bubble flow regime occurs at high liquid flow rates, where the liquid carries out the gas bubbles and no-slippage between phases occurs.

Slug flow: Most of the gas phase is located in large bullet-shape, gas pockets (Taylor bubbles) with a diameter slightly smaller than the pipe diameter that flow continuously through the pipe. A thin liquid film flows downward between the Taylor bubbles and the pipe wall, penetrating into the liquid slugs and creates a mixing zone aerated by small gas bubbles.

Churn flow: Characterized by an oscillatory movement. It is similar to slug flow, but looks more chaotic with remarkable differences between the two phases involved. This regime is present at high gas flow rates, in which case the slugs are blown through by

the gas phase, break, fall backwards and merge with the following slug. Finally, the Taylor bubble is distorted and churns occur.

Annular flow: Due to the symmetry of flow, a liquid film of uniform thickness is formed on the inside of the pipe wall. The liquid phase moves slower as a film around the pipe wall and as droplets entrained in the gas core.

All these flow regimes are shown in Figure A.1. Several authors have prepared flow regime maps, based on experimental observations, to help determine or predict what flow regime will prevail at any give conditions.

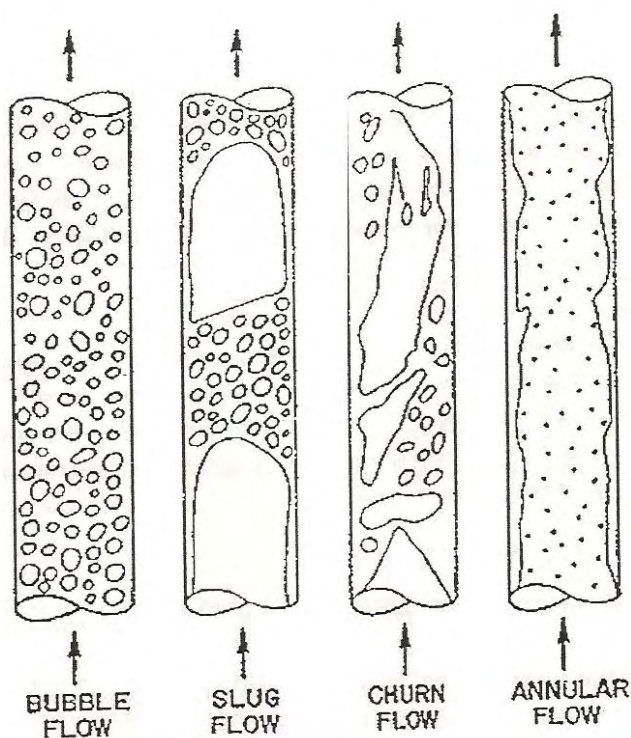


Figure A.1. Flow regimes for two-phase flow in vertical pipes (Shoham, 1998)

Taitel *et al.* (1980) proposed the classification mentioned by Shoham (1998) and the studied flow-regime transitions in pipes and considered transitions between regimes. They described in detail three of these transitions: bubble to slug flow, slug to churn flow, and churn to annular flow. These transitions are described in the following few pages.

The transition for bubble flow to slug flow: This transition requires a process of coalescence at low gas flow rates. However, when the liquid flow rate is increased, the larger bubbles breakup due to turbulent fluctuations and a dispersed bubble pattern can be maintained. Many studies demonstrate that bubbles behave as rigid spheres rising vertically in rectilinear motion when their diameter is below the so-called critical size. Above this critical size, the bubbles begin to deform and move randomly in zig-zag. At low gas and liquid flow rates, arrays of smaller bubbles move in zig-zag with Taylor bubbles appearing occasionally. When gas flow rate is increased maintaining the liquid flow rate low, the bubbles density increases and dispersed bubbles become closely packed, increasing the rate of coalescence and thus the transition to slug flow occurs. This phenomenon has been observed at bubble void fractions between 0.25 and 0.30. Taitel *et al.* (1980) proposed an expression for liquid superficial velocity to characterize this transition, which assumes that it happens at gas holdup of 0.25:

$$u_L = 3.0 u_G - 1.15 \left[\frac{g(\rho_L - \rho_G)\sigma}{\rho_L^2} \right]^{1/4} \quad (\text{A.1})$$

Equation (A.1) corresponds to line A in the flow pattern map presented by Taitel *et al.* (1980) in their work (Figure A.2).

Once turbulent fluctuations are vigorous, bubbles break into small critical size, coalescence no longer takes place, and dispersed bubble flow pattern prevails for gas holdups greater than 0.25. In this region of high flow rate, the slip velocity can be neglected.

Taitel *et al.* (1980) proposed the following equation to relate the flow rates at which turbulence-induced dispersion takes place:

$$u_L + u_G = 4.0 \frac{d_c^{0.429} (\sigma/\rho_L)^{0.089}}{\nu_L^{0.072}} \left[\frac{g(\rho_L - \rho_G)}{\rho_L} \right]^{0.446} \quad (\text{A.2})$$

where ν_L is the kinematic viscosity. Equation (A.2) corresponds to line B and C in the flow pattern map presented by the authors (Figure A.3). Taitel *et al.* (1980) concluded that, in tubes smaller than 0.05 m diameter, no bubbly flow can exist below line B and the entire zone I and III exists as slug flow pattern. The zone II can be present only at high liquid flow rates where dispersion takes place due to turbulence (Figure A.3).

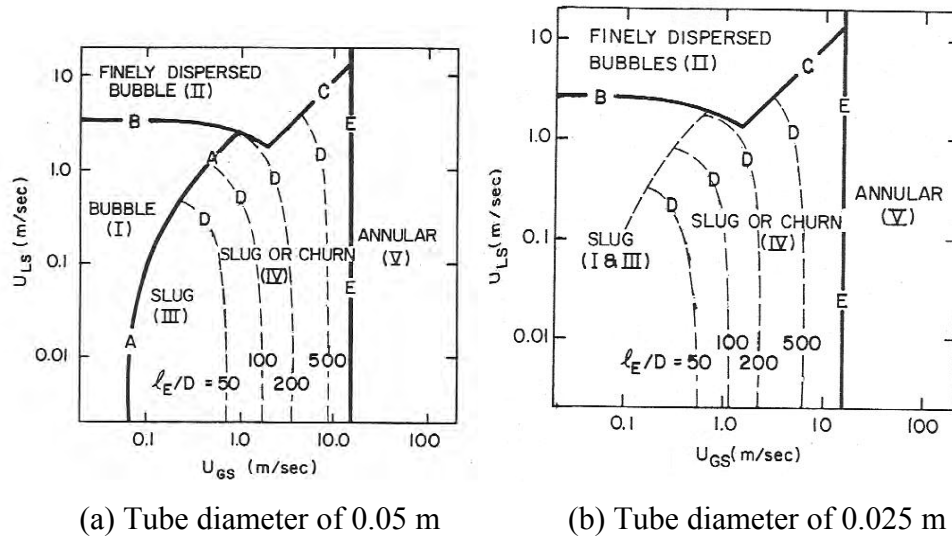


Figure A.2. Flow pattern maps obtained by Taitel *et al.* (1980) for water-air at 25 °C and 100 kPa

Transition for Slug flow to Churn flow: In the slug flow, the bubbles occupy most of the cross section of the pipe and are axially separated by a liquid slug in which small bubbles are dispersed. The transition occurs when the gas flow rate is increased. Taitel *et al.* (1980) proposed a Taylor gas bubble velocity:

$$\frac{u_G}{\varepsilon_G} = \frac{1.2 \frac{v_M}{1 - \varepsilon_G} + 0.35 \sqrt{gd_c}}{1 + 1.2 \frac{\varepsilon_G}{1 - \varepsilon_G}} \quad (\text{A.3})$$

$$\frac{u_L}{1 - \varepsilon_G} = \frac{v_M - u_G}{1 - \varepsilon_G} \quad (\text{A.4})$$

Transition from Churn flow to Annular flow: The flow pattern at high gas velocity is annular.

This transition occurs at gas superficial velocity given by:

$$\frac{u_G \rho_G^{0.5}}{[\sigma g (\rho_L - \rho_G)]^{0.25}} = 3.1 \quad (\text{A.5})$$

A.3. Gas holdup in pipes

In pipes, the gas holdup is defined in two ways depending on whether the slippage between gas and liquid phases occurs or not. The no-slip condition implies that the gas and the liquid have the same velocity so that the local or in situ gas holdup is equal to the no-slip gas holdup (the slip velocity is zero) and they can be expressed as:

$$\varepsilon_G = \frac{u_G}{u_G + u_L} = \varepsilon'_G \quad (\text{A.6})$$

where ε_G is the gas holdup and ε'_G the in situ gas holdup. Figure A.3 shows a sketch of both types of gas holdup.

The gas holdup has a strong relationship with pressure drop. The total pressure gradient is composed of three components: the frictional (f), gravitational (g), and accelerational (a) components (Shoham, 1998):

$$\left(\frac{dp}{dz}\right)_t = \left(\frac{dp}{dz}\right)_f + \left(\frac{dp}{dz}\right)_g + \left(\frac{dp}{dz}\right)_a \quad (\text{A.7})$$

The frictional pressure gradient component is given by the following expression:

$$-\left(\frac{dp}{dz}\right)_f = \frac{S}{A} \tau_w = \frac{4\tau_w}{d_c} \quad (\text{A.8})$$

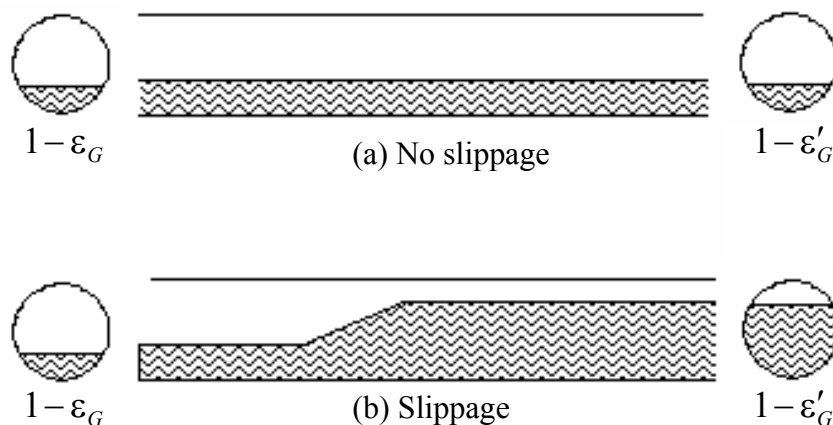


Figure A.3. In situ gas holdup and no-slip gas holdup

where A is the cross sectional area, S the pipe perimeter, and τ_w the shear stress at the wall.

The average wall shear stress can be expressed in terms of the friction factors obtaining:

$$\tau_w = \frac{1}{2} f_F \rho_M v_M^2 \quad (\text{A.9})$$

where f_F is the Fanning friction factor and ρ_M the mixture density. Combining the last two equations, the following expression for the frictional pressure gradient is obtained:

$$-\left(\frac{dp}{dz}\right)_f = \frac{2}{d_c} f_F \rho_M v_M^2 \quad (\text{A.10})$$

The Fanning friction factor is based on the mixture Reynolds number (Re_M) and an empirical relationship (correlation or chart) between f_F and Re_M (some correlations and charts use the Moody friction factor, which is four times the Fanning friction factor). The mixture viscosity used in the mixture Reynolds number is related to the phases viscosities. Several methods have been proposed by two-phase flow researchers to estimate this property. The methods mentioned by Shoham (1998) are the following:

- In-situ holdup:

$$\mu_M = (1 - \varepsilon'_G) \mu_L + \varepsilon'_G \mu_G \quad (\text{A.11})$$

- Dukler *et al.* (1964):

$$\mu_M = (1 - \varepsilon_G) \mu_L + \varepsilon_G \mu_G \quad (\text{A.12})$$

- Cicchitti:

$$\mu_M = (1 - x) \mu_L + x \mu_G \quad (\text{A.13})$$

where x is the quality or mass fraction of the gas phase.

- McAdams:

$$\frac{1}{\mu_g} = \frac{x}{\mu_g} + \frac{1-x}{\mu_L} \quad (\text{A.14})$$

The gravitational pressure gradient in Equation (A.7) is given by the expression:

$$-\left(\frac{dp}{dz}\right)_g = \rho_M g \sin \alpha \quad (\text{A.15})$$

where α is the inclination angle of the pipe from the horizontal. The mixture density has to be calculated with the slippage holdup because the gravitational head depends on the weight of the two phases, which is related to the in-situ volume or mass fractions of the phases (Shoham, 1998).

Finally, the accelerational pressure gradient in Equation (A.7) is the most difficult one to estimate. Shoham (1998) has expressed this term as follows:

$$-\left(\frac{dp}{dz}\right)_a = \frac{W}{A} \frac{d}{dz} \left(\frac{W}{A \rho_M} \right) \quad (\text{A.16})$$

where W is the mass flow rate. Using the definition of mixture density in Eq. (A.16), the expression obtained is the following:

$$\begin{aligned} -\left(\frac{dp}{dz}\right)_a = \left(\frac{W}{A}\right)^2 & \left\{ \left(\frac{1}{\rho_G} - \frac{1}{\rho_L} \right) \frac{dx}{dz} + \frac{d}{dz} \left[x \frac{d}{dz} \left(\frac{1}{\rho_G} \right) + (1-x) \frac{d}{dz} \left(\frac{1}{\rho_L} \right) \right] \right\} \\ & - \left(\frac{W}{A}\right)^2 \left[x \left(\frac{1}{\rho_G} - \frac{1}{\rho_L} \right) \right] \frac{1}{A} \frac{dA}{dz} \end{aligned} \quad (\text{A.17})$$

Several cases simplifies the final expression of total pressure drop when Eqs. (A.10), (A.15) and (A.17) are substituted into Eq. (A.7), for example:

- constant cross sectional area, $dA/dz = 0$

- no phase changes, $dx/dz = 0$
- incompressible liquid, $d(1/\rho_L)/dz = 0$

APPENDIX B. CALIBRATION CURVES

Table B.1. Calibration of micrometric valve. $u_G < 0.0206$ m/s

Micrometric valve		u_G (m/s)
Fixed scale	Mobile scale	
0	1	0.0010
0	2	0.0027
0	3	0.0034
0	4	0.0055
0	5	0.0065
0	6	0.0083
0	7	0.0095
0	8	0.0112
0	9	0.0129
0	10	0.0144
0	11	0.0162
0	12	0.0192

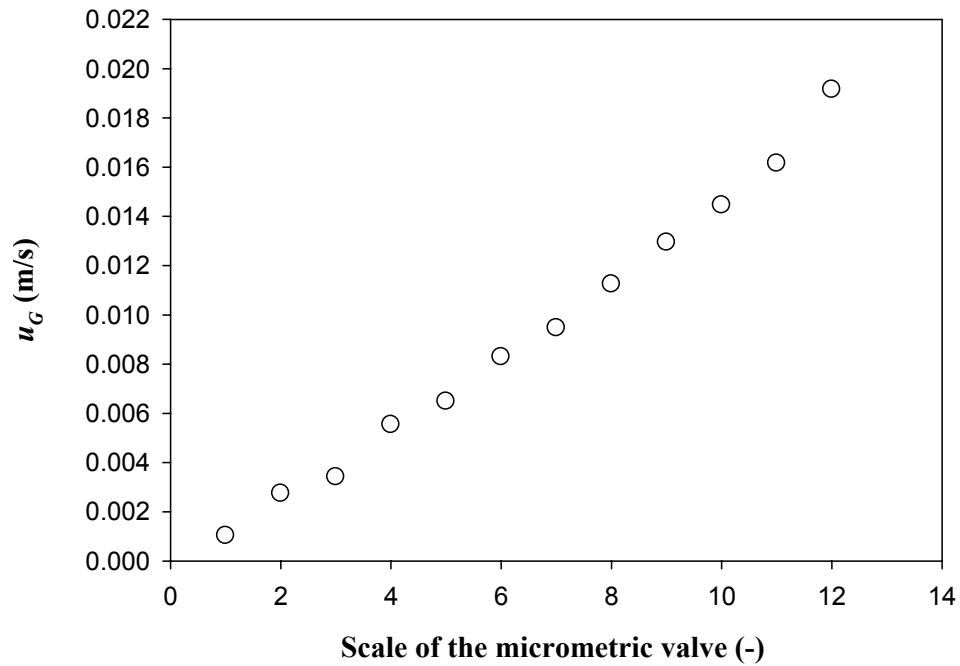


Figure B.1. Calibration of micrometric valve $u_G < 0.0206$ m/s

Table B.2. Calibration of rotameter. $u_G \geq 0.0206$ m/s

Rotameter (ft ³ /min STD)	u_G (m/s)
1.34	0.0206
2.00	0.0308
2.50	0.0385
3.00	0.0462
3.50	0.0539
4.00	0.0616

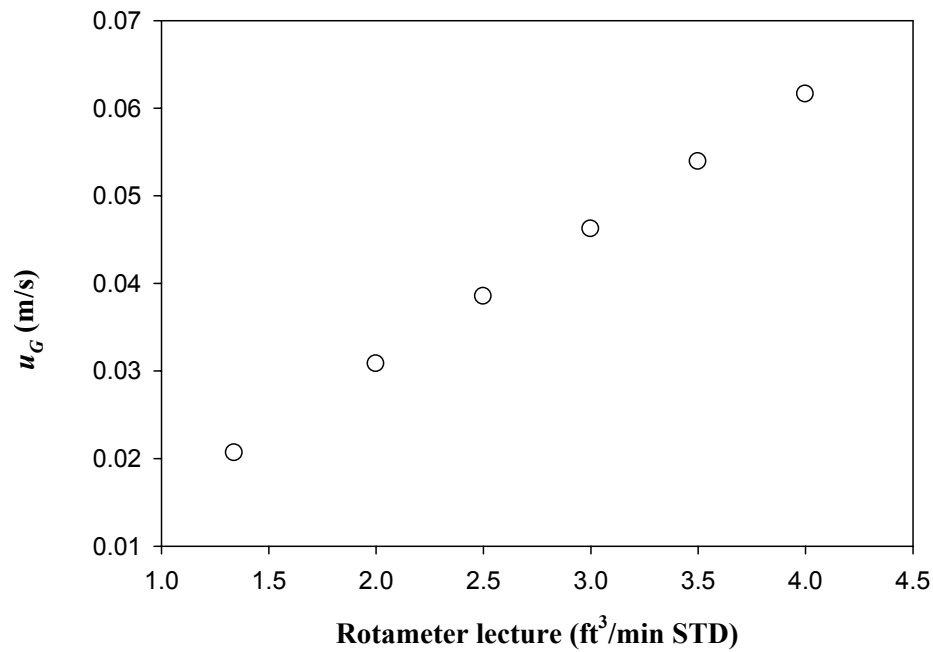
Figure B.2. Calibration of rotameter $u_G \geq 0.0206$ m/s

Table B.3. Calibration of the pump

Fixed scale	Mobile scale	u_L (m/s)
0	2	0.00051
0	4	0.00072
0	6	0.00166
0	7	0.00195
0	8	0.00214
10	0	0.00247
10	2	0.00317
10	3	0.00337
10	4	0.00355
10	5	0.00374
10	6	0.00398
10	8	0.00432
20	0	0.00451

Table B.4. Calibration of spectrophotometer for tap water at $\lambda=300$ nm

Absorbance	Concentration (kg/m^3)
2.700	0.04750
0.966	0.01188
0.270	0.00297
0.093	0.00074
0.065	0.00037
0.049	0.00019
0.042	0.00009
0.054	0.00025
0.041	0.00006
0.074	0.00050
0.043	0.00012
0.030	0.00000

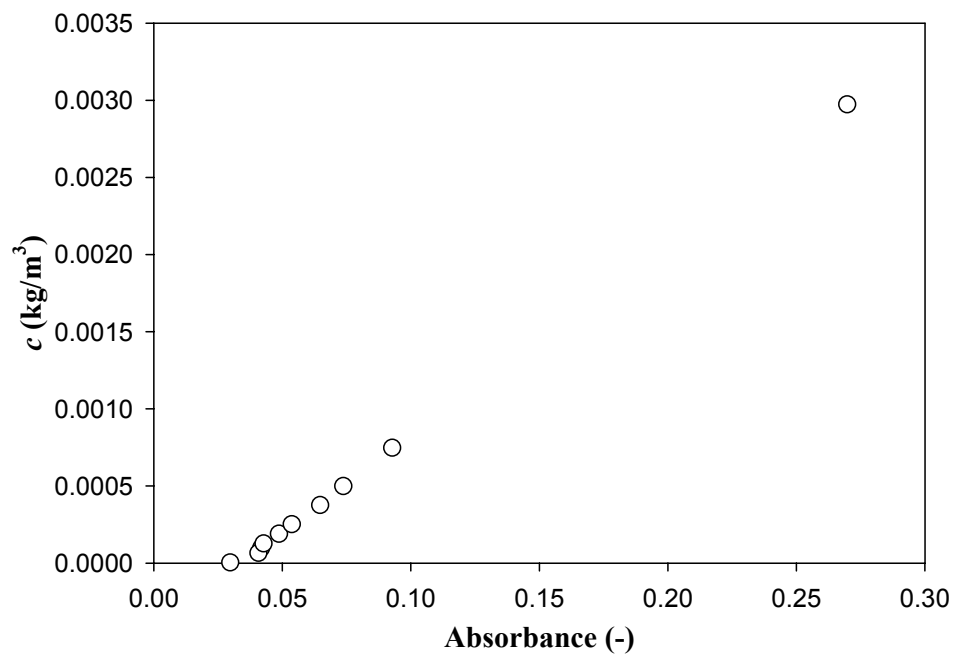
Figure B.3. Calibration curve of spectrophotometer for tap water at $\lambda=300$ nm

Table B.5. Calibration of spectrophotometer for 0.10% CMC solution at $\lambda=300$ nm and 24 h of dissolution

Absorbance	Concentration (kg/m^3)
1.532	0.02375
0.466	0.00594
0.262	0.00297
0.155	0.00148
0.097	0.00074
0.066	0.00037
0.050	0.00019
0.043	0.00009
0.035	0.00005
0.028	0.00000

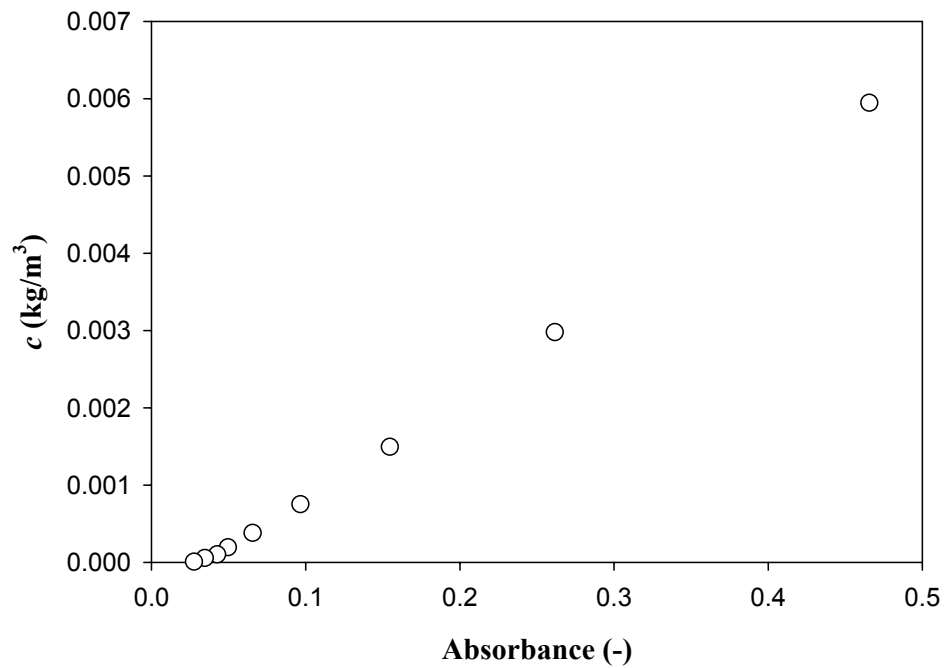


Figure B.4. Calibration curve of spectrophotometer for 0.10% CMC solution at $\lambda=300$ nm and 24 h of dissolution

Table B.6. Calibration of spectrophotometer for 0.20% CMC solution at $\lambda=300$ nm and 24 h of dissolution

Absorbance	Concentration (kg/m^3)
0.436	0.02375
0.152	0.00594
0.099	0.00297
0.072	0.00148
0.055	0.00074
0.047	0.00037
0.041	0.00019
0.035	0.00000

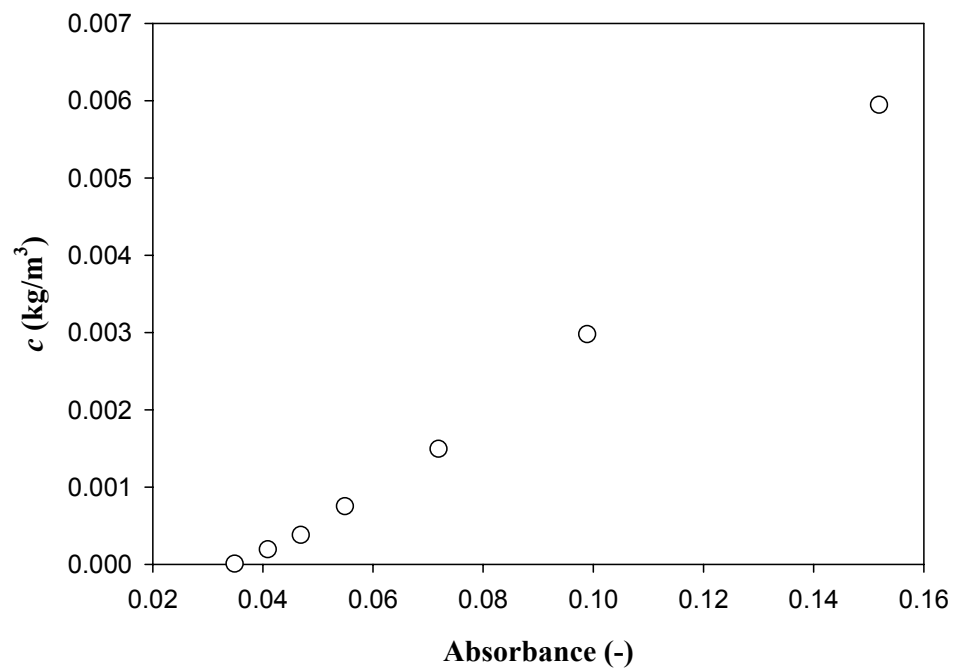


Figure B.5. Calibration curve of spectrophotometer for 0.20% CMC solution at $\lambda=300$ nm and 24 h of dissolution

Table B.7. Calibration of spectrophotometer for 0.30% CMC solution at $\lambda=300$ nm and 24 h of dissolution

Absorbance	Concentration (kg/m^3)
1.134	0.02375
0.382	0.00594
0.233	0.00297
0.153	0.00148
0.104	0.00074
0.078	0.00037
0.067	0.00019
0.056	0.00009
0.042	0.00000

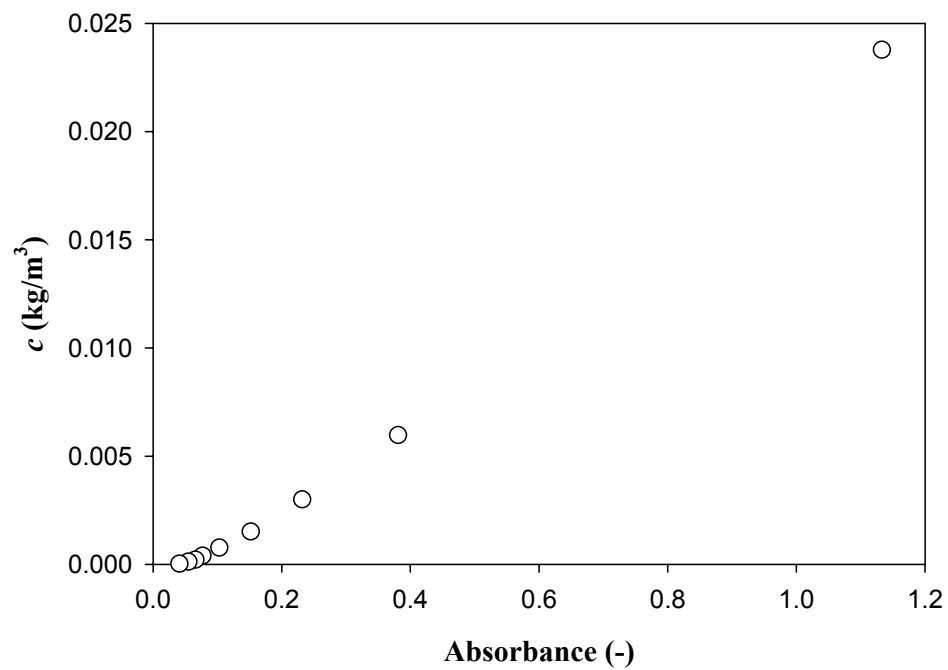


Figure B.6. Calibration curve of spectrophotometer for 0.30% CMC solution at $\lambda=300$ nm and 24 h of dissolution

Table B.8. Calibration of spectrophotometer for 0.40% CMC solution at $\lambda=300$ nm and 24 h of dissolution

Absorbance	Concentration (kg/m^3)
0.905	0.00594
0.334	0.00297
0.216	0.00148
0.153	0.00074
0.112	0.00037
0.092	0.00019
0.081	0.00009
0.076	0.00005
0.065	0.00000

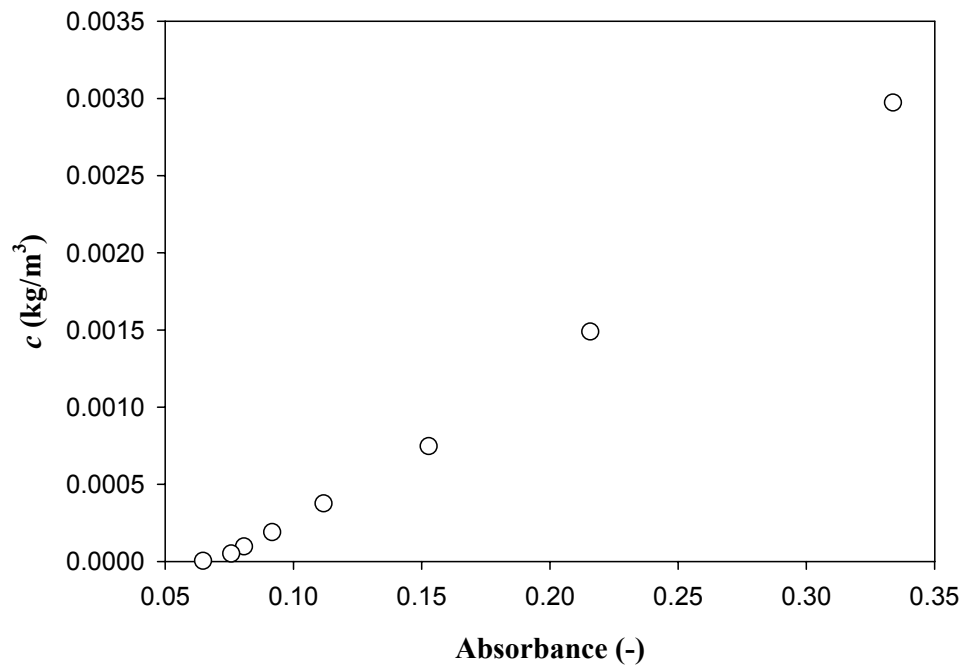


Figure B.7. Calibration curve of spectrophotometer for 0.40% CMC solution at $\lambda=300$ nm and 24 h of dissolution

APPENDIX C. TABLES OF DATA

Table C.1. Experimental data of pressure drop for tap water

Run	u_G (m/s)	u_L (m/s)	ΔP (Pa) Experimental	ΔP (Pa) Correlations
190	0.0010	0	20128.48	20236.32
191	0.0027	0	20051.21	19949.05
192	0.0034	0	19962.59	19885.42
193	0.0055	0	19873.07	19744.50
194	0.0083	0	19695.93	19628.03
235	0.0083	0	19723.34	19628.03
195	0.0112	0	19563.72	19540.63
196	0.0145	0	19303.55	19468.74
225	0.0145	0	19268.74	19468.74
197	0.0206	0	19157.75	
198	0.0308	0	18603.20	18587.41
199	0.0385	0	18338.95	18271.93
236	0.0385	0	18201.65	18271.93
200	0.0462	0	18034.23	18018.13
179	0.0010	0.0045	20105.43	20236.32
239	0.0010	0.0045	20058.98	20236.32
180	0.0027	0.0045	20040.34	19949.05
181	0.0034	0.0045	19962.32	19885.42
182	0.0055	0.0045	19880.86	19744.50
183	0.0083	0.0045	19715.27	19628.03
230	0.0083	0.0045	19615.10	19628.03
184	0.0112	0.0045	19526.47	19540.63
185	0.0145	0.0045	19526.47	19468.74
231	0.0145	0.0045	19247.87	19468.74
186	0.0206	0.0045	19127.97	
187	0.0308	0.0045	18583.34	18587.41
188	0.0385	0.0045	18326.56	18271.93
238	0.0385	0.0045	18195.46	18271.93
189	0.0462	0.0045	18015.92	18018.13

* Eq. (5.5) was used for $(1.04 \times 10^{-3} \leq u_G(m/s) \leq 1.44 \times 10^{-2})$ and Eq. (5.6) for $(3.07 \times 10^{-2} \leq u_G(m/s) \leq 4.62 \times 10^{-2})$

Table C.2. Experimental data of pressure drop for CMC solutions

Run	CMC concentration (% wt)	u_G (m/s)	u_L (m/s)	ΔP (Pa) Experimental
212	0.2	0.001036	0	20127.49
214	0.2	0.008297	0	19697.17
207	0.2	0.01446	0	19347.75
208	0.2	0.030795	0	18657.29
209	0.2	0.038494	0	18287.31
210	0.2	0.046193	0	18036.58
223	0.2	0.001036	0.004509	20093.38
216	0.2	0.008297	0.004509	19767.77
217	0.2	0.01446	0.004509	19339.74
218	0.2	0.030795	0.004509	18710.34
219	0.2	0.038494	0.004509	18282.80
220	0.2	0.046193	0.004509	18094.12
232	0.4	0.001036	0	20090.50
215	0.4	0.008297	0	19807.54
224	0.4	0.01446	0	19570.91
213	0.4	0.030795	0	18985.57
226	0.4	0.038494	0	18827.56
228	0.4	0.046193	0	18468.45
237	0.4	0.001036	0.004509	20090.36
222	0.4	0.008297	0.004509	19743.87
233	0.4	0.01446	0.004509	19502.14
227	0.4	0.030795	0.004509	19024.83
229	0.4	0.038494	0.004509	18831.26
234	0.4	0.046193	0.004509	18486.66

Table C.3. Correlation data of pressure drop for CMC solutions

Run	CMC concentration (% wt)	u_G (m/s)	u_L (m/s)	Consistency index k , (Pa·s ^{<i>n</i>})	Flow index n , (-)	ΔP (Pa) Correlations
212	0.2	0.001036	0	0.0113	0.9442	20126.30
214	0.2	0.008297	0	0.0161	0.9111	19614.50
207	0.2	0.01446	0	0.0074	0.9746	19423.51
208	0.2	0.030795	0	0.0135	0.9309	18666.55
209	0.2	0.038494	0	0.0121	0.9364	18296.78
210	0.2	0.046193	0	0.0107	0.9469	17989.41
223	0.2	0.001036	0.004509	0.0181	0.9063	20132.60
216	0.2	0.008297	0.004509	0.0110	0.9413	19591.95
217	0.2	0.01446	0.004509	0.0140	0.9338	19477.60
218	0.2	0.030795	0.004509	0.0212	0.9025	18799.11
219	0.2	0.038494	0.004509	0.0107	0.9525	18267.20
220	0.2	0.046193	0.004509	0.0173	0.9059	18136.85
232	0.4	0.001036	0	0.1678	0.7284	20101.77
215	0.4	0.008297	0	0.0773	0.8150	19703.93
224	0.4	0.01446	0	0.0928	0.7952	19585.77
213	0.4	0.030795	0	0.0421	0.8537	18941.18
226	0.4	0.038494	0	0.0651	0.8339	18743.95
228	0.4	0.046193	0	0.0553	0.8446	18468.82
237	0.4	0.001036	0.004509	0.1529	0.7530	20133.13
222	0.4	0.008297	0.004509	0.2462	0.7008	19697.87
233	0.4	0.01446	0.004509	0.0991	0.7894	19587.53
227	0.4	0.030795	0.004509	0.0941	0.7956	19036.53
229	0.4	0.038494	0.004509	0.1009	0.8041	18805.65
234	0.4	0.046193	0.004509	0.1950	0.7336	18540.13

* Eq. (5.7) was used for $(1.04 \times 10^{-3} \leq u_G(m/s) \leq 1.44 \times 10^{-2})$ and Eq. (5.8) for $(3.07 \times 10^{-2} \leq u_G(m/s) \leq 4.62 \times 10^{-2})$

Table C.4. Gas holdup for tap water through disengagement technique

Run	u_G (m/s)	u_L (m/s)	ε_G (-) Experimental	ε_G (-) Correlations
190	0.0010	0	0.00495	0.00206
191	0.0027	0	0.00702	0.00654
192	0.0034	0	0.01114	0.00846
193	0.0055	0	0.01624	0.01504
194	0.0083	0	0.02379	0.02425
235	0.0083	0	0.02417	0.02425
195	0.0112	0	0.03367	0.03477
196	0.0145	0	0.03999	0.04683
225	0.0145	0	0.05071	0.04683
197	0.0206	0	0.05426	
198	0.0308	0	0.07559	0.07679
199	0.0385	0	0.09335	0.09327
236	0.0385	0	0.09257	0.09327
200	0.0462	0	0.10609	0.10933
179	0.0010	0.0045		
239	0.0010	0.0045	0.00140	0.00206
180	0.0027	0.0045	0.00185	0.00654
230	0.0083	0.0045	0.03543	0.02425
184	0.0112	0.0045	0.03981	0.03477
231	0.0145	0.0045	0.04550	0.04683
186	0.0206	0.0045	0.05338	
187	0.0308	0.0045	0.08053	0.07679
238	0.0385	0.0045	0.09454	0.09327
189	0.0462	0.0045	0.11118	0.10933

* Eq. (5.7) was used for $(1.04 \times 10^{-3} \leq u_G (m/s) \leq 1.44 \times 10^{-2})$ and Eq. (5.8) for $(3.07 \times 10^{-2} \leq u_G (m/s) \leq 4.62 \times 10^{-2})$

Table C.5. Gas holdup for tap water through pressure drop technique

Run	u_G (m/s)	u_L (m/s)	ε_G (-) Experimental	ε_G (-) Correlations
190	0.0010	0		
191	0.0027	0	0.00288	0.00377
192	0.0034	0	0.00729	0.00522
193	0.0055	0	0.01175	0.01076
194	0.0083	0	0.02057	0.01965
235	0.0083	0	0.02050	0.01965
195	0.0112	0	0.02715	0.03094
196	0.0145	0	0.04011	0.04502
225	0.0145	0	0.04305	0.04502
197	0.0206	0	0.04736	
198	0.0308	0	0.07498	0.07660
199	0.0385	0	0.08813	0.09145
236	0.0385	0	0.09595	0.09145
200	0.0462	0	0.10330	0.10568
179	0.0010	0.0045	0.00018	0.00088
239	0.0010	0.0045	0.00414	0.00088
180	0.0027	0.0045	0.00342	0.00377
230	0.0083	0.0045	0.02568	0.01965
184	0.0112	0.0045	0.02901	0.03094
231	0.0145	0.0045	0.04432	0.04502
186	0.0206	0.0045	0.04885	
187	0.0308	0.0045	0.07596	0.07661
238	0.0385	0.0045	0.09667	0.09145
189	0.0462	0.0045	0.10422	0.10568

* Eq. (5.21) was used for $(1.04 \times 10^{-3} \leq u_G(m/s) \leq 1.44 \times 10^{-2})$ and Eq. (5.22) for $(3.07 \times 10^{-2} \leq u_G(m/s) \leq 4.62 \times 10^{-2})$

Table C.6. Gas holdup for CMC solutions through disengagement technique

Run	CMC concentration (% wt)	u_G (m/s)	u_L (m/s)	ε_G (-) Experimental
212-1	0.2	0.0010	0	0.00093
206-1	0.2	0.0083	0	0.02361
206-2	0.2	0.0083	0	0.02304
214	0.2	0.0083	0	0.02551
207-1	0.2	0.0145	0	0.03949
207-2	0.2	0.0145	0	0.04020
208-1	0.2	0.0308	0	0.07309
208-2	0.2	0.0308	0	0.07585
209-1	0.2	0.0385	0	0.09112
209-2	0.2	0.0385	0	0.09000
210	0.2	0.0462	0	0.10515
216	0.2	0.0083	0.0045	0.01461
217	0.2	0.0145	0.0045	0.04550
218	0.2	0.0308	0.0045	0.07703
219	0.2	0.0385	0.0045	0.09586
220	0.2	0.0462	0.0045	0.11118
211	0.3	0.0308	0	0.06526
232	0.4	0.0010	0	0.00509
215-1	0.4	0.0083	0	0.02004
215-2	0.4	0.0083	0	0.02005
224	0.4	0.0145	0	0.02508
213	0.4	0.0308	0	0.05504
226	0.4	0.0385	0	0.07390
228	0.4	0.0462	0	0.07536
237	0.4	0.0010	0.0045	0.00040
222	0.4	0.0083	0.0045	0.01598
233	0.4	0.0145	0.0045	0.03762
227	0.4	0.0308	0.0045	0.05951
229	0.4	0.0385	0.0045	0.06827
234	0.4	0.0462	0.0045	0.08491

Table C.7. Gas holdup of the proposed correlations for CMC solutions calculated through disengagement technique

Run	CMC concentration (% wt)	u_G (m/s)	u_L (m/s)	Consistency index k , (Pa·s ^{<i>n</i>})	Flow index n , (-)	ϵ_G (-) Correlations
212-1	0.2	0.0010	0	0.0113	0.9442	0.00070
206-1	0.2	0.0083	0			0.02542
206-2	0.2	0.0083	0			0.02542
214	0.2	0.0083	0	0.0161	0.9111	0.02630
207-1	0.2	0.0145	0	0.0074	0.9746	0.04252
207-2	0.2	0.0145	0	0.0074	0.9746	0.04252
208-1	0.2	0.0308	0	0.0135	0.9309	0.07398
208-2	0.2	0.0308	0	0.0135	0.9309	0.07398
209-1	0.2	0.0385	0	0.0121	0.9364	0.09258
209-2	0.2	0.0385	0	0.0121	0.9364	0.09258
210	0.2	0.0462	0	0.0107	0.9469	0.11223
216	0.2	0.0083	0.0045	0.0110	0.9413	0.02209
217	0.2	0.0145	0.0045	0.0140	0.9338	0.03977
218	0.2	0.0308	0.0045	0.0212	0.9025	0.06799
219	0.2	0.0385	0.0045	0.0107	0.9525	0.09478
220	0.2	0.0462	0.0045	0.0173	0.9059	0.10116
211	0.3	0.0308	0	0.0311	0.8824	0.06370
232	0.4	0.0010	0	0.1678	0.7284	0.00262
215-1	0.4	0.0083	0	0.0773	0.8150	0.01256
215-2	0.4	0.0083	0	0.0773	0.8150	0.01256
224	0.4	0.0145	0	0.0928	0.7952	0.03123
213	0.4	0.0308	0	0.0412	0.8596	0.06263
226	0.4	0.0385	0	0.0651	0.8339	0.07032
228	0.4	0.0462	0	0.0553	0.8446	0.08247
237	0.4	0.0010	0.0045	0.1529	0.7530	0.00108
222	0.4	0.0083	0.0045	0.2462	0.7008	0.02061
233	0.4	0.0145	0.0045	0.0991	0.7894	0.03137
227	0.4	0.0308	0.0045	0.0941	0.7956	0.06004
229	0.4	0.0385	0.0045	0.1009	0.8041	0.06829
234	0.4	0.0462	0.0045	0.1950	0.7336	0.08120

* Eq. (5.23) was used for $(1.04 \times 10^{-3} \leq u_G (m/s) \leq 1.44 \times 10^{-2})$ and Eq. (5.24) for $(3.07 \times 10^{-2} \leq u_G (m/s) \leq 4.62 \times 10^{-2})$

Table C.8. Gas holdup for CMC solutions through pressure drop technique

Run	CMC concentration (% wt)	u_G (m/s)	u_L (m/s)	ε_G (-) Experimental
212-1	0.2	0.0010	0	
206-1	0.2	0.0083	0	
206-2	0.2	0.0083	0	
214	0.2	0.0083	0	0.02870
207-1	0.2	0.0145	0	0.03732
207-2	0.2	0.0145	0	0.03732
208-1	0.2	0.0308	0	0.07186
208-2	0.2	0.0308	0	0.07186
209-1	0.2	0.0385	0	0.09078
209-2	0.2	0.0385	0	0.09078
210	0.2	0.0462	0	0.10254
216	0.2	0.0083	0.0045	0.01658
217	0.2	0.0145	0.0045	0.03752
218	0.2	0.0308	0.0045	0.06939
219	0.2	0.0385	0.0045	0.09033
220	0.2	0.0462	0.0045	0.10000
211	0.3	0.0308	0	0.05864
232	0.4	0.0010	0	0.00173
215-1	0.4	0.0083	0	0.01457
215-2	0.4	0.0083	0	0.01457
224	0.4	0.0145	0	0.02659
213	0.4	0.0308	0	0.05557
226	0.4	0.0385	0	0.06341
228	0.4	0.0462	0	0.08251
237	0.4	0.0010	0.0045	0.00189
222	0.4	0.0083	0.0045	0.01789
233	0.4	0.0145	0.0045	0.03065
227	0.4	0.0308	0.0045	0.05393
229	0.4	0.0385	0.0045	0.06430
234	0.4	0.0462	0.0045	0.08133

Table C.9. Gas holdup of the proposed correlations for CMC solutions through pressure drop technique

Run	CMC concentration (% wt)	u_G (m/s)	u_L (m/s)	Consistency index k , (Pa·s ^{n})	Flow index n , (-)	ϵ_G (-) Correlations
212-1	0.2	0.0010	0	0.0113	0.9442	0.00186
206-1	0.2	0.0083	0			
206-2	0.2	0.0083	0			
214	0.2	0.0083	0	0.0161	0.9111	0.02097
207-1	0.2	0.0145	0	0.0074	0.9746	0.03797
207-2	0.2	0.0145	0	0.0074	0.9746	0.03797
208-1	0.2	0.0308	0	0.0135	0.9309	0.07021
208-2	0.2	0.0308	0	0.0135	0.9309	0.07021
209-1	0.2	0.0385	0	0.0121	0.9364	0.08945
209-2	0.2	0.0385	0	0.0121	0.9364	0.08945
210	0.2	0.0462	0	0.0107	0.9469	0.11010
216	0.2	0.0083	0.0045	0.0110	0.9413	0.02070
217	0.2	0.0145	0.0045	0.0140	0.9338	0.03560
218	0.2	0.0308	0.0045	0.0212	0.9025	0.06422
219	0.2	0.0385	0.0045	0.0107	0.9525	0.09178
220	0.2	0.0462	0.0045	0.0173	0.9059	0.09875
211	0.3	0.0308	0	0.0311	0.8824	0.05995
232	0.4	0.0010	0	0.1678	0.7284	0.00204
215-1	0.4	0.0083	0	0.0773	0.8150	0.01548
215-2	0.4	0.0083	0	0.0773	0.8150	0.01548
224	0.4	0.0145	0	0.0928	0.7952	0.02939
213	0.4	0.0308	0	0.0412	0.8596	0.05827
226	0.4	0.0385	0	0.0651	0.8339	0.06687
228	0.4	0.0462	0	0.0553	0.8446	0.07979
237	0.4	0.0010	0.0045	0.1529	0.7530	0.00162
222	0.4	0.0083	0.0045	0.2462	0.7008	0.01651
233	0.4	0.0145	0.0045	0.0991	0.7894	0.02931
227	0.4	0.0308	0.0045	0.0941	0.7956	0.05568
229	0.4	0.0385	0.0045	0.1009	0.8041	0.06464
234	0.4	0.0462	0.0045	0.1950	0.7336	0.07756

* Eq. (5.23) was used for $(1.04 \times 10^{-3} \leq u_G (m/s) \leq 1.44 \times 10^{-2})$ and Eq. (5.24) for $(3.07 \times 10^{-2} \leq u_G (m/s) \leq 4.62 \times 10^{-2})$

Table C.10. Two-phase friction factor for tap water

Run	u_G (m/s)	u_L (m/s)	f_{GL} (-) Experimental	f_{GL} (-) Correlation
190	0.0010	0	261922.44	261922.44
191	0.0027	0	36995.58	36995.58
192	0.0034	0	23901.39	23901.39
193	0.0055	0	9091.23	9091.23
194	0.0083	0	4035.08	4035.08
235	0.0083	0	4043.50	4043.50
195	0.0112	0	2230.08	2230.08
196	0.0145	0	1308.01	1308.01
225	0.0145	0	1357.08	1357.08
197	0.0206	0	664.22	664.22
198	0.0308	0	283.29	283.29
199	0.0385	0	189.53	189.53
236	0.0385	0	181.51	181.51
200	0.0462	0	130.07	130.07
179	0.0010	0.0045	8892.46	8892.46
239	0.0010	0.0045	8787.77	8787.77
180	0.0027	0.0045	5162.07	5162.07
181	0.0034	0.0045		
182	0.0055	0.0045		
183	0.0083	0.0045		
230	0.0083	0.0045	1745.87	1745.87
184	0.0112	0.0045	1159.05	1159.05
185	0.0145	0.0045		
231	0.0145	0.0045	764.81	764.81
186	0.0206	0.0045	442.38	442.38
187	0.0308	0.0045	224.53	224.53
188	0.0385	0.0045		
238	0.0385	0.0045	146.38	146.38
189	0.0462	0.0045	110.26	110.26

* Equations (5.13) and (5.14) were used for $(1.04 \times 10^{-3} \leq u_G (m/s) \leq 1.44 \times 10^{-2})$ and $(3.07 \times 10^{-2} \leq u_G (m/s) \leq 4.62 \times 10^{-2})$ respectively at $u_L = 0$ m/s

* Equations (5.15) and (5.16) were used for $(1.04 \times 10^{-3} \leq u_G (m/s) \leq 1.44 \times 10^{-2})$ and $(3.07 \times 10^{-2} \leq u_G (m/s) \leq 4.62 \times 10^{-2})$ respectively at $u_L = 0.0045$ m/s

Table C.11. Two-phase friction factor for CMC solutions

Run	CMC concentration (% wt)	u_G (m/s)	u_L (m/s)	f_{GL} (-) Experimental	f_{GL} (-) Correlation
203-1	0.10	0.0010	0	259375.13	259375.13
203-2	0.10	0.0010	0	342371.71	342371.71
204-1	0.10	0.0083	0	3979.70	3979.69695
204-2	0.10	0.0083	0	3575.18	3575.17911
205-1	0.10	0.0083	0	4035.79	4035.78647
205-2	0.10	0.0083	0	4049.71	4049.7131
201-1	0.15	0.0010	0	257801.61	257801.612
201-2	0.15	0.0010	0	258418.53	258418.532
202-1	0.15	0.0010	0	258303.68	258303.679
202-2	0.15	0.0010	0	257820.90	257820.896
212-1	0.20	0.0010	0	257556.82	257556.82
212-2	0.20	0.0010	0	260898.00	260897.996
214	0.20	0.0083	0	4058.11	
207-1	0.20	0.0145	0	1349.28	
207-2	0.20	0.0145	0	1322.25	4058.10628
207-3	0.20	0.0145	0	1326.69	1349.28117
208-1	0.20	0.0308	0	266.32	1322.25063
208-2	0.20	0.0308	0	290.27	1326.6914
208-3	0.20	0.0308	0	294.23	266.315534
209-1	0.20	0.0385	0	188.74	290.270735
209-2	0.20	0.0385	0	184.97	294.226826
209-3	0.20	0.0385	0	183.93	188.742217
210-1	0.20	0.0462	0	129.95	184.969243
210-2	0.20	0.0462	0	142.44	183.931837
216	0.20	0.0083	0.0045	1653.32	129.946923
217	0.20	0.0145	0.0045	789.60	142.441587
218	0.20	0.0308	0.0045	227.85	
219	0.20	0.0385	0.0045	152.11	1653.32014
220	0.20	0.0462	0.0045	112.57	789.603809
211-1	0.30	0.0308	0	314.05	227.85492
211-2	0.30	0.0308	0	297.88	152.108573
232	0.40	0.0010	0	258909.75	112.574258
215-1	0.40	0.0083	0	4076.71	314.045328
215-2	0.40	0.0083	0	4113.80	297.882381
215-3	0.40	0.0083	0	4076.99	258909.748
224	0.40	0.0145	0	1299.45	4076.70583
213-1	0.40	0.0308	0	287.79	4113.80376
213-2	0.40	0.0308	0	304.62	4076.98757
213-3	0.40	0.0308	0	294.69	1299.45349
226	0.40	0.0385	0	194.24	287.787198
228	0.40	0.0462	0	123.69	304.6168
237	0.40	0.0010	0.0045	8839.08	294.692553
222	0.40	0.0083	0.0045	1653.84	194.237834
233	0.40	0.0145	0.0045	785.69	123.688493
227	0.40	0.0308	0.0045	225.51	8839.08181
229	0.40	0.0385	0.0045	150.85	1653.84263
234	0.40	0.0462	0.0045	108.35	785.691463

Table C.12. Tracer concentration for Run-86 ($u_L=0$ m/s, $u_G=0.0112$ m/s, tap water)

t (s)	$c(t)$ (kg/m ³) Experimental	$c(t)$ (kg/m ³) Model
0	0	1.962×10^{-6}
11	1.270×10^{-4}	9.853×10^{-5}
29	3.556×10^{-4}	3.801×10^{-4}
40	4.826×10^{-4}	4.650×10^{-4}
52	5.080×10^{-4}	5.154×10^{-4}
63	5.334×10^{-4}	5.404×10^{-4}
74	5.461×10^{-4}	5.542×10^{-4}
89	5.588×10^{-4}	5.637×10^{-4}
101	5.461×10^{-4}	5.674×10^{-4}
113	5.715×10^{-4}	5.694×10^{-4}
125	5.715×10^{-4}	5.704×10^{-4}
137	5.715×10^{-4}	5.709×10^{-4}
151	5.715×10^{-4}	5.712×10^{-4}
162	5.842×10^{-4}	5.713×10^{-4}
176	5.715×10^{-4}	5.714×10^{-4}
190	5.715×10^{-4}	5.715×10^{-4}
202	5.715×10^{-4}	5.715×10^{-4}
217	5.842×10^{-4}	5.715×10^{-4}
228	5.715×10^{-4}	5.715×10^{-4}
242	5.715×10^{-4}	5.715×10^{-4}
256	5.715×10^{-4}	5.715×10^{-4}
271	5.906×10^{-4}	5.715×10^{-4}
288	5.715×10^{-4}	5.715×10^{-4}
302	5.715×10^{-4}	5.715×10^{-4}
317	5.588×10^{-4}	5.715×10^{-4}
331	5.969×10^{-4}	5.715×10^{-4}
344	5.842×10^{-4}	5.715×10^{-4}
358	5.715×10^{-4}	5.715×10^{-4}
371	5.969×10^{-4}	5.715×10^{-4}
386	5.969×10^{-4}	5.715×10^{-4}
401	5.715×10^{-4}	5.715×10^{-4}
461	5.588×10^{-4}	5.715×10^{-4}

Table C.13. Tracer concentration for Run-87 ($u_L=0$ m/s, $u_G=0.0206$ m/s, tap water)

t (s)	$c(t)$ (kg/m ³) Experimental	$c(t)$ (kg/m ³) Model
0	0	1.831×10^{-6}
10	1.524×10^{-4}	1.645×10^{-4}
21	3.937×10^{-4}	3.757×10^{-4}
32	4.572×10^{-4}	4.678×10^{-4}
46	5.080×10^{-4}	5.119×10^{-4}
59	5.334×10^{-4}	5.258×10^{-4}
71	5.334×10^{-4}	5.305×10^{-4}
83	5.588×10^{-4}	5.323×10^{-4}
97	5.461×10^{-4}	5.330×10^{-4}
110	5.588×10^{-4}	5.333×10^{-4}
122	5.461×10^{-4}	5.333×10^{-4}
135	5.461×10^{-4}	5.333×10^{-4}
148	5.207×10^{-4}	5.333×10^{-4}
161	5.334×10^{-4}	5.334×10^{-4}
172	5.588×10^{-4}	5.334×10^{-4}
185	5.588×10^{-4}	5.334×10^{-4}
200	5.588×10^{-4}	5.334×10^{-4}
212	5.588×10^{-4}	5.334×10^{-4}
228	5.842×10^{-4}	5.334×10^{-4}
241	5.461×10^{-4}	5.334×10^{-4}
253	5.461×10^{-4}	5.334×10^{-4}
270	5.080×10^{-4}	5.334×10^{-4}
292	5.207×10^{-4}	5.334×10^{-4}
310	5.080×10^{-4}	5.334×10^{-4}
327	5.207×10^{-4}	5.334×10^{-4}
342	5.461×10^{-4}	5.334×10^{-4}
358	4.953×10^{-4}	5.334×10^{-4}
373	5.334×10^{-4}	5.334×10^{-4}
394	5.334×10^{-4}	5.334×10^{-4}
411	5.334×10^{-4}	5.334×10^{-4}
431	4.699×10^{-4}	5.334×10^{-4}
457	4.826×10^{-4}	5.334×10^{-4}
487	5.588×10^{-4}	5.334×10^{-4}
514	5.461×10^{-4}	5.334×10^{-4}
541	5.334×10^{-4}	5.334×10^{-4}

Table C.14. Tracer concentration for Run-88 ($u_L=0$ m/s, $u_G=0.0010$ m/s, tap water)

t (s)	$c(t)$ (kg/m ³) Experimental	$c(t)$ (kg/m ³) Model
0	0	1.875×10^{-6}
12	1.143×10^{-4}	8.096×10^{-5}
26	2.921×10^{-4}	2.862×10^{-4}
36	3.810×10^{-4}	3.808×10^{-4}
46	4.191×10^{-4}	4.415×10^{-4}
57	4.699×10^{-4}	4.830×10^{-4}
68	4.826×10^{-4}	5.080×10^{-4}
81	5.461×10^{-4}	5.251×10^{-4}
91	5.080×10^{-4}	5.329×10^{-4}
102	5.715×10^{-4}	5.381×10^{-4}
115	5.461×10^{-4}	5.417×10^{-4}
128	5.334×10^{-4}	5.437×10^{-4}
141	5.588×10^{-4}	5.448×10^{-4}
153	5.588×10^{-4}	5.453×10^{-4}
166	5.715×10^{-4}	5.457×10^{-4}
179	5.842×10^{-4}	5.459×10^{-4}
191	5.715×10^{-4}	5.460×10^{-4}
205	5.715×10^{-4}	5.460×10^{-4}
219	5.588×10^{-4}	5.461×10^{-4}
233	5.461×10^{-4}	5.461×10^{-4}
249	5.461×10^{-4}	5.461×10^{-4}
261	5.461×10^{-4}	5.461×10^{-4}
304	5.588×10^{-4}	5.461×10^{-4}
354	5.334×10^{-4}	5.461×10^{-4}
402	5.461×10^{-4}	5.461×10^{-4}
435	5.588×10^{-4}	5.461×10^{-4}
480	5.588×10^{-4}	5.461×10^{-4}
533	5.588×10^{-4}	5.461×10^{-4}
573	5.588×10^{-4}	5.461×10^{-4}
640	5.588×10^{-4}	5.461×10^{-4}
668	5.334×10^{-4}	5.461×10^{-4}
731	5.334×10^{-4}	5.461×10^{-4}
789	5.334×10^{-4}	5.461×10^{-4}
861	5.080×10^{-4}	5.461×10^{-4}
958	5.207×10^{-4}	5.461×10^{-4}
1004	5.207×10^{-4}	5.461×10^{-4}

Table C.15. Tracer concentration for Run-89 ($u_L=0$ m/s, $u_G=0.0055$ m/s, tap water)

t (s)	$c(t)$ (kg/m ³) Experimental	$c(t)$ (kg/m ³) Model
0	0	1.657×10^{-6}
13	2.032×10^{-4}	1.014×10^{-4}
25	2.540×10^{-4}	2.634×10^{-4}
33	3.175×10^{-4}	3.345×10^{-4}
40	3.810×10^{-4}	3.778×10^{-4}
48	3.937×10^{-4}	4.122×10^{-4}
56	3.937×10^{-4}	4.353×10^{-4}
63	4.445×10^{-4}	4.492×10^{-4}
71	4.445×10^{-4}	4.601×10^{-4}
78	4.318×10^{-4}	4.667×10^{-4}
84	4.445×10^{-4}	4.708×10^{-4}
91	4.572×10^{-4}	4.743×10^{-4}
97	4.572×10^{-4}	4.764×10^{-4}
105	4.953×10^{-4}	4.785×10^{-4}
111	4.699×10^{-4}	4.795×10^{-4}
178	4.699×10^{-4}	4.825×10^{-4}
125	4.826×10^{-4}	4.811×10^{-4}
132	5.080×10^{-4}	4.815×10^{-4}
138	4.699×10^{-4}	4.818×10^{-4}
143	4.699×10^{-4}	4.820×10^{-4}
149	4.699×10^{-4}	4.821×10^{-4}
156	4.699×10^{-4}	4.823×10^{-4}
162	4.699×10^{-4}	4.824×10^{-4}
168	4.699×10^{-4}	4.824×10^{-4}
175	4.953×10^{-4}	4.825×10^{-4}
198	4.699×10^{-4}	4.826×10^{-4}
211	4.699×10^{-4}	4.826×10^{-4}
221	4.826×10^{-4}	4.826×10^{-4}
234	4.826×10^{-4}	4.826×10^{-4}
247	4.826×10^{-4}	4.826×10^{-4}
262	4.445×10^{-4}	4.826×10^{-4}
304	4.826×10^{-4}	4.826×10^{-4}
362	4.953×10^{-4}	4.826×10^{-4}
422	4.826×10^{-4}	4.826×10^{-4}
484	4.826×10^{-4}	4.826×10^{-4}

Table C.16. Tracer concentration for Run-91 ($u_L=0$ m/s, $u_G=0.0055$ m/s, tap water)

t (s)	$c(t)$ (kg/m ³) Experimental	$c(t)$ (kg/m ³) Model
0	0	1.701×10^{-6}
17	1.270×10^{-5}	4.428×10^{-5}
25	1.270×10^{-4}	1.119×10^{-4}
31	1.651×10^{-4}	1.626×10^{-4}
38	2.286×10^{-4}	2.161×10^{-4}
45	2.540×10^{-4}	2.623×10^{-4}
53	3.175×10^{-4}	3.065×10^{-4}
61	3.429×10^{-4}	3.426×10^{-4}
70	4.064×10^{-4}	3.751×10^{-4}
77	3.937×10^{-4}	3.956×10^{-4}
85	4.064×10^{-4}	4.148×10^{-4}
92	4.064×10^{-4}	4.286×10^{-4}
100	4.445×10^{-4}	4.415×10^{-4}
107	4.572×10^{-4}	4.507×10^{-4}
115	4.445×10^{-4}	4.593×10^{-4}
123	4.445×10^{-4}	4.662×10^{-4}
130	4.572×10^{-4}	4.712×10^{-4}
138	4.699×10^{-4}	4.759×10^{-4}
144	4.699×10^{-4}	4.787×10^{-4}
151	4.699×10^{-4}	4.816×10^{-4}
158	4.953×10^{-4}	4.839×10^{-4}
166	4.826×10^{-4}	4.861×10^{-4}
173	4.826×10^{-4}	4.877×10^{-4}
181	4.826×10^{-4}	4.892×10^{-4}
189	4.826×10^{-4}	4.903×10^{-4}
196	4.826×10^{-4}	4.912×10^{-4}
204	4.826×10^{-4}	4.920×10^{-4}
212	5.080×10^{-4}	4.926×10^{-4}
222	5.080×10^{-4}	4.933×10^{-4}
229	4.953×10^{-4}	4.936×10^{-4}
271	4.953×10^{-4}	4.947×10^{-4}
327	4.826×10^{-4}	4.952×10^{-4}
388	4.953×10^{-4}	4.953×10^{-4}
450	4.699×10^{-4}	4.953×10^{-4}

Table C.17. Tracer concentration for Run-93 ($u_L=0$ m/s, $u_G=0.0034$ m/s, tap water)

t (s)	$c(t)$ (kg/m ³) Experimental	$c(t)$ (kg/m ³) Model
0	0	2.398×10^{-6}
14	1.778×10^{-4}	1.146×10^{-4}
23	3.175×10^{-4}	2.768×10^{-4}
32	3.937×10^{-4}	4.034×10^{-4}
40	4.699×10^{-4}	4.853×10^{-4}
48	5.969×10^{-4}	5.448×10^{-4}
57	5.715×10^{-4}	5.923×10^{-4}
64	5.334×10^{-4}	6.189×10^{-4}
72	6.477×10^{-4}	6.412×10^{-4}
81	6.350×10^{-4}	6.589×10^{-4}
90	6.604×10^{-4}	6.712×10^{-4}
98	6.604×10^{-4}	6.788×10^{-4}
106	6.604×10^{-4}	6.843×10^{-4}
115	6.223×10^{-4}	6.887×10^{-4}
123	6.477×10^{-4}	6.915×10^{-4}
131	6.604×10^{-4}	6.934×10^{-4}
140	6.985×10^{-4}	6.950×10^{-4}
149	6.223×10^{-4}	6.961×10^{-4}
157	6.223×10^{-4}	6.968×10^{-4}
165	5.969×10^{-4}	6.972×10^{-4}
175	6.477×10^{-4}	6.977×10^{-4}
184	6.477×10^{-4}	6.979×10^{-4}
193	6.731×10^{-4}	6.981×10^{-4}
203	6.731×10^{-4}	6.982×10^{-4}
226	6.731×10^{-4}	6.984×10^{-4}
237	6.731×10^{-4}	6.984×10^{-4}
249	6.858×10^{-4}	6.985×10^{-4}
271	7.112×10^{-4}	6.985×10^{-4}
318	6.985×10^{-4}	6.985×10^{-4}
364	6.985×10^{-4}	6.985×10^{-4}
412	6.731×10^{-4}	6.985×10^{-4}
457	6.985×10^{-4}	6.985×10^{-4}
491	7.112×10^{-4}	6.985×10^{-4}
535	6.477×10^{-4}	6.985×10^{-4}

Table C.18. Tracer concentration for Run-94 ($u_L=0$ m/s, $u_G=0.0112$ m/s, tap water)

t (s)	$c(t)$ (kg/m ³) Experimental	$c(t)$ (kg/m ³) Model
0	0	2.224×10^{-6}
14	3.937×10^{-4}	2.382×10^{-4}
22	3.937×10^{-4}	3.979×10^{-4}
30	4.699×10^{-4}	4.975×10^{-4}
38	4.953×10^{-4}	5.576×10^{-4}
46	5.461×10^{-4}	5.937×10^{-4}
53	5.207×10^{-4}	6.132×10^{-4}
61	5.715×10^{-4}	6.270×10^{-4}
70	5.969×10^{-4}	6.361×10^{-4}
77	5.588×10^{-4}	6.403×10^{-4}
85	6.223×10^{-4}	6.433×10^{-4}
94	6.350×10^{-4}	6.452×10^{-4}
102	5.969×10^{-4}	6.462×10^{-4}
109	6.223×10^{-4}	6.467×10^{-4}
116	6.223×10^{-4}	6.471×10^{-4}
124	6.350×10^{-4}	6.473×10^{-4}
131	6.350×10^{-4}	6.475×10^{-4}
138	6.604×10^{-4}	6.476×10^{-4}
146	5.969×10^{-4}	6.476×10^{-4}
153	6.350×10^{-4}	6.476×10^{-4}
161	4.953×10^{-4}	6.477×10^{-4}
170	6.223×10^{-4}	6.477×10^{-4}
178	5.588×10^{-4}	6.477×10^{-4}
185	6.604×10^{-4}	6.477×10^{-4}
201	6.477×10^{-4}	6.477×10^{-4}
211	6.477×10^{-4}	6.477×10^{-4}
222	6.477×10^{-4}	6.477×10^{-4}
230	6.350×10^{-4}	6.477×10^{-4}
247	6.223×10^{-4}	6.477×10^{-4}
275	6.350×10^{-4}	6.477×10^{-4}
298	6.223×10^{-4}	6.477×10^{-4}
343	6.477×10^{-4}	6.477×10^{-4}
382	6.477×10^{-4}	6.477×10^{-4}
427	6.477×10^{-4}	6.477×10^{-4}
475	5.969×10^{-4}	6.477×10^{-4}

Table C.19. Tracer concentration for Run-95 ($u_L=0$ m/s, $u_G=0.0462$ m/s, tap water)

t (s)	$c(t)$ (kg/m ³) Experimental	$c(t)$ (kg/m ³) Model
0	0	2.878×10^{-6}
40	6.731×10^{-4}	6.644×10^{-4}
48	7.239×10^{-4}	7.224×10^{-4}
55	7.620×10^{-4}	7.570×10^{-4}
62	7.620×10^{-4}	7.813×10^{-4}
69	8.636×10^{-4}	7.984×10^{-4}
76	8.001×10^{-4}	8.103×10^{-4}
84	7.620×10^{-4}	8.196×10^{-4}
91	8.255×10^{-4}	8.252×10^{-4}
99	7.747×10^{-4}	8.295×10^{-4}
107	8.255×10^{-4}	8.324×10^{-4}
114	7.874×10^{-4}	8.342×10^{-4}
122	8.255×10^{-4}	8.355×10^{-4}
128	8.128×10^{-4}	8.362×10^{-4}
134	8.382×10^{-4}	8.367×10^{-4}
141	8.382×10^{-4}	8.372×10^{-4}
149	8.001×10^{-4}	8.375×10^{-4}
155	8.255×10^{-4}	8.377×10^{-4}
162	8.255×10^{-4}	8.378×10^{-4}
170	8.382×10^{-4}	8.380×10^{-4}
177	8.255×10^{-4}	8.380×10^{-4}
184	8.255×10^{-4}	8.381×10^{-4}
191	7.620×10^{-4}	8.381×10^{-4}
198	8.128×10^{-4}	8.381×10^{-4}
219	8.636×10^{-4}	8.382×10^{-4}
227	8.128×10^{-4}	8.382×10^{-4}
234	8.128×10^{-4}	8.382×10^{-4}
242	8.382×10^{-4}	8.382×10^{-4}
250	7.874×10^{-4}	8.382×10^{-4}
287	8.382×10^{-4}	8.382×10^{-4}
327	7.239×10^{-4}	8.382×10^{-4}
361	7.747×10^{-4}	8.382×10^{-4}
405	7.366×10^{-4}	8.382×10^{-4}
438	6.985×10^{-4}	8.382×10^{-4}

Table C.20. Tracer concentration for Run-111 ($u_L=0$ m/s, $u_G=0.0027$ m/s, tap water)

t (s)	$c(t)$ (kg/m ³) Experimental	$c(t)$ (kg/m ³) Model
0	0	2.616×10^{-6}
12	7.620×10^{-5}	1.110×10^{-4}
20	2.032×10^{-4}	2.871×10^{-4}
27	4.191×10^{-4}	4.122×10^{-4}
36	5.080×10^{-4}	5.286×10^{-4}
42	5.715×10^{-4}	5.842×10^{-4}
48	6.731×10^{-4}	6.267×10^{-4}
55	7.239×10^{-4}	6.636×10^{-4}
62	7.239×10^{-4}	6.905×10^{-4}
68	6.858×10^{-4}	7.076×10^{-4}
74	7.620×10^{-4}	7.206×10^{-4}
81	7.493×10^{-4}	7.319×10^{-4}
87	7.620×10^{-4}	7.391×10^{-4}
93	7.747×10^{-4}	7.446×10^{-4}
100	8.128×10^{-4}	7.494×10^{-4}
107	7.874×10^{-4}	7.528×10^{-4}
115	8.255×10^{-4}	7.556×10^{-4}
122	7.874×10^{-4}	7.574×10^{-4}
129	7.874×10^{-4}	7.586×10^{-4}
137	7.747×10^{-4}	7.597×10^{-4}
145	7.493×10^{-4}	7.604×10^{-4}
154	7.620×10^{-4}	7.609×10^{-4}
164	7.747×10^{-4}	7.613×10^{-4}
172	7.493×10^{-4}	7.615×10^{-4}
194	7.874×10^{-4}	7.618×10^{-4}
210	7.620×10^{-4}	7.619×10^{-4}
226	7.493×10^{-4}	7.620×10^{-4}
243	8.128×10^{-4}	7.620×10^{-4}
261	7.493×10^{-4}	7.620×10^{-4}
284	7.366×10^{-4}	7.620×10^{-4}
303	7.493×10^{-4}	7.620×10^{-4}
319	7.493×10^{-4}	7.620×10^{-4}
334	8.001×10^{-4}	7.620×10^{-4}
352	7.112×10^{-4}	7.620×10^{-4}

Table C.21. Tracer concentration for Run-112 ($u_L=0$ m/s, $u_G=0.0308$ m/s, tap water)

t (s)	$c(t)$ (kg/m ³) Experimental	$c(t)$ (kg/m ³) Model
0	8.900×10^{-5}	4.361×10^{-6}
13	3.811×10^{-4}	2.547×10^{-4}
20	6.224×10^{-4}	5.215×10^{-4}
27	7.113×10^{-4}	7.310×10^{-4}
37	8.383×10^{-4}	9.368×10^{-4}
46	9.780×10^{-4}	1.055×10^{-3}
53	1.207×10^{-3}	1.117×10^{-3}
60	1.232×10^{-3}	1.161×10^{-3}
69	1.080×10^{-3}	1.200×10^{-3}
76	1.257×10^{-3}	1.220×10^{-3}
84	9.907×10^{-4}	1.236×10^{-3}
91	1.156×10^{-3}	1.246×10^{-3}
99	1.054×10^{-3}	1.254×10^{-3}
106	1.321×10^{-3}	1.258×10^{-3}
113	1.245×10^{-3}	1.262×10^{-3}
120	1.156×10^{-3}	1.264×10^{-3}
126	1.372×10^{-3}	1.266×10^{-3}
143	1.283×10^{-3}	1.268×10^{-3}
151	1.130×10^{-3}	1.269×10^{-3}
164	1.029×10^{-3}	1.269×10^{-3}
172	1.029×10^{-3}	1.270×10^{-3}
179	1.232×10^{-3}	1.270×10^{-3}
187	1.118×10^{-3}	1.270×10^{-3}
196	1.270×10^{-3}	1.270×10^{-3}

Table C.22. Tracer concentration for Run-235 ($u_L=0$ m/s, $u_G=0.0083$ m/s, tap water)

t (s)	$c(t)$ (kg/m ³) Experimental	$c(t)$ (kg/m ³) Model
0	0	3.488×10^{-6}
14	2.286×10^{-4}	3.260×10^{-4}
21	4.572×10^{-4}	5.482×10^{-4}
27	6.604×10^{-4}	6.849×10^{-4}
33	1.130×10^{-3}	7.825×10^{-4}
39	8.255×10^{-4}	8.515×10^{-4}
46	8.890×10^{-4}	9.067×10^{-4}
52	8.509×10^{-4}	9.390×10^{-4}
58	9.271×10^{-4}	9.618×10^{-4}
65	9.906×10^{-4}	9.800×10^{-4}
72	1.016×10^{-3}	9.921×10^{-4}
78	9.398×10^{-4}	9.992×10^{-4}
84	1.029×10^{-3}	1.004×10^{-3}
91	9.779×10^{-4}	1.008×10^{-3}
98	1.029×10^{-3}	1.011×10^{-3}
104	9.906×10^{-4}	1.012×10^{-3}
111	1.067×10^{-3}	1.014×10^{-3}
123	9.271×10^{-4}	1.015×10^{-3}
131	9.906×10^{-4}	1.015×10^{-3}
138	8.890×10^{-4}	1.015×10^{-3}
146	1.003×10^{-3}	1.016×10^{-3}
156	1.016×10^{-3}	1.016×10^{-3}
165	1.118×10^{-3}	1.016×10^{-3}
184	1.181×10^{-3}	1.016×10^{-3}

Table C.23. Tracer concentration for Run-236 ($u_L=0$ m/s, $u_G=0.0385$ m/s, tap water)

t (s)	$c(t)$ (kg/m ³) Experimental	$c(t)$ (kg/m ³) Model
0	0	4.142×10^{-6}
11	3.683×10^{-4}	2.506×10^{-4}
17	6.223×10^{-4}	5.096×10^{-4}
23	6.604×10^{-4}	7.101×10^{-4}
30	9.144×10^{-4}	8.753×10^{-4}
37	9.144×10^{-4}	9.862×10^{-4}
43	1.003×10^{-3}	1.051×10^{-3}
49	1.041×10^{-3}	1.097×10^{-3}
57	1.067×10^{-3}	1.138×10^{-3}
64	1.118×10^{-3}	1.161×10^{-3}
71	1.092×10^{-3}	1.176×10^{-3}
78	1.143×10^{-3}	1.186×10^{-3}
86	1.029×10^{-3}	1.194×10^{-3}
94	1.118×10^{-3}	1.199×10^{-3}
101	1.156×10^{-3}	1.201×10^{-3}
108	1.181×10^{-3}	1.203×10^{-3}
117	1.257×10^{-3}	1.204×10^{-3}
125	1.156×10^{-3}	1.205×10^{-3}
133	1.270×10^{-3}	1.206×10^{-3}
140	1.219×10^{-3}	1.206×10^{-3}
149	1.207×10^{-3}	1.206×10^{-3}
159	1.270×10^{-3}	1.206×10^{-3}
180	1.194×10^{-3}	1.206×10^{-3}
189	1.245×10^{-3}	1.206×10^{-3}

Table C.24. Tracer concentration for Run-92 ($u_L=0.0025$ m/s, $u_G=0.0010$ m/s, tap water)

t (s)	$c(t)$ (kg/m ³) Experimental	$c(t)$ (kg/m ³) Model
0	0	0
16	1.270×10^{-5}	1.470×10^{-4}
24	1.270×10^{-4}	1.819×10^{-4}
33	2.286×10^{-4}	2.134×10^{-4}
41	2.540×10^{-4}	2.367×10^{-4}
48	2.540×10^{-4}	2.544×10^{-4}
55	2.921×10^{-4}	2.700×10^{-4}
62	2.921×10^{-4}	2.839×10^{-4}
69	3.429×10^{-4}	2.962×10^{-4}
75	3.175×10^{-4}	3.058×10^{-4}
82	3.429×10^{-4}	3.158×10^{-4}
89	3.556×10^{-4}	3.248×10^{-4}
95	3.175×10^{-4}	3.318×10^{-4}
102	3.556×10^{-4}	3.391×10^{-4}
110	3.810×10^{-4}	3.465×10^{-4}
116	3.683×10^{-4}	3.514×10^{-4}
124	3.937×10^{-4}	3.572×10^{-4}
131	3.556×10^{-4}	3.617×10^{-4}
137	3.683×10^{-4}	3.651×10^{-4}
146	3.302×10^{-4}	3.694×10^{-4}
153	3.810×10^{-4}	3.723×10^{-4}
160	3.683×10^{-4}	3.747×10^{-4}
168	3.556×10^{-4}	3.770×10^{-4}
187	3.556×10^{-4}	3.805×10^{-4}
194	3.937×10^{-4}	3.812×10^{-4}
204	3.937×10^{-4}	3.817×10^{-4}
212	3.810×10^{-4}	3.818×10^{-4}
224	3.937×10^{-4}	3.812×10^{-4}
233	3.937×10^{-4}	3.804×10^{-4}
242	3.556×10^{-4}	3.792×10^{-4}
254	3.556×10^{-4}	3.772×10^{-4}
270	3.556×10^{-4}	3.738×10^{-4}
283	3.810×10^{-4}	3.705×10^{-4}
304	3.302×10^{-4}	3.643×10^{-4}
330	3.556×10^{-4}	3.554×10^{-4}
357	3.429×10^{-4}	3.451×10^{-4}
385	3.175×10^{-4}	3.335×10^{-4}
428	3.048×10^{-4}	3.147×10^{-4}
447	3.048×10^{-4}	3.061×10^{-4}

Table C.24. Tracer concentration for Run-92 ($u_L=0.0025$ m/s, $u_G=0.0010$ m/s, tap water).

Cont...

t (s)	$c(t)$ (kg/m ³) Experimental	$c(t)$ (kg/m ³) Model
479	2.921×10^{-4}	2.915×10^{-4}
501	2.413×10^{-4}	2.814×10^{-4}
533	2.794×10^{-4}	2.669×10^{-4}
576	2.667×10^{-4}	2.477×10^{-4}
612	2.413×10^{-4}	2.321×10^{-4}
658	1.905×10^{-4}	2.130×10^{-4}
720	2.032×10^{-4}	1.888×10^{-4}
796	1.651×10^{-4}	1.620×10^{-4}
846	1.524×10^{-4}	1.460×10^{-4}
882	1.270×10^{-4}	1.354×10^{-4}
951	1.270×10^{-4}	1.167×10^{-4}
994	1.016×10^{-4}	1.062×10^{-4}
1045	1.016×10^{-4}	9.489×10^{-5}
1097	1.016×10^{-4}	8.446×10^{-5}
1154	8.890×10^{-5}	7.422×10^{-5}
1220	8.890×10^{-5}	6.379×10^{-5}
1280	6.350×10^{-5}	5.551×10^{-5}
1333	5.080×10^{-5}	4.904×10^{-5}
1387	5.080×10^{-5}	4.318×10^{-5}
1449	5.080×10^{-5}	3.727×10^{-5}
1490	3.810×10^{-5}	3.380×10^{-5}
1517	3.810×10^{-5}	3.168×10^{-5}
1567	3.810×10^{-5}	2.809×10^{-5}
1634	2.540×10^{-5}	2.388×10^{-5}
1699	2.540×10^{-5}	2.039×10^{-5}
1748	2.540×10^{-5}	1.808×10^{-5}
1797	2.540×10^{-5}	1.603×10^{-5}
1850	1.270×10^{-5}	1.407×10^{-5}
1897	1.270×10^{-5}	1.253×10^{-5}

Table C.25. Tracer concentration for Run-96 ($u_L=0.0025$ m/s, $u_G=0.0034$ m/s, tap water)

t (s)	$c(t)$ (kg/m ³) Experimental	$c(t)$ (kg/m ³) Model
0	0	0
10	2.286×10^{-4}	3.223×10^{-4}
17	2.286×10^{-4}	3.812×10^{-4}
24	2.921×10^{-4}	4.229×10^{-4}
32	3.556×10^{-4}	4.590×10^{-4}
38	4.699×10^{-4}	4.808×10^{-4}
44	5.080×10^{-4}	4.993×10^{-4}
50	5.588×10^{-4}	5.152×10^{-4}
58	6.223×10^{-4}	5.331×10^{-4}
65	6.350×10^{-4}	5.463×10^{-4}
72	6.223×10^{-4}	5.575×10^{-4}
79	6.477×10^{-4}	5.672×10^{-4}
86	6.223×10^{-4}	5.754×10^{-4}
94	6.604×10^{-4}	5.833×10^{-4}
100	6.604×10^{-4}	5.884×10^{-4}
113	6.604×10^{-4}	5.970×10^{-4}
123	6.731×10^{-4}	6.018×10^{-4}
130	6.350×10^{-4}	6.044×10^{-4}
138	6.477×10^{-4}	6.066×10^{-4}
144	6.350×10^{-4}	6.078×10^{-4}
151	6.223×10^{-4}	6.087×10^{-4}
157	6.350×10^{-4}	6.092×10^{-4}
164	6.096×10^{-4}	6.093×10^{-4}
171	6.096×10^{-4}	6.090×10^{-4}
191	5.969×10^{-4}	6.065×10^{-4}
198	6.096×10^{-4}	6.050×10^{-4}
205	6.096×10^{-4}	6.033×10^{-4}
212	5.969×10^{-4}	6.014×10^{-4}
220	5.842×10^{-4}	5.989×10^{-4}
227	5.842×10^{-4}	5.965×10^{-4}
235	5.588×10^{-4}	5.935×10^{-4}
243	5.461×10^{-4}	5.903×10^{-4}
252	5.207×10^{-4}	5.865×10^{-4}
260	5.461×10^{-4}	5.829×10^{-4}
269	5.461×10^{-4}	5.787×10^{-4}
279	5.207×10^{-4}	5.737×10^{-4}
289	5.080×10^{-4}	5.686×10^{-4}
297	5.461×10^{-4}	5.643×10^{-4}
316	5.207×10^{-4}	5.538×10^{-4}

Table C.25. Tracer concentration for Run-96 ($u_L=0.0025$ m/s, $u_G=0.0034$ m/s, tap water).

Cont...

t (s)	$c(t)$ (kg/m ³) Experimental	$c(t)$ (kg/m ³) Model
324	4.826×10^{-4}	5.492×10^{-4}
332	5.334×10^{-4}	5.446×10^{-4}
377	4.953×10^{-4}	5.173×10^{-4}
417	4.572×10^{-4}	4.922×10^{-4}
462	4.318×10^{-4}	4.636×10^{-4}
513	3.683×10^{-4}	4.315×10^{-4}
549	3.810×10^{-4}	4.094×10^{-4}
606	3.556×10^{-4}	3.755×10^{-4}
666	3.175×10^{-4}	3.417×10^{-4}
764	3.048×10^{-4}	2.913×10^{-4}
824	2.667×10^{-4}	2.633×10^{-4}
890	2.413×10^{-4}	2.352×10^{-4}
941	2.413×10^{-4}	2.153×10^{-4}
1013	2.286×10^{-4}	1.897×10^{-4}
1078	1.905×10^{-4}	1.689×10^{-4}
1145	1.651×10^{-4}	1.497×10^{-4}
1222	1.524×10^{-4}	1.301×10^{-4}
1288	1.524×10^{-4}	1.152×10^{-4}
1354	1.270×10^{-4}	1.020×10^{-4}
1411	1.270×10^{-4}	9.171×10^{-5}
1489	1.016×10^{-4}	7.924×10^{-5}
1554	8.890×10^{-5}	7.009×10^{-5}
1635	7.620×10^{-5}	6.011×10^{-5}
1700	8.890×10^{-5}	5.311×10^{-5}
1761	7.620×10^{-5}	4.726×10^{-5}
1831	5.080×10^{-5}	4.131×10^{-5}
1859	6.350×10^{-5}	3.915×10^{-5}
1940	5.080×10^{-5}	3.348×10^{-5}
2029	2.540×10^{-5}	2.817×10^{-5}

Table C.26. Tracer concentration for Run-97 ($u_L=0.0025$ m/s, $u_G=0.0112$ m/s, tap water)

t (s)	$c(t)$ (kg/m ³) Experimental	$c(t)$ (kg/m ³) Model
0	0	0
9	1.016×10^{-4}	3.115×10^{-4}
17	2.159×10^{-4}	3.904×10^{-4}
23	3.175×10^{-4}	4.328×10^{-4}
31	4.826×10^{-4}	4.772×10^{-4}
38	5.842×10^{-4}	5.084×10^{-4}
45	6.223×10^{-4}	5.347×10^{-4}
52	6.731×10^{-4}	5.571×10^{-4}
68	7.112×10^{-4}	5.976×10^{-4}
76	7.112×10^{-4}	6.135×10^{-4}
99	7.112×10^{-4}	6.481×10^{-4}
128	7.112×10^{-4}	6.745×10^{-4}
135	6.985×10^{-4}	6.788×10^{-4}
142	6.985×10^{-4}	6.824×10^{-4}
150	7.112×10^{-4}	6.857×10^{-4}
157	7.112×10^{-4}	6.881×10^{-4}
172	6.985×10^{-4}	6.914×10^{-4}
192	6.858×10^{-4}	6.928×10^{-4}
200	6.858×10^{-4}	6.925×10^{-4}
209	6.731×10^{-4}	6.917×10^{-4}
217	6.731×10^{-4}	6.906×10^{-4}
226	6.477×10^{-4}	6.889×10^{-4}
235	6.477×10^{-4}	6.868×10^{-4}
275	6.223×10^{-4}	6.733×10^{-4}
289	6.096×10^{-4}	6.672×10^{-4}
351	5.969×10^{-4}	6.350×10^{-4}
379	5.842×10^{-4}	6.183×10^{-4}
403	5.715×10^{-4}	6.034×10^{-4}
427	5.588×10^{-4}	5.881×10^{-4}
454	5.461×10^{-4}	5.704×10^{-4}
497	4.953×10^{-4}	5.420×10^{-4}
531	4.699×10^{-4}	5.194×10^{-4}
588	4.572×10^{-4}	4.820×10^{-4}
620	4.191×10^{-4}	4.615×10^{-4}
655	4.064×10^{-4}	4.395×10^{-4}
683	4.191×10^{-4}	4.223×10^{-4}
713	4.191×10^{-4}	4.044×10^{-4}
766	3.937×10^{-4}	3.740×10^{-4}
840	3.429×10^{-4}	3.343×10^{-4}

Table C.26. Tracer concentration for Run-97 ($u_L=0.0025$ m/s, $u_G=0.0112$ m/s, tap water).

Cont...

t (s)	$c(t)$ (kg/m ³) Experimental	$c(t)$ (kg/m ³) Model
986	2.794×10^{-4}	2.657×10^{-4}
1043	2.413×10^{-4}	2.423×10^{-4}
1162	2.286×10^{-4}	1.992×10^{-4}
1265	1.651×10^{-4}	1.676×10^{-4}
1416	1.524×10^{-4}	1.295×10^{-4}
1548	1.143×10^{-4}	1.030×10^{-4}
1660	1.016×10^{-4}	8.465×10^{-5}
1772	1.016×10^{-4}	6.943×10^{-5}
1870	7.620×10^{-5}	5.831×10^{-5}
2003	7.620×10^{-5}	4.593×10^{-5}
2110	3.810×10^{-5}	3.786×10^{-5}
2228	3.810×10^{-5}	3.056×10^{-5}
2318	3.810×10^{-5}	2.593×10^{-5}
2410	3.810×10^{-5}	2.191×10^{-5}

Table C.27. Tracer concentration for Run-98 ($u_L=0.0025$ m/s, $u_G=0.0462$ m/s, tap water)

t (s)	$c(t)$ (kg/m ³) Experimental	$c(t)$ (kg/m ³) Model
0	0	0
14	2.794×10^{-4}	5.516×10^{-4}
23	5.334×10^{-4}	5.989×10^{-4}
31	5.588×10^{-4}	6.259×10^{-4}
39	6.731×10^{-4}	6.451×10^{-4}
48	7.493×10^{-4}	6.606×10^{-4}
56	7.620×10^{-4}	6.705×10^{-4}
63	7.747×10^{-4}	6.770×10^{-4}
81	7.747×10^{-4}	6.867×10^{-4}
89	7.620×10^{-4}	6.886×10^{-4}
97	7.493×10^{-4}	6.894×10^{-4}
113	7.366×10^{-4}	6.882×10^{-4}
122	7.239×10^{-4}	6.863×10^{-4}
146	6.858×10^{-4}	6.777×10^{-4}
153	6.731×10^{-4}	6.745×10^{-4}
162	6.985×10^{-4}	6.699×10^{-4}
175	6.731×10^{-4}	6.627×10^{-4}
183	6.985×10^{-4}	6.579×10^{-4}
191	6.858×10^{-4}	6.529×10^{-4}
198	5.969×10^{-4}	6.483×10^{-4}
234	6.096×10^{-4}	6.232×10^{-4}
289	4.572×10^{-4}	5.814×10^{-4}
311	4.699×10^{-4}	5.642×10^{-4}
328	4.318×10^{-4}	5.509×10^{-4}
381	3.810×10^{-4}	5.097×10^{-4}
413	4.318×10^{-4}	4.854×10^{-4}
456	3.683×10^{-4}	4.536×10^{-4}
494	3.302×10^{-4}	4.267×10^{-4}
598	3.429×10^{-4}	3.587×10^{-4}
647	2.921×10^{-4}	3.298×10^{-4}
701	2.540×10^{-4}	3.003×10^{-4}
764	2.413×10^{-4}	2.687×10^{-4}
847	2.413×10^{-4}	2.317×10^{-4}
942	1.905×10^{-4}	1.950×10^{-4}
1226	1.270×10^{-4}	1.153×10^{-4}
1469	1.270×10^{-4}	7.285×10^{-5}
1618	1.397×10^{-4}	5.482×10^{-5}
1747	1.016×10^{-4}	4.280×10^{-5}
1819	7.620×10^{-5}	3.726×10^{-5}

Table C.27. Tracer concentration for Run-98 ($u_L=0.0025$ m/s, $u_G=0.0462$ m/s, tap water).

Cont...

t (s)	$c(t)$ (kg/m ³) Experimental	$c(t)$ (kg/m ³) Model
1951	5.080×10^{-5}	2.887×10^{-5}
2028	5.080×10^{-5}	2.487×10^{-5}
2076	7.620×10^{-5}	2.266×10^{-5}
2114	5.080×10^{-5}	2.105×10^{-5}
2152	1.270×10^{-5}	1.955×10^{-5}
2182	3.810×10^{-5}	1.844×10^{-5}
2223	2.540×10^{-5}	1.702×10^{-5}
2270	2.540×10^{-5}	1.553×10^{-5}
2304	2.540×10^{-5}	1.454×10^{-5}
2349	2.540×10^{-5}	1.331×10^{-5}
2397	2.540×10^{-5}	1.212×10^{-5}
2437	2.540×10^{-5}	1.121×10^{-5}
2475	2.540×10^{-5}	1.041×10^{-5}
2521	1.270×10^{-5}	9.510×10^{-6}

Table C.28. Tracer concentration for Run-99 ($u_L=0.0017$ m/s, $u_G=0.0010$ m/s, tap water)

t (s)	$c(t)$ (kg/m ³) Experimental	$c(t)$ (kg/m ³) Model
0	0	0
16	2.540×10^{-5}	2.774×10^{-4}
25	5.080×10^{-5}	3.291×10^{-4}
32	1.524×10^{-4}	3.610×10^{-4}
41	2.667×10^{-4}	3.954×10^{-4}
49	3.810×10^{-4}	4.215×10^{-4}
56	4.572×10^{-4}	4.417×10^{-4}
63	4.699×10^{-4}	4.599×10^{-4}
72	4.953×10^{-4}	4.809×10^{-4}
80	5.588×10^{-4}	4.978×10^{-4}
88	6.350×10^{-4}	5.131×10^{-4}
95	6.096×10^{-4}	5.255×10^{-4}
102	6.604×10^{-4}	5.370×10^{-4}
110	6.477×10^{-4}	5.491×10^{-4}
117	6.604×10^{-4}	5.590×10^{-4}
124	6.477×10^{-4}	5.682×10^{-4}
132	6.223×10^{-4}	5.780×10^{-4}
139	6.223×10^{-4}	5.860×10^{-4}
147	6.604×10^{-4}	5.946×10^{-4}
162	6.604×10^{-4}	6.090×10^{-4}
169	6.604×10^{-4}	6.151×10^{-4}
177	6.731×10^{-4}	6.217×10^{-4}
185	6.477×10^{-4}	6.277×10^{-4}
203	6.731×10^{-4}	6.399×10^{-4}
210	6.731×10^{-4}	6.442×10^{-4}
218	6.731×10^{-4}	6.487×10^{-4}
226	6.731×10^{-4}	6.529×10^{-4}
235	6.731×10^{-4}	6.572×10^{-4}
243	6.731×10^{-4}	6.608×10^{-4}
259	6.604×10^{-4}	6.671×10^{-4}
267	6.604×10^{-4}	6.699×10^{-4}
275	6.477×10^{-4}	6.724×10^{-4}
282	6.604×10^{-4}	6.745×10^{-4}
344	6.604×10^{-4}	6.863×10^{-4}
358	6.604×10^{-4}	6.876×10^{-4}
373	6.350×10^{-4}	6.885×10^{-4}
395	6.477×10^{-4}	6.891×10^{-4}
485	6.096×10^{-4}	6.833×10^{-4}
519	6.223×10^{-4}	6.784×10^{-4}

Table C.28. Tracer concentration for Run-99 ($u_L=0.0017$ m/s, $u_G=0.0010$ m/s, tap water).

Cont....

t (s)	$c(t)$ (kg/m ³) Experimental	$c(t)$ (kg/m ³) Model
583	5.969×10^{-4}	6.664×10^{-4}
689	5.461×10^{-4}	6.402×10^{-4}
765	5.334×10^{-4}	6.183×10^{-4}
878	5.080×10^{-4}	5.828×10^{-4}
1018	4.445×10^{-4}	5.368×10^{-4}
1109	4.318×10^{-4}	5.067×10^{-4}
1312	3.810×10^{-4}	4.413×10^{-4}
1410	3.810×10^{-4}	4.114×10^{-4}
1611	3.175×10^{-4}	3.540×10^{-4}
1774	3.048×10^{-4}	3.120×10^{-4}
2048	2.667×10^{-4}	2.504×10^{-4}
2494	2.032×10^{-4}	1.725×10^{-4}
2920	1.524×10^{-4}	1.193×10^{-4}
3328	1.143×10^{-4}	8.314×10^{-5}
3793	1.016×10^{-4}	5.469×10^{-5}
4139	7.620×10^{-5}	3.988×10^{-5}
4718	5.080×10^{-5}	2.337×10^{-5}
5154	3.810×10^{-5}	1.556×10^{-5}

Table C.29. Tracer concentration for Run-100 ($u_L=0.0017$ m/s, $u_G=0.0034$ m/s, tap water)

t (s)	$c(t)$ (kg/m ³) Experimental	$c(t)$ (kg/m ³) Model
0	0	0
12	3.429×10^{-4}	4.284×10^{-4}
20	3.048×10^{-4}	4.819×10^{-4}
27	4.953×10^{-4}	5.152×10^{-4}
34	5.334×10^{-4}	5.414×10^{-4}
43	6.223×10^{-4}	5.684×10^{-4}
50	6.604×10^{-4}	5.857×10^{-4}
58	6.858×10^{-4}	6.026×10^{-4}
66	6.985×10^{-4}	6.170×10^{-4}
90	7.112×10^{-4}	6.499×10^{-4}
130	6.985×10^{-4}	6.829×10^{-4}
153	6.858×10^{-4}	6.943×10^{-4}
169	6.985×10^{-4}	6.999×10^{-4}
177	6.604×10^{-4}	7.022×10^{-4}
220	6.731×10^{-4}	7.089×10^{-4}
523	5.969×10^{-4}	6.429×10^{-4}
622	5.461×10^{-4}	6.061×10^{-4}
736	5.207×10^{-4}	5.620×10^{-4}
870	4.572×10^{-4}	5.104×10^{-4}
1015	3.937×10^{-4}	4.568×10^{-4}
1388	3.175×10^{-4}	3.364×10^{-4}
1762	2.667×10^{-4}	2.430×10^{-4}
2346	1.524×10^{-4}	1.432×10^{-4}
2768	1.397×10^{-4}	9.668×10^{-5}
3087	8.890×10^{-5}	7.157×10^{-5}
3386	8.890×10^{-5}	5.386×10^{-5}
3783	5.080×10^{-5}	3.682×10^{-5}
4108	3.810×10^{-5}	2.691×10^{-5}
4803	2.540×10^{-5}	1.370×10^{-5}
4908	2.540×10^{-5}	1.237×10^{-5}
5010	1.270×10^{-5}	1.119×10^{-5}

Table C.30. Tracer concentration for Run-101 ($u_L=0.0017$ m/s, $u_G=0.0112$ m/s, tap water)

t (s)	$c(t)$ (kg/m ³) Experimental	$c(t)$ (kg/m ³) Model
0	0	0
13	1.397×10^{-4}	3.894×10^{-4}
21	3.683×10^{-4}	4.289×10^{-4}
30	4.064×10^{-4}	4.596×10^{-4}
39	5.461×10^{-4}	4.825×10^{-4}
45	5.715×10^{-4}	4.949×10^{-4}
53	5.715×10^{-4}	5.091×10^{-4}
60	5.842×10^{-4}	5.196×10^{-4}
82	6.096×10^{-4}	5.450×10^{-4}
97	6.096×10^{-4}	5.575×10^{-4}
107	5.969×10^{-4}	5.643×10^{-4}
113	6.223×10^{-4}	5.679×10^{-4}
135	6.096×10^{-4}	5.786×10^{-4}
143	5.969×10^{-4}	5.816×10^{-4}
156	5.969×10^{-4}	5.857×10^{-4}
162	6.096×10^{-4}	5.873×10^{-4}
169	5.969×10^{-4}	5.889×10^{-4}
176	5.969×10^{-4}	5.904×10^{-4}
199	6.096×10^{-4}	5.937×10^{-4}
207	5.842×10^{-4}	5.945×10^{-4}
214	5.969×10^{-4}	5.950×10^{-4}
222	6.096×10^{-4}	5.954×10^{-4}
243	5.969×10^{-4}	5.957×10^{-4}
252	5.842×10^{-4}	5.955×10^{-4}
273	5.715×10^{-4}	5.945×10^{-4}
288	5.842×10^{-4}	5.933×10^{-4}
302	5.842×10^{-4}	5.918×10^{-4}
310	5.842×10^{-4}	5.909×10^{-4}
317	5.715×10^{-4}	5.900×10^{-4}
339	5.588×10^{-4}	5.868×10^{-4}
380	5.334×10^{-4}	5.795×10^{-4}
424	5.207×10^{-4}	5.701×10^{-4}
462	5.334×10^{-4}	5.611×10^{-4}
496	5.207×10^{-4}	5.525×10^{-4}
577	4.826×10^{-4}	5.304×10^{-4}
731	4.572×10^{-4}	4.854×10^{-4}
1176	3.810×10^{-4}	3.591×10^{-4}
1398	2.921×10^{-4}	3.047×10^{-4}

Table C.30. Tracer concentration for Run-101 ($u_L=0.0017$ m/s, $u_G=0.0112$ m/s, tap water). Cont...

t (s)	$c(t)$ (kg/m ³) Experimental	$c(t)$ (kg/m ³) Model
2161	1.778×10^{-4}	1.674×10^{-4}
2718	1.524×10^{-4}	1.061×10^{-4}
3106	1.016×10^{-4}	7.676×10^{-5}
3159	8.890×10^{-5}	7.342×10^{-5}
3217	8.890×10^{-5}	6.993×10^{-5}
3304	7.620×10^{-5}	6.499×10^{-5}
3404	7.620×10^{-5}	5.973×10^{-5}
3603	7.620×10^{-5}	5.047×10^{-5}
3729	5.080×10^{-5}	4.535×10^{-5}
3875	6.350×10^{-5}	4.005×10^{-5}
3984	5.080×10^{-5}	3.649×10^{-5}
4043	5.080×10^{-5}	3.469×10^{-5}
4106	3.810×10^{-5}	3.287×10^{-5}

Table C.31. Tracer concentration for Run-102 ($u_L=0.0017$ m/s, $u_G=0.0462$ m/s, tap water)

t (s)	$c(t)$ (kg/m ³) Experimental	$c(t)$ (kg/m ³) Model
0	0	0
11	8.890×10^{-5}	2.519×10^{-4}
18	1.905×10^{-4}	2.928×10^{-4}
24	2.921×10^{-4}	3.188×10^{-4}
33	4.064×10^{-4}	3.490×10^{-4}
43	4.826×10^{-4}	3.748×10^{-4}
51	5.080×10^{-4}	3.916×10^{-4}
91	5.207×10^{-4}	4.454×10^{-4}
119	5.207×10^{-4}	4.660×10^{-4}
170	5.080×10^{-4}	4.846×10^{-4}
197	4.699×10^{-4}	4.881×10^{-4}
211	4.826×10^{-4}	4.887×10^{-4}
219	4.699×10^{-4}	4.887×10^{-4}
262	4.572×10^{-4}	4.854×10^{-4}
269	4.572×10^{-4}	4.844×10^{-4}
276	4.699×10^{-4}	4.834×10^{-4}
283	4.572×10^{-4}	4.822×10^{-4}
290	4.572×10^{-4}	4.809×10^{-4}
298	4.572×10^{-4}	4.793×10^{-4}
340	4.445×10^{-4}	4.695×10^{-4}
348	4.572×10^{-4}	4.674×10^{-4}
357	4.445×10^{-4}	4.649×10^{-4}
511	4.064×10^{-4}	4.136×10^{-4}
712	3.429×10^{-4}	3.396×10^{-4}
892	2.794×10^{-4}	2.781×10^{-4}
1019	2.159×10^{-4}	2.394×10^{-4}
1156	2.032×10^{-4}	2.026×10^{-4}
1460	1.651×10^{-4}	1.377×10^{-4}
1735	7.620×10^{-5}	9.590×10^{-5}
2059	7.620×10^{-5}	6.196×10^{-5}
2384	3.810×10^{-5}	3.965×10^{-5}
2715	2.540×10^{-5}	2.501×10^{-5}
3041	1.270×10^{-5}	1.581×10^{-5}
3290	1.270×10^{-5}	1.111×10^{-5}
3645	0	6.693×10^{-6}

Table C.32. Tracer concentration for Run 103 ($u_L=0.0017$ m/s, $u_G=0.0027$ m/s, tap water)

t (s)	$c(t)$ (kg/m ³) Experimental	$c(t)$ (kg/m ³) Model
0	0	0
12	2.286×10^{-4}	3.939×10^{-4}
19	2.667×10^{-4}	4.428×10^{-4}
27	3.683×10^{-4}	4.832×10^{-4}
35	4.826×10^{-4}	5.143×10^{-4}
41	5.842×10^{-4}	5.338×10^{-4}
49	5.842×10^{-4}	5.560×10^{-4}
55	6.731×10^{-4}	5.704×10^{-4}
64	6.858×10^{-4}	5.894×10^{-4}
70	7.112×10^{-4}	6.005×10^{-4}
80	6.985×10^{-4}	6.169×10^{-4}
139	7.366×10^{-4}	6.789×10^{-4}
146	7.239×10^{-4}	6.836×10^{-4}
154	7.366×10^{-4}	6.885×10^{-4}
175	7.366×10^{-4}	6.994×10^{-4}
191	7.366×10^{-4}	7.058×10^{-4}
199	7.366×10^{-4}	7.086×10^{-4}
214	7.239×10^{-4}	7.129×10^{-4}
248	7.112×10^{-4}	7.196×10^{-4}
277	7.112×10^{-4}	7.223×10^{-4}
293	6.985×10^{-4}	7.229×10^{-4}
338	6.858×10^{-4}	7.217×10^{-4}
354	6.858×10^{-4}	7.203×10^{-4}
362	6.858×10^{-4}	7.195×10^{-4}
394	6.731×10^{-4}	7.154×10^{-4}
434	6.604×10^{-4}	7.084×10^{-4}
627	5.969×10^{-4}	6.584×10^{-4}
782	5.715×10^{-4}	6.084×10^{-4}
891	5.461×10^{-4}	5.717×10^{-4}
1076	4.572×10^{-4}	5.100×10^{-4}
1658	3.302×10^{-4}	3.409×10^{-4}
1926	2.794×10^{-4}	2.794×10^{-4}
2068	2.794×10^{-4}	2.509×10^{-4}
2695	1.778×10^{-4}	1.540×10^{-4}
3167	1.524×10^{-4}	1.056×10^{-4}
3388	1.397×10^{-4}	8.830×10^{-5}
3866	1.143×10^{-4}	5.974×10^{-5}
4196	1.143×10^{-4}	4.550×10^{-5}

Table C.33. Tracer concentration for Run 104 ($u_L=0.0025$ m/s, $u_G=0.0027$ m/s, tap water)

t (s)	$c(t)$ (kg/m ³) Experimental	$c(t)$ (kg/m ³) Model
0	0	0
15	1.778×10^{-4}	4.536×10^{-4}
23	2.286×10^{-4}	5.207×10^{-4}
30	3.683×10^{-4}	5.655×10^{-4}
38	5.842×10^{-4}	6.068×10^{-4}
44	6.604×10^{-4}	6.329×10^{-4}
51	7.874×10^{-4}	6.593×10^{-4}
58	6.985×10^{-4}	6.821×10^{-4}
67	8.509×10^{-4}	7.073×10^{-4}
74	8.382×10^{-4}	7.243×10^{-4}
80	8.382×10^{-4}	7.373×10^{-4}
88	8.763×10^{-4}	7.528×10^{-4}
96	8.636×10^{-4}	7.662×10^{-4}
104	8.636×10^{-4}	7.780×10^{-4}
110	8.890×10^{-4}	7.859×10^{-4}
131	8.890×10^{-4}	8.079×10^{-4}
145	8.763×10^{-4}	8.186×10^{-4}
159	8.763×10^{-4}	8.267×10^{-4}
166	8.636×10^{-4}	8.299×10^{-4}
173	8.763×10^{-4}	8.325×10^{-4}
182	8.636×10^{-4}	8.353×10^{-4}
201	8.255×10^{-4}	8.388×10^{-4}
209	8.255×10^{-4}	8.395×10^{-4}
216	8.382×10^{-4}	8.397×10^{-4}
225	7.874×10^{-4}	8.395×10^{-4}
234	7.874×10^{-4}	8.389×10^{-4}
241	7.874×10^{-4}	8.381×10^{-4}
266	8.128×10^{-4}	8.333×10^{-4}
306	7.747×10^{-4}	8.205×10^{-4}
314	7.747×10^{-4}	8.173×10^{-4}
322	7.620×10^{-4}	8.140×10^{-4}
331	7.366×10^{-4}	8.100×10^{-4}
339	7.493×10^{-4}	8.063×10^{-4}
348	7.239×10^{-4}	8.020×10^{-4}
356	7.239×10^{-4}	7.980×10^{-4}
389	7.239×10^{-4}	7.804×10^{-4}
414	6.731×10^{-4}	7.660×10^{-4}
500	6.477×10^{-4}	7.121×10^{-4}

Table C.33. Tracer concentration for Run 104 ($u_L=0.0025$ m/s, $u_G=0.0027$ m/s, tap water). Cont...

t (s)	$c(t)$ (kg/m ³) Experimental	$c(t)$ (kg/m ³) Model
577	5.969×10^{-4}	6.609×10^{-4}
784	4.953×10^{-4}	5.262×10^{-4}
952	4.191×10^{-4}	4.289×10^{-4}
1079	3.302×10^{-4}	3.647×10^{-4}
1238	2.921×10^{-4}	2.957×10^{-4}
1575	2.032×10^{-4}	1.862×10^{-4}
1787	1.651×10^{-4}	1.380×10^{-4}
2070	1.016×10^{-4}	9.176×10^{-5}
2860	5.080×10^{-5}	2.850×10^{-5}
3339	2.540×10^{-5}	1.382×10^{-5}
3404	1.270×10^{-5}	1.252×10^{-5}
3452	1.270×10^{-5}	1.164×10^{-5}
3493	1.270×10^{-5}	1.094×10^{-5}
3545	2.540×10^{-5}	1.010×10^{-5}
3863	0	6.211×10^{-6}

Table C.34. Tracer concentration for Run 105 ($u_L=0.0025$ m/s, $u_G=0.0308$ m/s, tap water)

t (s)	$c(t)$ (kg/m ³) Experimental	$c(t)$ (kg/m ³) Model
0	0	0
14	3.556×10^{-4}	5.898×10^{-4}
20	5.207×10^{-4}	6.417×10^{-4}
28	6.858×10^{-4}	6.921×10^{-4}
35	8.128×10^{-4}	7.255×10^{-4}
44	9.017×10^{-4}	7.591×10^{-4}
94	9.525×10^{-4}	8.521×10^{-4}
129	9.144×10^{-4}	8.727×10^{-4}
136	9.398×10^{-4}	8.744×10^{-4}
143	9.271×10^{-4}	8.756×10^{-4}
149	9.398×10^{-4}	8.761×10^{-4}
162	9.017×10^{-4}	8.760×10^{-4}
169	9.017×10^{-4}	8.753×10^{-4}
175	8.382×10^{-4}	8.744×10^{-4}
193	9.017×10^{-4}	8.701×10^{-4}
208	8.382×10^{-4}	8.649×10^{-4}
244	7.747×10^{-4}	8.483×10^{-4}
287	7.493×10^{-4}	8.226×10^{-4}
335	7.366×10^{-4}	7.892×10^{-4}
343	7.239×10^{-4}	7.834×10^{-4}
366	7.112×10^{-4}	7.661×10^{-4}
386	7.366×10^{-4}	7.508×10^{-4}
409	6.604×10^{-4}	7.329×10^{-4}
454	6.477×10^{-4}	6.974×10^{-4}
516	6.096×10^{-4}	6.487×10^{-4}
590	5.588×10^{-4}	5.919×10^{-4}
644	5.080×10^{-4}	5.522×10^{-4}
710	4.445×10^{-4}	5.060×10^{-4}
795	4.191×10^{-4}	4.506×10^{-4}
865	3.937×10^{-4}	4.086×10^{-4}
1066	2.921×10^{-4}	3.058×10^{-4}
1247	2.540×10^{-4}	2.337×10^{-4}
1350	2.032×10^{-4}	2.000×10^{-4}
1703	1.397×10^{-4}	1.160×10^{-4}
1999	8.890×10^{-5}	7.282×10^{-5}
2470	5.080×10^{-5}	3.431×10^{-5}
2797	2.540×10^{-5}	2.023×10^{-5}
3317	1.270×10^{-5}	8.667×10^{-6}

Table C.35. Tracer concentration for Run 106 ($u_L=0.0007$ m/s, $u_G=0.0034$ m/s, tap water)

t (s)	$c(t)$ (kg/m ³) Experimental	$c(t)$ (kg/m ³) Model
0	0	0
14	1.905×10^{-4}	4.891×10^{-4}
22	3.175×10^{-4}	5.301×10^{-4}
28	4.953×10^{-4}	5.529×10^{-4}
36	5.969×10^{-4}	5.772×10^{-4}
45	6.350×10^{-4}	5.990×10^{-4}
55	7.366×10^{-4}	6.187×10^{-4}
63	6.858×10^{-4}	6.321×10^{-4}
71	7.366×10^{-4}	6.437×10^{-4}
78	7.112×10^{-4}	6.527×10^{-4}
85	7.366×10^{-4}	6.609×10^{-4}
93	7.493×10^{-4}	6.693×10^{-4}
100	7.366×10^{-4}	6.760×10^{-4}
133	7.493×10^{-4}	7.010×10^{-4}
139	7.493×10^{-4}	7.046×10^{-4}
147	7.366×10^{-4}	7.090×10^{-4}
167	7.620×10^{-4}	7.186×10^{-4}
174	7.620×10^{-4}	7.215×10^{-4}
219	7.493×10^{-4}	7.358×10^{-4}
226	7.366×10^{-4}	7.374×10^{-4}
240	7.493×10^{-4}	7.403×10^{-4}
248	7.620×10^{-4}	7.418×10^{-4}
291	7.493×10^{-4}	7.474×10^{-4}
326	7.493×10^{-4}	7.496×10^{-4}
340	7.493×10^{-4}	7.500×10^{-4}
348	7.239×10^{-4}	7.501×10^{-4}
355	7.366×10^{-4}	7.502×10^{-4}
405	7.112×10^{-4}	7.491×10^{-4}
470	7.112×10^{-4}	7.445×10^{-4}
524	7.112×10^{-4}	7.387×10^{-4}
573	6.858×10^{-4}	7.321×10^{-4}
676	6.350×10^{-4}	7.156×10^{-4}
834	6.096×10^{-4}	6.852×10^{-4}
1280	4.953×10^{-4}	5.879×10^{-4}
1869	4.445×10^{-4}	4.637×10^{-4}
2062	3.810×10^{-4}	4.269×10^{-4}
2508	3.302×10^{-4}	3.507×10^{-4}
2673	3.175×10^{-4}	3.255×10^{-4}

Table C.35. Tracer concentration for Run 106 ($u_L=0.0007$ m/s, $u_G=0.0034$ m/s, tap water). Cont...

t (s)	$c(t)$ (kg/m ³) Experimental	$c(t)$ (kg/m ³) Model
2951	3.048×10^{-4}	2.867×10^{-4}
3514	2.540×10^{-4}	2.206×10^{-4}
4099	1.778×10^{-4}	1.672×10^{-4}
4530	1.778×10^{-4}	1.359×10^{-4}
5069	1.651×10^{-4}	1.047×10^{-4}
5703	1.143×10^{-4}	7.680×10^{-5}
5891	1.143×10^{-4}	7.003×10^{-5}
6472	7.620×10^{-5}	5.258×10^{-5}
6783	7.620×10^{-5}	4.508×10^{-5}
7778	6.350×10^{-5}	2.747×10^{-5}

Table C.36. Tracer concentration for Run 109 ($u_L=0.0017$ m/s, $u_G=0.0112$ m/s, tap water)

t (s)	$c(t)$ (kg/m ³) Experimental	$c(t)$ (kg/m ³) Model
0	0	0
13	1.524×10^{-4}	3.462×10^{-4}
22	2.413×10^{-4}	3.936×10^{-4}
27	3.302×10^{-4}	4.133×10^{-4}
36	4.572×10^{-4}	4.417×10^{-4}
42	4.699×10^{-4}	4.573×10^{-4}
49	4.826×10^{-4}	4.730×10^{-4}
55	4.953×10^{-4}	4.847×10^{-4}
62	5.588×10^{-4}	4.969×10^{-4}
68	5.842×10^{-4}	5.062×10^{-4}
74	5.842×10^{-4}	5.147×10^{-4}
81	6.096×10^{-4}	5.236×10^{-4}
87	6.223×10^{-4}	5.305×10^{-4}
94	5.969×10^{-4}	5.379×10^{-4}
141	6.096×10^{-4}	5.729×10^{-4}
148	6.223×10^{-4}	5.765×10^{-4}
190	6.096×10^{-4}	5.923×10^{-4}
255	5.969×10^{-4}	6.031×10^{-4}
302	5.842×10^{-4}	6.041×10^{-4}
364	5.715×10^{-4}	5.997×10^{-4}
385	5.461×10^{-4}	5.971×10^{-4}
475	5.334×10^{-4}	5.816×10^{-4}
537	5.080×10^{-4}	5.678×10^{-4}
911	3.937×10^{-4}	4.654×10^{-4}
1127	3.556×10^{-4}	4.050×10^{-4}
1334	3.048×10^{-4}	3.513×10^{-4}
1543	2.794×10^{-4}	3.023×10^{-4}
1857	2.286×10^{-4}	2.392×10^{-4}
2105	2.032×10^{-4}	1.977×10^{-4}
2439	1.651×10^{-4}	1.522×10^{-4}
2593	1.524×10^{-4}	1.346×10^{-4}
2720	1.397×10^{-4}	1.216×10^{-4}
2796	1.397×10^{-4}	1.144×10^{-4}
2995	1.270×10^{-4}	9.736×10^{-5}
3201	1.143×10^{-4}	8.231×10^{-5}
3328	1.143×10^{-4}	7.418×10^{-5}
3786	1.016×10^{-4}	5.082×10^{-5}
4184	1.016×10^{-4}	3.647×10^{-5}

Table C.37. Tracer concentration for Run 110 ($u_L=0.0017$ m/s, $u_G=0.0112$ m/s, tap water)

t (s)	$c(t)$ (kg/m ³) Experimental	$c(t)$ (kg/m ³) Model
0	0	0
13	1.905×10^{-4}	3.584×10^{-4}
19	2.286×10^{-4}	3.860×10^{-4}
25	3.810×10^{-4}	4.067×10^{-4}
34	4.572×10^{-4}	4.303×10^{-4}
41	5.461×10^{-4}	4.448×10^{-4}
48	5.461×10^{-4}	4.569×10^{-4}
55	5.588×10^{-4}	4.672×10^{-4}
75	5.715×10^{-4}	4.898×10^{-4}
144	5.715×10^{-4}	5.281×10^{-4}
156	5.588×10^{-4}	5.313×10^{-4}
237	5.334×10^{-4}	5.395×10^{-4}
242	5.461×10^{-4}	5.395×10^{-4}
255	5.207×10^{-4}	5.392×10^{-4}
299	5.207×10^{-4}	5.360×10^{-4}
325	5.334×10^{-4}	5.329×10^{-4}
373	5.080×10^{-4}	5.255×10^{-4}
435	4.953×10^{-4}	5.135×10^{-4}
590	4.318×10^{-4}	4.767×10^{-4}
728	3.937×10^{-4}	4.404×10^{-4}
790	3.683×10^{-4}	4.239×10^{-4}
923	3.556×10^{-4}	3.890×10^{-4}
1027	3.175×10^{-4}	3.625×10^{-4}
1684	2.159×10^{-4}	2.237×10^{-4}
2144	1.651×10^{-4}	1.560×10^{-4}
2509	1.270×10^{-4}	1.164×10^{-4}
2940	1.143×10^{-4}	8.190×10^{-5}
3233	7.620×10^{-5}	6.432×10^{-5}
3594	6.350×10^{-5}	4.764×10^{-5}
3929	5.080×10^{-5}	3.599×10^{-5}
4279	3.810×10^{-5}	2.681×10^{-5}
4529	3.810×10^{-5}	2.170×10^{-5}
5120	3.810×10^{-5}	1.314×10^{-5}

Table C.38. Tracer concentration for Run 113 ($u_L=0.0017$ m/s, $u_G=0.0112$ m/s, tap water)

t (s)	$c(t)$ (kg/m ³) Experimental	$c(t)$ (kg/m ³) Model
0	0	0
13	1.524×10^{-4}	3.947×10^{-4}
19	2.413×10^{-4}	4.346×10^{-4}
26	4.191×10^{-4}	4.697×10^{-4}
32	5.334×10^{-4}	4.938×10^{-4}
38	5.842×10^{-4}	5.141×10^{-4}
45	6.604×10^{-4}	5.344×10^{-4}
51	6.985×10^{-4}	5.495×10^{-4}
128	7.239×10^{-4}	6.526×10^{-4}
147	7.366×10^{-4}	6.648×10^{-4}
170	7.366×10^{-4}	6.758×10^{-4}
199	7.239×10^{-4}	6.852×10^{-4}
207	7.239×10^{-4}	6.871×10^{-4}
221	7.239×10^{-4}	6.897×10^{-4}
238	7.239×10^{-4}	6.920×10^{-4}
253	6.985×10^{-4}	6.931×10^{-4}
268	6.858×10^{-4}	6.936×10^{-4}
275	6.985×10^{-4}	6.936×10^{-4}
282	6.985×10^{-4}	6.935×10^{-4}
305	6.604×10^{-4}	6.925×10^{-4}
313	6.731×10^{-4}	6.918×10^{-4}
321	6.604×10^{-4}	6.911×10^{-4}
330	6.604×10^{-4}	6.901×10^{-4}
361	6.350×10^{-4}	6.857×10^{-4}
395	6.223×10^{-4}	6.793×10^{-4}
534	5.588×10^{-4}	6.424×10^{-4}
650	5.080×10^{-4}	6.041×10^{-4}
766	4.953×10^{-4}	5.632×10^{-4}
974	4.445×10^{-4}	4.894×10^{-4}
1232	3.810×10^{-4}	4.042×10^{-4}
1528	3.175×10^{-4}	3.199×10^{-4}
1828	2.540×10^{-4}	2.497×10^{-4}
2634	1.397×10^{-4}	1.244×10^{-4}
2937	1.143×10^{-4}	9.501×10^{-5}
3278	7.620×10^{-5}	6.991×10^{-5}
3680	6.350×10^{-5}	4.851×10^{-5}
3898	6.350×10^{-5}	3.973×10^{-5}
4233	3.810×10^{-5}	2.919×10^{-5}

Table C.39. Tracer concentration for Run 126 ($u_L=0.0045$ m/s, $u_G=0.0308$ m/s, tap water)

t (s)	$c(t)$ (kg/m ³) Experimental	$c(t)$ (kg/m ³) Model
0	0	0
11	4.191×10^{-4}	5.409×10^{-4}
18	5.461×10^{-4}	5.934×10^{-4}
25	6.096×10^{-4}	6.266×10^{-4}
33	7.112×10^{-4}	6.518×10^{-4}
55	7.493×10^{-4}	6.849×10^{-4}
76	7.493×10^{-4}	6.911×10^{-4}
83	7.493×10^{-4}	6.900×10^{-4}
90	7.366×10^{-4}	6.878×10^{-4}
102	7.239×10^{-4}	6.818×10^{-4}
108	7.239×10^{-4}	6.779×10^{-4}
115	6.858×10^{-4}	6.729×10^{-4}
123	6.858×10^{-4}	6.664×10^{-4}
130	6.477×10^{-4}	6.603×10^{-4}
137	6.477×10^{-4}	6.538×10^{-4}
144	6.477×10^{-4}	6.469×10^{-4}
150	6.096×10^{-4}	6.409×10^{-4}
157	6.223×10^{-4}	6.335×10^{-4}
163	5.969×10^{-4}	6.271×10^{-4}
185	5.842×10^{-4}	6.025×10^{-4}
193	5.842×10^{-4}	5.932×10^{-4}
209	5.334×10^{-4}	5.745×10^{-4}
216	5.334×10^{-4}	5.663×10^{-4}
223	5.080×10^{-4}	5.580×10^{-4}
234	5.080×10^{-4}	5.450×10^{-4}
242	5.080×10^{-4}	5.356×10^{-4}
251	4.953×10^{-4}	5.250×10^{-4}
260	4.953×10^{-4}	5.145×10^{-4}
270	4.953×10^{-4}	5.029×10^{-4}
288	4.572×10^{-4}	4.822×10^{-4}
296	4.445×10^{-4}	4.732×10^{-4}
304	4.445×10^{-4}	4.643×10^{-4}
312	4.318×10^{-4}	4.554×10^{-4}
327	4.064×10^{-4}	4.391×10^{-4}
351	4.064×10^{-4}	4.138×10^{-4}
359	3.937×10^{-4}	4.056×10^{-4}
395	3.556×10^{-4}	3.701×10^{-4}
429	3.175×10^{-4}	3.388×10^{-4}

Table C.39. Tracer concentration for Run 126 ($u_L=0.0045$ m/s, $u_G=0.0308$ m/s, tap water). Cont...

t (s)	$c(t)$ (kg/m ³) Experimental	$c(t)$ (kg/m ³) Model
520	2.794×10^{-4}	2.657×10^{-4}
588	2.286×10^{-4}	2.205×10^{-4}
679	1.778×10^{-4}	1.710×10^{-4}
732	1.651×10^{-4}	1.472×10^{-4}
784	1.397×10^{-4}	1.269×10^{-4}
859	1.270×10^{-4}	1.022×10^{-4}
955	8.890×10^{-5}	7.736×10^{-5}
1053	7.620×10^{-5}	5.805×10^{-5}
1172	5.080×10^{-5}	4.085×10^{-5}
1303	2.540×10^{-5}	2.767×10^{-5}
1351	2.540×10^{-5}	2.397×10^{-5}
1398	2.540×10^{-5}	2.083×10^{-5}
1467	1.270×10^{-5}	1.693×10^{-5}
1500	1.270×10^{-5}	1.534×10^{-5}
1548	0	1.327×10^{-5}

Table C.40. Tracer concentration for Run 128 ($u_L=0.0045$ m/s, $u_G=0.0112$ m/s, tap water)

t (s)	$c(t)$ (kg/m ³) Experimental	$c(t)$ (kg/m ³) Model
0	0	0
13	2.286×10^{-4}	4.016×10^{-4}
20	3.937×10^{-4}	4.458×10^{-4}
27	4.318×10^{-4}	4.767×10^{-4}
34	5.461×10^{-4}	4.997×10^{-4}
49	6.223×10^{-4}	5.330×10^{-4}
55	6.350×10^{-4}	5.422×10^{-4}
82	6.350×10^{-4}	5.657×10^{-4}
96	6.350×10^{-4}	5.701×10^{-4}
122	6.096×10^{-4}	5.698×10^{-4}
141	5.842×10^{-4}	5.647×10^{-4}
148	5.715×10^{-4}	5.620×10^{-4}
154	5.842×10^{-4}	5.595×10^{-4}
189	5.461×10^{-4}	5.406×10^{-4}
205	5.334×10^{-4}	5.303×10^{-4}
213	5.080×10^{-4}	5.248×10^{-4}
220	4.826×10^{-4}	5.200×10^{-4}
227	5.080×10^{-4}	5.150×10^{-4}
235	4.826×10^{-4}	5.092×10^{-4}
243	4.826×10^{-4}	5.033×10^{-4}
252	4.699×10^{-4}	4.966×10^{-4}
259	4.572×10^{-4}	4.913×10^{-4}
267	4.445×10^{-4}	4.851×10^{-4}
274	4.191×10^{-4}	4.797×10^{-4}
282	4.572×10^{-4}	4.736×10^{-4}
299	4.445×10^{-4}	4.603×10^{-4}
307	4.191×10^{-4}	4.541×10^{-4}
324	4.191×10^{-4}	4.408×10^{-4}
336	4.064×10^{-4}	4.314×10^{-4}
352	3.937×10^{-4}	4.190×10^{-4}
368	3.810×10^{-4}	4.068×10^{-4}
391	3.810×10^{-4}	3.894×10^{-4}
463	3.048×10^{-4}	3.376×10^{-4}
607	2.286×10^{-4}	2.490×10^{-4}
681	2.159×10^{-4}	2.115×10^{-4}
813	1.651×10^{-4}	1.568×10^{-4}
936	1.143×10^{-4}	1.178×10^{-4}
1001	1.143×10^{-4}	1.011×10^{-4}

Table C.40. Tracer concentration for Run 128 ($u_L=0.0045$ m/s, $u_G=0.0112$ m/s, tap water). Cont...

t (s)	$c(t)$ (kg/m ³) Experimental	$c(t)$ (kg/m ³) Model
1103	8.890×10^{-5}	7.930×10^{-5}
1207	7.620×10^{-5}	6.176×10^{-5}
1358	6.350×10^{-5}	4.281×10^{-5}
1398	5.080×10^{-5}	3.882×10^{-5}
1445	3.810×10^{-5}	3.460×10^{-5}
1490	3.810×10^{-5}	3.098×10^{-5}
1537	3.810×10^{-5}	2.759×10^{-5}
1598	2.540×10^{-5}	2.374×10^{-5}
1654	2.540×10^{-5}	2.066×10^{-5}
1726	2.540×10^{-5}	1.728×10^{-5}
1786	2.540×10^{-5}	1.489×10^{-5}
1835	2.540×10^{-5}	1.317×10^{-5}
1878	2.540×10^{-5}	1.183×10^{-5}

Table C.41. Tracer concentration for Run 130 ($u_L=0.0045$ m/s, $u_G=0.0206$ m/s, tap water)

t (s)	$c(t)$ (kg/m ³) Experimental	$c(t)$ (kg/m ³) Model
0	0	0
31	4.953×10^{-4}	6.135×10^{-4}
50	6.731×10^{-4}	6.494×10^{-4}
61	6.858×10^{-4}	6.587×10^{-4}
124	6.858×10^{-4}	6.446×10^{-4}
145	6.477×10^{-4}	6.278×10^{-4}
154	6.477×10^{-4}	6.197×10^{-4}
164	6.223×10^{-4}	6.103×10^{-4}
182	6.350×10^{-4}	5.924×10^{-4}
194	5.842×10^{-4}	5.800×10^{-4}
205	5.969×10^{-4}	5.684×10^{-4}
216	5.461×10^{-4}	5.566×10^{-4}
228	5.334×10^{-4}	5.436×10^{-4}
237	5.207×10^{-4}	5.339×10^{-4}
247	5.334×10^{-4}	5.231×10^{-4}
257	4.953×10^{-4}	5.122×10^{-4}
268	5.080×10^{-4}	5.004×10^{-4}
279	4.572×10^{-4}	4.886×10^{-4}
301	4.572×10^{-4}	4.654×10^{-4}
314	4.064×10^{-4}	4.519×10^{-4}
326	4.191×10^{-4}	4.396×10^{-4}
337	3.810×10^{-4}	4.286×10^{-4}
349	3.810×10^{-4}	4.167×10^{-4}
361	3.683×10^{-4}	4.050×10^{-4}
382	3.556×10^{-4}	3.852×10^{-4}
393	3.429×10^{-4}	3.750×10^{-4}
404	3.429×10^{-4}	3.651×10^{-4}
447	3.048×10^{-4}	3.282×10^{-4}
458	3.048×10^{-4}	3.193×10^{-4}
469	3.048×10^{-4}	3.105×10^{-4}
479	2.921×10^{-4}	3.028×10^{-4}
499	2.794×10^{-4}	2.877×10^{-4}
510	2.667×10^{-4}	2.797×10^{-4}
533	2.540×10^{-4}	2.636×10^{-4}
556	2.413×10^{-4}	2.483×10^{-4}
581	2.286×10^{-4}	2.325×10^{-4}
766	1.397×10^{-4}	1.416×10^{-4}
818	1.143×10^{-4}	1.228×10^{-4}

Table C.41. Tracer concentration for Run 130 ($u_L=0.0045$ m/s, $u_G=0.0206$ m/s, tap water). Cont...

t (s)	$c(t)$ (kg/m ³) Experimental	$c(t)$ (kg/m ³) Model
852	1.143×10^{-4}	1.118×10^{-4}
963	1.016×10^{-4}	8.215×10^{-5}
1030	7.620×10^{-5}	6.810×10^{-5}
1143	6.350×10^{-5}	4.952×10^{-5}
1234	3.810×10^{-5}	3.824×10^{-5}
1315	3.810×10^{-5}	3.035×10^{-5}
1362	3.810×10^{-5}	2.653×10^{-5}
1429	2.540×10^{-5}	2.189×10^{-5}
1483	2.540×10^{-5}	1.874×10^{-5}
1713	2.540×10^{-5}	9.641×10^{-6}
1897	2.540×10^{-5}	5.646×10^{-6}
1934	2.540×10^{-5}	5.069×10^{-6}
1968	1.270×10^{-5}	4.590×10^{-6}
2011	1.270×10^{-5}	4.048×10^{-6}

Table C.42. Tracer concentration for Run 131 ($u_L=0.0045$ m/s, $u_G=0.0206$ m/s, tap water)

t (s)	$c(t)$ (kg/m ³) Experimental	$c(t)$ (kg/m ³) Model
0	0	0
13	2.921×10^{-4}	5.052×10^{-4}
20	4.572×10^{-4}	5.508×10^{-4}
27	5.715×10^{-4}	5.813×10^{-4}
35	6.477×10^{-4}	6.055×10^{-4}
42	6.985×10^{-4}	6.204×10^{-4}
49	7.239×10^{-4}	6.313×10^{-4}
93	7.239×10^{-4}	6.486×10^{-4}
101	7.112×10^{-4}	6.463×10^{-4}
108	7.112×10^{-4}	6.434×10^{-4}
128	6.731×10^{-4}	6.319×10^{-4}
135	6.731×10^{-4}	6.270×10^{-4}
143	6.604×10^{-4}	6.209×10^{-4}
150	6.477×10^{-4}	6.151×10^{-4}
157	6.223×10^{-4}	6.092×10^{-4}
173	6.223×10^{-4}	5.946×10^{-4}
180	5.842×10^{-4}	5.880×10^{-4}
196	5.334×10^{-4}	5.722×10^{-4}
204	5.334×10^{-4}	5.642×10^{-4}
227	4.699×10^{-4}	5.405×10^{-4}
234	4.826×10^{-4}	5.332×10^{-4}
242	4.699×10^{-4}	5.248×10^{-4}
261	4.445×10^{-4}	5.049×10^{-4}
268	4.318×10^{-4}	4.976×10^{-4}
282	4.191×10^{-4}	4.831×10^{-4}
290	4.191×10^{-4}	4.749×10^{-4}
298	4.191×10^{-4}	4.667×10^{-4}
305	4.064×10^{-4}	4.595×10^{-4}
312	4.064×10^{-4}	4.525×10^{-4}
327	3.810×10^{-4}	4.375×10^{-4}
335	3.683×10^{-4}	4.296×10^{-4}
344	3.937×10^{-4}	4.209×10^{-4}
355	3.556×10^{-4}	4.103×10^{-4}
381	3.175×10^{-4}	3.860×10^{-4}
402	3.429×10^{-4}	3.671×10^{-4}
504	2.667×10^{-4}	2.853×10^{-4}
855	1.270×10^{-4}	1.126×10^{-4}

Table C.42. Tracer concentration for Run 131 ($u_L=0.0045$ m/s, $u_G=0.0206$ m/s, tap water). Cont...

t (s)	$c(t)$ (kg/m ³) Experimental	$c(t)$ (kg/m ³) Model
988	8.890×10^{-5}	7.803×10^{-5}
1051	6.350×10^{-5}	6.549×10^{-5}
1110	6.350×10^{-5}	5.553×10^{-5}
1287	3.810×10^{-5}	3.372×10^{-5}
1326	3.810×10^{-5}	3.019×10^{-5}
1445	2.540×10^{-5}	2.152×10^{-5}
1577	2.540×10^{-5}	1.475×10^{-5}
1877	1.270×10^{-5}	6.215×10^{-6}
1894	1.270×10^{-5}	5.917×10^{-6}
1914	1.270×10^{-5}	5.584×10^{-6}

Table C.43. Tracer concentration for Run 230 ($u_L=0.0045$ m/s, $u_G=0.0083$ m/s, tap water)

t (s)	$c(t)$ (kg/m ³) Experimental	$c(t)$ (kg/m ³) Model
0	0	0
12	2.794×10^{-4}	4.465×10^{-4}
18	4.191×10^{-4}	5.347×10^{-4}
24	5.969×10^{-4}	6.029×10^{-4}
30	7.239×10^{-4}	6.578×10^{-4}
44	8.128×10^{-4}	7.515×10^{-4}
51	8.636×10^{-4}	7.855×10^{-4}
59	9.525×10^{-4}	8.166×10^{-4}
98	9.271×10^{-4}	8.897×10^{-4}
113	9.144×10^{-4}	8.951×10^{-4}
127	8.890×10^{-4}	8.928×10^{-4}
136	8.763×10^{-4}	8.883×10^{-4}
144	8.636×10^{-4}	8.827×10^{-4}
153	8.255×10^{-4}	8.748×10^{-4}
164	8.509×10^{-4}	8.631×10^{-4}
174	8.001×10^{-4}	8.510×10^{-4}
184	7.874×10^{-4}	8.376×10^{-4}
194	7.493×10^{-4}	8.231×10^{-4}
343	5.207×10^{-4}	5.682×10^{-4}
380	4.699×10^{-4}	5.080×10^{-4}
498	3.556×10^{-4}	3.454×10^{-4}
553	2.794×10^{-4}	2.855×10^{-4}
608	2.667×10^{-4}	2.347×10^{-4}
751	1.524×10^{-4}	1.386×10^{-4}
823	1.397×10^{-4}	1.055×10^{-4}
884	1.143×10^{-4}	8.346×10^{-5}
997	7.620×10^{-5}	5.375×10^{-5}
1066	5.080×10^{-5}	4.094×10^{-5}
1113	3.810×10^{-5}	3.397×10^{-5}
1165	5.080×10^{-5}	2.761×10^{-5}
1211	3.810×10^{-5}	2.296×10^{-5}
1246	2.540×10^{-5}	1.994×10^{-5}
1286	2.540×10^{-5}	1.697×10^{-5}
1318	0	1.491×10^{-5}

Table C.44. Tracer concentration for Run 231 ($u_L=0.0045$ m/s, $u_G=0.0145$ m/s, tap water)

t (s)	$c(t)$ (kg/m ³) Experimental	$c(t)$ (kg/m ³) Model
0	0	0
11	5.207×10^{-4}	6.814×10^{-4}
19	7.239×10^{-4}	7.969×10^{-4}
25	8.001×10^{-4}	8.563×10^{-4}
32	9.906×10^{-4}	9.085×10^{-4}
39	1.041×10^{-3}	9.481×10^{-4}
47	1.092×10^{-3}	9.824×10^{-4}
76	1.118×10^{-3}	1.046×10^{-3}
91	1.105×10^{-3}	1.056×10^{-3}
98	1.092×10^{-3}	1.057×10^{-3}
114	1.067×10^{-3}	1.054×10^{-3}
130	1.041×10^{-3}	1.043×10^{-3}
139	1.029×10^{-3}	1.034×10^{-3}
148	1.016×10^{-3}	1.025×10^{-3}
163	9.779×10^{-4}	1.006×10^{-3}
175	9.525×10^{-4}	9.887×10^{-4}
190	9.144×10^{-4}	9.659×10^{-4}
210	8.636×10^{-4}	9.332×10^{-4}
274	7.493×10^{-4}	8.208×10^{-4}
346	6.477×10^{-4}	6.948×10^{-4}
427	5.334×10^{-4}	5.660×10^{-4}
545	3.937×10^{-4}	4.112×10^{-4}
586	3.810×10^{-4}	3.665×10^{-4}
702	2.921×10^{-4}	2.624×10^{-4}
775	2.413×10^{-4}	2.116×10^{-4}
836	2.159×10^{-4}	1.763×10^{-4}
897	1.778×10^{-4}	1.467×10^{-4}
1016	1.397×10^{-4}	1.020×10^{-4}
1093	1.270×10^{-4}	8.047×10^{-5}
1158	8.890×10^{-5}	6.576×10^{-5}
1220	7.620×10^{-5}	5.419×10^{-5}
1272	7.620×10^{-5}	4.604×10^{-5}
1337	6.350×10^{-5}	3.753×10^{-5}
1395	6.350×10^{-5}	3.125×10^{-5}

Table C.45. Tracer concentration for Run 238 ($u_L=0.0045$ m/s, $u_G=0.0385$ m/s, tap water)

t (s)	$c(t)$ (kg/m ³) Experimental	$c(t)$ (kg/m ³) Model
0	0	0
10	3.810×10^{-4}	5.995×10^{-4}
18	6.731×10^{-4}	7.216×10^{-4}
24	7.874×10^{-4}	7.835×10^{-4}
31	9.144×10^{-4}	8.372×10^{-4}
38	1.003×10^{-3}	8.773×10^{-4}
49	1.016×10^{-3}	9.216×10^{-4}
55	1.016×10^{-3}	9.386×10^{-4}
90	9.906×10^{-4}	9.761×10^{-4}
103	9.906×10^{-4}	9.729×10^{-4}
110	9.525×10^{-4}	9.687×10^{-4}
117	9.398×10^{-4}	9.631×10^{-4}
124	9.271×10^{-4}	9.563×10^{-4}
132	9.144×10^{-4}	9.471×10^{-4}
178	8.382×10^{-4}	8.762×10^{-4}
186	8.001×10^{-4}	8.619×10^{-4}
255	6.477×10^{-4}	7.300×10^{-4}
358	4.953×10^{-4}	5.425×10^{-4}
429	4.318×10^{-4}	4.335×10^{-4}
486	3.556×10^{-4}	3.594×10^{-4}
531	3.302×10^{-4}	3.088×10^{-4}
570	2.794×10^{-4}	2.701×10^{-4}
621	2.159×10^{-4}	2.262×10^{-4}
682	2.159×10^{-4}	1.823×10^{-4}
744	1.905×10^{-4}	1.460×10^{-4}
795	1.651×10^{-4}	1.214×10^{-4}
874	1.270×10^{-4}	9.090×10^{-5}
940	1.016×10^{-4}	7.122×10^{-5}
1001	8.890×10^{-5}	5.676×10^{-5}
1060	7.620×10^{-5}	4.551×10^{-5}
1115	5.080×10^{-5}	3.700×10^{-5}
1174	3.810×10^{-5}	2.960×10^{-5}
1223	3.810×10^{-5}	2.458×10^{-5}
1267	2.540×10^{-5}	2.079×10^{-5}
1321	1.270×10^{-5}	1.692×10^{-5}
1383	2.540×10^{-5}	1.334×10^{-5}

Table C.46. Tracer concentration for Run 239 ($u_L=0.0045$ m/s, $u_G=0.0010$ m/s, tap water)

t (s)	$c(t)$ (kg/m ³) Experimental	$c(t)$ (kg/m ³) Model
0	0	0
12	6.350×10^{-4}	5.842×10^{-4}
18	6.096×10^{-4}	6.642×10^{-4}
26	4.953×10^{-4}	7.396×10^{-4}
36	8.382×10^{-4}	8.054×10^{-4}
44	8.763×10^{-4}	8.435×10^{-4}
52	9.144×10^{-4}	8.725×10^{-4}
58	9.144×10^{-4}	8.897×10^{-4}
68	9.779×10^{-4}	9.113×10^{-4}
75	9.906×10^{-4}	9.223×10^{-4}
82	9.652×10^{-4}	9.303×10^{-4}
91	9.652×10^{-4}	9.372×10^{-4}
99	9.652×10^{-4}	9.404×10^{-4}
106	9.652×10^{-4}	9.414×10^{-4}
118	9.652×10^{-4}	9.396×10^{-4}
126	9.525×10^{-4}	9.364×10^{-4}
133	9.144×10^{-4}	9.325×10^{-4}
145	8.890×10^{-4}	9.237×10^{-4}
153	9.017×10^{-4}	9.165×10^{-4}
161	8.763×10^{-4}	9.085×10^{-4}
170	8.636×10^{-4}	8.986×10^{-4}
178	8.255×10^{-4}	8.891×10^{-4}
186	8.128×10^{-4}	8.791×10^{-4}
194	9.525×10^{-4}	8.685×10^{-4}
221	7.620×10^{-4}	8.304×10^{-4}
326	5.969×10^{-4}	6.676×10^{-4}
387	5.842×10^{-4}	5.765×10^{-4}
462	4.191×10^{-4}	4.754×10^{-4}
602	2.921×10^{-4}	3.238×10^{-4}
787	1.905×10^{-4}	1.891×10^{-4}
950	1.270×10^{-4}	1.157×10^{-4}
1220	8.890×10^{-5}	5.013×10^{-5}
1529	5.080×10^{-5}	1.882×10^{-5}
1648	3.810×10^{-5}	1.285×10^{-5}

Table C.47. Tracer concentration for Run 206 ($u_L=0.0$ m/s, $u_G=0.0083$ m/s, 0.20% CMC)

t (s)	$c(t)$ (kg/m ³) Experimental	$c(t)$ (kg/m ³) Model
0	0	1.550×10^{-5}
9	1.026×10^{-3}	5.411×10^{-4}
17	1.949×10^{-3}	1.816×10^{-3}
24	2.565×10^{-3}	2.670×10^{-3}
31	3.488×10^{-3}	3.266×10^{-3}
39	3.642×10^{-3}	3.717×10^{-3}
47	3.591×10^{-3}	4.006×10^{-3}
55	3.694×10^{-3}	4.190×10^{-3}
63	4.361×10^{-3}	4.308×10^{-3}
72	3.899×10^{-3}	4.390×10^{-3}
80	5.284×10^{-3}	4.435×10^{-3}
87	3.950×10^{-3}	4.461×10^{-3}
94	4.104×10^{-3}	4.478×10^{-3}
102	4.720×10^{-3}	4.491×10^{-3}
111	4.771×10^{-3}	4.501×10^{-3}
120	4.720×10^{-3}	4.506×10^{-3}
128	4.874×10^{-3}	4.509×10^{-3}
136	4.309×10^{-3}	4.511×10^{-3}
145	4.258×10^{-3}	4.512×10^{-3}
153	4.207×10^{-3}	4.513×10^{-3}
162	4.361×10^{-3}	4.514×10^{-3}
171	4.925×10^{-3}	4.514×10^{-3}
179	5.797×10^{-3}	4.514×10^{-3}
187	4.309×10^{-3}	4.514×10^{-3}
218	4.258×10^{-3}	4.514×10^{-3}
228	4.412×10^{-3}	4.514×10^{-3}
249	5.079×10^{-3}	4.514×10^{-3}
257	4.258×10^{-3}	4.514×10^{-3}
266	4.514×10^{-3}	4.514×10^{-3}
275	4.361×10^{-3}	4.514×10^{-3}
283	5.335×10^{-3}	4.514×10^{-3}
292	4.617×10^{-3}	4.514×10^{-3}
300	4.514×10^{-3}	4.514×10^{-3}
309	4.412×10^{-3}	4.514×10^{-3}
319	4.720×10^{-3}	4.514×10^{-3}
327	4.258×10^{-3}	4.514×10^{-3}
336	4.925×10^{-3}	4.514×10^{-3}
345	4.771×10^{-3}	4.514×10^{-3}

Table C.47. Tracer concentration for Run 206 ($u_L=0.0$ m/s, $u_G=0.0083$ m/s, 0.20% CMC). Cont...

t (s)	$c(t)$ (kg/m ³) Experimental	$c(t)$ (kg/m ³) Model
355	4.822×10^{-3}	4.514×10^{-3}
364	4.822×10^{-3}	4.514×10^{-3}
373	4.412×10^{-3}	4.514×10^{-3}
382	5.233×10^{-3}	4.514×10^{-3}
390	4.514×10^{-3}	4.514×10^{-3}
399	4.258×10^{-3}	4.514×10^{-3}
408	4.104×10^{-3}	4.514×10^{-3}
417	4.514×10^{-3}	4.514×10^{-3}
425	4.309×10^{-3}	4.514×10^{-3}
434	4.720×10^{-3}	4.514×10^{-3}

Table C.48. Tracer concentration for Run 207 ($u_L=0.0$ m/s, $u_G=0.0145$ m/s, 0.20% CMC)

t (s)	$c(t)$ (kg/m ³) Experimental	$c(t)$ (kg/m ³) Model
0	0	1.462×10^{-5}
20	2.668×10^{-3}	2.358×10^{-3}
32	2.975×10^{-3}	3.360×10^{-3}
42	3.642×10^{-3}	3.779×10^{-3}
53	4.001×10^{-3}	4.019×10^{-3}
65	4.668×10^{-3}	4.146×10^{-3}
81	3.848×10^{-3}	4.217×10^{-3}
91	4.053×10^{-3}	4.236×10^{-3}
102	4.053×10^{-3}	4.247×10^{-3}
114	4.925×10^{-3}	4.253×10^{-3}
124	4.668×10^{-3}	4.255×10^{-3}
135	4.053×10^{-3}	4.257×10^{-3}
146	4.258×10^{-3}	4.257×10^{-3}
157	4.258×10^{-3}	4.258×10^{-3}
167	4.155×10^{-3}	4.258×10^{-3}
179	4.155×10^{-3}	4.258×10^{-3}
191	4.155×10^{-3}	4.258×10^{-3}
201	4.258×10^{-3}	4.258×10^{-3}
212	4.258×10^{-3}	4.258×10^{-3}
224	5.079×10^{-3}	4.258×10^{-3}
236	4.104×10^{-3}	4.258×10^{-3}
247	4.207×10^{-3}	4.258×10^{-3}
258	4.412×10^{-3}	4.258×10^{-3}
269	4.207×10^{-3}	4.258×10^{-3}
296	4.258×10^{-3}	4.258×10^{-3}
311	4.258×10^{-3}	4.258×10^{-3}
324	4.309×10^{-3}	4.258×10^{-3}
337	4.309×10^{-3}	4.258×10^{-3}
350	4.412×10^{-3}	4.258×10^{-3}
363	4.566×10^{-3}	4.258×10^{-3}
376	4.207×10^{-3}	4.258×10^{-3}
390	4.463×10^{-3}	4.258×10^{-3}
405	4.258×10^{-3}	4.258×10^{-3}
418	4.463×10^{-3}	4.258×10^{-3}
430	4.361×10^{-3}	4.258×10^{-3}
442	4.309×10^{-3}	4.258×10^{-3}
456	4.155×10^{-3}	4.258×10^{-3}
472	4.874×10^{-3}	4.258×10^{-3}

Table C.48. Tracer concentration for Run 207 ($u_L=0.0$ m/s, $u_G=0.0145$ m/s, 0.20% CMC). Cont...

t (s)	$c(t)$ (kg/m ³) Experimental	$c(t)$ (kg/m ³) Model
485	4.463×10^{-3}	4.258×10^{-3}
500	4.617×10^{-3}	4.258×10^{-3}
518	4.566×10^{-3}	4.258×10^{-3}
569	4.566×10^{-3}	4.258×10^{-3}
582	4.463×10^{-3}	4.258×10^{-3}
606	4.463×10^{-3}	4.258×10^{-3}

Table C.49. Tracer concentration for Run 208 ($u_L=0.0$ m/s, $u_G=0.0308$ m/s, 0.20%

CMC)

t (s)	$c(t)$ (kg/m ³) Experimental	$c(t)$ (kg/m ³) Model
0	0	1.603×10^{-5}
16	2.616×10^{-3}	2.545×10^{-3}
24	3.540×10^{-3}	3.519×10^{-3}
31	3.540×10^{-3}	4.000×10^{-3}
38	4.463×10^{-3}	4.280×10^{-3}
45	4.463×10^{-3}	4.442×10^{-3}
52	4.925×10^{-3}	4.537×10^{-3}
61	4.566×10^{-3}	4.603×10^{-3}
69	4.822×10^{-3}	4.633×10^{-3}
78	4.463×10^{-3}	4.651×10^{-3}
85	4.822×10^{-3}	4.658×10^{-3}
93	4.207×10^{-3}	4.663×10^{-3}
109	4.771×10^{-3}	4.667×10^{-3}
117	4.822×10^{-3}	4.667×10^{-3}
125	4.412×10^{-3}	4.668×10^{-3}
133	4.514×10^{-3}	4.668×10^{-3}
141	4.361×10^{-3}	4.668×10^{-3}
149	4.207×10^{-3}	4.668×10^{-3}
157	4.463×10^{-3}	4.668×10^{-3}
165	4.566×10^{-3}	4.668×10^{-3}
173	5.130×10^{-3}	4.668×10^{-3}
182	4.925×10^{-3}	4.668×10^{-3}
190	4.412×10^{-3}	4.668×10^{-3}
208	5.027×10^{-3}	4.668×10^{-3}
217	4.412×10^{-3}	4.668×10^{-3}
226	4.463×10^{-3}	4.668×10^{-3}
235	4.361×10^{-3}	4.668×10^{-3}
244	4.668×10^{-3}	4.668×10^{-3}
253	4.566×10^{-3}	4.668×10^{-3}
262	4.514×10^{-3}	4.668×10^{-3}
271	5.181×10^{-3}	4.668×10^{-3}
280	4.771×10^{-3}	4.668×10^{-3}
289	4.361×10^{-3}	4.668×10^{-3}
297	5.130×10^{-3}	4.668×10^{-3}
306	4.822×10^{-3}	4.668×10^{-3}
316	4.566×10^{-3}	4.668×10^{-3}
325	4.720×10^{-3}	4.668×10^{-3}

Table C.49. Tracer concentration for Run 208 ($u_L=0.0$ m/s, $u_G=0.0308$ m/s, 0.20% CMC). Cont...

t (s)	$c(t)$ (kg/m ³) Experimental	$c(t)$ (kg/m ³) Model
336	4.668×10^{-3}	4.668×10^{-3}
348	4.668×10^{-3}	4.668×10^{-3}
382	4.822×10^{-3}	4.668×10^{-3}
392	4.463×10^{-3}	4.668×10^{-3}
402	4.566×10^{-3}	4.668×10^{-3}
412	4.668×10^{-3}	4.668×10^{-3}
423	4.566×10^{-3}	4.668×10^{-3}
432	4.720×10^{-3}	4.668×10^{-3}
442	4.720×10^{-3}	4.668×10^{-3}
453	4.925×10^{-3}	4.668×10^{-3}

Table C.50. Tracer concentration for Run 209 ($u_L=0.0$ m/s, $u_G=0.0385$ m/s, 0.20%

CMC)

t (s)	$c(t)$ (kg/m ³) Experimental	$c(t)$ (kg/m ³) Model
0	0	1.497×10^{-5}
11	1.796×10^{-3}	1.319×10^{-3}
21	2.462×10^{-3}	2.833×10^{-3}
28	3.232×10^{-3}	3.434×10^{-3}
35	3.950×10^{-3}	3.799×10^{-3}
44	4.104×10^{-3}	4.066×10^{-3}
52	3.899×10^{-3}	4.195×10^{-3}
59	3.899×10^{-3}	4.260×10^{-3}
66	4.720×10^{-3}	4.300×10^{-3}
73	4.566×10^{-3}	4.324×10^{-3}
81	5.387×10^{-3}	4.340×10^{-3}
87	3.950×10^{-3}	4.347×10^{-3}
94	4.309×10^{-3}	4.352×10^{-3}
101	4.514×10^{-3}	4.356×10^{-3}
108	5.592×10^{-3}	4.358×10^{-3}
116	4.258×10^{-3}	4.359×10^{-3}
123	4.207×10^{-3}	4.359×10^{-3}
131	4.258×10^{-3}	4.360×10^{-3}
138	4.720×10^{-3}	4.360×10^{-3}
145	5.335×10^{-3}	4.360×10^{-3}
154	4.309×10^{-3}	4.360×10^{-3}
170	5.489×10^{-3}	4.360×10^{-3}
177	4.463×10^{-3}	4.360×10^{-3}
204	5.284×10^{-3}	4.360×10^{-3}
214	4.617×10^{-3}	4.360×10^{-3}
222	4.771×10^{-3}	4.360×10^{-3}
230	4.412×10^{-3}	4.360×10^{-3}
240	4.361×10^{-3}	4.360×10^{-3}
248	4.463×10^{-3}	4.360×10^{-3}
256	4.207×10^{-3}	4.360×10^{-3}
265	4.412×10^{-3}	4.360×10^{-3}
274	4.463×10^{-3}	4.360×10^{-3}
282	4.822×10^{-3}	4.360×10^{-3}
306	4.925×10^{-3}	4.360×10^{-3}
315	4.309×10^{-3}	4.360×10^{-3}
325	4.668×10^{-3}	4.360×10^{-3}

Table C.50. Tracer concentration for Run 209 ($u_L=0.0$ m/s, $u_G=0.0385$ m/s, 0.20% CMC). Cont...

t (s)	$c(t)$ (kg/m ³) Experimental	$c(t)$ (kg/m ³) Model
334	4.668×10^{-3}	4.360×10^{-3}
343	4.617×10^{-3}	4.360×10^{-3}
352	4.566×10^{-3}	4.360×10^{-3}
361	4.925×10^{-3}	4.360×10^{-3}
369	4.617×10^{-3}	4.360×10^{-3}
378	4.617×10^{-3}	4.360×10^{-3}
387	4.361×10^{-3}	4.360×10^{-3}
398	4.617×10^{-3}	4.360×10^{-3}
409	4.668×10^{-3}	4.360×10^{-3}

Table C.51. Tracer concentration for Run 210 ($u_L=0.0$ m/s, $u_G=0.0462$ m/s, 0.20%

CMC)

t (s)	$c(t)$ (kg/m ³) Experimental	$c(t)$ (kg/m ³) Model
0	0	1.638×10^{-5}
14	2.206×10^{-3}	2.250×10^{-3}
22	2.975×10^{-3}	3.401×10^{-3}
30	4.412×10^{-3}	4.033×10^{-3}
38	4.976×10^{-3}	4.374×10^{-3}
46	4.155×10^{-3}	4.558×10^{-3}
53	4.566×10^{-3}	4.647×10^{-3}
61	4.822×10^{-3}	4.704×10^{-3}
70	4.617×10^{-3}	4.738×10^{-3}
82	5.694×10^{-3}	4.758×10^{-3}
90	4.771×10^{-3}	4.764×10^{-3}
98	4.514×10^{-3}	4.767×10^{-3}
115	5.284×10^{-3}	4.770×10^{-3}
124	5.233×10^{-3}	4.770×10^{-3}
132	4.720×10^{-3}	4.771×10^{-3}
141	4.771×10^{-3}	4.771×10^{-3}
150	4.720×10^{-3}	4.771×10^{-3}
159	4.668×10^{-3}	4.771×10^{-3}
167	4.771×10^{-3}	4.771×10^{-3}
176	4.925×10^{-3}	4.771×10^{-3}
186	4.668×10^{-3}	4.771×10^{-3}
195	4.822×10^{-3}	4.771×10^{-3}
203	4.617×10^{-3}	4.771×10^{-3}
223	4.361×10^{-3}	4.771×10^{-3}
232	4.771×10^{-3}	4.771×10^{-3}
241	4.207×10^{-3}	4.771×10^{-3}
251	3.950×10^{-3}	4.771×10^{-3}
260	4.155×10^{-3}	4.771×10^{-3}
269	4.771×10^{-3}	4.771×10^{-3}
278	4.361×10^{-3}	4.771×10^{-3}
288	4.053×10^{-3}	4.771×10^{-3}
297	4.309×10^{-3}	4.771×10^{-3}
306	4.463×10^{-3}	4.771×10^{-3}
315	4.463×10^{-3}	4.771×10^{-3}
324	4.874×10^{-3}	4.771×10^{-3}
334	4.361×10^{-3}	4.771×10^{-3}

Table C.51. Tracer concentration for Run 210 ($u_L=0.0$ m/s, $u_G=0.0462$ m/s, 0.20% CMC). Cont...

t (s)	$c(t)$ (kg/m ³) Experimental	$c(t)$ (kg/m ³) Model
352	4.361×10^{-3}	4.771×10^{-3}
361	4.463×10^{-3}	4.771×10^{-3}
370	4.309×10^{-3}	4.771×10^{-3}
380	4.361×10^{-3}	4.771×10^{-3}
389	4.668×10^{-3}	4.771×10^{-3}
399	4.514×10^{-3}	4.771×10^{-3}
409	4.720×10^{-3}	4.771×10^{-3}
420	4.361×10^{-3}	4.771×10^{-3}
430	4.617×10^{-3}	4.771×10^{-3}

Table C.52. Tracer concentration for Run 216 ($u_L=0.0045$ m/s, $u_G=0.0083$ m/s, 0.20%

CMC)

t (s)	$c(t)$ (kg/m ³) Experimental	$c(t)$ (kg/m ³) Model
0	0	0
12	7.196×10^{-4}	2.082×10^{-3}
19	1.233×10^{-3}	2.476×10^{-3}
26	2.413×10^{-3}	2.760×10^{-3}
33	2.464×10^{-3}	2.975×10^{-3}
64	3.849×10^{-3}	3.477×10^{-3}
70	3.695×10^{-3}	3.522×10^{-3}
77	3.182×10^{-3}	3.561×10^{-3}
100	3.746×10^{-3}	3.608×10^{-3}
107	3.387×10^{-3}	3.604×10^{-3}
117	3.387×10^{-3}	3.585×10^{-3}
134	3.131×10^{-3}	3.528×10^{-3}
150	2.772×10^{-3}	3.453×10^{-3}
162	3.028×10^{-3}	3.386×10^{-3}
175	2.669×10^{-3}	3.305×10^{-3}
192	2.618×10^{-3}	3.191×10^{-3}
203	2.515×10^{-3}	3.114×10^{-3}
227	2.823×10^{-3}	2.938×10^{-3}
250	2.566×10^{-3}	2.766×10^{-3}
300	3.028×10^{-3}	2.396×10^{-3}
340	1.746×10^{-3}	2.116×10^{-3}
367	1.746×10^{-3}	1.939×10^{-3}
411	1.438×10^{-3}	1.673×10^{-3}
479	1.387×10^{-3}	1.319×10^{-3}
544	1.130×10^{-3}	1.043×10^{-3}
587	9.248×10^{-4}	8.888×10^{-4}
648	8.735×10^{-4}	7.060×10^{-4}
704	7.709×10^{-4}	5.695×10^{-4}
790	5.657×10^{-4}	4.072×10^{-4}
824	6.683×10^{-4}	3.561×10^{-4}
880	3.605×10^{-4}	2.850×10^{-4}
912	3.092×10^{-4}	2.508×10^{-4}
953	4.118×10^{-4}	2.127×10^{-4}
979	3.092×10^{-4}	1.915×10^{-4}
1016	3.092×10^{-4}	1.648×10^{-4}
1049	1.553×10^{-4}	1.441×10^{-4}
1074	1.553×10^{-4}	1.302×10^{-4}
1094	2.066×10^{-4}	1.200×10^{-4}

Table C.53. Tracer concentration for Run 217 ($u_L=0.0045$ m/s, $u_G=0.0145$ m/s, 0.20%

CMC)

t (s)	$c(t)$ (kg/m ³) Experimental	$c(t)$ (kg/m ³) Model
0	0	0
11	1.796×10^{-3}	2.026×10^{-3}
18	1.796×10^{-3}	2.481×10^{-3}
25	2.103×10^{-3}	2.804×10^{-3}
32	3.181×10^{-3}	3.045×10^{-3}
46	3.591×10^{-3}	3.367×10^{-3}
53	3.488×10^{-3}	3.472×10^{-3}
62	3.437×10^{-3}	3.568×10^{-3}
69	3.796×10^{-3}	3.617×10^{-3}
85	3.283×10^{-3}	3.667×10^{-3}
92	3.386×10^{-3}	3.668×10^{-3}
109	2.822×10^{-3}	3.628×10^{-3}
116	3.181×10^{-3}	3.599×10^{-3}
138	2.719×10^{-3}	3.470×10^{-3}
146	2.770×10^{-3}	3.413×10^{-3}
158	3.129×10^{-3}	3.320×10^{-3}
175	2.411×10^{-3}	3.178×10^{-3}
188	2.309×10^{-3}	3.063×10^{-3}
201	2.462×10^{-3}	2.946×10^{-3}
236	2.206×10^{-3}	2.627×10^{-3}
252	2.873×10^{-3}	2.483×10^{-3}
312	2.411×10^{-3}	1.979×10^{-3}
383	1.180×10^{-3}	1.478×10^{-3}
462	1.642×10^{-3}	1.047×10^{-3}
520	8.721×10^{-4}	8.054×10^{-4}
565	7.182×10^{-4}	6.542×10^{-4}
692	4.104×10^{-4}	3.582×10^{-4}
769	2.565×10^{-4}	2.465×10^{-4}

Table C.54. Tracer concentration for Run 218 ($u_L=0.0045$ m/s, $u_G=0.0308$ m/s, 0.20%

CMC)

t (s)	$c(t)$ (kg/m ³) Experimental	$c(t)$ (kg/m ³) Model
0	0	0
13	3.232×10^{-3}	2.920×10^{-3}
22	2.873×10^{-3}	3.146×10^{-3}
29	3.232×10^{-3}	3.250×10^{-3}
129	3.437×10^{-3}	3.206×10^{-3}
138	3.181×10^{-3}	3.161×10^{-3}
146	3.129×10^{-3}	3.119×10^{-3}
154	3.027×10^{-3}	3.076×10^{-3}
161	2.873×10^{-3}	3.037×10^{-3}
170	3.129×10^{-3}	2.987×10^{-3}
179	2.873×10^{-3}	2.936×10^{-3}
195	2.770×10^{-3}	2.844×10^{-3}
268	2.462×10^{-3}	2.425×10^{-3}
302	2.309×10^{-3}	2.239×10^{-3}
357	2.103×10^{-3}	1.958×10^{-3}
419	1.590×10^{-3}	1.674×10^{-3}
514	1.693×10^{-3}	1.307×10^{-3}
637	1.026×10^{-3}	9.388×10^{-4}
730	1.026×10^{-3}	7.275×10^{-4}
766	6.669×10^{-4}	6.585×10^{-4}
824	6.156×10^{-4}	5.604×10^{-4}
884	5.130×10^{-4}	4.737×10^{-4}
935	4.617×10^{-4}	4.104×10^{-4}
991	4.104×10^{-4}	3.504×10^{-4}
1063	2.052×10^{-4}	2.856×10^{-4}
1121	2.052×10^{-4}	2.421×10^{-4}
1180	1.539×10^{-4}	2.046×10^{-4}
1207	5.130×10^{-5}	1.893×10^{-4}

Table C.55. Tracer concentration for Run 219 ($u_L=0.0045$ m/s, $u_G=0.0385$ m/s, 0.20%

CMC)

t (s)	$c(t)$ (kg/m ³) Experimental	$c(t)$ (kg/m ³) Model
0	0	0
14	1.642×10^{-3}	2.586×10^{-3}
21	3.283×10^{-3}	2.869×10^{-3}
30	3.693×10^{-3}	3.113×10^{-3}
69	3.745×10^{-3}	3.550×10^{-3}
129	3.386×10^{-3}	3.537×10^{-3}
144	3.437×10^{-3}	3.483×10^{-3}
159	3.591×10^{-3}	3.418×10^{-3}
173	3.078×10^{-3}	3.350×10^{-3}
183	3.283×10^{-3}	3.298×10^{-3}
190	3.181×10^{-3}	3.260×10^{-3}
219	3.129×10^{-3}	3.095×10^{-3}
227	3.129×10^{-3}	3.048×10^{-3}
248	3.078×10^{-3}	2.922×10^{-3}
259	2.770×10^{-3}	2.855×10^{-3}
270	2.462×10^{-3}	2.789×10^{-3}
407	2.001×10^{-3}	2.010×10^{-3}
482	1.590×10^{-3}	1.652×10^{-3}
665	1.129×10^{-3}	9.937×10^{-4}
712	8.208×10^{-4}	8.683×10^{-4}
814	6.669×10^{-4}	6.449×10^{-4}
1022	4.617×10^{-4}	3.466×10^{-4}
1147	3.591×10^{-4}	2.371×10^{-4}
1243	2.565×10^{-4}	1.767×10^{-4}
1322	1.026×10^{-4}	1.385×10^{-4}
1419	1.026×10^{-4}	1.025×10^{-4}
1499	5.130×10^{-5}	7.992×10^{-5}

Table C.56. Tracer concentration for Run 220 ($u_L=0.0045$ m/s, $u_G=0.0462$ m/s, 0.20%

CMC)

t (s)	$c(t)$ (kg/m ³) Experimental	$c(t)$ (kg/m ³) Model
0	0	0
11	1.642×10^{-3}	2.276×10^{-3}
18	2.462×10^{-3}	2.602×10^{-3}
23	3.232×10^{-3}	2.766×10^{-3}
35	3.335×10^{-3}	3.035×10^{-3}
80	3.694×10^{-3}	3.382×10^{-3}
97	3.540×10^{-3}	3.391×10^{-3}
144	2.975×10^{-3}	3.266×10^{-3}
150	3.181×10^{-3}	3.240×10^{-3}
192	2.873×10^{-3}	3.029×10^{-3}
249	2.616×10^{-3}	2.698×10^{-3}
293	2.309×10^{-3}	2.437×10^{-3}
379	1.847×10^{-3}	1.960×10^{-3}
447	1.693×10^{-3}	1.629×10^{-3}
497	1.488×10^{-3}	1.415×10^{-3}
548	1.180×10^{-3}	1.222×10^{-3}
689	8.721×10^{-4}	8.033×10^{-4}
770	8.208×10^{-4}	6.272×10^{-4}
823	6.156×10^{-4}	5.323×10^{-4}
943	4.617×10^{-4}	3.656×10^{-4}
994	3.591×10^{-4}	3.111×10^{-4}
1134	2.565×10^{-4}	1.989×10^{-4}
1152	2.052×10^{-4}	1.877×10^{-4}
1186	2.565×10^{-4}	1.683×10^{-4}
1271	1.539×10^{-4}	1.278×10^{-4}
1318	1.539×10^{-4}	1.097×10^{-4}

Table C.57. Tracer concentration for Run 223 ($u_L=0.0045$ m/s, $u_G=0.0010$ m/s, 0.20%

CMC)

t (s)	$c(t)$ (kg/m ³) Experimental	$c(t)$ (kg/m ³) Model
0	0	0
15	5.130×10^{-4}	1.615×10^{-3}
21	1.231×10^{-3}	1.827×10^{-3}
29	2.155×10^{-3}	2.041×10^{-3}
36	2.001×10^{-3}	2.185×10^{-3}
43	2.462×10^{-3}	2.301×10^{-3}
62	2.668×10^{-3}	2.519×10^{-3}
69	2.822×10^{-3}	2.574×10^{-3}
76	2.873×10^{-3}	2.618×10^{-3}
91	2.873×10^{-3}	2.683×10^{-3}
97	2.873×10^{-3}	2.700×10^{-3}
106	2.873×10^{-3}	2.718×10^{-3}
119	2.719×10^{-3}	2.729×10^{-3}
136	2.668×10^{-3}	2.723×10^{-3}
144	2.360×10^{-3}	2.713×10^{-3}
157	2.514×10^{-3}	2.690×10^{-3}
165	2.360×10^{-3}	2.672×10^{-3}
175	2.360×10^{-3}	2.646×10^{-3}
183	2.257×10^{-3}	2.622×10^{-3}
190	2.309×10^{-3}	2.600×10^{-3}
237	2.052×10^{-3}	2.424×10^{-3}
247	1.847×10^{-3}	2.382×10^{-3}
255	2.001×10^{-3}	2.348×10^{-3}
266	1.898×10^{-3}	2.300×10^{-3}
278	1.898×10^{-3}	2.248×10^{-3}
288	1.796×10^{-3}	2.203×10^{-3}
301	1.539×10^{-3}	2.145×10^{-3}
311	1.693×10^{-3}	2.100×10^{-3}
391	2.668×10^{-3}	1.750×10^{-3}
462	1.334×10^{-3}	1.465×10^{-3}
538	1.077×10^{-3}	1.197×10^{-3}
658	7.695×10^{-4}	8.562×10^{-4}
726	5.643×10^{-4}	7.033×10^{-4}
787	5.643×10^{-4}	5.876×10^{-4}
848	4.617×10^{-4}	4.897×10^{-4}
914	4.104×10^{-4}	4.011×10^{-4}
969	4.617×10^{-4}	3.390×10^{-4}
1015	2.565×10^{-4}	2.942×10^{-4}

Table C.57. Tracer concentration for Run 223 ($u_L=0.0045$ m/s, $u_G=0.0010$ m/s, 0.20% CMC). Cont...

t (s)	$c(t)$ (kg/m ³) Experimental	$c(t)$ (kg/m ³) Model
1076	5.130×10^{-4}	2.434×10^{-4}
1130	2.052×10^{-4}	2.056×10^{-4}
1150	2.565×10^{-4}	1.931×10^{-4}
1198	2.052×10^{-4}	1.661×10^{-4}
1252	2.565×10^{-4}	1.400×10^{-4}
1342	1.539×10^{-4}	1.051×10^{-4}

Table C.58. Tracer concentration for Run 213 ($u_L=0.0$ m/s, $u_G=0.0308$ m/s, 0.40%

CMC)

t (s)	$c(t)$ (kg/m ³) Experimental	$c(t)$ (kg/m ³) Model
0	0	2.719×10^{-6}
13	6.336×10^{-4}	5.894×10^{-4}
21	6.732×10^{-4}	7.259×10^{-4}
30	7.326×10^{-4}	7.733×10^{-4}
39	6.831×10^{-4}	7.867×10^{-4}
59	9.009×10^{-4}	7.917×10^{-4}
68	8.514×10^{-4}	7.919×10^{-4}
77	7.425×10^{-4}	7.920×10^{-4}
86	7.524×10^{-4}	7.920×10^{-4}
95	7.722×10^{-4}	7.920×10^{-4}
104	8.118×10^{-4}	7.920×10^{-4}
114	8.217×10^{-4}	7.920×10^{-4}
124	6.831×10^{-4}	7.920×10^{-4}
134	7.128×10^{-4}	7.920×10^{-4}
142	8.118×10^{-4}	7.920×10^{-4}
152	7.227×10^{-4}	7.920×10^{-4}
168	7.920×10^{-4}	7.920×10^{-4}
187	7.722×10^{-4}	7.920×10^{-4}
197	9.009×10^{-4}	7.920×10^{-4}
218	8.217×10^{-4}	7.920×10^{-4}
229	7.128×10^{-4}	7.920×10^{-4}
251	8.019×10^{-4}	7.920×10^{-4}
261	7.524×10^{-4}	7.920×10^{-4}
271	7.623×10^{-4}	7.920×10^{-4}
282	8.217×10^{-4}	7.920×10^{-4}
293	8.415×10^{-4}	7.920×10^{-4}
303	7.425×10^{-4}	7.920×10^{-4}
315	7.920×10^{-4}	7.920×10^{-4}
337	9.009×10^{-4}	7.920×10^{-4}
348	8.316×10^{-4}	7.920×10^{-4}
358	8.118×10^{-4}	7.920×10^{-4}
369	7.821×10^{-4}	7.920×10^{-4}
380	7.425×10^{-4}	7.920×10^{-4}
390	7.821×10^{-4}	7.920×10^{-4}
401	8.019×10^{-4}	7.920×10^{-4}
412	7.920×10^{-4}	7.920×10^{-4}
423	8.415×10^{-4}	7.920×10^{-4}

Table C.59. Tracer concentration for Run 215 ($u_L=0.0$ m/s, $u_G=0.0083$ m/s, 0.40%

CMC)

t (s)	$c(t)$ (kg/m ³) Experimental	$c(t)$ (kg/m ³) Model
0	0	2.005×10^{-6}
16	1.584×10^{-4}	1.538×10^{-4}
27	1.980×10^{-4}	3.152×10^{-4}
39	5.049×10^{-4}	4.272×10^{-4}
50	5.643×10^{-4}	4.889×10^{-4}
62	3.366×10^{-4}	5.289×10^{-4}
106	4.851×10^{-4}	5.766×10^{-4}
126	5.049×10^{-4}	5.811×10^{-4}
137	5.346×10^{-4}	5.823×10^{-4}
151	5.049×10^{-4}	5.831×10^{-4}
173	5.643×10^{-4}	5.837×10^{-4}
185	5.148×10^{-4}	5.839×10^{-4}
198	5.742×10^{-4}	5.840×10^{-4}
210	5.445×10^{-4}	5.840×10^{-4}
227	5.049×10^{-4}	5.841×10^{-4}
255	5.445×10^{-4}	5.841×10^{-4}
290	6.534×10^{-4}	5.841×10^{-4}
302	6.039×10^{-4}	5.841×10^{-4}
318	5.841×10^{-4}	5.841×10^{-4}
330	6.732×10^{-4}	5.841×10^{-4}
362	6.633×10^{-4}	5.841×10^{-4}
384	8.811×10^{-4}	5.841×10^{-4}
421	6.237×10^{-4}	5.841×10^{-4}
434	6.138×10^{-4}	5.841×10^{-4}
454	5.445×10^{-4}	5.841×10^{-4}
480	5.742×10^{-4}	5.841×10^{-4}
495	6.930×10^{-4}	5.841×10^{-4}
509	6.435×10^{-4}	5.841×10^{-4}
522	5.643×10^{-4}	5.841×10^{-4}
567	6.138×10^{-4}	5.841×10^{-4}
594	6.633×10^{-4}	5.841×10^{-4}

Table C.60. Tracer concentration for Run 224 ($u_L=0.0$ m/s, $u_G=0.0145$ m/s, 0.40%

CMC)

t (s)	$c(t)$ (kg/m ³) Experimental	$c(t)$ (kg/m ³) Model
0	0	2.379×10^{-6}
15	1.287×10^{-4}	2.997×10^{-4}
27	5.445×10^{-4}	5.153×10^{-4}
37	6.138×10^{-4}	6.023×10^{-4}
83	6.336×10^{-4}	6.889×10^{-4}
94	6.039×10^{-4}	6.911×10^{-4}
104	7.524×10^{-4}	6.920×10^{-4}
114	6.336×10^{-4}	6.925×10^{-4}
147	6.732×10^{-4}	6.929×10^{-4}
181	7.524×10^{-4}	6.930×10^{-4}
193	7.326×10^{-4}	6.930×10^{-4}
204	6.831×10^{-4}	6.930×10^{-4}
215	6.633×10^{-4}	6.930×10^{-4}
228	6.930×10^{-4}	6.930×10^{-4}
273	7.821×10^{-4}	6.930×10^{-4}
311	7.227×10^{-4}	6.930×10^{-4}
337	6.930×10^{-4}	6.930×10^{-4}
348	7.524×10^{-4}	6.930×10^{-4}
362	7.128×10^{-4}	6.930×10^{-4}
375	6.633×10^{-4}	6.930×10^{-4}
388	7.821×10^{-4}	6.930×10^{-4}

Table C.61. Tracer concentration for Run 226 ($u_L=0.0$ m/s, $u_G=0.0385$ m/s, 0.40%

CMC)

t (s)	$c(t)$ (kg/m ³) Experimental	$c(t)$ (kg/m ³) Model
0	0	2.889×10^{-6}
12	1.881×10^{-4}	2.776×10^{-4}
20	4.455×10^{-4}	5.106×10^{-4}
31	7.821×10^{-4}	6.867×10^{-4}
40	7.920×10^{-4}	7.586×10^{-4}
50	8.514×10^{-4}	8.001×10^{-4}
60	8.613×10^{-4}	8.208×10^{-4}
69	1.059×10^{-3}	8.304×10^{-4}
80	1.010×10^{-3}	8.363×10^{-4}
90	1.010×10^{-3}	8.389×10^{-4}
100	8.316×10^{-4}	8.402×10^{-4}
111	7.920×10^{-4}	8.409×10^{-4}
121	9.108×10^{-4}	8.412×10^{-4}
132	9.009×10^{-4}	8.414×10^{-4}
143	8.019×10^{-4}	8.414×10^{-4}
155	8.613×10^{-4}	8.415×10^{-4}
166	8.613×10^{-4}	8.415×10^{-4}
178	8.514×10^{-4}	8.415×10^{-4}
188	8.415×10^{-4}	8.415×10^{-4}
199	8.910×10^{-4}	8.415×10^{-4}
210	8.811×10^{-4}	8.415×10^{-4}
221	8.217×10^{-4}	8.415×10^{-4}
231	9.108×10^{-4}	8.415×10^{-4}
243	9.108×10^{-4}	8.415×10^{-4}

Table C.62. Tracer concentration for Run 228 ($u_L=0.0$ m/s, $u_G=0.0462$ m/s, 0.40%

CMC)

t (s)	$c(t)$ (kg/m ³) Experimental	$c(t)$ (kg/m ³) Model
0	0	2.991×10^{-6}
15	3.663×10^{-4}	3.936×10^{-4}
26	5.840×10^{-4}	6.468×10^{-4}
38	8.514×10^{-4}	7.740×10^{-4}
49	8.811×10^{-4}	8.261×10^{-4}
60	8.410×10^{-4}	8.503×10^{-4}
70	9.603×10^{-4}	8.608×10^{-4}
87	8.910×10^{-4}	8.680×10^{-4}
97	8.910×10^{-4}	8.696×10^{-4}
106	8.712×10^{-4}	8.704×10^{-4}
116	8.415×10^{-4}	8.708×10^{-4}
125	9.405×10^{-4}	8.710×10^{-4}
144	8.910×10^{-4}	8.711×10^{-4}
154	8.712×10^{-4}	8.712×10^{-4}
165	9.306×10^{-4}	8.712×10^{-4}
175	9.009×10^{-4}	8.712×10^{-4}
184	9.009×10^{-4}	8.712×10^{-4}
194	8.811×10^{-4}	8.712×10^{-4}
205	9.009×10^{-4}	8.712×10^{-4}
216	8.712×10^{-4}	8.712×10^{-4}
226	9.108×10^{-4}	8.712×10^{-4}
236	9.108×10^{-4}	8.712×10^{-4}
262	9.009×10^{-4}	8.712×10^{-4}
271	9.207×10^{-4}	8.712×10^{-4}
281	9.108×10^{-4}	8.712×10^{-4}
291	8.712×10^{-4}	8.712×10^{-4}
302	9.009×10^{-4}	8.712×10^{-4}
323	8.316×10^{-4}	8.712×10^{-4}
333	9.207×10^{-4}	8.712×10^{-4}
354	8.910×10^{-4}	8.712×10^{-4}
364	8.910×10^{-4}	8.712×10^{-4}
374	8.712×10^{-4}	8.712×10^{-4}
386	8.613×10^{-4}	8.712×10^{-4}
397	9.108×10^{-4}	8.712×10^{-4}
407	9.207×10^{-4}	8.712×10^{-4}
417	9.108×10^{-4}	8.712×10^{-4}
435	8.910×10^{-4}	8.712×10^{-4}
453	8.118×10^{-4}	8.712×10^{-4}

Table C.63. Tracer concentration for Run 232 ($u_L=0.0$ m/s, $u_G=0.0010$ m/s, 0.40%

CMC)

t (s)	$c(t)$ (kg/m ³) Experimental	$c(t)$ (kg/m ³) Model
0	0	1.768×10^{-6}
29	1.188×10^{-4}	2.745×10^{-7}
43	1.683×10^{-4}	4.210×10^{-6}
63	1.683×10^{-4}	2.392×10^{-5}
87	2.376×10^{-4}	6.466×10^{-5}
110	2.079×10^{-4}	1.101×10^{-4}
152	2.673×10^{-4}	1.906×10^{-4}
186	2.277×10^{-4}	2.470×10^{-4}
240	2.475×10^{-4}	3.189×10^{-4}
286	4.653×10^{-4}	3.652×10^{-4}
354	2.970×10^{-4}	4.147×10^{-4}
419	2.673×10^{-4}	4.467×10^{-4}
455	3.663×10^{-4}	4.597×10^{-4}
545	4.059×10^{-4}	4.825×10^{-4}
604	3.465×10^{-4}	4.920×10^{-4}
666	3.861×10^{-4}	4.990×10^{-4}
752	6.039×10^{-4}	5.053×10^{-4}
826	5.148×10^{-4}	5.087×10^{-4}
895	5.247×10^{-4}	5.107×10^{-4}
971	4.851×10^{-4}	5.122×10^{-4}
1062	5.148×10^{-4}	5.133×10^{-4}
1155	5.742×10^{-4}	5.139×10^{-4}
1267	5.643×10^{-4}	5.144×10^{-4}
1348	5.742×10^{-4}	5.145×10^{-4}

Table C.64. Tracer concentration for Run 239 ($u_L=0.0$ m/s, $u_G=0.0308$ m/s, tap water)

t (s)	$c(t)$ (kg/m ³) Experimental	$c(t)$ (kg/m ³) Model
0	0	3.059×10^{-6}
12	4.158×10^{-4}	3.008×10^{-4}
23	4.158×10^{-4}	6.127×10^{-4}
36	7.425×10^{-4}	7.795×10^{-4}
59	7.722×10^{-4}	8.690×10^{-4}
70	7.722×10^{-4}	8.809×10^{-4}
80	9.702×10^{-4}	8.860×10^{-4}
92	8.811×10^{-4}	8.888×10^{-4}
104	9.801×10^{-4}	8.901×10^{-4}
115	8.712×10^{-4}	8.906×10^{-4}
126	8.415×10^{-4}	8.908×10^{-4}
161	8.118×10^{-4}	8.910×10^{-4}
172	8.910×10^{-4}	8.910×10^{-4}
184	8.118×10^{-4}	8.910×10^{-4}
196	7.524×10^{-4}	8.910×10^{-4}
207	7.623×10^{-4}	8.910×10^{-4}
219	8.910×10^{-4}	8.910×10^{-4}
244	8.712×10^{-4}	8.910×10^{-4}
255	8.217×10^{-4}	8.910×10^{-4}
268	9.009×10^{-4}	8.910×10^{-4}
292	9.108×10^{-4}	8.910×10^{-4}
307	8.712×10^{-4}	8.910×10^{-4}
318	9.702×10^{-4}	8.910×10^{-4}
330	8.316×10^{-4}	8.910×10^{-4}
342	8.613×10^{-4}	8.910×10^{-4}
412	8.514×10^{-4}	8.910×10^{-4}
457	9.108×10^{-4}	8.910×10^{-4}
475	9.108×10^{-4}	8.910×10^{-4}

Table C.65. Tracer concentration for Run 222 ($u_L=0.0045$ m/s, $u_G=0.0083$ m/s, 0.40%

CMC)

t (s)	$c(t)$ (kg/m ³) Experimental	$c(t)$ (kg/m ³) Model
0	0	0
10	4.851×10^{-4}	3.414×10^{-4}
19	2.178×10^{-4}	3.831×10^{-4}
27	2.277×10^{-4}	4.019×10^{-4}
36	3.663×10^{-4}	4.129×10^{-4}
45	4.455×10^{-4}	4.174×10^{-4}
54	2.871×10^{-4}	4.176×10^{-4}
66	3.465×10^{-4}	4.135×10^{-4}
76	3.762×10^{-4}	4.075×10^{-4}
101	6.336×10^{-4}	3.861×10^{-4}
110	2.277×10^{-4}	3.771×10^{-4}
118	1.584×10^{-4}	3.687×10^{-4}
125	1.980×10^{-4}	3.612×10^{-4}
132	8.118×10^{-4}	3.535×10^{-4}
155	1.584×10^{-4}	3.280×10^{-4}
163	2.871×10^{-4}	3.192×10^{-4}
171	8.019×10^{-4}	3.104×10^{-4}
193	3.465×10^{-4}	2.866×10^{-4}
201	2.574×10^{-4}	2.781×10^{-4}
222	3.267×10^{-4}	2.567×10^{-4}
232	2.574×10^{-4}	2.469×10^{-4}
241	3.267×10^{-4}	2.383×10^{-4}
266	4.356×10^{-4}	2.155×10^{-4}
284	2.079×10^{-4}	2.002×10^{-4}
322	1.584×10^{-4}	1.709×10^{-4}
340	1.188×10^{-4}	1.583×10^{-4}
347	8.910×10^{-5}	1.536×10^{-4}
359	1.584×10^{-4}	1.459×10^{-4}
371	1.188×10^{-4}	1.386×10^{-4}
384	1.287×10^{-4}	1.310×10^{-4}
401	1.287×10^{-4}	1.216×10^{-4}
415	1.089×10^{-4}	1.144×10^{-4}
440	6.930×10^{-5}	1.024×10^{-4}
453	6.930×10^{-5}	9.667×10^{-5}
466	6.930×10^{-5}	9.123×10^{-5}
513	6.930×10^{-5}	7.387×10^{-5}
571	2.970×10^{-5}	5.678×10^{-5}
640	2.970×10^{-5}	4.137×10^{-5}

Table C.66. Tracer concentration for Run 227 ($u_L=0.0045$ m/s, $u_G=0.0308$ m/s, 0.40%

CMC)

t (s)	$c(t)$ (kg/m ³) Experimental	$c(t)$ (kg/m ³) Model
0	0	0
15	3.069×10^{-4}	5.140×10^{-4}
22	6.732×10^{-4}	5.700×10^{-4}
29	7.326×10^{-4}	6.094×10^{-4}
84	7.623×10^{-4}	7.039×10^{-4}
111	7.029×10^{-4}	6.950×10^{-4}
140	6.732×10^{-4}	6.699×10^{-4}
154	6.435×10^{-4}	6.543×10^{-4}
188	6.138×10^{-4}	6.113×10^{-4}
201	5.544×10^{-4}	5.937×10^{-4}
223	5.445×10^{-4}	5.632×10^{-4}
250	4.950×10^{-4}	5.255×10^{-4}
400	3.366×10^{-4}	3.381×10^{-4}
463	3.069×10^{-4}	2.760×10^{-4}
519	2.772×10^{-4}	2.292×10^{-4}
578	2.376×10^{-4}	1.877×10^{-4}
659	2.079×10^{-4}	1.418×10^{-4}
805	1.188×10^{-4}	8.450×10^{-5}
854	9.900×10^{-5}	7.083×10^{-5}
897	7.920×10^{-5}	6.060×10^{-5}
947	1.089×10^{-4}	5.051×10^{-5}
998	7.920×10^{-5}	4.190×10^{-5}
1060	4.950×10^{-5}	3.335×10^{-5}
1108	1.980×10^{-5}	2.792×10^{-5}
1184	1.980×10^{-5}	2.105×10^{-5}
1231	9.900×10^{-6}	1.766×10^{-5}
1275	9.900×10^{-6}	1.498×10^{-5}

Table C.67. Tracer concentration for Run 229 ($u_L=0.0045$ m/s, $u_G=0.0385$ m/s, 0.40%

CMC)

t (s)	$c(t)$ (kg/m ³) Experimental	$c(t)$ (kg/m ³) Model
0	0	0
13	5.940×10^{-4}	6.054×10^{-4}
21	6.138×10^{-4}	6.513×10^{-4}
35	7.623×10^{-4}	6.920×10^{-4}
73	6.732×10^{-4}	7.138×10^{-4}
81	7.623×10^{-4}	7.110×10^{-4}
89	7.722×10^{-4}	7.068×10^{-4}
113	6.831×10^{-4}	6.882×10^{-4}
120	6.633×10^{-4}	6.816×10^{-4}
137	6.237×10^{-4}	6.638×10^{-4}
144	6.633×10^{-4}	6.560×10^{-4}
152	6.039×10^{-4}	6.468×10^{-4}
167	5.841×10^{-4}	6.290×10^{-4}
212	5.940×10^{-4}	5.733×10^{-4}
250	5.247×10^{-4}	5.261×10^{-4}
264	5.148×10^{-4}	5.091×10^{-4}
369	4.059×10^{-4}	3.917×10^{-4}
464	3.465×10^{-4}	3.044×10^{-4}
561	2.673×10^{-4}	2.332×10^{-4}
613	2.277×10^{-4}	2.016×10^{-4}
680	2.079×10^{-4}	1.668×10^{-4}
728	1.683×10^{-4}	1.454×10^{-4}
788	1.584×10^{-4}	1.223×10^{-4}
860	1.089×10^{-4}	9.929×10^{-5}
919	7.920×10^{-5}	8.359×10^{-5}
1024	5.940×10^{-5}	6.140×10^{-5}
1072	3.960×10^{-5}	5.329×10^{-5}
1107	1.980×10^{-5}	4.804×10^{-5}
1159	1.980×10^{-5}	4.117×10^{-5}
1210	3.960×10^{-5}	3.538×10^{-5}
1245	9.900×10^{-6}	3.187×10^{-5}

Table C.68. Tracer concentration for Run 233 ($u_L=0.0045$ m/s, $u_G=0.0145$ m/s, 0.40%

CMC)

t (s)	$c(t)$ (kg/m ³) Experimental	$c(t)$ (kg/m ³) Model
0	0	0
16	5.643×10^{-4}	7.410×10^{-4}
47	6.831×10^{-4}	7.745×10^{-4}
56	7.425×10^{-4}	7.729×10^{-4}
66	7.920×10^{-4}	7.685×10^{-4}
74	7.920×10^{-4}	7.636×10^{-4}
84	7.623×10^{-4}	7.562×10^{-4}
99	7.722×10^{-4}	7.432×10^{-4}
107	7.029×10^{-4}	7.355×10^{-4}
115	7.128×10^{-4}	7.275×10^{-4}
130	6.930×10^{-4}	7.117×10^{-4}
142	5.643×10^{-4}	6.986×10^{-4}
151	6.831×10^{-4}	6.886×10^{-4}
159	6.435×10^{-4}	6.796×10^{-4}
166	8.613×10^{-4}	6.716×10^{-4}
184	7.524×10^{-4}	6.510×10^{-4}
213	5.544×10^{-4}	6.179×10^{-4}
229	6.633×10^{-4}	5.998×10^{-4}
248	5.148×10^{-4}	5.786×10^{-4}
275	5.049×10^{-4}	5.491×10^{-4}
305	4.752×10^{-4}	5.176×10^{-4}
326	4.455×10^{-4}	4.962×10^{-4}
378	4.059×10^{-4}	4.463×10^{-4}
485	4.554×10^{-4}	3.566×10^{-4}
615	3.168×10^{-4}	2.696×10^{-4}
755	1.782×10^{-4}	1.984×10^{-4}
845	1.386×10^{-4}	1.625×10^{-4}
1002	1.089×10^{-4}	1.145×10^{-4}
1033	6.930×10^{-5}	1.068×10^{-4}
1065	5.940×10^{-5}	9.939×10^{-5}
1130	8.910×10^{-5}	8.586×10^{-5}
1159	4.950×10^{-5}	8.043×10^{-5}
1210	1.980×10^{-5}	7.168×10^{-5}
1277	9.900×10^{-6}	6.160×10^{-5}

Table C.69. Tracer concentration for Run 234 ($u_L=0.0045$ m/s, $u_G=0.0462$ m/s, 0.40%

CMC)

t (s)	$c(t)$ (kg/m ³) Experimental	$c(t)$ (kg/m ³) Model
0	0	0
14	3.861×10^{-4}	5.448×10^{-4}
22	6.930×10^{-4}	6.327×10^{-4}
29	7.425×10^{-4}	6.835×10^{-4}
36	7.722×10^{-4}	7.186×10^{-4}
44	7.821×10^{-4}	7.453×10^{-4}
75	7.623×10^{-4}	7.690×10^{-4}
95	7.326×10^{-4}	7.476×10^{-4}
130	6.732×10^{-4}	6.802×10^{-4}
153	5.841×10^{-4}	6.270×10^{-4}
163	5.841×10^{-4}	6.031×10^{-4}
171	5.346×10^{-4}	5.839×10^{-4}
179	5.742×10^{-4}	5.648×10^{-4}
195	5.247×10^{-4}	5.271×10^{-4}
202	5.049×10^{-4}	5.109×10^{-4}
210	5.049×10^{-4}	4.926×10^{-4}
251	3.960×10^{-4}	4.051×10^{-4}
268	3.663×10^{-4}	3.721×10^{-4}
327	2.970×10^{-4}	2.736×10^{-4}
374	2.574×10^{-4}	2.118×10^{-4}
499	1.485×10^{-4}	1.040×10^{-4}
631	3.960×10^{-5}	4.753×10^{-5}

Table C.70. Tracer concentration for Run 237 ($u_L=0.0045$ m/s, $u_G=0.0010$ m/s, 0.40%

CMC)

t (s)	$c(t)$ (kg/m ³) Experimental	$c(t)$ (kg/m ³) Model
0	0	0
18	3.960×10^{-5}	1.081×10^{-4}
30	2.079×10^{-4}	1.439×10^{-4}
50	2.178×10^{-4}	1.848×10^{-4}
64	8.910×10^{-5}	2.046×10^{-4}
75	1.782×10^{-4}	2.165×10^{-4}
90	1.782×10^{-4}	2.286×10^{-4}
151	1.782×10^{-4}	2.456×10^{-4}
202	2.079×10^{-4}	2.374×10^{-4}
217	1.881×10^{-4}	2.329×10^{-4}
237	1.188×10^{-4}	2.258×10^{-4}
251	1.782×10^{-4}	2.204×10^{-4}
316	2.079×10^{-4}	1.922×10^{-4}
344	1.584×10^{-4}	1.795×10^{-4}
385	1.386×10^{-4}	1.611×10^{-4}
399	7.920×10^{-5}	1.550×10^{-4}
415	8.910×10^{-5}	1.481×10^{-4}
437	1.089×10^{-4}	1.389×10^{-4}
467	1.089×10^{-4}	1.270×10^{-4}
491	1.089×10^{-4}	1.180×10^{-4}
526	7.920×10^{-5}	1.056×10^{-4}
582	4.950×10^{-5}	8.800×10^{-5}
609	7.920×10^{-5}	8.039×10^{-5}
679	5.940×10^{-5}	6.323×10^{-5}
699	1.089×10^{-4}	5.896×10^{-5}
739	9.900×10^{-5}	5.118×10^{-5}
756	9.900×10^{-5}	4.816×10^{-5}
825	2.970×10^{-5}	3.751×10^{-5}
955	5.940×10^{-5}	2.314×10^{-5}

Table C.71. Tracer concentration for Run 240 ($u_L=0.0045$ m/s, $u_G=0.0308$ m/s, 0.40%

CMC)

t (s)	$c(t)$ (kg/m ³) Experimental	$c(t)$ (kg/m ³) Model
0	0	0
11	2.079×10^{-4}	2.088×10^{-4}
20	2.475×10^{-4}	2.904×10^{-4}
87	4.851×10^{-4}	5.076×10^{-4}
113	5.247×10^{-4}	5.179×10^{-4}
122	6.138×10^{-4}	5.170×10^{-4}
155	5.940×10^{-4}	5.000×10^{-4}
165	4.950×10^{-4}	4.918×10^{-4}
183	4.158×10^{-4}	4.747×10^{-4}
192	4.455×10^{-4}	4.652×10^{-4}
209	3.663×10^{-4}	4.462×10^{-4}
217	4.752×10^{-4}	4.369×10^{-4}
226	3.762×10^{-4}	4.262×10^{-4}
247	3.366×10^{-4}	4.007×10^{-4}
399	3.168×10^{-4}	2.311×10^{-4}
563	1.287×10^{-4}	1.143×10^{-4}
699	7.920×10^{-5}	6.100×10^{-5}
763	9.900×10^{-6}	4.499×10^{-5}
699	7.920×10^{-5}	6.100×10^{-5}
763	9.900×10^{-6}	4.499×10^{-5}

APPENDIX D. SAMPLE CALCULATIONS

In this section an example of calculations of each parameter in the bubble column is shown.

D.1. Gas holdup

The gas holdup was calculated by two methods. The first method was the disengagement of the gas, in which two volumes are measured: the total volume when two phases are present in the system during the operation of the bubble column and the volume when the valves that fed the bubble column are closed suddenly, and the gas go out from the bubble column. Taking for example Run 238 (tap water at $u_L = 0.0045$ m/s, $u_G = 0.0385$ m/s):

$$\varepsilon_G = \frac{V - V_0}{V} = \frac{7.175 \times 10^{-2} \text{ m}^3 - 6.497 \times 10^{-2} \text{ m}^3}{7.175 \times 10^{-2} \text{ m}^3} = 0.0945$$

The second method was through the pressure drop, where the friction and acceleration contribution to total pressure drop were neglected. The acceleration contribution was neglected because no changes in crosssectional area and phase are present, while friction contribution was neglected due to the size of the diameter compared to the traditional pipes as it is made by the majority of researchers; however, latter a calculation of two-phase friction factor was made to verify this assumption.

Considering again Run 238, the calculation of gas holdup with this method results in:

$$\varepsilon_G = \frac{\rho_L - \Delta P / gH}{\rho_L - \rho_G} = \frac{977.6 \text{ kg/m}^3 - 18195 \text{ Pa} / (9.806 \text{ m/s}^2 \times 2.126 \text{ m})}{977.6 \text{ kg/m}^3 - 1.207 \text{ kg/m}^3} = 0.0967$$

It is important to mention that the density of the gas phase was calculated using the gas ideal equation.

D.2. Two-phase friction factor

The two-phase friction factor was calculated from Eq. (3.47), in which the liquid density was substituted by the mixture density and the liquid velocity by mixture velocity as follows:

$$u_M = u_G + u_L = (0.0385 + 0.0045) \text{ m/s} = 0.0430 \text{ m/s}$$

$$\rho_M = \varepsilon_G \rho_G + (1 - \varepsilon_G) \rho_L = [0.0945 \times 1.2066 + (1 - 0.0945) \times 977.6] \text{ kg/m}^3 = 885.31 \text{ kg/m}^3$$

$$f_{GL} = \left(\frac{\Delta P}{\Delta Z} - \frac{\rho_M}{g} \right) \frac{d_c}{2\rho_M u_M^2} = \left(\frac{18195 \text{ Pa}}{1.642 \text{ m}} - \frac{885.3 \text{ kg/m}^3}{9.806 \text{ m/s}^2} \right) \frac{0.2 \text{ m}}{2 \times 885.3 \text{ kg/m}^3 \times (0.0430 \text{ m/s})^2}$$

$$f_{GL} = 146.38$$

In this work, the distance between the two pressure ports was 1.642 m.

D.2. Axial dispersion coefficient

The bubble column used in this work was operated in two modes: in batch and in continuous mode. In batch mode, experimental data were fit to the axial dispersion model neglecting the convective term of the liquid phase because there is not net circulation of the liquid phase in the column (Eq. 3.95). The dispersion coefficient was found through the best fit of the model to experimental data, using MathCad®. An example of the calculations for Run 208 (0.20% CMC, $u_G = 0.0308 \text{ m/s}$ and $u_L = 0 \text{ m/s}$) in MathCad® is as follows:

Datos

$$H := 2.1258$$

$$z := 1.682$$

$$\text{lambda} := 0.00031831$$

$$\text{Dz} := 0.02$$

$$\text{cinf} := 0.0046683$$

$$\text{ORIGIN} \equiv 1 \quad i := 1..48$$

	(0)		(0)
	16		0.0026163
	24		0.0035397
	31		0.0035397
	38		0.0044631
	45		0.0044631
	52		0.0049248
	61		0.0045657
	69		0.0048222
	78		0.0044631
	85		0.0048222
	93		0.0042066
	101		0.0080028
	109		0.0047709
	117		0.0048222
	125		0.0044118
	133		0.0045144
	141		0.0043605
	149		0.0042066
	157		0.0044631
	165		0.0045657
	173		0.00513
	182		0.0049248
t :=	190	Gexp :=	0.0044118
	208		0.0050274
	217		0.0044118
	226		0.0044631
	235		0.0043605
	244		0.0046683
	253		0.0045657
	262		0.0045144
	271		0.0051813
	280		0.0047709
	289		0.0043605
	297		0.00513
	306		0.0048222
	316		0.0045657
	325		0.0047196
	336		0.0046683
	348		0.0046683
	382		0.0048222
	392		0.0044631
	402		0.0045657
	412		0.0046683
	423		0.0045657
	432		0.0047196
	442		0.0047196
	(453)		(0.0049248)

$$\text{CTOL} \equiv 1 \cdot 10^{-10}$$

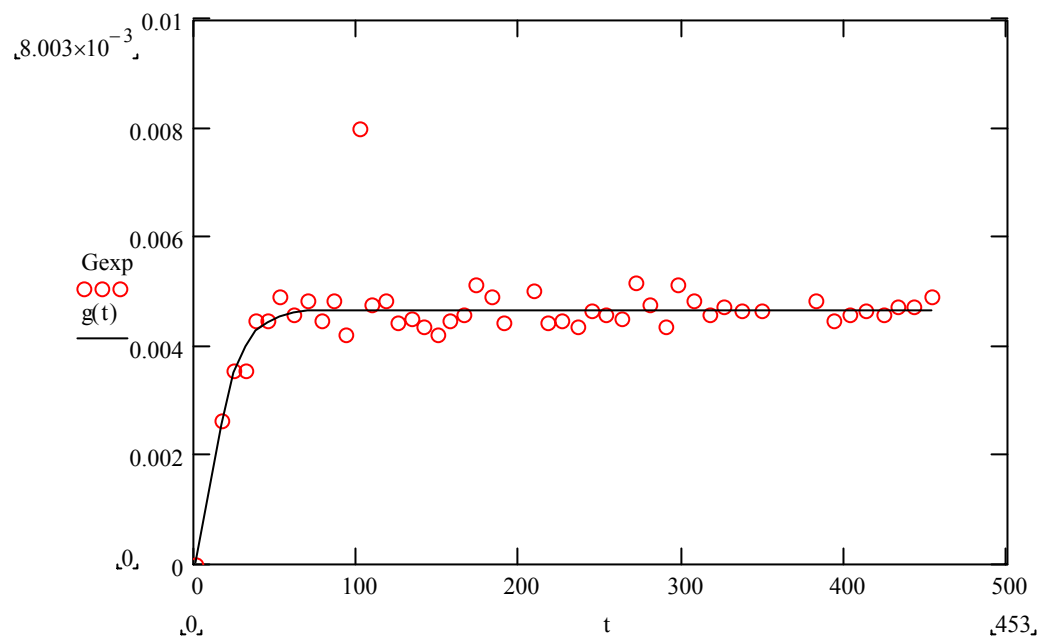
$$F(t, Dz) := \begin{bmatrix} \text{cinf} + \text{cinf} \cdot \frac{2 \cdot H}{\pi \cdot \text{lambda}} \cdot \sum_{m=1}^{45} \left[\frac{1}{m} \cdot \cos\left(m \cdot \pi \cdot \frac{z}{H}\right) \cdot \exp\left[-Dz \cdot t \cdot \left(\frac{m \cdot \pi}{H}\right)^2\right] \cdot \sin\left(m \cdot \pi \cdot \frac{\text{lambda}}{H}\right) \right] \\ -\text{cinf} \cdot 2 \cdot \frac{H}{\pi \cdot \text{lambda}} \cdot \sum_{m=1}^{45} \left[\left(\frac{m \cdot \pi}{H}\right)^2 \cdot \frac{1}{m} \cdot \cos\left(m \cdot \pi \cdot \frac{z}{H}\right) \cdot \exp\left[-Dz \cdot t \cdot \left(\frac{m \cdot \pi}{H}\right)^2\right] \cdot \sin\left(m \cdot \pi \cdot \frac{\text{lambda}}{H}\right) \right] \cdot t \end{bmatrix}$$

$$\text{vg} := .005$$

$$Dz := \text{genfit}(t, \text{Gexp}, \text{vg}, F)$$

$$Dz = \blacksquare$$

$$g(t) := F(t, Dz)_1$$



The function `genfit` minimizes the sum of the squared errors (SSE) from each data point to the resulting function. The `genfit` algorithm will begin iterating at a guess value by computing the gradient of $\text{SSE}(\text{parameter})$ at this point. The gradient vector moves between steep path ascent and steep path descent, guiding the algorithm to the minimum. The function `genfit` takes a step in the direction of the negative gradient and computes a new value; and will continue until it can no longer take any steps and returns the value of the parameter sought in the function SSE. For this reason the guess value is important.

In the case of continuous mode, the tanks-in-series model was also programmed in Mathcad®. An example of the program is shown for Run 229 that corresponds to 0.40% CMC, $u_G = 0.0385$ m/s and $u_L = 0.0045$ m/s).

$t :=$	$C_{exp} :=$
0	0
13	0.000594
21	0.0006138
73	0.0006732
113	0.0006831
120	0.0006633
137	0.0006237
144	0.0006633
152	0.0006039
167	0.0005841
212	0.000594
250	0.0005247
264	0.0005148
369	0.0004059
464	0.0003465
561	0.0002673
613	0.0002277
680	0.0002079
728	0.0001683
788	0.0001584
860	0.0001089
919	0.0000792
1024	0.0000594
1072	$3.96 \cdot 10^{-5}$
1107	0.0000198
1159	0.0000198
1210	$3.96 \cdot 10^{-5}$
1245	$9.9 \cdot 10^{-6}$

Data

$$MQ := 0.3478662$$

$$\mu := 355.7265354$$

$$C(N, \text{tao}, t) := \frac{MQ}{\text{tao}} \cdot \left(\frac{t}{\text{tao}}\right)^{(N-1)} \cdot \binom{N}{N} \cdot \left(\frac{1}{\Gamma(N)}\right) \cdot \exp\left(-t \cdot \frac{N}{\text{tao}}\right)$$

Initial guesses

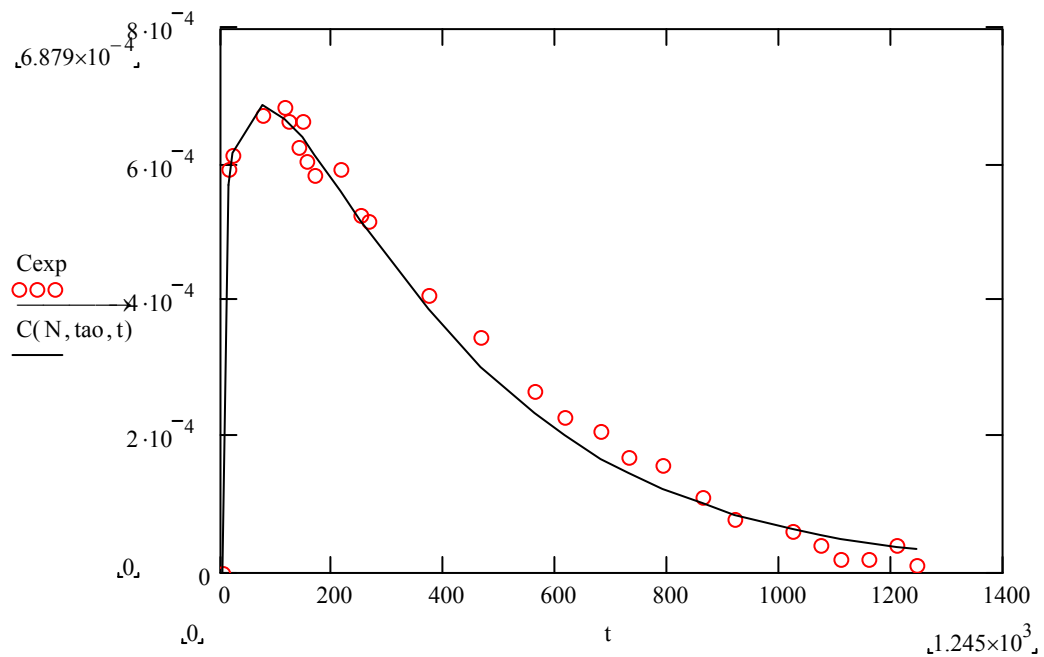
$$N := 5 \quad \text{tao} := 500$$

$$\text{SSE}(N, \text{tao}) := \sum_{i=0}^{27} \left[\left(\text{Cexp}_i - C(N, \text{tao}, t_i) \right)^2 \right]$$

$$\begin{pmatrix} N \\ \text{tao} \end{pmatrix} := \text{Minimize}(\text{SSE}, N, \text{tao})$$

$$N = 1.217 \quad \text{tao} = 388.9529$$

$$\text{SSE}(N, \text{tao}) = 1.478 \times 10^{-8}$$



When the number of tanks is obtained, the calculations of the moments are made in the program to obtain the axial dispersion coefficient for each boundary condition. These results of the same test (Run 229) are shown as follows:

Dispersion model

$$\text{sigmac} := \frac{\text{tao}^2}{N} \qquad \text{sigmac} = 1.243 \times 10^5$$

$$\text{sesgo} := \frac{2 \cdot \text{tao}^3}{N^2} \qquad \text{sesgo} = 7.943 \times 10^7$$

Model Open-Open

$$\frac{\mu}{\text{tao}} = 0.915 \qquad \text{Bo1} := \frac{2 \cdot \text{tao}}{\mu - \text{tao}} \qquad \text{Bo1} = -23.41232$$

$$\text{root} \left(\frac{2}{\text{Bo2}} + \frac{8}{\text{Bo2}^2} - \frac{\text{sigmac}}{\text{tao}^2}, \text{Bo2}, 0.0000000000000000, 1100 \right) = 4.56677$$

$$\text{root} \left(\frac{12}{\text{Bo3}^2} + \frac{64}{\text{Bo3}^3} - \frac{\text{sesgo}}{\text{tao}^3}, \text{Bo3}, 0.0000000001100 \right) = 4.42712$$

Model Open-Closed

$$\frac{\mu}{\text{tao}} = 0.91457 \qquad \text{Bo1} := \frac{\text{tao}}{\mu - \text{tao}} \qquad \text{Bo1} = -11.70616$$

$$\text{root} \left(\frac{2}{\text{Bo2}} + \frac{3}{\text{Bo2}^2} - \frac{\text{sigmac}}{\text{tao}^2}, \text{Bo2}, 0.0000000000000000, 1100 \right) = 3.48291$$

